University of Southampton

Faculty of Environmental and Life Sciences

School of Biological Sciences

Investigating the mode of action of fluensulfone on the plant parasitic nematode, *Globodera pallida*

by

Emily Feist

Thesis for the degree of Doctor of Philosophy

December 2020

University of Southampton

Abstract

Faculty of Environmental and Life Sciences

School of Biological Sciences

Doctor of Philosophy

Investigating the mode of action of fluensulfone on the plant parasitic nematode,

Globodera pallida

by

Emily Feist

Plant parasitic nematodes (PPNs) are a major agricultural pest that infest crops and affect food production worldwide. Current measures that exist for controlling PPN infestation are limited, with the majority of chemical control agents being withdrawn from use due to their off-target toxicity and impact on the environment. New nematicides are therefore required for safe and improved PPN management strategies.

Fluensulfone (FLS) is a novel nematicide with a distinct profile of effects on PPN, suggesting a unique mode of action. Here, I investigate the effects of fluensulfone on *G. pallida* at two critical life cycle stages; the egg- and cyst-enclosed J2, and the free-living, non-feeding, infective J2.

Investigation of the ability of fluensulfone to inhibit *G. pallida* hatching, relative to the efficacy of other distinct classes of nematicides, reinforced that fluensulfone has a distinct mode of action among existing nematicides and demonstrated that it is a potent inhibitor of hatching. At concentrations as low as 1µM (0.29 ppm), fluensulfone exhibited complete inhibition of *G. pallida* root diffusate-induced hatching. This effect was reversible at concentrations ≤5µM (1.46 ppm), partially reversible at concentrations ≤50µM (14.6 ppm) and irreversible at the maximum concentration tested of 500µM (146 ppm). Despite hatching inhibition being reversible at low concentrations, J2s that emerged under these conditions exhibited impaired motility. This suggests that fluensulfone impacts on the viability of the unhatched J2. The irreversibility of hatch inhibition at concentrations >50µM coincided with a granulated appearance of the egg-encased J2 and suggests a nematicidal action of fluensulfone on the unhatched J2.

To inform mechanistic understanding of the nematastatic and nematicidal action of fluensulfone, I combined inhibitor studies to highlight the role played by distinct metabolic fluxes and provide evidence that lipid utilization is selectively disrupted. This was reinforced using Coherent anti-Stokes Raman scattering (CARS) spectroscopy to image lipid stores.

I optimized approaches to extract major lipids from the PPN and probed for levels of key lipid. Interestingly, this failed to identify significant changes in the gross levels of lipids in *G. pallida* juveniles treated with fluensulfone. I discuss this mismatch.

The effects of fluensulfone on lipid utilization were accompanied by morphological changes, manifest by the appearance of enlarged, lipid-bound organelles. These highlight that fluensulfone impacts lipid and/or membrane trafficking processes, accumulating vacuole-like structures. The gross features of these effects appear to be consistent with degradative and cell death pathways. In particular, the appearance of these structures show striking similarities to the accumulation of degradative water and lipid filled vacuoles associated with the cell death process of methuosis.

Taken together, the data presented here present an increased understanding of the mode of action of fluensulfone. They support a model in which fluensulfone brings about a slowly developing metabolic insult that is nematicidal. This involves a disruption in lipid homeostasis and the nematicidal action of fluensulfone may be explained by the accumulation of toxic metabolic intermediates.

Table of Contents

Table of Tables

Table of Figures

Table of Figures

Research Thesis: Declaration of Authorship

Print name: Emily Feist

Title of thesis: Investigating the mode of action of fluensulfone on the plant parasitic nematode, *Globodera pallida*

I declare that this thesis and the work presented in it are my own and has been generated by me as the result of my own original research.

I confirm that:

1. This work was done wholly or mainly while in candidature for a research degree at this University;
2. Where any part of this thesis has previously been submitted for a degree or any other qualification at this University or any other institution, this has been clearly stated;
3. Where I have consulted the published work of others, this is always clearly attributed;
4. Where I have quoted from the work of others, the source is always given. With the exception of such quotations, this thesis is entirely my own work;
5. I have acknowledged all main sources of help;
6. Where the thesis is based on work done by myself jointly with others, I have made clear exactly what was done by others and what I have contributed myself;
7. Parts of this work have been published as:-

Feist, E., Kearn, J., Gaihre, Y., O'Connor, V., Holden-Dye, L., 2020. The distinct profiles of the inhibitory effects of fluensulfone, abamectin, aldicarb and fluopyram on Globodera pallida hatching. Pestic. Biochem. Physiol. 165. doi:10.1016/j.pestbp.2020.02.007

Signature: ..... Date: .....

Acknowledgements

I would firstly like to thank my supervisors, Lindy Holden-Dye and Vincent O'Connor. I have benefited hugely from your time, patience and knowledge. I am at this point out of words to justly articulate my gratitude towards you, but will be forever thankful for your supervision.

I thank ADAMA agricultural solutions Ltd. for their financial support for this project and helpful discussions with Ionit Iberkleid.

Thank you to all of my WormLab colleagues, whose advice and friendship has been invaluable, and to Ellie and Kate; our coffee dates and lunches have kept me sane!

Lacrosse and the SULLC girls have been a massive part of my University experience, both as an undergraduate and postgraduate. Coaching you alongside my PhD has been an absolute joy and much needed refuge away from the lab.

Thank you to my fiancé, Vince. Your support and love for the last 4+ years has been unquestionable and unequivocal. At times when I have doubted myself, you never have, encouraging me to work harder and better, and for that I am so grateful.

Lastly, my parents, Stuart and Sarah Feist. It goes without saying that I would not be where I am today without your unwavering support and guidance. Your work ethic and ambition continues to amaze and inspire me. I am eternally grateful for the opportunities you have enabled me to pursue.

Definitions and Abbreviations

5-HT 5-hydroxytryptamine

AAK ..... AMP-activated kinase

ABM ..... Abamectin

ACAD ..... Acyl-CoA dehydrogenase

ACC ..... Acetyl-CoA carboxylase

ACOX ..... Acyl-CoA oxidase

ALD ..... Aldicarb

AMP ..... Adenosine monophosphate

AMPK ..... AMP-activated protein kinase

ANOVA ..... Analysis of variance

ANT ..... Adenine nucleotide translocator

ASD ..... Anaerobic soil disinfestation

ATP ..... Adenosine triphosphate

CARS ..... Coherent anti-Stokes Raman scattering

CE ..... Cholesterol ester

CER ..... Ceramide

CID ..... Collision induced dissociation

CPT ..... Carnitine palmitoyltransferase

DA ..... Dafachronic acid

DAF ..... Dauer formation

DCM ..... Dichloromethane

DIC ..... Differential interference contrast

DMSO ..... Dimethyl sulfoxide

ER ..... Endoplasmic reticulum

ESI..... Electrospray ionisation

EST..... Expressed sequence tag

ETC ..... Electron transport chain

ETF..... Electron transfer flavoprotein

FA ..... Fatty acid

FAA ..... Fluoroacetic acid

FAD ..... Flavin adenine dinucleotide

FAO..... Food and Agriculture Organisation

FFA..... Free fatty acid

FID ..... Flame ionization detection

FLS ..... Fluensulfone

FPM ..... Fluopyram

GC..... Gas chromatography

GL ..... Glycerolipid

GP ..... Glycerophospholipid

HF ..... Hatching factor

HI ..... Hatching inhibitor

HPLC ..... High performance liquid chromatography

HS ..... Hatching stimulant

ICL..... Isocitrate lyase

IGF ..... Insulin-like growth factor

IMS ..... Imaging mass spectrometry

IRAC..... Insecticide resistance action committee

ITC ..... Itaconic acid

J2 ..... Juvenile stage 2

LC..... Liquid chromatography

LPC..... Lyso-phosphotidylcholine

MAL ..... Malonic acid

MALDI..... Matrix assisted laser desorption ionization

MCSR ..... Mitochondrial-to-cytosolic stress response

MS ..... Mass spectrometry

MTBE ..... Methyl-tert-butyl ether

MTT ..... 2-(4,5-dimethyl-2-thiazolyl)-3,5-diphenyl-2H-tetrazolium bromide

NAD ..... Nicotinamide adenine dinucleotide

NGM ..... Nematode growth medium

NHR ..... Nuclear hormone receptor

OCR..... Oxygen consumption rate

OPO ..... Optical parametric oscillator

PA ..... Phosphatidic acid

PC ..... Phosphatidylcholine

PCN..... Potato cyst nematode

PER ..... Perhexiline

PG..... Phosphatidylglycerol

PK ..... Polyketide

PL..... Prenol lipid

PPN..... Plant parasitic nematode

PRD..... Potato root diffusate

PS..... Phosphatidylserine

PVN..... Plant virus nanoparticle

RCNMV ..... Red clover necrotic mosaic virus

ROI ..... Region of interest

ROS ..... Reactive oxygen species

SCD ..... Stearoyl-CoA desaturase

SDH(I) ..... Succinate dehydrogenase (inhibitor)

SL ..... Saccharolipid

SM ..... Sphingomyelin

SPT ..... Spirotetramat

SQR ..... Succinate-ubiquinone oxidoreductase

SREBP ..... Sterol regulatory element-binding protein

ST ..... Sterol lipid

TAG ..... Triglyceride

TCA ..... Tricarboxylic acid

TGF ..... Transforming growth factor

TLC ..... Thin layer chromatography

TOF ..... Time of flight

WHO ..... World Health Organisation

Chapter 1 General Introduction

1.1 Plant Parasitic Nematode burden

Nematodes are highly diverse organisms, occupying a large range of ecological niches. This includes free-living nematodes through to parasites of plants and animals (Blaxter et al., 1998). Plant parasitic nematodes (PPNs) are major agricultural pests that infect crops and affect food production worldwide (Bernard et al., 2017). PPNs were first described in the 1700's by Needham, who outlined symptoms of galling in wheat caused by nematodes (Needham, 1742). There are over 4,000 identified species of PPNs (Decraemer and Hunt, 2013). It is estimated that collectively, they result in annual global losses of between $80 and $125 billion dollars (Chitwood, 2003; Bernard et al., 2017).

The most economically important species of PPNs, root-knot nematodes (*Meloidogyne* spp.), directly target the roots of major production crops, resulting in reduced agronomic performance due to the prevention of water and nutrient uptake by the host(Bernard et al., 2017). Second in agricultural and economic importance to root-knot nematodes are cyst nematodes, *Heterodera* and *Globodera* spp. The most significant cyst nematodes are the potato cyst nematodes *G. pallida* and *G. rostochiensis,* soybean cyst nematode *Heterodera glycines* and cereal cyst nematodes (Bernard et al., 2017). *G. pallida* and *G. rostochiensis* are known parasites of the solanaceae family, resulting in prolific losses in potato yields. In the UK, it is estimated that *G. pallida* and *G. rostochiensis* result in annual losses of £50 million (Jones et al., 2017).

1.2 PPN life cycle

Plant-parasitic nematodes follow a life cycle with an egg stage, four larval stages and a reproductively mature adult stage. The larval stages of plant-parasitic nematodes are often referred to as juveniles. The first-stage juvenile (J1) develops and undergoes its first moult within the egg, hatching as infective second-stage juveniles (J2s) (Lee, 2002).

J2s are specialised for dispersal and can adapt to survive harsh environmental conditions. In many species, this is the non-feeding stage in the PPN life cycle (Decraemer and Hunt, 2013). The most extensively studied plant-parasitic nematodes are species from cyst, *Globodera* spp. and *Heterodera* spp., and root-knot, *Meloidogyne* spp., nematodes. These species hatch in the soil either from cysts (cyst nematodes) or egg-masses (root-knot nematodes). Root-knot nematodes have a much larger host range than the cyst nematodes (Bird and Bird, 2001). The life cycle stages of these nematodes are described below.

1.2.1 The stylet

As a result of plant-nematode association, PPNs have developed specific feeding structures called stylets (Figure 1.1), which are located at the anterior end of the nematode and connect to the intestines via the esophageal gland (Bernard et al., 2017). This specialised structure enables the nematode to compromise the plant cells by secreting products, such as cellulases, from the subventral and dorsal glands, aiding in the development of host entry and establishment of a feeding site (Davis et al., 2008).

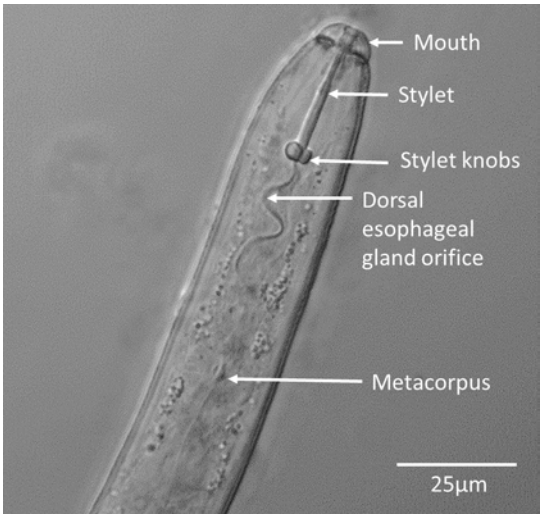

Figure 1.1 Anterior anatomy of potato cyst nematode, *Globodera pallida.* At the head of a plant parasitic nematode is a specialised mouth spear called a stylet. *Globodera pallida* juveniles feature a stylet with stylet knobs that is able to protrude from the mouth and push into plant cells. The stylet is a distinguishable feature of PPNs.

1.2.2 Root-Knot Nematodes

Under favourable environmental conditions, root-knot nematodes hatch from eggs as J2s, which can occur with or without the presence of a chemical stimulus (Bernard et al., 2017). Infective J2s invade the roots of host plants and move intercellularly towards the root tip, where they infiltrate at the elongation zone and enter the vascular cylinder (Bernard et al., 2017). Stylet thrusting and secretion of cell wall degrading enzymes aids migration through root cortex cells. Secretions through the stylet emanate from subventral and dorsal esophageal glands, playing a critical role in PPN infectivity by enabling the juvenile to establish a feeding site. This is achieved by inducing nuclear division of the invaded cell, leading to formation of multinucleate giant cells. Infection by root knot nematodes leads to swelling of root tissues, which is observed as galls or root-knots on the infected plants (Williamson and Gleason, 2003). As the nematodes feed, J2 larvae moult into larval stage 3 (J3). Two further moults take place whilst the juvenile feeds, leading to the J4 and final adult stage. Females continue to feed once at the final adult stage, whereas males leave the root and move through the soil. Females lay eggs in masses in the soil, completing the life cycle (Eisenback and Triantaphyllou, 1991). This is summarised in Figure 1.2.

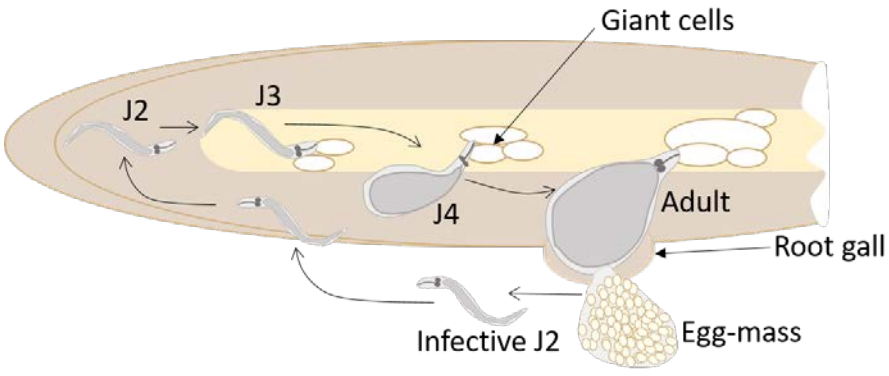

Figure 1.2 Life cycle stages of root-knot nematodes. Root-knot nematodes invade the roots and enter the vascular cylinder near to the root tip. They form giant cells and establish a feeding site. They undergo three moults inside the root before becoming adults. They reproduce either by amphimixis or parthenogenesis and the female lays her eggs in an egg-mass/sac. Figure adapted from Williamson and Gleason, 2003.

1.2.3 Cyst Nematodes

The cyst nematode life cycle is similar to that of root-knot nematodes. A distinguishing feature of cyst nematodes in comparison to root-knot nematodes is that cyst nematodes require a chemical stimulus to induce hatching (Perry et al., 2013). Once hatched, the infective juveniles enter the roots of host plants and move to the vascular cylinder, piercing the cell walls with their stylets and disrupting cells as they go, until they reach the vascular cylinder. It is here that they establish a feeding site. Like root knot nematodes, they break down cell walls between the initial feeding site cell and neighbouring cells by injecting stylet secretions to form a multinucleate syncytium and undergo three moults inside the root to become adults. Male adults go in search of females, which remain attached to their feeding site, and reproduce sexually. In contrast to root-knot nematodes, eggs produced by cyst nematodes are preserved within the body of the female, which becomes a protective cyst casing surrounding the eggs after her death (Williamson and Gleason, 2003). The cysts protrude from the roots or fall into the soil, where they can remain viable for up to 20 years (Jones, 1970). This is summarised in Figure 1.3.

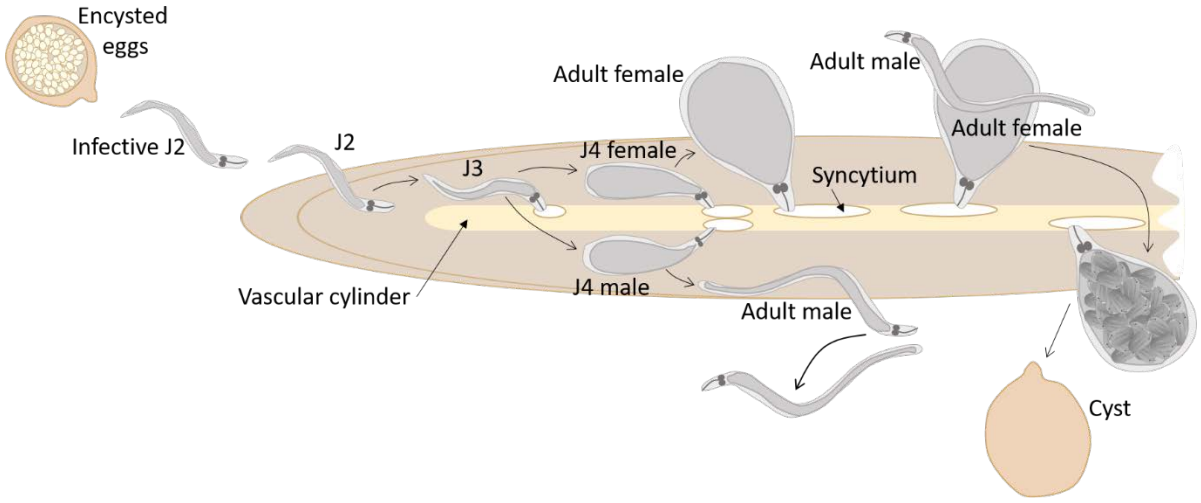

Figure 1.3 Life cycle stages of cyst nematodes. Cyst nematodes infect the roots of host plants and establish feeding sites in the vascular cylinder. They undergo three moults within the root before becoming adults. Males will leave their feeding sites and go in search of a female to reproduce sexually. The female then lays eggs inside her body and once full of eggs, becomes a protective cyst around the eggs. Figure adapted from Cotton et al., 2014.

1.2.4 Quiescence and diapause

Quiescence and diapause are two forms of dormancy that enable PPN survival during adverse environmental conditions (Perry and Moens, 2011). Diapause is a period of dormancy that the juvenile must enter prior to hatching, usually associated with a period of cold, such as winter, and cannot be broken until the end of this essential period, even if favourable conditions return (Perry and Moens, 2011). Following diapause, in host-specific species such as *G. pallida,* juveniles will enter quiescence, still exhibiting limited metabolic flux, however in contrast to diapause, are able to resume their development when favourable conditions return. Juveniles therefore exit quiescence prior to hatching (Perry and Moens, 2011; Palomares-Rius et al., 2013). In *Globodera* spp., exiting quiescence is synchronised with host availability, the majority of juveniles only able to hatch when in the presence of potato root diffusate (PRD) (Palomares-Rius et al., 2013). In the field the stimulus for hatching is determined by hatching factors in root diffusates, emanating from host roots (Perry and Moens, 2011) and in the lab can be triggered by application of PRD, which is generated by soaking roots of potato plants in distilled water (Palomares-Rius et al., 2013). A metabolic switch occurs in the transition from a quiescent juvenile to a PRD-activated juvenile, observed as an increase in juvenile movement within the egg (Gaihre et al., 2019) and evidenced by large-scale upregulation of transcription, including the upregulation of carbohydrate metabolism (Cotton et al., 2014) and increase in cyclic AMP (Atkinson et al., 1987). These suggest an increase in metabolic activity of the juvenile (Figure 1.4).

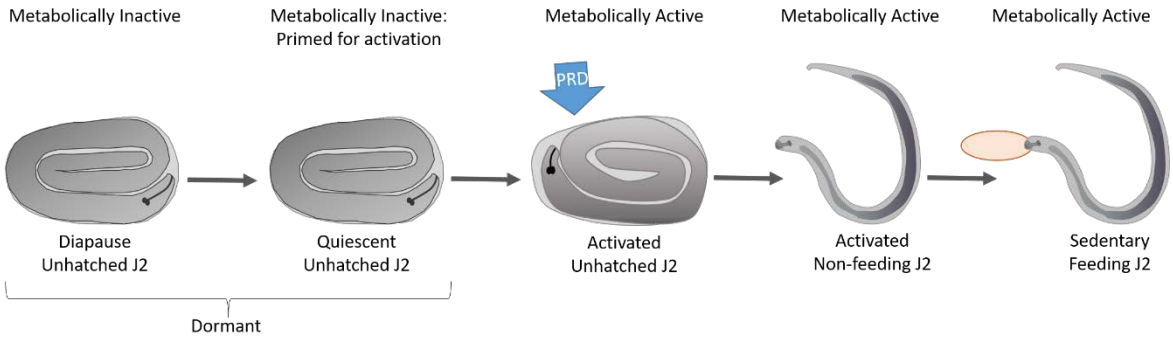

Figure 1.4 Metabolic states of the PPN life cycle. Prior to hatching, *G. pallida* juveniles exist in a dormant metabolic state, enabling long-term survival and preservation of stored energy. Juveniles must exit diapause and enter quiescence prior to activation of hatching and increased metabolic activity.

The genetic and neurosecretory control of diapause and quiescence is not well understood in cyst nematodes in contrast to the extensive studies that have investigated development arrest in the free-living model nematode *Caenorhabditis elegans* dauer larvae (Palomares-Rius et al., 2013). Like parasitic nematodes, *C. elegans* dauers are arrested, non-feeding, and act as a dispersal stage to enable colonisation of high nutrient microenvironments (Crook, 2014). This allows their survival when environmental conditions are unfavourable (Palomares-Rius et al., 2013).

1.2.4.1 *Caenorhabditis elegans* dauer larvae

Caenorhabditis elegans is the most extensively studied free-living nematode, first selected for use as a model organism in the 1970s by Sydney Brenner, due to its suitability for genetic study (Brenner, 1974). This suitability was further contributed to in 1998 when its genome was sequenced (The *C. elegans* sequencing consortium, 1998). The short life cycle and well-defined life stages of *C. elegans* make it an easy organism to work with and maintain in the laboratory. In favourable environmental conditions, *C. elegans* develop from embryo, through four larval stages (L1-4), to reproductive adults. If conditions are unfavourable, developmental arrest occurs at larval stage 2, forming the specialized L3 diapause form, the dauer larvae (Figure 1.5).

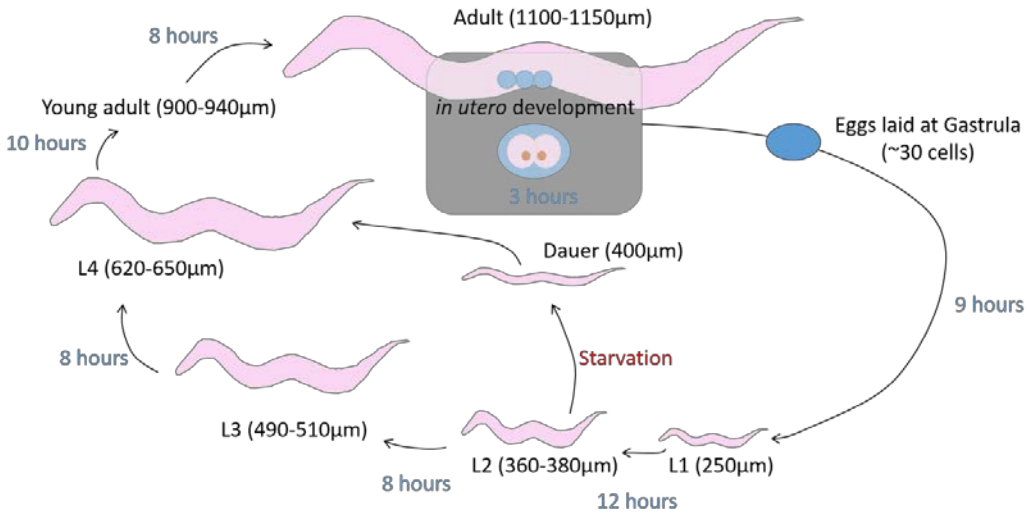

Figure 1.5 *Caenorhabditis elegans* life cycle at 20°C. The time spent at each stage is indicated in blue text. The approximate length of the animal during each stage is indicated next in µm. Figure adapted from wormatlas.org

Entry into and exit from dauer formation is determined by three environmental cues; food, temperature and population density, which is sensed as a constitutively produced ascaroside pheromone complex (Golden and Riddle, 1984). Dauer formation genes (*daf* genes) integrate these environmental signals to mediate dauer arrest (Golden and Riddle, 1984). Pathways controlling dauer formation include cyclic guanosine monophosphate (cGMP) and transforming growth factor β (TGF-β) signalling that control neurosensory function, and an insulin/IGF-1-like receptor signalling pathway (Antebi et al., 2000). These pathways converge on a DAF-12 nuclear hormone receptor (NHR), which is regulated by dafachronic acid (DA) steroid ligands (Stoltzfus et al., 2014), regulating the switch between dauer and normal development (Antebi et al., 2000; Fielenbach and Antebi, 2008). Neurosensory perception of the environment and dietary intake, coupled to endocrine signalling pathways, therefore coordinates survival, growth and development (Fielenbach and Antebi, 2008).

When conditions are unfavourable, cGMP production is down regulated, decreasing the expression of the dauer TGF-β ligand (DAF-7) and inhibiting the production of DAs. In contrast, when favourable conditions return, these pathways are hypothesized to act in reverse (Stoltzfus et al., 2014).

The four molecular pathways that regulate dauer entry and exit in free-living nematodes have been identified in a number of parasitic nematodes. The role of the insulin signalling pathway, *daf-12* and DAs appear to be conserved, whilst *daf-7* signalling is divergent (Crook, 2014). It is therefore surprising that sequence comparison of diapause-related genes in *C. elegans* and *G. pallida* revealed few orthologues between the species, including orthologues for insulin signalling, TGF-β and steroid hormone pathways (Palomares-Rius et al., 2013). This is in contrast to other studies in PPNs, such as *Bursaphelenchus xylophilusm,* where orthologues of most genes involved in pathways that regulate *C. elegans* dauer formation were identified (Kikuchi et al., 2011), and *M. hapla,* which encodes strong orthologues of many *C. elegans daf* genes (Opperman et al., 2008). The absence of orthologues in *G. pallida* may therefore be as a result of some genes being missed during genome assembly or annotation and/or differences in the parameters used when comparing nematode genes between different studies (Palomares-Rius et al., 2013). Clarifying how PPNs control their exit from developmental arrest, and the conservation and divergence of those control mechanisms between free-living nematodes, is vital in better understanding the activation of unhatched juveniles and could provide opportunities to interfere with this stage in the nematodes life cycle.

1.3 Potato cyst nematode hatching

Three phases of hatching have been described for potato cyst nematodes (PCN); changes in the eggshell, activation of the juvenile and eclosion (Perry et al., 2013). These stages are summarised in Figure 1.6.

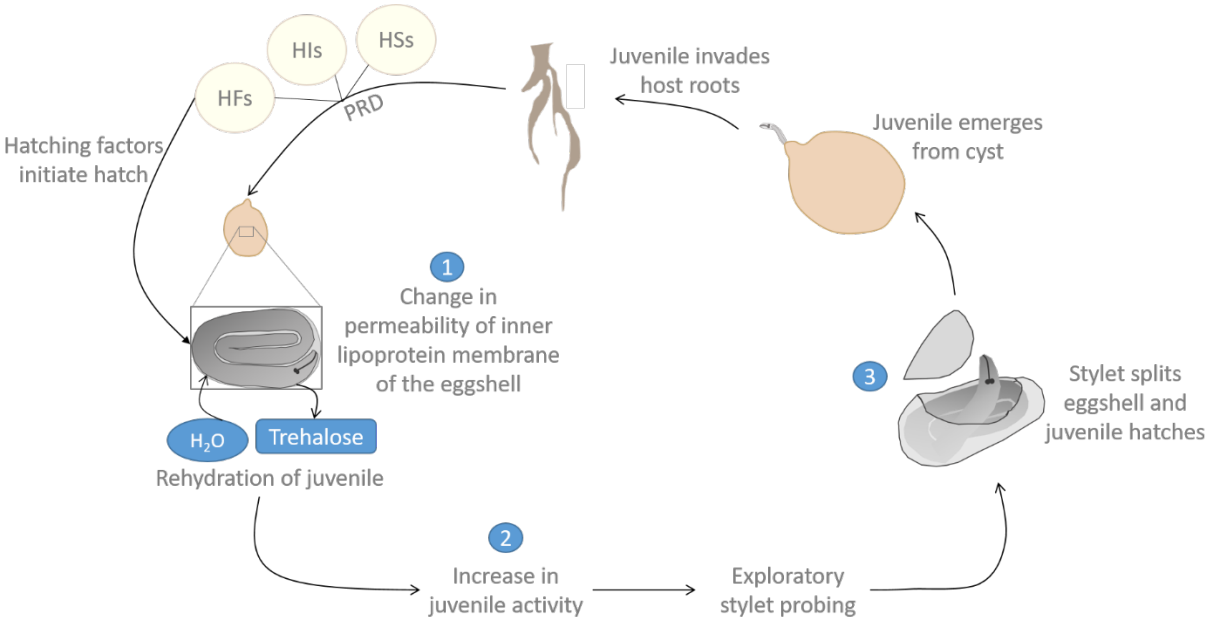

Figure 1.6 Summary of PCN hatching. (1) Changes to the juvenile eggshell, (2) activation of the juvenile and (3) juvenile eclosion. PRD: potato root diffusate, HFs: hatching factors, HIs: hatching inhibitors, HSs: hatching stimulants.

1.3.1 Initiation of hatching

The hatching process differs between different PPN species, including different requirements for initiation of hatching. Some species, such as the potato cyst nematodes *Globodera* spp., require activation from hatching factors that are released from host roots to stimulate J2 hatching (Perry et al., 2013). This can be mimicked experimentally by generating host root diffusate as a source of hatching factors. Host-nematode synchronization is a survival strategy common to cyst nematodes, as it ensures hatching does not commence until a suitable host is present (Perry et al., 2013). Other species of PPNs, such as the root-knot nematodes *Meloidogyne* spp., do not require host root diffusate to hatch and will hatch readily in water (Perry and Moens, 2011).

1.3.1.1 Root diffusate components

It has been shown that *G. rostochiensis* hatch in response to potato root diffusate (PRD) in a concentration-dependent manner (Devine and Jones, 2000). Hatching activity peaks at an optimum concentration of PRD, with increases in PRD concentration above optimum resulting in a decline in hatching. This could be as a result of the increase in concentration of hatching inhibitors (HIs) with more concentrated PRD (Byrne et al., 1998). HIs are present in PRD with hatching factors (HFs) and hatching stimulants (HSs). HFs induce hatching, HIs reversibly inhibit this induction of hatching, whereas HSs have a synergistic effect on HF-induced hatching (Byrne et al., 1998). The ratio of HF: HI influences the hatching activity of potato cyst nematodes in the soil, with a low HF: HI ratio limiting hatching. A low HF: HI ratio is found in root exudates from young plants, suggesting that young plants produce HIs as a survival mechanism, limiting nematode hatching activity until they become more established plants (Byrne et al., 1998). HF: HI ratio of root exudates increases as the plants age, which is paralleled with an increase in nematode hatching activity (Byrne et al., 1998).

Chemical analysis of root diffusates has resulted in identification of HFs (Perry, 1996), such as potato-specific glycoalkaloids α-solanine and α-chaconine (Byrne et al., 2001). Artificial HFs, such as sodium metavanadate and picrolonic acid, have also been identified (Byrne et al., 2001). Inducing 'suicide hatch' of PPNs by direct application of HFs to infested soils in the absence of a host plant has the potential to be used as a control method for PPN infestation. It has been shown that application of natural HFs to soil in the field is able to reduce *G. rostochiensis* populations (Devine and Jones, 2000) via such an approach.

1.3.2 Eggshell and permeability changes

The nematode eggshell is typically comprised of three layers; the outer protein-rich vitelline layer, a thick, middle chitinous layer and an inner lipid layer that is made up of lipids and proteolipids (Perry and Moens, 2011). Perivitelline fluid surrounds the unhatched juvenile and in combination with the eggshell, provides protection from environmental challenges. The constituents of the eggshell are summarised in Figure 1.7.

The inner lipid layer is responsible for the limited permeability of the eggshell and prevents the passage of small molecules (Ebrahimi, 2015). Initiation of hatching is associated with a change in the permeability of the lipid layer of the eggshell (Palomares-Rius et al., 2016). For potato cyst nematodes *Globodera* spp*.,* this is thought to occur via a calcium-mediated process by which Ca^{2+} is taken up by the juvenile and egg-shell and may have a binding site located on the egg-shell surface to mediate these permeability changes (Perry and Clarke, 1981). Sodium- and zinc-mediated changes in egg permeability have also been described for other parasitic nematode species (Perry and Clarke, 1981; Tefft and Bone, 1985). This change in permeability is thought to be triggered by egg exposure to hatching factors in host root diffusate, synchronizing nematode hatching with host availability (Perry and Clarke, 1981).

It is thought that HFs interact with the eggshell to bring about the changes in permeability described, and so it can be considered that compounds that inhibit hatching may interfere with domains of receptors located on the eggshell that are responsible for identifying hatching factors and stimulants (Charlson and Tylka, 2003) and could represent a route to prevent hatching. Juvenile death within the eggshell can also cause changes to the permeability of the lipid layer (Ebrahimi, 2015), a phenomenon that does not rely on an interaction with the eggshell from external components, but that is driven by a change to the juvenile itself. It should therefore be considered whether HFs and other components of root diffusate interact solely with the eggshell to bring about changes or whether they are able to alter the behaviour of the enclosed juvenile and so trigger the hatching cascade. This would complement the fact that not all juveniles hatch in response to host diffusate. In *Globodera* spp*.,* after exposure to host root diffusate, there is only a 60-80% hatch, with juveniles that do not hatch remaining unaffected by the stimulus and in unaltered eggshells (Atkinson and Fowler, 1990).

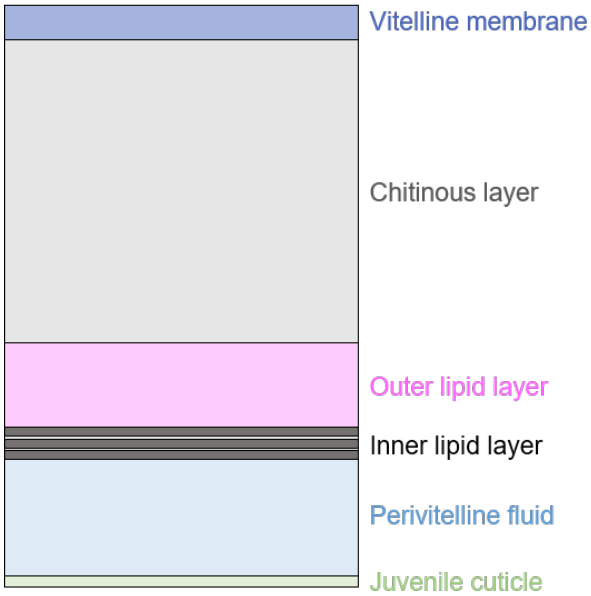

Figure 1.7 Typical components of a nematode eggshell. The eggshell is made up of an outer vitelline layer, a middle chitinous layer and an inner lipid layer. Perivitelline fluid surrounds the unhatched nematode. Figure adapted from (Perry and Trett, 1986).

1.3.2.1 Role of trehalose in hatching

Trehalose leakage is reported to follow changes in the permeability of the eggshell and be a key factor in the initiation of hatching of PPNs (Perry and Clarke, 1981). The present description suggests that this happens after receptor activation. The presence of trehalose in the perivitelline fluid provides an osmotic stress on the unhatched juvenile, inducing quiescence and inhibiting locomotion of the nematode (Palomares-Rius et al., 2016). When trehalose leaks out of the eggshell, water uptake by the juvenile can occur and the osmotic stress is removed, allowing the juvenile to become activated (Perry et al., 2013).

Synthesis of trehalose has long been associated with desiccation tolerance in anhydrobiotic organisms, including nematodes (Crowe and Madin, 1975). Due to it being a non-reducing sugar, storage of trehalose during prolonged periods of environmental stress is more favourable over reducing sugars, such as glucose, as it causes less damage to cells and tissues (Watanabe, 2006).

Dauer larvae of *C. elegans* have been described as anhydrobiotes, displaying a four- to five-fold increase in trehalose levels in response to harsh desiccation (Abusharkh et al., 2014). Supporting the role of trehalose in desiccation tolerance in *C. elegans,* mutants that cannot produce trehalose are unable to survive desiccation to the same extent as wild-type animals (Erkut et al., 2011). Trehalose is also important in the ability of animals to undergo controlled rehydration, with *C. elegans* larvae that are deficient in trehalose suffering membrane rupture upon rehydration (Abusharkh et al., 2014).

It is well documented that trehalose is a protective agent during dehydration and subsequent rehydration. Its presence in the egg of PPNs suggests it is acting to protect the metabolically inactive juvenile from dessication stress, whilst allowing for its rehydration and activation following its leakage from the egg. Furthermore, trehalose can be hydrolysed into glucose and can be readily utilised as an energy source by parasitic nematodes (Behm, 1997; Grewal et al., 2006).

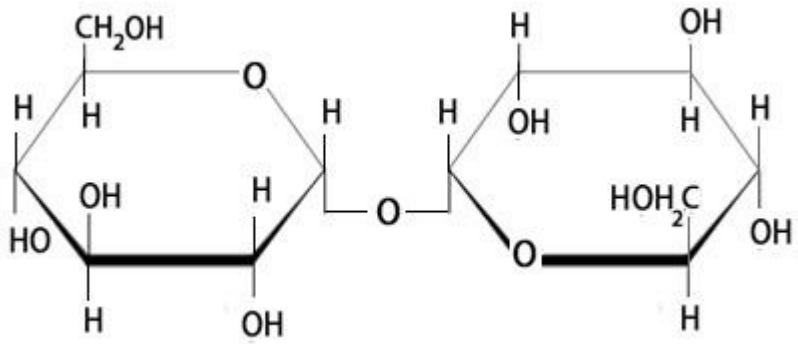

Figure 1.8 Chemical structure of trehalose. Trehalose is a disaccharide formed by an α,α-1,1-glucoside bond between two α-glucose units. It is a non-reducing sugar that can be broken down into glucose by the enzyme trehalase.

1.3.3 Water uptake and rehydration

Following trehalose leakage from the egg, water uptake occurs, leading to the rehydration of the juvenile. An increase in water uptake increases volume and pressure within the egg, aiding juvenile eclosion (Perry and Clarke, 1981).

Larvae stimulated by HFs have an increased water content in comparison to unstimulated larvae (Ellenby and Perry, 1976), however full hydration of the unhatched juvenile does not occur until after eclosion, the eggshell preventing full rehydration by limiting water uptake (Holz et al., 1998b). If HFs interact directly with the juvenile rather than causing changes to the eggshell, it could be possible that they trigger a response in the juvenile, such as activation of neurosecretory activity, which leads to processes, such as increased water uptake, that result in hatching (Ellenby and Perry, 1976).

Interestingly, juveniles of species that have a higher water content than *Globodera* spp. do not require water uptake prior to hatch and are able to hatch without stimulation from HFs (Perry and Clarke, 1981). Species include the sugarbeet nematode, *Heterodera schachtii,* which can readily hatch in water and has an extensive host range. In comparison *Globodera* spp. have a very narrow host range and require stimulation by host root diffusate to hatch (Perry et al., 2013).

1.3.4 Utilization of lipids

Stimulation of unhatched juveniles by host root diffusates has been shown to increase utilization of lipid reserves in *Globodera* spp. (Atkinson and Fowler, 1990; Holz et al., 1997). This suggests that lipid stores are utilized during hatching to provide energy for the hatching process (Perry et al., 2013).

Anhydrobiotic species also display high levels of lipid reserves (Perry and Moens, 2011), including the well-studied anhydrobiotic organisms, tardigrades, whose main repository of energy is stored as lipid, peptide and glycogen (Reuner et al., 2010). Lipid stores are therefore important as an energy reserve during times of environmental stress and are potentially utilized by animals during rehydration. Increased water uptake and utilization of lipids are events both stimulated by host root diffusate (Holz et al., 1997). Furthermore, stimulated unhatched juveniles use their lipid reserves more rapidly than unstimulated juveniles and have a fatty acid profile that is similar to that of hatched juveniles (Holz et al., 1998b). This is again suggesting a direct interaction of host root diffusate with the enclosed juvenile, leading to activation of the juvenile and eclosion.

1.3.5 Eclosion

Before the juvenile exits the eggshell, three main events have been reported to take place within the encapsulated egg. Firstly, widespread exploration, where the nematode circulates the intact egg. Secondly, local exploration, where the nematodes lips explore the surface of the eggshell, and thirdly, stylet thrusting (Perry and Clarke, 1981; Gaihre et al., 2019). Stylet protractor muscles control stylet protrusion and are relaxed during retention, which is caused by tension in the alimentary tract (Rolfe and Perry, 2001). Stylet thrusting differs between different species of nematode. *Globodera* spp. display coordinated thrusts that cause a slit in the eggshell from which the juvenile can escape. Other species thrust in a more random manner and it is their increased bodily movements that results in the eggshell breaking and the nematode hatching (Perry et al., 2013). In species such as *Globodera* spp., where stylet thrusting is required for eclosion, this phase of hatching could be a potential target for nematicides to reduce nematode populations.

1.4 PPN control

1.4.1 Biological control

Biological control of pests maintains or enhances naturally occurring nematode-suppressive mechanisms that occur in agricultural soils (Stirling, 2011). This can involve application of antagonistic organisms and/or conservation and enhancement of indigenous antagonists to provide an alternative method to chemical control (Timper, 2011) (see 1.4.3 for chemical control). Despite the many advances that have been seen in biological control methods in the past two decades, it is still rarely solely used in nematode management strategies (Timper, 2011; Viane et al., 2013). To be successful, a strategy must combine different management methods, be flexible to changes in diseases and pests and adapt as our knowledge on pest management grows (Viane et al., 2013). Methods that are used in the biological control of nematodes are discussed in this section.

1.4.1.1 Agricultural soils and their treatment

Physical soil treatments to disinfest soils are used in nematode management strategies to improve crop yield and reduce nematode populations. This can be achieved by dry heat, steam, solarisation, flooding or anaerobic soil disinfestation (Viane et al., 2013).

Surface burning and roasting are long established methods for applying dry heat to soils, resulting in high temperatures that kill nematode larvae. This is based on the principal that most PPNs have low thermal death points, and so increasing temperature decreases nematode populations (Newhall, 1955). Microwave radiation is based on this same principal and involves treating infested soil in commercial microwave ovens. This has shown elimination of soil-borne pathogens (Ferriss, 1984), however is not widely used due to its impracticality of treating field soil (Viane et al., 2013). Steam treatment of soil non-selectively kills pests and results in better growth of plants in subsequent crops (Newhall, 1955), however is expensive and is mainly used for small volumes of soil, such as in a greenhouse (Viane et al., 2013).

Soil solarisation is an approach to soil disinfestation that can be employed effectively to reduce nematode populations, primarily used in hot climates (Viane et al., 2013). Like with the other soil disinfestation methods that use heat to kill pests, solarisation acts by the same mechanism. This approach utilizes passive solar heating of moist soils that are covered with plastic sheeting, usually transparent polyethylene (Stapleton, 2000). In addition to the destruction of soil-borne pests by thermal deactivation, solarisation can improve soil nutrient availability, leading to an increase in plant health and growth (Stapleton, 2000). Solarisation relies greatly on climate and weather and so has its limitations. The combination of soil solarisation with other nematode management strategies, however, could prove to be an important agricultural solution to soil disinfestation (Stapleton, 2000).

Flooding is an alternative soil disinfestation method that effectively kills soil nematodes without relying on heat. This method is mainly utilised in agricultural land that is prone to natural flooding, rather than artificial flooding, which is expensive and not cost-efficient (Bridge, 1996). This method relies on the basis that PPNs require oxygen tensions above what is available in water for respiration (Newhall, 1955).

Anaerobic soil disinfestations (ASDs) were developed in Japan and The Netherlands (Momma et al., 2013). This method consists of applying large amounts of organic matter followed by irrigation and then sealing the amended soil. Sealing the soil results in the trapping of gases to establish the anaerobic conditions necessary to kill the soil pathogens, including PPNs (Viane et al., 2013). Nematode populations can be suppressed under anaerobic conditions, as is observed during flooding. This suppression can be enhanced by application of organic matter (Momma et al., 2013), forming the basis of ASD development. Accumulation of organic acids, acetic acid and butyric acid during ASDs contributes to the suppression of some nematode populations (Momma et al., 2006). Further optimization of this technique could be a promising approach for disinfesting soil. A combination of ASDs and soil solarisation has shown to effectively control soil-borne pathogens, including PPNs (Butler et al., 2014), highlighting the effectiveness of combining biological control and physical methods for nematode management.

1.4.1.2 Natural enemies of nematodes

The rhizosphere is the zone of soil that surrounds roots, differing from bulk soil biologically, chemically and physically (Kerry, 2000). Plant-parasitic nematodes must pass through this zone in order to reach their host. The amount of time spent in the rhizosphere, however, depends on the mode of parasitism (Kerry, 2000). In a particular rhizosphere, many microorganisms exist. The presence of more than one microorganism and their constant interactions with each other, the environment and microbial biological control agents results in a biological balance (Jatala, 1986; Viane et al., 2013). Microorganisms that grow in the rhizosphere provide defence for the roots of host plants against plant-parasitic nematodes (Jatala, 1986). Pathogens and antagonists of PPNs include nematode-trapping fungi, such as *Arthrobotrys oligospora*, egg-parasitic fungi, such as *Verticillium chlamydosporium* and antagonistic rhizobacteria, such as *Agrobacterium radiobacter* and *Bacillus subtilis* (Kerry, 2000). A greater understanding of the dynamics of the microbial community in the rhizosphere would improve application of biological control agents in agricultural soil to enhance the pathogenic and antagonistic effects of naturally occurring PPN parasites. Soil amendments, such as addition of organic matter, can increase the numbers and variety of microorganisms within the rhizosphere, including microorganisms that are able to suppress nematode populations (Viane et al., 2013). Soil amendments could therefore be integrated as part of a nematode management strategy.

Most organisms that are able to suppress PPN populations are nematophagous fungi and antagonistic bacteria (Viane et al., 2013). To maintain nematode populations below their damage threshold densities, an understanding of how these biological control agents can be manipulated for use in nematode management programmes must be sought.

1.4.1.3 Nematophagous fungi

Nematophagous fungi include nematode-trapping, egg-parasitic and cyst-parasitic fungi. Nematode-trapping fungi occur in many different soil types where they exist mainly as saprophytes, living on dead or decaying organic matter (Nordbring-Hertz et al., 2006). Their ability to develop infection structures allows them to trap and subsequently feed on nematodes, giving them a nutritional advantage over other saprophytes (Nordbring-Hertz et al., 2006). Formation of trapping structures is induced by nematode contact with the mycelium (Nordbring-Hertz et al., 2006) and include constricting and non-constricting rings, adhesive knobs, adhesive networks and adhesive columns (Li et al., 2015). Nematode-trapping fungi can be classified according to the type of trapping structures that they form. *Arthrobotrys* form adhesive networks, *Dactylellina* develop adhesive knobs and non-constricting rings, and *Drechslerella,* constricting rings (Li et al. 2015).

Egg-parasitic fungi grow towards nematode eggs and form a specialized penetration peg, which is used to infect the eggshell. The fungi then feeds on the contents of the egg (Nordbring-Hertz et al., 2006; Li et al., 2015). Species include *Pochonia chlamydosporia, Paecilomyces lilacinus, Clonostachys rosea,and Lecanicillium psalliotae* (Li et al., 2015). Nematode eggshells are composed of several layers, including a middle chitinous layer, which provides a target for chitinases secreted by egg-parasitic fungi (Nordbring-Hertz et al., 2006). Fungi and the fungal chitinases they produce have been associated with nematode population decline (Gortari and Hours, 2008) and have therefore shown great potential as biological control agents.

Most egg-parasitic fungi can also parasitize cysts (Indarti et al., 2010), infection occurring either directly through the nematode cuticle, through the natural openings of the vulval cone or after colonisation of the feeding site in the root when the female is feeding (Kerry, 1988).

1.4.1.4 Nematophagous bacteria

Nematophagous bacteria interfere with nematodes by producing toxins, antibiotics or enzymes that have strong antagonistic properties, and are able to reduce the damage caused by nematode parasitism (Viane et al., 2013). These bacteria have a wide range of suppressive activities on a range of nematodes and are broadly distributed (Tian et al., 2007).

Pasteuria penetrans has been widely studied as a nematode parasite (Siddiqui & Mahmood 1999). Bacterial species of the genus *Pasteuria* are obligate, endospore- forming bacterial parasites of PPNs that have considerable biocontrol potential, naturally existing world-wide (Siddiqui and Mahmood, 1999; Tian et al., 2007). Spores of *P. penetrans* can attach to the cuticles of *Meloidogyne* spp. juveniles, germinating once the juvenile has infected the root. Germ tubes of the bacteria then penetrate the nematode cuticle and microcolonies form and proliferate through the feeding nematodes body (Tian et al., 2007). A limitation to the application of *P. penetrans* for biocontrol is that it has low mobility and so therefore relies on dispersal by water or cultivation practices (Jatala, 1986).

Rhizobacteria, such as *Bacillus* and *Pseudomonas* strains, are able to suppress nematode populations and enhance plant growth (Tian et al., 2007). This is achieved by their ability to colonize roots and reduce nematode root invasion (Siddiqui and Mahmood, 1999). They can also prevent growth- promoting mechanisms, such as nitrogen fixing, when nitrogen in the soil is limited (Bloemberg and Lugtenberg, 2001). The mechanisms responsible for suppressing nematode populations include competition for nutritional resources, antibiotic production, binding to and altering the root surface to prevent host recognition by nematodes and production of metabolites (Chet et al., 1990; Siddiqui and Mahmood, 1999; Bloemberg and Lugtenberg, 2001).

The successful use of biological control agents relies on a thorough understanding of the organism's interactions with other microorganisms in the rhizosphere. The application of biological agents is difficult; effective isolates must be selected and then an inoculum produced. This must consider the nematode species and the stage of development being targeted. Further to initial application, the biological control agents must be maintained and this may require subsequent application.

1.4.2 Biological control and integration

Crop rotation can be a very effective way of managing PPN populations. The aim of this practice is to rotate with different crops on the same area of land so that there are sufficient time-periods between planting of host crops to allow for the number of nematodes to decline, improving yield of the next host crop (Trivedi and Barker, 1986). Crop rotation is rarely used in the management of PCNs due to the decrease in revenue associated with this method (Scholte, 2000) and the ability of cyst nematodes to remain viable in the soil between rotations, due to their host-synchronized hatch.

Trap cropping could provide an alternative control method for the control of PCNs. Trap crops can be planted to attract pests, such as insects or nematodes, to allow pest invasion and development and protect target crops. This is achieved by concentrating the pests in a desired location, the trap crop, and then destroying them (Hokkanen, 1991; Viane et al., 2013). The use of potato as a trap crop has been shown to effectively control *Globodera* spp (Scholte, 2000). Success of using trap cropping as a control method for nematodes must consider the nematodes host range, specifically what stimulates nematode activity, and proper removal of the trap crop once invasion of nematodes has occurred. In addition, some trap crops produce nematicidal derivatives that are able to reduce nematode populations. The main antagonistic plants tested for the control of nematodes are *Tagetes* spp., particularly *T. erecta*, *T. patula* and *T. minuta,* all species of marigolds (Bridge 1996). These plants reduce numbers of *Pratylenchus* spp. and *Meloidogyne* spp. by producing the toxic root exudate, α-terthienyl, (Viane et al., 2013). However, the detrimental effect of these plants on crop yield often outweighs their nematode control benefits (Bridge, 1996).

Trap cropping can be quite costly (Viane et al., 2013) and so is not always a viable option for farmers. An alternative can be to implement the use of cover crops. Cover crops have additional functions that make them more appealing for the farmer, such as having their own commercial value, conserving the soil in the off season or providing forage for livestock (Bridge, 1996; Viane et al., 2013).

1.4.3 Chemical control

Nematicides are chemical compounds that are used to control unwanted nematodes. A range of nematicides are used worldwide to reduce damage caused by nematodes and increase crop yield and productivity (Tobin et al., 2008). The insecticide resistance action committee (IRAC) are a specialist technical group that provide a coordinated industry response to prevent or delay the development of resistance in insect and mite pests. The nematode working group is the most recently established IRAC team, with an initial objective to develop a mode of action classification scheme (https://irac-online.org/mode-of-action/). This has enabled the grouping of nematicides based on mechanism of action, whilst also highlighting the nematicides that are available with unknown modes of action. The classification also includes biologicals, grouped as bacterium, fungus and botanical/animal derivatives. The chemical nematicides that are available for nematode management are described below, according to their mode of action classification.

1.4.3.1 Acetylcholinesterase inhibitors

Acetylcholinesterase (AChE) inhibitors prevent the hydrolysis of acetylcholine (ACh) at the neuromuscular synapse and thus result in paralysis (Opperman and Chang, 1991). AChE inhibitors include compounds from the carbamate (Figure 1.9) and organophosphate (Figure 1.10) chemical groups (Haydock et al., 2013).

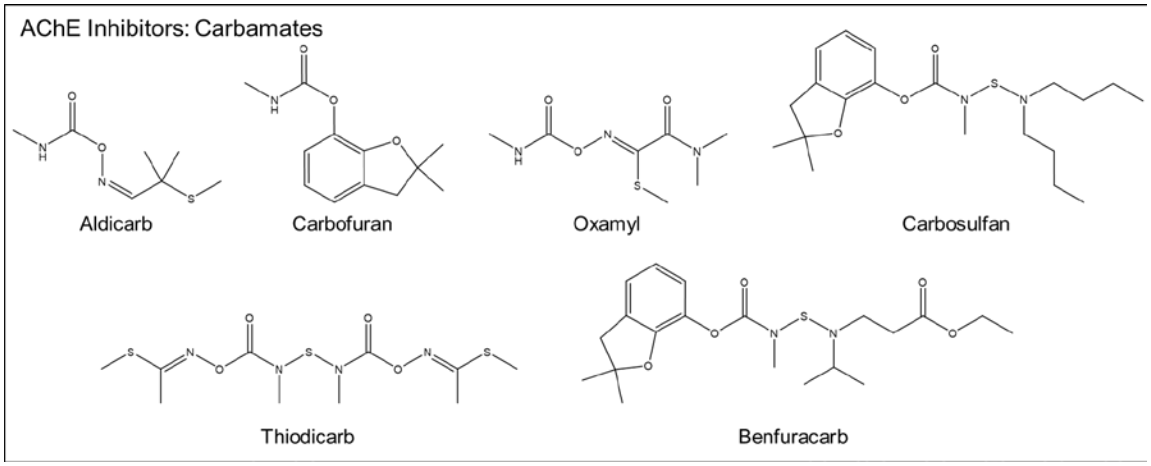

Figure 1.9 Chemical structures of carbamate nematicides. Major representatives of the carbamate acetylcholinesterase (AChE) inhibitors.

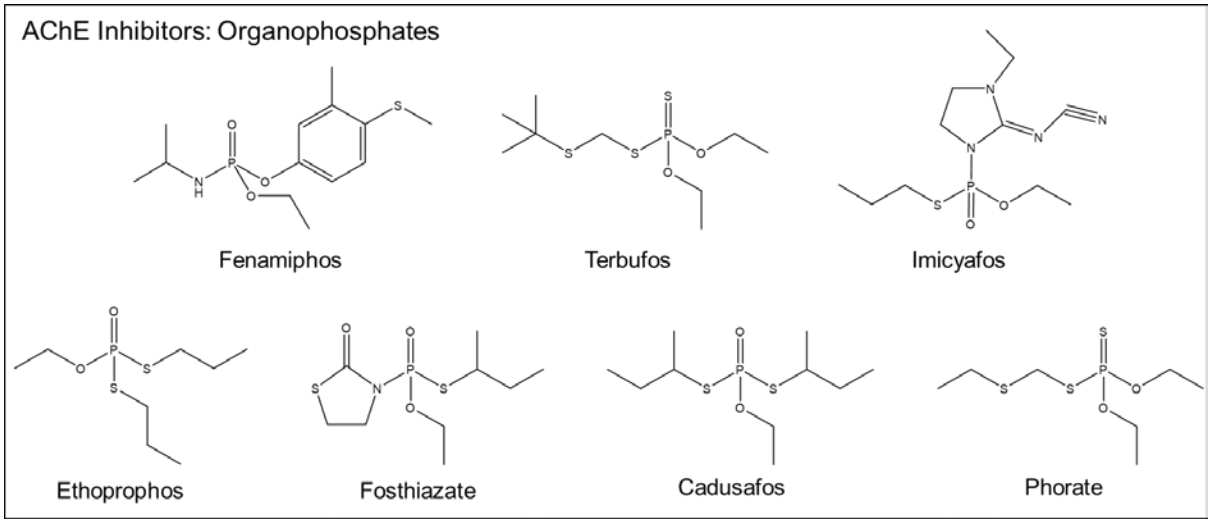

Figure 1.10 Chemical structures of organophosphate nematicides. Major representatives of the organophosphate acetylcholinesterase (AChE) inhibitors.

The amount of ACh that builds up as a result of nematicide treatment depends on the rate of ACh release from the pre-synapse. This accumulation then results in the onset of paralysis by translating the cholinergic signal into a sustained muscle contraction and causing spastic paralysis (Mulcahy et al., 2012). Rapid nematode recovery has been reported following short exposure to carbamate and organophosphate nematicide treatment. This was shown in a study looking at AChE activity and percentage motility in *C. elegans* (Opperman and Chang, 1991). Recovery after longer exposure to organophosphates was conditional and slower when compared to carbamate exposure. These results explain why AChE inhibitor nematicides are often referred to as nematistats or nematostatics, due to their reversible biochemical effects (Haydock et al., 2013).

At the end of the 20th Century, aldicarb was one of the most widely used non-fumigant nematicides in the UK, making up nearly half of the market share (Minnis et al., 2004). However, by 2003, under EU legislation, aldicarb was no longer approved for use due to its high non-target toxicity. The acute median lethal dose (LD50) of aldicarb was found to be 0.65–1.0 mg kg^{-1} body weight for rats via oral administration (International programme on chemical safety, World Health Organization, Geneva, 1991). The organophosphate and carbamate nematicides are referred to as old-generation nematicides due to the majority of them being banned or withdrawn due to their high toxicity to non-target organisms, including humans (Oka, 2020a).

Oxamyl (Vydate; Corteva, developed by Du Pont) is still registered in many countries as a nematicide and insecticide, despite a relatively low LD_{50} (5.4 mg kg^{-1}) (Oka, 2020a).

1.4.3.2 Glutamate-gated chloride channel allosteric modulators

Abamectin and emamectin benzoate make up the glutamate-gated chloride channel (GluCl) allosteric modulators.

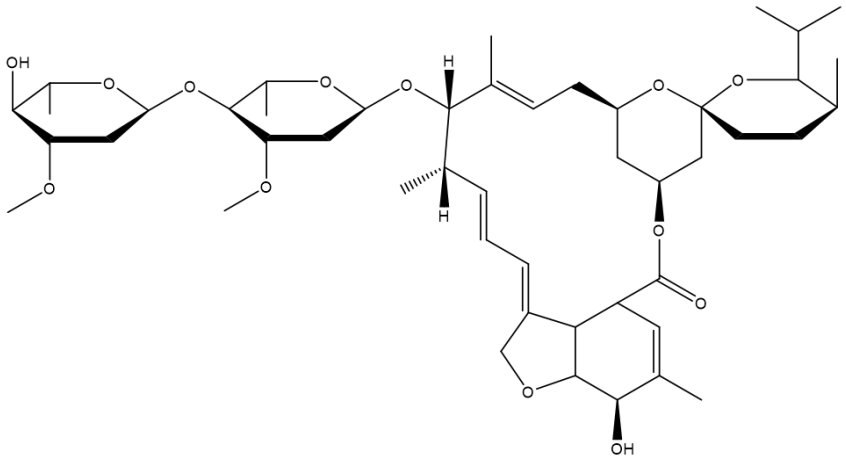

Figure 1.11 Chemical structure of abamectin. Abamectin is classified as a GluCl allosteric modulator, along with the 4'-deoxy-4'-methylamino derivative of abamectin, emamectin benzoate.

Abamectin is a mixture of avermectins B_{1a} and $B_{1b,}$ which are macrocyclic lactones synthesised by *Streptomyces avermitilis*, a gram-positive bacterium. Abamectin can be applied directly to the soil as a granular formulation or applied as a foliar spray (Qiao et al., 2012). Abamectin impacts glutamate-gated chloride channels that regulate motility and nerve signalling (Cully et al., 1994), resulting in rapid paralysis of nematodes without hypercontraction, which is reversible following short-exposure and irreversible following exposure exceeding 120 minutes (Fisher and Mrozik, 1992; Faske and Starr, 2006; Cabrera et al., 2013).

Initially, studies investigated the effect of applying abamectin directly to the soil in a liquid or granular formulation, allowing wide distribution of the active compound through the soil profile (Cabrera et al., 2013). However, it was found that the effects of abamectin were short-lived due to its binding to soil particles and insolubility in water (Faske and Starr, 2006; Cabrera et al., 2013). The ability of abamectin to bind tightly with soil particles, however, prevents its run off into rivers and lakes, reducing its bioavailability (Fisher and Mrozik, 1992). Abamectin is also degraded rapidly by sunlight in water, and in the soil is metabolised to less toxic metabolites by soil microorganisms (Fisher and Mrozik, 1992).

Abamectin has been developed as a seed treatment, marketed as 'Avicta' by Syngenta Crop Protection (Cao et al., 2015). Seed treatment is an attractive approach for nematode control, as it usually requires less application of chemicals to the field, limiting its action to a specific site and reducing its negative environmental impact (Cabrera et al., 2013). However, it has been shown that a large ratio of the abamectin dose remains on the seed coat and there is minimal uptake into the root system. Due to its insolubility and poor movement through soil, the liquid formulation of abamectin also shows poor uptake into the root system and provides a limited area of protection to crops (Cao et al., 2015).

A new method for abamectin application has been developed which has shown enhanced protection against root-knot nematodes. The method involves encapsulating abamectin into a *red clover necrotic mosaic virus* (RCNMV) -derived plant virus nanoparticle (PVN). RCNMV-derived PVN technology allows for controlled delivery of abamectin that results in improved soil mobility, an enlarged protection zone against root- knot nematodes and increased efficacy (Cao et al., 2015).

Abamectin provides a promising alternative to fumigant and non-fumigant nematicides that have a negative environmental impact and display high toxicity toward non-target organisms. Steps to improve its application so that it is able to have a greater effect on agriculturally important nematodes, such as RCNMV-derived PVN technology, will further increase its nematicidal efficacy and importance in nematode control strategies.

1.4.3.3 Mitochondrial complex II electron transport inhibitors. Succinate-coenzyme Q reductase

Fluopyram is a succinate dehydrogenase inhibitor (SDHI) fungicide of the pyridinyl-ethyl benzamide chemical group (Avenot and Michailides, 2010) (Figure 1.12). SDHI fungicides target the mitochondrial succinate dehydrogenase (SDH) complex in the electron transport chain, which is also referred to as mitochondrial complex II or succinate-ubiquinone oxidoreductase (SQR) (Avenot and Michailides, 2010). SDH couples the oxidation of succinate to fumerate with the reduction of quinone to quinol (Horsefield et al., 2006). Fluopyram binds at the ubiquinone binding site (Q-site). In *C. elegans*, fluopyram inhibits SDH with a potent IC_{50} of 1.8 nM (Burns et al., 2015).

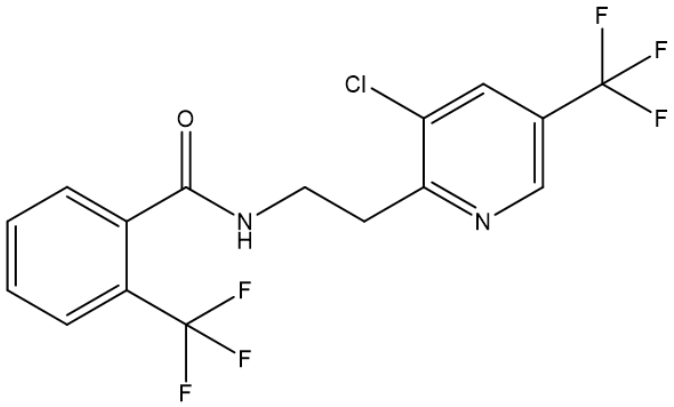

Figure 1.12 Chemical structure of fluopyram. Fluopyram (N-{2-[3-chloro-5-(trifluoromethyl)-2-pyridyl]ethyl}-a,a,a-trifluoro-o-toluami) is a fungicide and nematicide of the pyridinyl-ethyl benzamide chemical group.

In addition to its well-known fungicide properties, fluopyram is nematicidal (Faske and Hurd, 2015). For nematode control, fluopyram can be applied as a seed treatment (ILevo; Bayer CropScience, Inc.) (Beeman and Tylka, 2018) or as an in-furrow spray, applied at the time of planting (Storelli et al., 2020). It has shown efficacy against a number of plant parasitic nematodes including root-knot nematodes *Meloidogyne incognita* and *M. javanica* (Faske and Hurd, 2015; Oka and Saroya, 2019), soybean cyst nematode *Heterodera glycines* (Beeman and Tylka, 2018), sugar beet nematode *Ditylenchus dipsaci* (Storelli et al., 2020) and the reniform nematode *Rotylenchus reniformis* (Faske and Hurd, 2015).

To effectively supress nematode populations, fluopyram requires direct contact with the nematode, as the drug exhibits limited movement in the xylem (Faske and Hurd, 2015). Because of this, reduced efficacy has been reported in field use of fluopyram against reniform nematodes, due to the vertical distribution of reniform nematodes in the soil (Schumacher et al., 2020). Therefore, there is differential susceptibility of nematodes to in-furrow application of fluopyram depending on the root systems, as only nematodes in contact with fluopyram will be affected, resulting in a small effective zone (Faske and Hurd, 2015; Schumacher et al., 2020).

Given the potent effect of fluopyram on *C. elegans* SDH (Burns et al., 2015), it is unsurprising that fluopyram reduces numbers of both beneficial and plant parasitic nematodes in the field (Waldo et al., 2019). It also effects nematode feeding groups, reducing bacterivores, fungivores and omnivores, resulting in a less stable environment that reduces ecosystem service benefits (Waldo et al., 2019).

1.4.3.4 Lipid synthesis, growth regulation. Inhibitors of acetyl CoA carboxylase

Spirotetramat (Movento; Bayer CropScience) is a keto-enol insecticide with phloem and xylem motility (Nauen et al., 2008). Upon hydrolysis to spirotetramat-enol, it inhibits lipid biosynthesis by targeting acetyl-coA carboxylase (ACC) (Nauen et al., 2008; Smiley et al., 2011). As well as insecticide activity, it also displays nematicidal activity against cereal cyst nematode *Heterodera avenae* (Smiley et al., 2011), root knot nematode *M. incognita* (Leah E Vang et al., 2016) and soybean cyst nematode *H. glycines* (Leah E Vang et al., 2016).

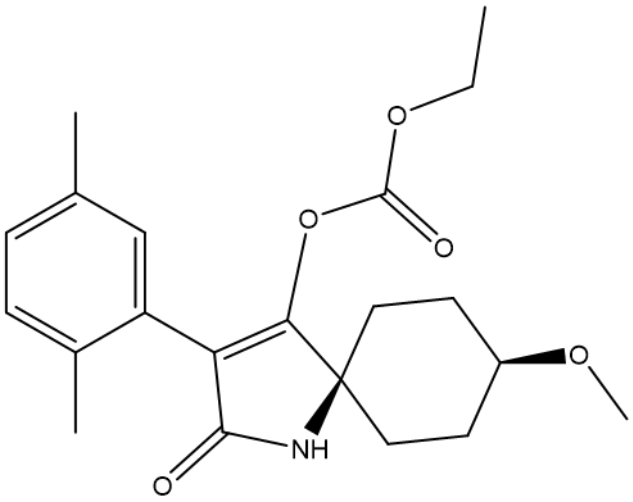

Figure 1.13 Chemical structure of spirotetramat. Spirotetramat (cis-3-(2,5-Xylyl)-4-(ethoxycarbonyloxy)-8-methoxy-1-azaspiro[4.5]dec-3-en-2-one) is an insecticide and nematicide of the keto-enol group.

Like in insects, spirotetramat targets ACC in nematodes (Gutbrod et al., 2020). ACC converts acetyl-coA to malonyl-coA, providing the substrate for fatty acid biosynthesis. Inhibition of ACC activity in *C. elegans* and *H. schachtii* therefore leads to a depletion of storage lipid and results in developmental arrest (Gutbrod et al., 2020). Developmental arrest of *M. incognita* and *H. glycines* juveniles has also been reported, however spirotetramat has no effect on hatching rates of either nematode or on *C. elegans* hatching (Vang et al., 2016).

1.4.3.5 Nematicides with unknown mode of actions, presumed to act at multiple sites

Nematicides with unknown modes of action that are presumed to act at multiple sites include the fumigant nematicides methyl bromide and 1,3-D (Haydock et al., 2013).

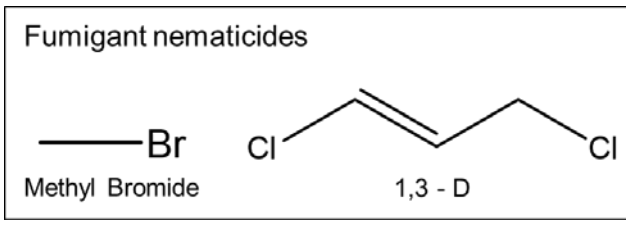

Figure 1.14 Chemical structures of fumigant nematicides. Structures of methyl brominde and 1,3-D (1,3-dichloropropene).

The fumigant nematicides methyl bromide and 1,3-D will be discussed below. Exposure to fumigant nematicides results in an initial hyperactivity in the nematode, which progresses to a decline in activity and paralysis. If exposure time is insufficient, removal of fumigant nematicides can see recovery (Wright, 1981). Furthermore, eggs of some nematode species, such as *Globodera* spp., are unaffected by concentrations which are lethal to juveniles. This could be due to the protective cyst that surrounds the unhatched eggs preventing uptake of the nematicide. Higher concentrations of the fumigant nematicide would therefore be required to have an effect at this stage and reduce nematode populations (Wright, 1981). In both circumstances, application of higher concentrations and over a longer time period presents drawbacks to fumigant nematicide use, due to the high toxicity and low selectivity associated with these nematicides (Haydock et al., 2013).

1.4.3.5.1 Methyl bromide

Methyl bromide is a volatile, short-chained halogenated hydrocarbon which is an odourless gas above 4°C. It is used as a pre-plant management practice, where it is applied into the soil in combination with chloropicrin (Ou, 1998; Zasada et al., 2010). Chloropicrin is combined to add an odour to the fumigant so that operators are able to detect the presence of the toxic chemical (Haydock et al., 2013) and to provide additional control over soil borne fungal pathogens (Ou, 1998).

However, methyl bromide depletes the ozone layer in the atmosphere (Ristaino and Thomas, 1996). It is now only applied when there are critical use exemptions, under the Montreal Protocol. This means that it can only be used when there are no feasible alternatives or where its use is crucial to avoid disruption to the market of high-value crops (Zasada et al., 2010).

1.4.3.5.2 1,3-dichloropropene

1,3-dichloropropene (1,3-D), manufactured by Dow AgroSciences as 'Telone II,' offers good PPN control (Zasada et al., 2010). 1,3-D is, however, under restricted use in many countries and is currently not approved for use in the EU due to its reported contribution to air pollution and human health problems. One potential solution to reduce 1,3-D volatilization, and hence its contribution to air pollution, is to accelerate its degradation in the soil. This can be achieved by the application of organic matter to alter the biological and chemical properties of the soil to improve nematicide degradation (Dungan et al., 2001). Application of 1,3-D in combination with non-fumigant, granular nematicides has shown some promise in controlling PCNs in an economically beneficial way (Minnis et al., 2004).

1.4.3.6 Nematicides with unknown modes of action

Along with fluopyram (section 1.4.3.3), fluazaindolizine and fluensulfone are described as the three main next-generation nematicides (Oka, 2020a). All three nematicides contain trifluoromethyl (-CF3) and so are often referred to as 3F or fluorinated nematicides (Desaeger and Watson, 2019). The modes of action of fluazaindolizine and fluensulfone are, however, unknown, leading to their IRAC classification of 'Group N-UN: Unknown.' Furfural, iprodione and tioxazafen join fluazaindolizine and fluensulfone in the unknown group. Tioxazafen, like the 3F nematicides, is also a relatively new nematicide and is due to be released as a seed treatment for soybean, cotton, and corn against several nematode species, however, very little information is available on its action (Oka, 2020a).

1.4.3.6.1 Fluazaindolizine

Fluazaindolizine (Salibro; Corteva Agriscience) is a sulfonamide nematicide from the imidazopyridine group (Lahm et al., 2017) (Figure 1.15). Adverse effects for 1-50ppm fluazaindolizine have been reported for the root-knot nematodes *M. incognita, M. hapla* and *M. javanica* (Thoden et al., 2019; Thoden and Wiles, 2019). Once the juveniles have been exposed to fluazaindolizine, they are unable to recover, even after rinsing in water (Thoden and Wiles, 2019). In fact, *M. incognita* juveniles that appeared motile at the end of the treatment period displayed impaired motility with time when incubated in water (Wram and Zasada, 2019). Treatment of tomatoes infected with *M. javanica* with fluazaindolizine displayed less root-galling, suggesting the in vitro effects reported may translate to a field setting (Desaeger and Watson, 2019).

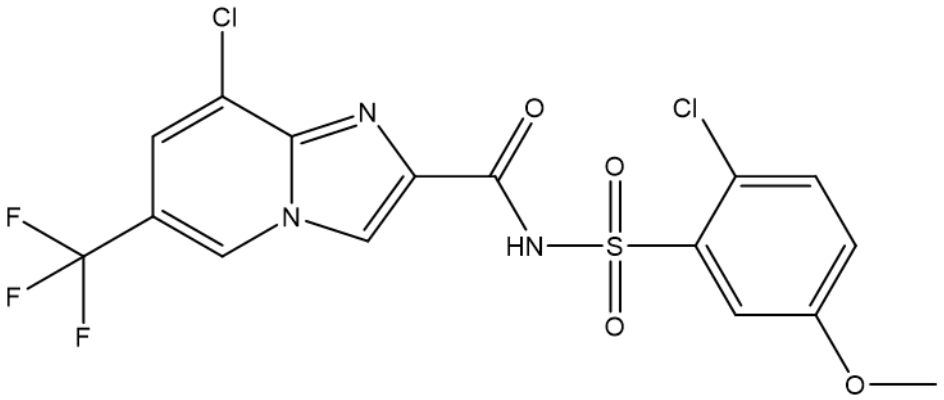

Figure 1.15 Chemical structure of fluazaindolizine. Fluazaindolizine (8-chloro-N-[(2-chloro-5-methoxyphenyl)sulfonyl]-6-(trifluoromethyl)imidazo [1,2-a]pyridine-2-carboxamide) is a novel nematicide of the imidazopyridine group.

The mode of action of fluazaindolizine is currently unknown, however, known target sites of nematicides including AChE, SDH and GluCl channels were not affected by application (Lahm et al., 2017). Importantly, it displays favourable mammalian and eco-toxicity profiles and has a suggested low impact on beneficial nematodes (Thoden and Wiles, 2019).

1.5 Fluensulfone

Fluensulfone (Nimitz; ADAMA) is a novel nematicide of the heterocyclic fluoroalkenyl sulfones group (Figure 1.16).

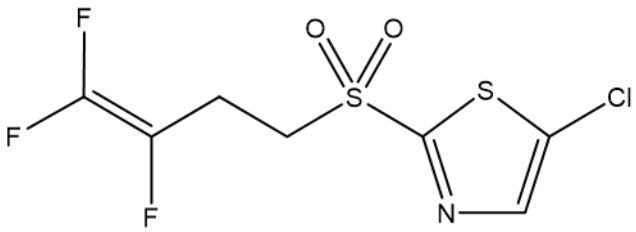

Figure 1.16 Chemical structure of fluensulfone. Fluensulfone (5-chloro-2-(3,4,4-trifluoro-but-3-ene-1-sulfonyl)- thiazole) is a novel nematicide of the heterocyclic fluoroalkenyl sulfones group.

Fluensulfone has a favourable toxicity profile when compared to the old-generation nematicides (Table 1.1).

Fluensulfone displays a selective toxicity within the nematode genera, able to significantly reduce damage caused by root-knot nematodes whilst maintaining non-target, free-living nematode population densities at control levels (Kawanobe et al., 2019). Free-living nematodes, bacterivores and omnivores in turf grass systems are also not negatively impacted by fluensulfone (Waldo et al., 2019). However, it displays some phytotoxicity to plants if applied after planting, resulting in the recommendation that it be used pre-planting (Giannakou and Panopoulou, 2019).

Active substance	**Chemical group**	**LD_{50} (acute oral male rats) mg kg^{-1}**
1,3-dichloropropene	Halogenated hydrocarbon	150
Methyl Bromide	Halogenated hydrocarbon	214
Abamectin	Avermectins	10
Aldicarb	Carbamate	0.93
Oxamyl	Carbamate	3.1
Cadusafos	Organophosphate	37
Fenamiphos	Organophosphate	6
Fluensulfone	**Fluoroalkenyl**	**500-1000**

Table 1.1 Acute oral toxicity (LD_{50}) of globally important nematicides in comparison to new nematicide fluensulfone. LD_{50} values (acute oral male rats) <50 mg kg^{-1}: high toxicity, 50-500 mg kg^{-1}: moderate toxicity, >500 mg kg^{-1}: low toxicity. Data summarised from (Haydock et al., 2013) and Joint FAO/WHO Meeting on Pesticide Residues (JMPR), Fluensulfone (265) Report 2013, 2014 & 2016.

1.5.1 Fluensulfone profile of effects on Plant Parasitic Nematodes

Fluensulfone exhibits nematostatic and nematicidal activity against a range of nematode species including root-knot nematodes *M. javanica* (Oka et al., 2009) and *M. incognita* (Oka et al., 2012), migratory nematodes, *Pratylenchus penetrans, P. thornei* and *Xiphinema index* (Oka, 2014), and the potato cyst nematode *Globodera pallida* (Norshie et al., 2016; Kearn et al., 2017). The irreversible paralysis that fluensulfone elicits is in contrast to the effects of the organophosphate and carbamate nematicides (section 1.4.3.1), which are reversed upon drug wash-out (Oka et al., 2009). Interestingly, as was described for fluazaindolizine, juveniles that are exposed to fluensulfone for a short period of time that do not show an immediate inhibition in motility become immotile after chemical wash out and incubation in water (Oka et al., 2009). This suggests that once the nematodes have been exposed to fluensulfone, they are unable to recover from the exposure and indicates that fluensulfone is eliciting a slow accumulating effect.

1.5.2 Field application

Fluensulfone is registered for use in several crops, including: tomato, cucumber, bell pepper, squash, potato, cabbage, broccoli, melon, lettuce, strawberry, and turf grass (Oka, 2020a). These crops are associated with a range of nematode species, including the root-knot and potato cyst nematodes. The half-life of fluensulfone in the soil is up to 24 days (Patrick M Norshie et al., 2017). Despite the short persistence of fluensulfone, the remaining concentrations could be sufficient to control PPNs, given that *M. hapla* juveniles are immobilized by exposure to 0.25 mg L^{-1} for 48 h in vitro (Oka, 2020b).

Fluensulfone soil treatments applied at planting reduce the infection of potato roots by *G. pallida* (Norshie et al., 2016). Application of fluensulfone in the field has also been shown to reduce *M. incognita* populations and subsequent root-galling in carrots, lima bean, cucumber, and tomato (Morris et al., 2015; Jones et al., 2017; Becker et al., 2019; Grabau et al., 2019). Additionally, when compared to fluopyram and fluzaindolizine, fluensulfone showed the most consistent nematode suppression for managing *M. javanica* in tomato production (Desaeger and Watson, 2019).

1.5.3 Fluensulfone mode of action studies

The molecular target of fluensulfone is currently unknown. However based on comparisons with aldicarb and ivermectin, it has a different mode of action to the AChE inhibitors and GluCl channel modulators (Kearn et al., 2014). Fluensulfone impacts *C. elegans* motility, development, egg-laying, hatching and pharyngeal pumping, summarised in Table 1.2 (Kearn et al., 2014). These effects are observed at much higher concentrations than those seen to inhibit activity of *Meloidogyne* spp. (Oka et al., 2009; Oka et al., 2012).

Interestingly, fluensulfone inhibits *C. elegans* pharyngeal pumping on food and 5-HT-induced pumping (Kearn et al., 2014). *C. elegans* exhibit high levels of pharyngeal pumping in the presence of food and can also be stimulated by 5-HT. This suggests that fluensulfone could be interfering with the serotonergic signalling pathway that regulates pharyngeal pumping in *C. elegans* (Kearn, 2015). Fluensulfone also interacts with serotonergic signalling to stimulate stylet thrusting and inhibits 5-HT induced stylet thrusting in potato cyst nematode *G. pallida* (Kearn et al., 2017). These effects, which were induced at concentrations ≥300µM, were blocked by the 5-HT receptor antagonist, methiothepin (Kearn, 2015), suggesting potential agonist activity at 5-HT receptors. However, these effects could also be as a result of stimulated 5-HT release at the synapse or prevention of 5-HT re-uptake.

Behaviour	Concentration	Effect
Reproduction[a]	1mM	Egg laying and egg hatching both reduced. Embryo viability also reduced.
Thrashing[b]	1mM	Inhibition of motility in liquid of L2/3. Near-maximal inhibition of thrashing after 1 hour.
Body bends[c]	500µM	Reduced rate of body bends off food. Increases number of body bends on food.
Pharyngeal pumping[d]	100µM	No effect on food. Inhibits off food.
	500µM	Inhibits pumping on and off food.
	1mM	Abolishes pumping on and off food. Inhibits 5-HT-induced pumping
Food-leaving[e]	500µM	Increases food-leaving

Table 1.2 A summary of the effects of fluensulfone on model organism, *C. elegans.* Data summarised from (Kearn et al., 2014). [a]Reproduction was measured by allowing gravid *C. elegans* worms to lay eggs on NGM plates seeded with OP50 in the presence of vehicle control or 1mM fluensulfone. [b]*C. elegans* exhibit a stereotypical flexing movement around the midpoint of its body when in liquid. Stage-synchronised worms were placed in BSA-supplemented M9 buffer with fluensulfone and the number of thrashes performed in 30 s was scored by visual observation. [c]Movement of worms on and off food was scored by counting the number of body bends in 30 s. [d]Pharyngeal pumping was scored by visual observation of the contraction-relaxation cycle of the terminal bulb of the pharynx in the freely moving worm. [e]Food-leaving was measured on OP50 seeded plates, prepared with vehicle or fluensulfone. A food leaving event was defined as an incident in which the whole body of the worm completely left the bacterial lawn. Wild-type *C. elegans* typically dwell on high quality food sources and exhibit a low frequency of food-leaving.

1.5.4 Metabolic impairment underlies the novel nematicidal action of fluensulfone

Exposure to fluensulfone results in a progressive, concentration-dependent decrease in motility of *G. pallida* juveniles. At concentrations ≥30µM, paralysis was associated with the internal structures of the juveniles appearing granular. This granular appearance is taken to arise through tissue cell death (Kearn et al., 2017). The slow progressive paralysis in *G. pallida* is comparable to the accumulating effect that fluensulfone has on *M. javanica* juveniles (Oka et al., 2009). Furthermore, removal of juveniles from fluensulfone is not sufficient for them to recover from the insult (Oka et al., 2009). To determine whether paralysis was accompanied with metabolic impairment and subsequent mortality, histological staining was used to determine metabolic activity (Kearn et al., 2017).

1.5.4.1 Assessing metabolic activity with histological staining

MTT (3-(4,5-dimethylthiazol-2-yl)-2,5-diphenyl tetrazolium bromide) is a tetrazolium salt that can be used in a tetrazolium-based dye reduction colorimetric assay to evaluate cell viability (Mosmann, 1983). MTT undergoes a reduction reaction in metabolically active cells that results in a colour change from yellow to dark purple (Figure 1.17).

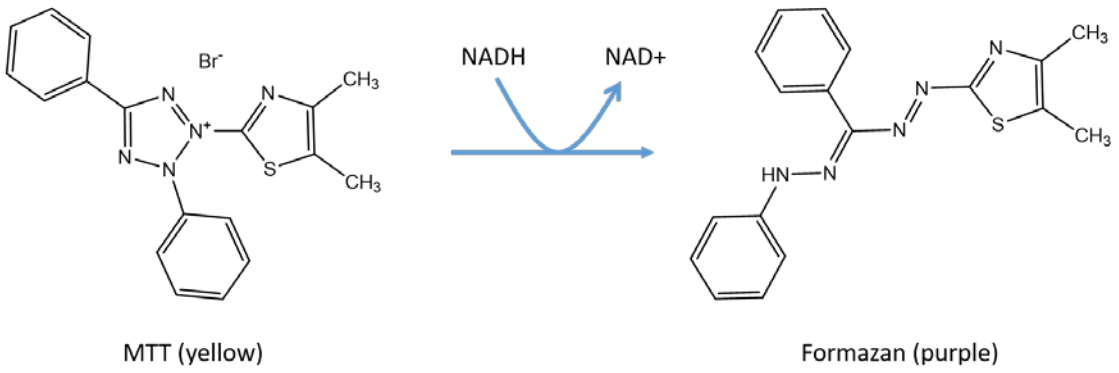

Figure 1.17 MTT reduction reaction to MTT formazan. MTT undergoes a reduction reaction to MTT formazan, which precipitates as a dark purple stain. In the reaction above, the reducing agent is NADH, however, MTT can be reduced by other reducing agents, such as NADPH.

The assay can also be used to assess the viability of *C. elegans* following drug treatment (James and Davey, 2007) and was used to assess metabolic activity and mortality in *G. pallida* (Kearn et al., 2017).

In untreated *G. pallida* juveniles, staining was visible in the head region in nearly 100% of the worms tested. Fluensulfone treatment resulted in a reduction in staining, suggesting metabolic impairment. Longer exposure to fluensulfone resulted in a progressive decrease in the percentage of worms stained which indicated loss of metabolism and death (Kearn et al., 2017). Furthermore, there was an interesting re-distribution of staining described, in which the predominant anterior staining was lost and a shift to predominant posterior staining prior to a complete loss of staining, suggesting that fluensulfone alters *G. pallida* metabolism prior to its nematicidal effects (Kearn et al., 2017).

Additionally, *M. javanica* juveniles pre-treated with fluopyram were less sensitive to fluensulfone than untreated active juveniles (Oka, 2020b). This could suggest that the fluensulfone target is related to that of fluopyram, which is a succinate dehydrogenase inhibitor (SDHI) (Section 1.4.3.3). The mechanism of this interaction is not clear, however the author suggests that at low concentrations, fluopyram may compete with fluensulfone by binding to common or related target sites (Oka, 2020b). As SDH is a critical component of the TCA cycle and the electron transport chain, it could mean that fluensulfone is targeting one of these critical pathways to induce metabolic impairment.

1.5.5 Impaired lipid utilization following fluensulfone treatment

Nile Red (9-diethylamino-5H-benzo[a]phenoxazine-5-one) is a dye that can be used as a stain for detection of intracellular lipid droplets by fluorescence microscopy (Greenspan et al., 1985). Nile red staining was used to determine the lipid content of *G. pallida* juveniles following fluensulfone exposure. Fluensulfone treated juveniles showed increased fluorescence relative to controls. This was taken to indicate an enhanced lipid content that in this case results from reduced lipid consumption relative to the control (Kearn et al., 2017). This suggests that fluensulfone treatment alters lipid metabolism and prevents the nematode from accessing its lipid stores. This could be via interference with β-oxidation of fatty acids or impairment of lipolysis, both preventing the use of stored lipids for energy metabolism. A summary of the effects of fluensulfone on the PCN *G. pallida* are tabulated below.

Behaviour	Concentration	Effect
Stylet thrusting	500µM	Induces stylet thrusting
	1mM	Induces stylet thrusting. Inhibits 5-HT-, tryptamine- and fluoxetine-induced thrusting
Coiling	500µM	Elicits protracted coiling
Motility	1-10µM	50% immobility after 10 days exposure
	30µM	100% immobility after 7 days exposure
	200-500µM	100% immobility after 3 days exposure
Morphology	1-10µM	No granular appearance
	30µM	Granular appearance and death after 14 days exposure
	500µM	Granular appearance and death after 7 days exposure
MTT staining	1-10µM	15-50% staining after 14 days exposure
	30µM	Loss of staining after 10 days exposure
	200-500µM	Loss of staining after 3 days exposure
Lipid consumption (Nile Red staining)	10µM	Reduced lipid consumption

Table 1.3 A summary of the effects of fluensulfone on PPN, *G. pallida*. Data summarised from (Kearn et al., 2017).

1.5.5.1 Investigating lipids in nematodes

Traditionally, lipid deposits are labelled with fluorescent dyes that accumulate in hydrophobic environments (Witting and Schmitt-Kopplin, 2016).

Nile red preferentially interacts with extremely hydrophobic environments, i.e. neutral lipid droplets, when examined at wavelengths ≤570nm. When examined at fluorescence emission wavelengths >590nm, Nile red can interact and shift fluoresce in the presence of phospholipids, cholesterol, cholesterol esters and triglycerides, (P Greenspan et al., 1985).

BODIPY, 4,4-difluoro-1,3,5,7,8-pentamethyl-4-bora-3a,4a-diaza-s-indacene, is also a fluorescent stain. BODIPY-stained fluorescent signals have been described to correspond to lipid droplets (Guo et al., 2008). Both Nile red and BODIPY stains have been used as vital dyes to assess lipids in live *C. elegans.* This can be achieved by mixing the *C. elegans* food source, *E. coli,* with Nile red and BODIPY-labelled fatty acids and subsequently measuring fluorescence (K et al., 2003; Mak et al., 2006).

Insufficient permeabilization of the nematode cuticle can prevent staining. Fixation methods are frequently employed prior to staining, however, excessive permeabilization and/or poor tissue fixation can lead to the animal breaking apart (Barros et al., 2012). Fixation and staining of nematodes is prone to error, resulting in variability and poor reproducibility (Barros et al., 2012; Escorcia et al., 2018). This can be due to fixation methods altering the morphology of lipid deposits. Furthermore, fats readily dissolve in alcohol, which is used during the dehydration and staining steps, contributing to the extensive variability and low resolution that is observed via this approach (Barros et al., 2012). Staining techniques are therefore preferentially utilized for comparisons between conditions when the differences in fat stores are likely to be substantial (Barros et al., 2012).

1.5.5.1.1 CARS microscopy

Coherent anti-Stokes Raman scattering (CARS) microscopy enables imaging of dye free, live samples. Lipids consist of fatty acid side chains, which are rich in CH_2 groups. Lipids can be selectively imaged using the characteristic vibration that corresponds to the large number of these methylene groups. For *C. elegans,* it has been shown that the peak in a CARS spectrum corresponding to the vibrational frequency of neutral lipids in the C-H stretching region is at $\sim$2850cm^{-1}, validating CARS as an approach for detection of lipid in nematodes (Smus et al., 2017).

CARS is based on the principle that a pump beam at frequency ω_p and a Stokes beam at frequency ω_s interact with a sample via a wave-mixing process. When $\omega_p - \omega_s$ is equal to the frequency of a Raman active molecular vibration, there is activation of the resonant oscillators driven by the excitation fields, generating a strong anti-Stokes signal ($\omega_{as} = 2\ \omega_p - \omega_s$) (Evans and Xie, 2008). $\omega_p - \omega_s$ can be tuned to a particular vibrational frequency to enhance this anti-Stokes signal. For lipids, CARS images are taken at the CH_2 symmetrical stretching vibration at 2845 cm^{-1} (Evans and Xie, 2008). It has good sensitivity towards lipids due to the abundance of C-H bonds in a lipid molecule (Cheng and Xie, 2004).

CARS microscopy has been used to quantitatively assess the impact of genetic variations in metabolic pathways on lipid storage in *C. elegans* (Hellerer et al., 2007). Furthermore, CARS microscopy can be coupled with fingerprint confocal Raman analysis to analyse the level of unsaturation of fatty acids in lipids in wild-type and mutant *C. elegans,* providing information on the dynamic interactions between lipid storage, peroxidation and desaturation in a single, living *C. elegans* (Le et al., 2010).

The capability of CARS microscopy for quantitative analysis of lipid storage in *C. elegans* has been compared with dye-labelled imaging and biochemical quantification of extracted triglyceride. This identified Nile red and BODIPY staining did not correlate well to biochemically measured lipid stores. A significant confound was the presence of auto-fluorescent organelles in the gut that were associated with the lysosome (Yen et al., 2010). These structures, which altered the levels and distribution of dye labelling, are modulated by the physiological state of the organism and as an example, readily increase upon oxidative stress (Teuscher and Ewald, 2018).

1.6 Metabolic pathways in nematodes

The evidence in section 1.5 highlights that fluensulfone induces a slowly accumulating insult that is irreversible, leading to death. It is suggested that this is as a result of a progressive metabolic impairment, with preliminary evidence that altered lipid utilization may underpin its effects. The focus of this current investigation is therefore to better understand the nature of the metabolic impairment and the effect of fluensulfone on PPN lipids.

Most nematodes are able to generate energy in the form of ATP by oxidising substrates via reactions of the TCA cycle and the electron transport chain (Behm, 2002). In this section, an overview of energy utilization, generation and storage in nematodes will be provided. The glyoxylate shunt, a shortcut of the TCA cycle, which is utilized when nutrient intake is limited, will be discussed.

1.6.1 Energy storage in nematodes

Lipids are an essential fuel reserve for nematodes, with high levels of lipid stores found in aerobic nematodes, particularly in non-feeding juvenile stages and eggs (Behm, 2002). This is exemplified by neutral lipids constituting approximately 70% of total lipid content in non-feeding *G. pallida* juveniles (Holz et al., 1997). Non-feeding *G. pallida* juveniles rely on the mobilisation of lipid stores until they have located and established a feeding site. Furthermore, cyst nematode males do not feed and so rely solely on the utilisation of stored lipids. This is reflected by upregulation of lipid mobilisation genes in adult males of *G. pallida* (Cotton et al., 2014).

Glycogen, which is synthesised from glucose 1-phosphate, is the most common carbohydrate reserve. Glycogen is catabolised to generate glucose-6-phosphate by glycogen phosphorylase. Carbohydrate can also be stored as the disaccharide, trehalose (Behm, 2002). In section 1.3.2.1, the role of trehalose as an anhydrous buffer surrounding the unhatched juvenile is discussed. Trehalose is readily hydrolysed to glucose by trehalase and evidence that trehalose levels decrease after rehydration suggest that it may be used as an energy source during rehydration (Behm, 1997; Grewal et al., 2006).

1.6.2 Intermediary metabolism

Intermediary metabolism includes the pathways of metabolism that are involved with the utilization, generation and storage of metabolic energy (Behm, 2002). These pathways of intermediary metabolism are highly conserved in eukaryotes and generate ATP from lipid, carbohydrates and proteins. *C. elegans* possess orthologues for most enzymes and proteins that are essential for intermediary metabolism that are present in other organisms (Holt and Riddle, 2003).

1.6.2.1 Carbohydrate metabolism

Glycolysis generates pyruvate from glucose or glucose-6- phosphate and provides the major source of ATP in nematodes undergoing anaerobic metabolism (Behm, 2002). Pyruvate is converted to acetyl-CoA, which enters the tricarboxylic acid (TCA) cycle. Many nematodes, including egg and larval stages, utilize the TCA cycle and electron transport chain to generate energy (Behm, 2002).

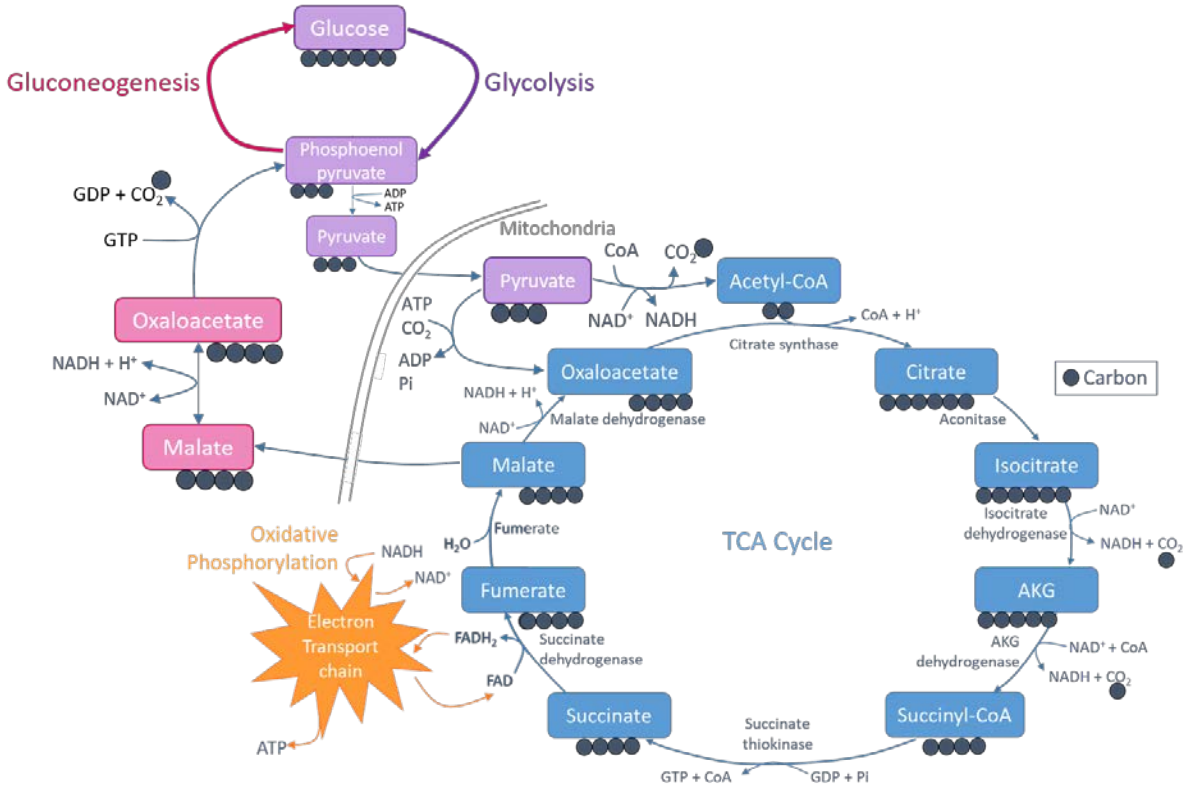

Figure 1.18 Metabolic pathways for the utilization of carbohydrates. Pyruvate is generated from glucose during glycolysis (purple). Acetyl-CoA is liberated from pyruvate in the mitochondria and enters the TCA cycle (blue). The TCA cycle generates electron donors, NADH, $FADH_2$ and succinate, which are utilized by the electron transport chain (orange) to produce ATP. Glucose is generated during gluconeogenesis (pink).

The TCA cycle is the common pathway for oxidation of substrates in many organisms, involving a series of oxidation reactions to generate NADH, $FADH_2$ and CO_2. NADH, $FADH_2$ and succinate are electron donors that can be utilised in oxidative phosphorylation, resulting in the transfer of electrons out of the mitochondrial matrix to generate a proton gradient, which allows the flow of protons back into the mitochondrial matrix, through ATP synthase, to generate ATP (Berg et al., 2002). These pathways have been demonstrated to be active in free-living and plant- parasitic nematode species, identified by the presence of key enzymes (Behm, 2002).

In *G. pallida,* the relative levels of carbohydrate metabolism increase across developmental transitions from the unhatched juvenile, described as being dormant, to the emerged juvenile, which is in a metabolically active state (Cotton et al., 2014). Other changes identified during this transition include upregulation of genes involved in lipid metabolism and proteolysis.

1.6.2.2 Lipid metabolism

In aerobic conditions, acetyl-CoA is derived from β-oxidation of fatty acids, allowing ATP and energy generation from lipid stores. Fatty acids must first be liberated from triglycerides, which are stored in lipid storage organelles called lipid droplets (Olzmann and Carvalho, 2019). During starvation, mobilization of fatty acids from lipid droplets is induced (Zhang et al., 2010). Fatty acids are broken down with the sequential removal of two-carbon units from the acyl chain (Eaton, 2002). This yields molecules of acetyl-CoA which can enter the TCA cycle (Berg et al., 2002).

β-oxidation can be mitochondrial or peroxisomal, where multiple pathways with common substrates are used (Figure 1.19). Enzymes encoded by the *C. elegans* genome have been identified that act in both of these pathways (Mak et al., 2006). Acyl CoA dehydrogenase, a key enzyme in mitochondrial β-oxidation, is encoded by the most abundant transcript in the expressed sequence tag (EST) dataset of the non-feeding juvenile (Jones et al., 2009). This highlights the importance of lipid catabolism during the non-feeding stage of the plant parasitic nematode's life cycle.

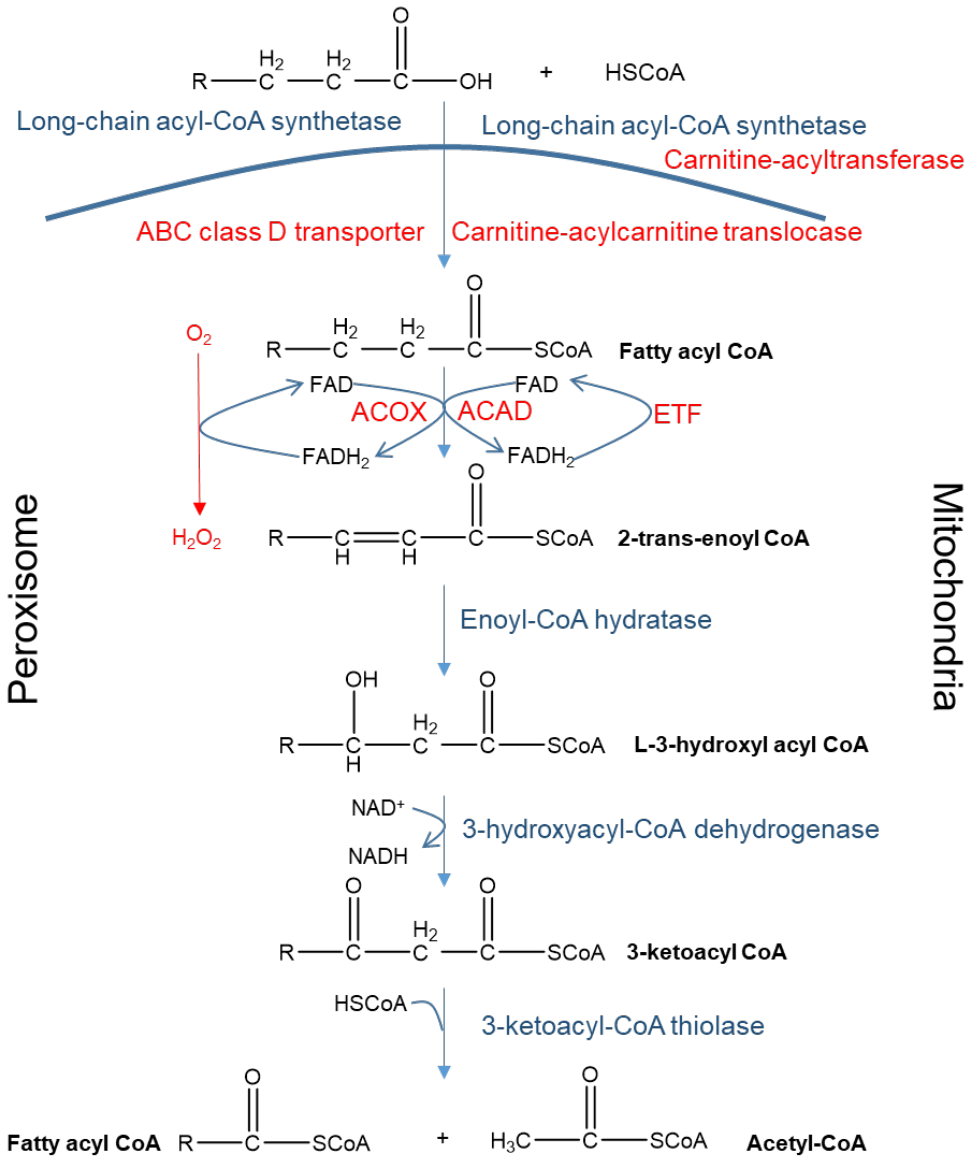

Figure 1.19 Peroxisomal and mitochondrial β-oxidation. Fatty acids are actively transported across both peroxisomal and mitochondrial membranes. Fatty acids are broken down to yield acetyl-CoA. Differences in fatty acid import and catabolic breakdown are indicated in red, with reactions specific to the peroxisome on the left-hand side and mitochondria on the right-hand side. Note that conversion of fatty acyl CoA to 2-treans-enoyl CoA is regulated by ACOX (acyl-CoA oxidase) in peroxisomes and ACAD (acyl-CoA dehydrogenase) and ETF (electron transfer flavoprotein) in mitochondria.

1.6.2.3 The glyoxylate shunt

In addition to the TCA cycle, liberation of acetyl-CoA from the breakdown of fatty acids can flux via the glyoxylate shunt. The glyoxylate shunt operates in bacteria, fungi, some protists, plants and nematodes (Kondrashov et al., 2006). The glyoxylate shunt permits synthesis of succinate and malate from acetyl-CoA and isocitrate, regulated by the enzymes isocitrate lyase (ICL) and malate synthase (MS). Malate is oxidised to oxaloacetate, which is converted to glucose- 6-phosphate via the process of gluconeogenesis. This allows two decarboxylation steps of the TCA cycle to be bypassed, resulting in net synthesis of carbohydrates from acetyl-CoA (Behm, 2002). Mammals were thought to be unable to utilize the glyoxylate shunt, however, it has been shown that the glyoxylate shunt can be activated in mammalian tissue by adrenaline, allowing the mobilization of carbohydrates and lipids (Morgunov et al., 2005).

Reproductive stage *C. elegans* feed on bacteria, which provides a source of lipids, proteins and sugars for energy metabolism via glycolysis and the TCA cycle. Dauer larvae of *C. elegans,* however, are non-feeding and must find an alternative pathway for energy generation. This is achieved via β-oxidation of lipid reserves and the glyoxylate shunt (Erkut et al., 2016).

It has been shown that the gene encoding glyoxylate enzymes is upregulated in *C. elegans* dauer larvae and *daf-2* adults (McElwee et al., 2006). *Daf-2* mutants display dauer-like behaviour, including termination of feeding and adoption of a dauer-like posture (Gems et al., 1998). In *C. elegans,* the two enzymes required for glyoxylate shunt activity, ICL and MS, are encoded by a single gene and expressed as a single bifunctional polypeptide (ICL-1) (Liu et al., 1997). There is evidence that these enzymes were acquired into the *C. elegans* lineage following horizontal gene transfer from bacteria (Kondrashov et al., 2006).

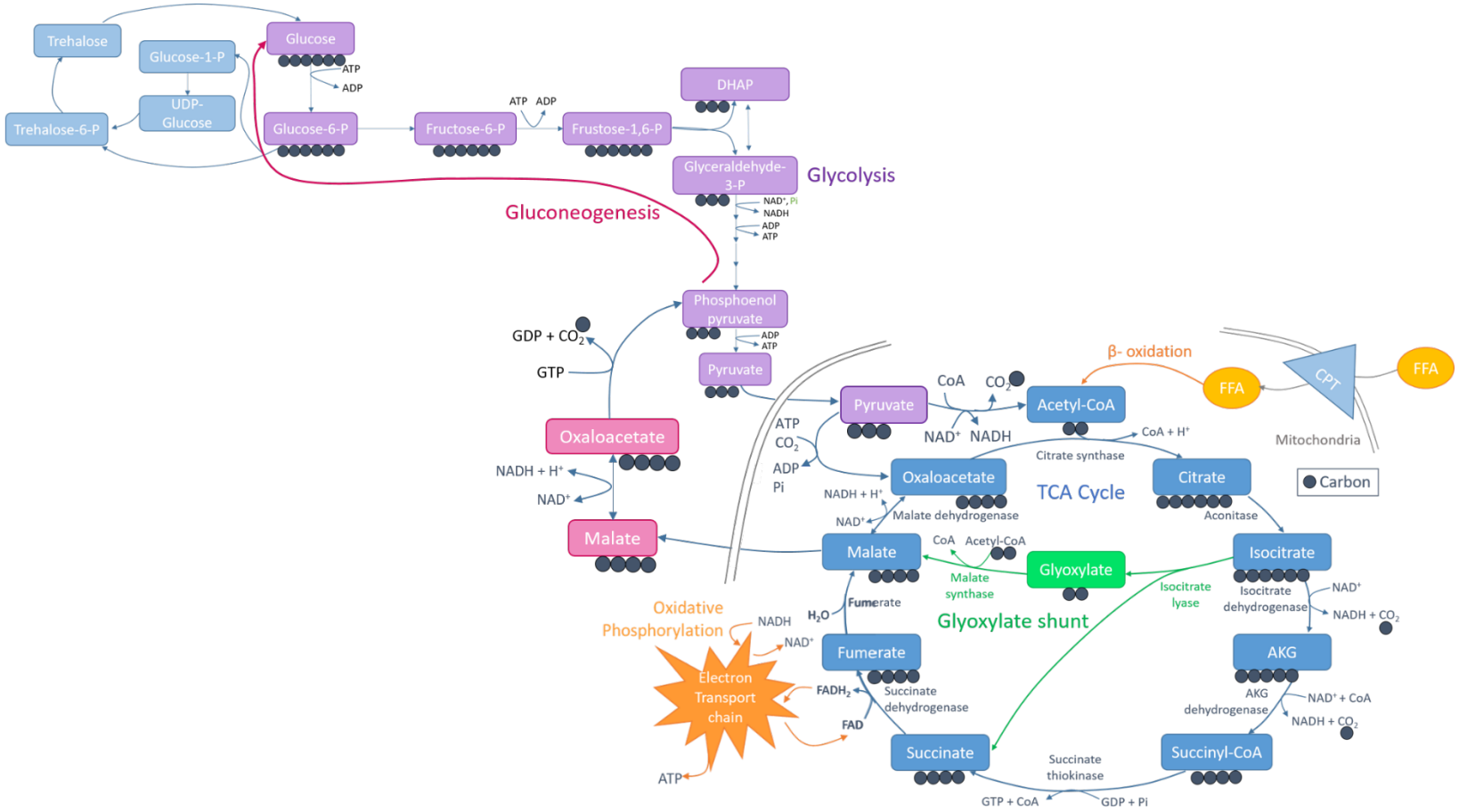

Figure 1.20 Overview of metabolic pathways, including the glyoxylate shunt. The glyoxylate shunt (green) bypasses decarboxylation steps of the TCA cycle (blue). Acetyl-CoA, generated from β-oxidation of fatty acids can flux via the glyoxylate shunt to generate carbohydrate via gluconeogenesis (purple).

A *C. elegans* strain with a deletion mutation in *icl-1* and a *daf-2* background (*daf- 2;icl-1* strain) was used to investigate the role of the glyoxylate shunt in dauer larvae (Erkut et al., 2016). Without a functional glyoxylate shunt, worms were unable to utilize fatty acids for gluconeogenesis and trehalose biosynthesis. It was previously shown by the same authors that trehalose accumulation was essential for desiccation tolerance in *C. elegans* (Erkut et al., 2011) (Chapter 1.3.2.1). Supporting the role of the glyoxylate shunt in trehalose biosynthesis and thus desiccation tolerance, in order to survive desiccation, worms required a functional glyoxylate shunt. While preparing for desiccation, *C. elegans* can change their metabolism to shift towards creating carbohydrates rather than releasing energy. This involves utilising the glyoxylate shunt to produce carbohydrates from lipid or acetic acid, without the need for glucose uptake. This dependence on the glyoxylate shunt for trehalose accumulation and desiccation tolerance was also observed in *Saccharomyces cerevisiae* cells (Erkut et al., 2016), showing that the role of the glyoxylate shunt in regulating metabolism and transition to a gluconeogenic state in response to environmental stress is conserved in different organisms.

In *C. elegans,* its major role is to prepare for desiccation, providing a pathway to directly link lipid utilization with carbohydrate synthesis, specifically trehalose. Transcripts encoding glyoxylate shunt enzymes have been identified in non-feeding larval stages of the root-knot nematode, *M. incognita* (Mccarter et al., 2003). Glyoxylate shunt activity is thought to regulate metabolism during non-feeding larval stages, demonstrated in the upregulation of *ICL* during non-feeding stages of *M. incognita* (Lourenço-Tessutti et al., 2015). It could therefore be speculated that glyoxylate shunt activity is important prior to, during and immediately after hatching, whilst the nematode is not feeding, as a mechanism to tolerate stress. Knock-down of *ICL* gene expression was shown to reduce *M. incognita* reproduction (Lourenço-Tessutti et al., 2015), suggesting that targeting the glyoxylate shunt in PPNs could be a potential route to controlling PPN populations.

1.7 Targeting metabolic pathways as a route to nematicidal activity

Targeting key metabolic activities that are specialized to PPNs may be a potential route to achieving selective toxicity, with reduced side-effects against non-target, free-living nematodes. Currently available nematicides, fluopyram and spirotetramat, which target the mitochondrial electron transport chain and lipid synthesis, respectively (Chapter 1.4.3.3 and 1.4.3.4), demonstrate the effectiveness of targeting metabolic pathways as a route to nematicidal activity. However, both targets are conserved in the free-living nematode, *C. elegans*¸ and so whilst they display nematicidal efficacy against PPNs (Smiley et al., 2011; Faske and Hurd, 2015; Leah E. Vang et al., 2016; Beeman and Tylka, 2018; Oka and Saroya, 2019), they also negatively impact non-target nematodes (Burns et al., 2015; Waldo et al., 2019; Gutbrod et al., 2020).

1.7.1 Metabolic potential

Metabolic potential is a critical factor that determines a pathogen's development and pathogenicity (Taylor et al., 2013; Tyagi et al., 2015). Identifying differences in the metabolic potential of parasitic and non-parasitic nematodes provides an opportunity to identify targets for anthelminthic and nematicide development (Tyagi et al., 2015). For example, many parasitic nematodes spend part of their life cycle outside of the host and require expanded biochemical functions to meet the metabolic requirements of diverse developmental stages (Tyagi et al., 2015). In a study focusing on compact reaction cascades, termed metabolic modules, they provide detail on the metabolic potential of parasitic and non-parasitic nematodes to identify specific modular differences that could be exploited as drug targets (Tyagi et al., 2015). They also examined module structures to determine variation in enzyme usage between plants (*A. thaliana, S. tuberosum* and *S. lycopersicum*) and PPNs (*M. incognita, M. hapla* and *B. xylophilus*). This identified mutually exclusive use of enzymes by all PPN-host pairs in the module for β-oxidation, suggesting broadly conserved differences in this pathway between PPNs and plants (Tyagi et al., 2015). Specifically, differences were identified in the last two reactions in module M00087 (β-oxidation), where different orthologue groups, termed KOs, were used for completion of the reactions in plants vs PPNs. Different KOs are likely to be mapped to genes that are not orthologues to each other, presenting an opportunity for selective targeting (Tyagi et al., 2015).

Comparative metabolomics as described above can be combined with the identification of chokepoint enzymes, which are enzymes catalysing a reaction that produces or consumes a unique compound (Taylor et al., 2013), identifying potential targets for drug discovery. Targeting metabolic chokepoints results in lethality due to a lack of alternative pathways and the essentiality of the reaction within the metabolic network (Palumbo et al., 2007; Taylor et al., 2013). Identifying metabolic chokepoints from KEGG REACTION, which is a database of enzymatic reactions that appear in the Kyoto Encyclopedia of Genes and Genomes (KEGG) metabolic pathway maps, and linking these to targets in the KEGG Drug database and DrugBank enabled the identification of potential drugs that bind to chokepoints in nematode metabolic pathways (Taylor et al., 2013). This identified perhexiline, which is an approved small molecule drug that is used in the treatment of angina (Ashrafian et al., 2007) and inhibits carnitine palmitoyltransferase (CPT) (Kennedy et al., 1996), as a promising compound that targets chokepoint enzyme CPT in *C. elegans* and parasitic nematodes *H. contortus* and *O. lienalis* (Taylor et al., 2013). This exemplifies how investigating metabolic pathways in nematodes can lead to the identification of novel anthelmintic/nematicide targets. Furthering this analysis to identify specialised targets in PPNs that are distinct from their host and non-target nematodes would potentially enable the identification of novel compounds that offer selective toxicity.

1.8 Project aims

The overarching aim of this project is to more precisely elucidate the mode of action of the novel nematicide, fluensulfone. This will involve analysis of the effects of fluensulfone on the plant parasitic nematode, *Globodera pallida,* at two key life cycle stages; hatching and the infective juvenile stage.

Aim 1: To provide a detailed profile of the effects of fluensulfone on PPN intermediary metabolism by comparing the actions of fluensulfone with that of known metabolic inhibitors in a range of viability assays.

Aim 2: To detail the nematicidal action of fluensulfone through an investigation of its effects on lipid content and tissue integrity.

Aim 3: To use imaging, including CARS, to investigate the effects of fluensulfone on lipid metabolism.

Aim 4: To refine a model for the mode of action of fluensulfone.

Chapter 2 Methods and Materials

2.1 *Globodera pallida* maintenance and hatching assays

2.1.1 *Globodera pallida* culture

Globodera pallida were cultured on potato plants (*Solanum tuberosum* "Desiree") as described (Urwin et al., 2002). All cysts were kindly provided by Leeds University and were stored at 8˚C in sealed Eppendorf tubes until use.

2.1.2 Generation of potato root diffusate

Potato root diffusate (PRD) was generated by soaking cut roots of three-week old potato plants (*Solanum tuberosum* "Desiree") in water at a concentration of 80g of roots per litre of water. Roots were soaked for 24 hours at 4˚C in darkness. PRD was collected by straining out the roots and filter- sterilised through a 0.45µm syringe filter (Bell et al., 2019). PRD was kept at 8˚C until use and each batch was used within 3 months. All PRD was obtained from Leeds University.

2.1.3 *Globodera pallida* cyst hatching assays

Prior to the start of cyst hatching assays, dry *G. pallida* cysts were soaked in tap water for 24 hours. Individual cysts were transferred to wells of a 24-well plate, with one cyst per well (Figure 2.1A). PRD solution was one part PRD to three parts tap water. Wells contained PRD solution or active ingredient (a.i.) made up in PRD solution. Nematicides were dissolved in 100% vehicle and added to PRD solution to give a final vehicle concentration that was the same across all treatment wells. The vehicle used and final concentration of vehicle in solution is indicated. A vehicle control was performed for each experiment.

Juvenile emergence was scored by counting the number of free-living juveniles in each well at the indicated intervals. The hatching solutions were replaced after each of the indicated time points.

In experiments in which recovery from a.i. treatment was measured, cysts were washed with tap water at the indicated time point (up to 32 days) and transferred to another 24-well plate that contained fresh PRD solution to ensure a continual hatching trigger. Juvenile emergence was counted as before, with hatching solutions replaced after each count. After the final time point, the cysts were transferred to dd.H_2O and cracked open with a blade and tweezers. The number of unhatched eggs, empty egg cases and juveniles that had not emerged were scored per cyst and the final cumulative hatching represented as:

(Number of emerged juveniles/ (Total number of emerged juveniles + unhatched eggs + non-emerged juveniles within cyst)) x 100

Data are plotted as cumulative percentage juvenile emergence per cyst over time.

2.1.4 Isolated egg preparation

Isolated eggs were generated as previously described (Gaihre et al., 2019). Briefly, dry *G. pallida* cysts were soaked in tap water for 24 hours before being broken open to release eggs. Cyst casings were discarded and the remaining cyst contents were passed through a 50µm mesh sieve. The sieve was washed gently with water and eggs passed through onto an underlying 25µm mesh. Contaminating juveniles passed through the 25µm mesh into a collecting dish and were discarded. Eggs collected on the 25µm sieve were washed off with water into a clean collecting dish. If a large number of juveniles remained in the egg inoculum, the contents of the 25µm sieve were passed back through the sieves and re-collected. This re-washing was performed up to five times. The isolated egg preparation was then quantified as number of eggs per ml and the volume was adjusted to give approximately 1000 eggs/ml.

2.1.5 *Globodera pallida* egg hatching assay

Egg based hatching assays were conducted in 24-well culture plates using translucent inserts as described previously (Gaihre et al., 2019) (Figure 2.1B). The inserts are the same as those used in tissue culture studies and are made from translucent polystyrene materials (Corning Limited) with dimensions of 7mm diameter, 18mm height and 9mm depth. Originally, these inserts had 0.4µm collagen-treated polytetrafluoroethylene (PTFE) membrane. The membrane was removed and replaced with a 25µm pore size nylon mesh (Normesh Limited) which was glued with superglue.

400µl of egg inoculum (~400 eggs) was transferred to each insert. Inserts were transferred to 24-well assay plates, which contained 500µl of solution. Solutions are as described for cyst hatching assays. Juvenile emergence was counted by transferring the inserts to fresh plates with new solutions and counting the number of juveniles that remained in the wells.

Where recovery is reported, the egg inserts were washed with tap water at the indicated time point (up to 32 days) and transferred to another 24-well plate that contained PRD solution only. Juvenile emergence was counted as before, with inserts transferred to fresh hatching solutions at each time point and cumulative hatch over time recorded. To calculate juvenile emergence as a percentage, juvenile emergence was represented as:

(Number of emerged juveniles/ Number of unhatched eggs on insert at beginning of experiment (400)) x 100

Data are plotted as cumulative percentage juvenile emergence per well over time.

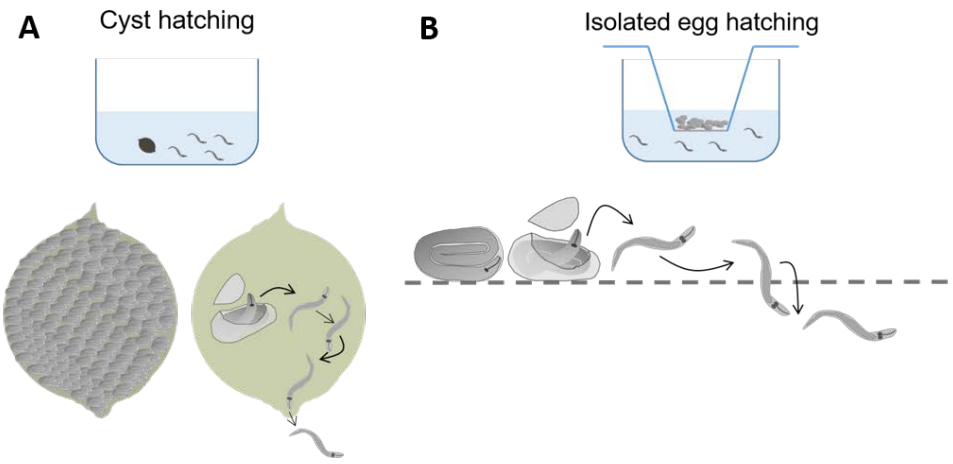

Figure 2.1 Hatching assays. A cartoon to show the experimental set-up of cyst hatching assays (A) and isolated egg hatching assays (B). Both assays are carried out in 24-well plates with 500µl of solution. Where possible, cyst hatching assays and isolated egg hatching assays were performed in parallel.

2.1.6 *In ovo* motility assays with fluensulfone treated *Globodera pallida* cysts

The motility of juveniles that emerged from cysts during the recovery period were assessed to observe the effect of *in ovo* fluensulfone exposure. Scoring of motility was performed for each well at each time point during the recovery period when juvenile emergence was counted. Individual juveniles were observed for 10-second intervals, with each juvenile that hatched during the recovery period being assessed for motility. Motility was assessed by scoring each juvenile as motile, coiled or rod-shaped (Figure 2.2). Juveniles were scored as coiled if their head or tail consistently touched another part of the body during the 10-second observation period. Juveniles were scored as rod-shaped if they appeared straight and did not move during the 10-second observation period. Juveniles that did not remain coiled throughout the observation period and were freely moving were scored as motile.

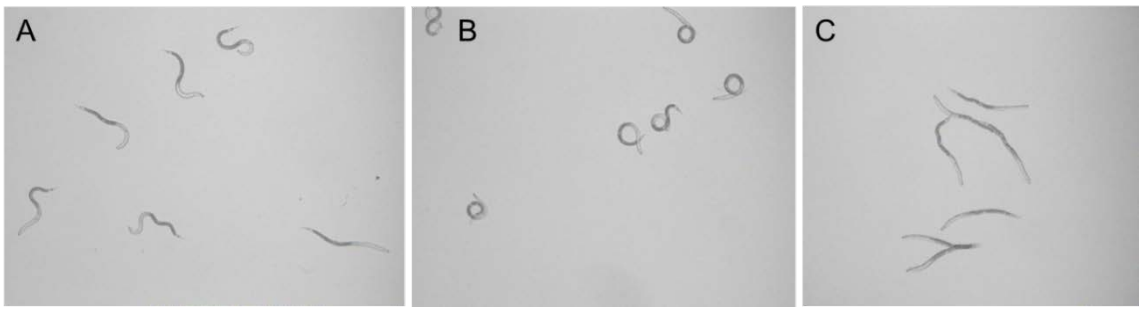

Figure 2.2 Representative images of *G. pallida* juveniles. Juveniles were scored as motile, coiled or rod-shaped. Representative motile juveniles are displayed in panel A, coiled in panel B and rod-shaped in panel C. Juveniles were only scored as coiled or rod-shaped if they remained in the posture for the duration of the 10-second observation period.

2.1.6.1 Assessment of Continuous Movement for Motility Assays

A 10-second observation period was used to assess motility after careful consideration of the time individual control juveniles were moving in a 60-second period. Freshly hatched juveniles were observed continuously during a 60-second period and the time spent moving/ immotile recorded. During analysis, no juvenile was stopped for longer than 1.56 seconds (Figure 2.3).

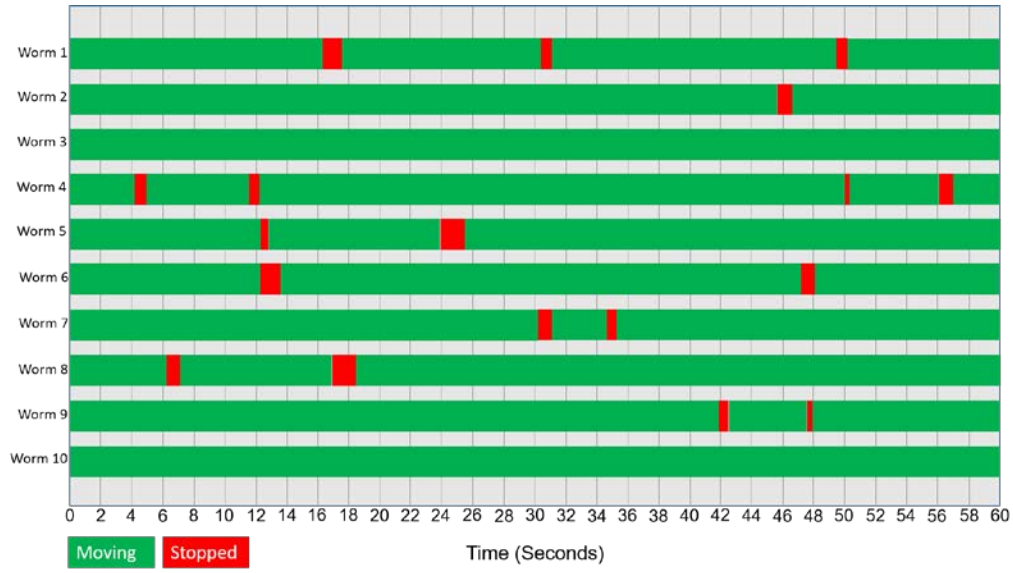

Figure 2.3 Continuous movement of control *G. pallida* juveniles. Freshly hatched juveniles were recorded as being motile (green) or immotile (red) for a 60-second period. Individual measurements are displayed across the 60 second period.

2.1.7 Granulation unhatched egg

At the end of hatching assays when cysts were cracked open, cysts that had been exposed to relatively high concentrations of fluensulfone (>50µM) contained 'granular' eggs. Thus, an assay designed to quantify this phenomenon was developed to assess the effect of prolonged exposure of *G. pallida* cysts to fluensulfone on the integrity of unhatched juveniles. Dry *G. pallida* cysts were soaked in dd.H_2O for 24 hours prior to the start of the assay. Individual cysts were transferred to wells of a 24-well plate containing dd.H_2O, vehicle control or the indicated concentration of nematicide. Nematicide solutions were made up as described for the hatching assays, but with dd.H_2O in place of PRD solution, thus, the granulation that is observed is on quiescent eggs which have not been activated by root diffusate. Cysts were exposed to treatment conditions for up to 28 days. At the time points indicated (1, 2, 3, 7, 10, 14, 21 and 28 days) individual cysts were removed from treatment solutions, washed with dd.H_2O and transferred to a clean well of a 24-well plate containing dd.H_2O only. Cysts were cracked open with a blade and tweezers and their contents dislodged. The number of unhatched eggs and 'granular' unhatched eggs were then scored. Unhatched eggs were considered 'granular' when the enclosed juvenile could not be distinguished, appeared dark and had a loss of internal structures. At each time point, the proportion of granular unhatched eggs was represented as:

(Number of granular unhatched eggs/ (number of granular unhatched eggs + unhatched eggs)) x 100

Data are plotted as the percentage of unhatched eggs that appear granular per cyst over time.

2.2 *Globodera pallida* juvenile assays

2.2.1 *Globodera pallida* hatching for juvenile assays

To induce J2 hatching, cysts were placed in a solution of 1 part PRD to 3 parts dd.H_2O at ~20 °C in the dark (Feist et al., 2020). J2s were age synchronised so that they were collected every 24 hours for use in each experiment.

2.2.2 Motility assays

Newly emerged J2s were washed three times in double distilled H_2O and then treated with vehicle control or drug at the indicated concentration. J2s were incubated in treatment solutions at 20°C for up to 14 days. At the indicated time points, ~10 J2s were removed from treatment solution, rinsed and transferred to a single well in a 24-well plate. This was repeated so there were six wells of ~10 J2s per treatment group at each time point. J2s were scored as immotile if they failed to move during the 10-second observation period. The percentage motility per well was then calculated. Following motility scoring, the same population of J2s were stained with MTT to assess metabolic activity. The number of independent repeats performed is indicated for each experiment.

2.2.3 MTT staining

MTT (2-(4,5-dimethyl-2-thiazolyl)-3,5-diphenyl-2H-tetrazolium bromide) undergoes an NADH/NADPH reduction reaction to produce MTT formazan, which precipitates as a dark purple insoluble product in metabolically active cells and organisms. MTT solution (5mg/ml) was made fresh in M9 buffer (In 1L distilled water: KH_2PO_4, 3g; Na_2HPO_4, 6g; NaCl, 5g; 1 M $MgSO_4$, 1ml). J2s that had been scored for motility as described above were transferred to a single well in a 24-well plate containing MTT and incubated at 20°C for 24-h in the dark. After 24-h in the MTT solution, each well was observed and J2s were scored for the presence, absence and relative distribution of staining. The percentage of stained J2s per well was then calculated and the location of predominant staining. J2s that had been exposed to control treatment and remained motile displayed predominant staining in their anterior end.

2.2.4 Exposure of juveniles to treatment conditions prior to CARS imaging

Newly emerged J2s were washed three times and then incubated for up to 14 days in tubes containing vehicle control, 30µM fluensulfone or 50µM perhexiline made up in M9 solution.

2.2.5 Preparing juveniles for CARS imaging

J2s were removed from treatment solutions and washed three times in M9. J2s were re-suspended in M9 solution to give a concentration of ~5 J2s/µl. A small drop of 2% agar was pipetted onto a clean glass slide and incubated at 37°C for ≥1-h. Parafilm was then cut with scissors to form a border around the agar pad and to create a spacer between the glass slide and the cover slip, avoiding damage to the J2s. 10µl of *G. pallida* suspension was then transferred to the agar pad and gently spread across the area. A glass cover slip was then placed over the sample and sealed.

2.2.6 CARS imaging

Live *G. pallida* were imaged with coherent anti-Stokes Raman scattering (CARS). Scan Image 5.1 (Vidrio Technologies), an open source software, was used for acquiring images with a home-built laser scanning microscope.

For CARS imaging the fundamental of a fibre laser (1031 nm, 2 picosecond, 80 MHz, Emerald Engine, APE) was used as a Stokes beam, and the output of an optical parametric oscillator (OPO) (APE, Levante Emerald, 650–950 nm) which was synchronously pumped by the second harmonic (516 nm) of the fibre laser, was used as a pump beam. The multimodal platform is unique in that it utilises 2 ps pulses. Non-linear interactions increase with shorter pulse widths; however, with CARS since vibrational line-widths are of the order of 10 cm^{-1}, therefore, 2 ps pulse-widths are near ideal for CARS in ensuring efficient excitation and reduction of non-resonant background. The two beams were made collinear and then coupled through a galvanometric scanner to an inverted microscope (Nikon Ti-U) configured for epi-detection. Their temporal overlap was controlled with a delay line. For imaging lipids in the *G. pallida*, the C–H stretching mode at 2845 cm^{-1} was targeted, and for this reason the OPO was tuned to 797.2 nm.

A long pass dichroic beam splitter with cut-off at 775 nm with a 643±20 nm band pass filter was used to separate the laser excitation and collect the anti-Stokes signal from the epi-collected emission. A further long pass dichroic beam splitter with cut-off at 442 nm (Semrock Di02-R442) and 594 nm (Semrock Di02-R594) was used in the collection path with short focal length lenses on the respective detectors.

Each sample was imaged using a 20x/0.5 NA air objective, with 3 x optical zoom using galvanometric scanning. The total incident power on the sample was approximately 70 mW.

2.2.7 CARS image analysis

ImageJ was used to analyse all images. Images shown are representative of >10 J2s per treatment group. In *G. pallida,* CARS signal for storage lipids is predominant in the posterior (Smus et al., 2017) and so analysis was made on images taken of the posterior region. Threshold limits were applied to each image to remove background signal. Binary images were created to enable the selection of signal above threshold, which related to lipid area. Using the binary images, a region of interest (ROI) was created and saved for each image. ROI were applied to the original CARS images to measure mean grey values and total area occupied by lipid stores in the tail; this signal relates to merged signal and does not reflect 3 dimensional area. Integrated density (IntDensity) was calculated for each image as area occupied by lipid multiplied by the mean grey value from the ROI.

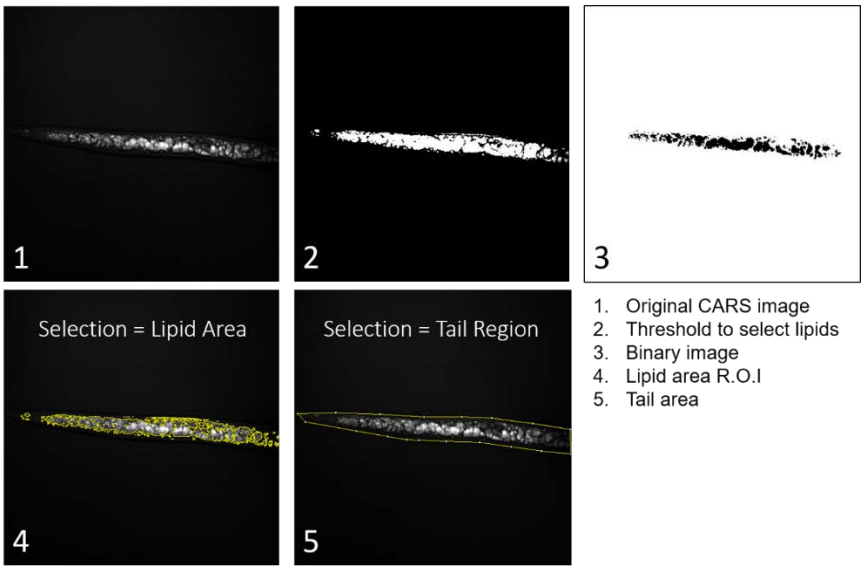

Figure 2.4 CARS image analysis. Steps in image analysis following CARS spectroscopy. CARS signal tuned to neutral lipid allows visualization of lipids (1). A threshold is then set to select lipids (2) and a binary image created (3). This allows the selection to be saved, which can then be applied to the original CARS image to measure intensity of signal and area occupied by lipid (4). This results in the calculation of IntDensity, which is reflective of both the intensity of the signal and the area that corresponds to signal. IntDensity is divided by the area of the tail region that has been imaged for normalization (5).

Light microscopy was used to define the tail boundary and used to determine the tail area imaged for each sample. Tail area was not significantly different between treatment groups (Figure 2.5). IntDensity was divided by the tail area in each image. Data are presented as ±S.E.M IntDensity/Area of tail and is normalised to the mean IntDensity/Area of tail from control day 0 samples.

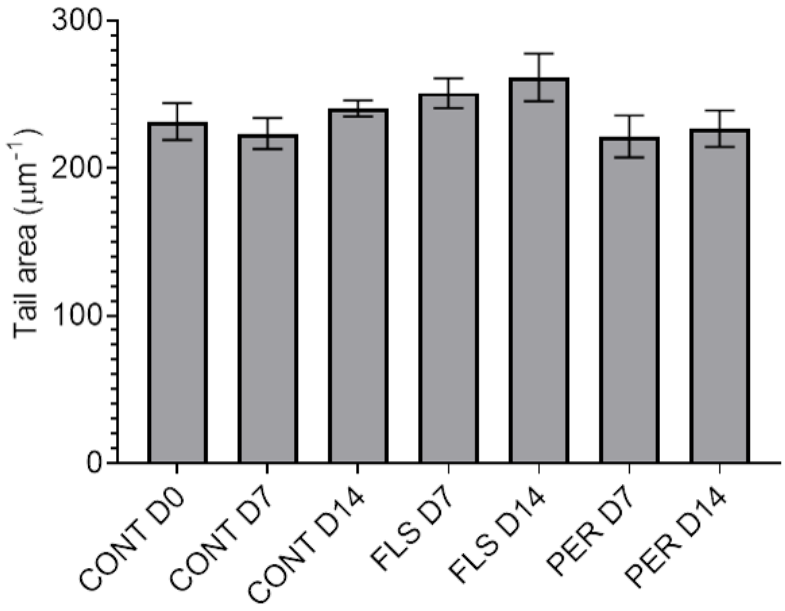

Figure 2.5 Area of tail imaged in CARS analysis. There were no significant differences between the tail area for representative control (CONT), 30µM fluensulfone (FLS) and 50µM perhexiline (PER) treated J2s at day 0 (D0), day 7 post-hatch (D7) or day 14 post-hatch (D14). Data plotted is Tail area, as determined by drawing around the tail boundary on ImageJ and using the measure function to measure area (μm^{-1}), ± S.E.M.

2.3 Biochemical analysis

2.3.1 *Globodera pallida* preparation for biochemical analysis

Glass hatching wells were set up with approximately 50 cysts per well and 1.5ml of PRD solution. Juveniles that hatched within the same 24 hours were collected and transferred to clean eppendorfs. If multiple samples were collected, samples were pooled and subsamples taken to perform a nematode count. For each treatment group, population numbers were carefully matched to ensure accurate comparisons.

Worms were pelleted using a table-top centrifuge, spun at 1000 x g for 3 minutes at room temperature. Supernatant was removed and wash repeated 3 times.

Nematode pellets were re-suspended in 500µl of treatment solution and stored at room temperature. At set time points, ~100 worms from each treatment group were removed for motility and MTT staining analysis, as described above. The remaining worms were pelleted and supernatant removed. A wash was performed three times to remove any treatment solution before worms were pelleted and then frozen at -80˚C until lipidomic analysis could be performed.

2.3.2 Lipid extraction

Juvenile pellets were formed as described above. Juvenile pellets were transferred to polystyrene sonication tubes and kept on ice. Sonication tubes provide more efficient energy transfer during sonication. A FisherBrand Q700 sonicator, with CL-334 converter and cup horn accessory, was used to homogenize the samples. This was equilibrated to 4°C and set up with the parameters 50 amplitude, 6 minute process time, 10 seconds on, 30 seconds off. Following sonication, total tube contents were transferred from the sonication tube into a clean glass tube. Sonication tube was rinsed with 1000µl methanol (100%) and added to glass tube.

To each tube, 2000µl chloroform (100%) and a further 1000µl methanol was added and vortexed. 800µl Saline solution (0.9% sodium chloride made in dd.H_2O) was added and vortexed to a single phase. Samples were titrated with methanol if single phase did not form. 1000µl chloroform and 1000µl dd.H_2O were added and vortexed. Tubes were sealed and incubated at -20°C overnight.

Using a Pasteur pipette, the bottom lipid layer was transferred into a clean Eppendorf and the sample was dried under nitrogen flow at 37°C or by spinning at 30°C under vacuum.

Samples were stored at -20°C if not analysed immediately.

2.3.3 Thin Layer Chromatography

2.3.3.1 TLC tank saturation

The required solvents (depending on lipid separation) were mixed immediately prior to performing Thin Layer Chromatography (TLC). To saturate the tank, the tank was lined with filter paper and tanks filled with solvent to ~1cm. Tanks were left to saturate whilst the samples were spotted on to the plate.

2.3.3.2 Spotting samples

The origin line was drawn 2cm from the bottom of the plate in pencil. Samples that were prepared as described above (section 2.3.2) were re-suspended in 10µl 100% methanol. A fine glass capillary tube with a diameter of 0.58mm was used to draw up sample and spot onto TLC plate (aluminium backed, Plain Silica gel60). Samples were spotted at least 1-1.5cm apart. Plates were left to dry in fume hood whilst tank was saturating.

2.3.3.3 Separation of neutral lipids with single phase system

A single phase solvent system was used to separate neutral lipids. The solvents used were hexane: diethyl ether: acetic acid at 75 mL: 25 mL: 2 mL (vol/vol/vol) ratio. The tank was saturated as described above. The plate was developed to the top of the plate and then removed and dried in the fume hood.

2.3.3.4 Separation of polar and non-polar lipids using two phase system

The first solvent system used was chloroform: methanol: H_2O at 32.5 mL: 12.5 mL: 2 mL (vol/vol/vol) ratio. The tank was saturated as described above. Plates were developed up to 15cm on the plate. The plate was removed from the tank and left to dry in the fume hood. The first solvent system and filter paper were disposed of and the tank was saturated with the second solvent system of hexane: diethyl ether at 4 mL: 1mL (vol/vol) ratio. The plate was developed in the second solvent system to the top of the plate. The plate was then dried in the fume hood.

2.3.3.5 Visualisation of TLC bands

10% phosphomolybdic acid was made up in 10mL immediately prior to staining. An airbrush was used to spray the plate evenly with phosphomolybdic acid. The plate was dried in 100°C drying oven for 10 minutes. Plates were scanned and imaged to enable quantification of bands.

2.3.3.6 TLC image analysis

ImageJ was used to analyse TLC plates. The area and greyscale profile of the lipid band was determined for each standard and compared to each lipid species detected in samples to give an estimate of lipid quantity. This was achieved by thresholding the image to identify the standard bands from the background. Using the wand feature, each band was selected and the area and mean gray values measured.

2.3.4 Mass spectrometry

2.3.4.1 Lipidomics standards

Lipid extraction was performed as described in section 2.3.2. For samples prepared for mass spectrometry, standards were added to the glass tube that the sample was transferred to prior to lipid extraction. The standards and concentrations used for lipidomic analysis are listed below.

Standard	Concentration (µMol/vial)
Triglyceride (TAG 16:0/16:0/16:0)	10
Dimyristoyl Phosphatidylethanolamine (PE)	4
Dimyristoyl Phosphatidylcholine (PC 14:0/14:0)	10
Lyso-phosphatidylcholine (LPC 17:0)	1
Dimyristoyl Phosphatidylglycerol (PG)	2
Dimyristoyl Phosphatidylserine (PS)	2
Dimyristoyl Phosphatidic acid (PA)	1
Cardiolipin	0.1
Sphingomyelin (SM 6:0)	1
Ceramide (14:0 CER)	1

Table 2.1 Standards used for lipidomic analysis. Standards were dissolved in DCM and total volume was made up to 100ml.

2.3.4.2 Mass spectrometer

Dried samples were dissolved in methanol: butanol: H_2O: 25% NH_4OH (6:2:1.6:0.4 vol/vol/vol/vol) and infused directly into a triple quadruple mass spectrometer with an electrospray interface (XEVO TQD triple quad from Waters, UK) and delivered by direct infusion at 8 µl/min. The mass spectra were acquired in both positive (ES+) and negative (ES-) ionization modes with an m/z range of 2–3000. Specific precursor scans were performed by collision induced dissociation (CID) by tandem MS/MS (ESI-MS/MS) to produce diagnostic fragment ions. Fragment of mass to charge ratio (m/z) +184 was used to identify sphingomyelin, phosphatidylcholine and Lyso-phosphatidylcholine species. Triglyceride species were identified from the full positive scans.

2.3.4.3 Extracting and analysing mass spectrometry data

The data was extracted from MS spectra after smoothing and baseline subtraction using Masslynx software (Version 4). This was subsequently exported into an Excel spreadsheet and analysed using an in-house Excel macro analyser.

2.4 Statistical analysis

Data are shown as ± S.E.M, unless otherwise stated. The statistical test employed, along with the number of cysts/worms and number of repeats for each experiment, is indicated in the figure legends. It is indicated where data has been pooled from multiple experiments. One-way ANOVA's and two-way ANOVA's were used where appropriate and were followed by Tukey post-hoc tests, with significance level set at $P<0.05$. Statistical analysis performed was carried out using GraphPad Prism software.

2.5 Materials

Chemicals and drugs were largely obtained from Merck at Sigma Aldrich.
Lipid standards were obtained from Avanti Polar Lipids.

Fluensulfone was provided by ADAMA Agricultural Solutions Ltd. Fluensulfone is shown in units of micromolar (µM), where 1 µM is equivalent to 0.29 ppm or 0.29mg l^{-1}.

Chapter 3 The Distinct Profiles of the Inhibitory Effects of Fluensulfone, Abamectin, Aldicarb and Fluopyram on *Globodera pallida* hatching

3.1 Introduction

Previous investigations into the mechanism of action of fluensulfone have focused on the way in which fluensulfone inhibits the free-living J2 stage. At concentrations in the micro molar range, fluensulfone causes a progressive impairment of *G. pallida* juveniles. This is observed as impaired motility, reduced metabolic activity and coincident reduction in the use of stored lipids that act as a primary source of energy for the J2 stage (Kearn et al., 2017). In the context of field exposure, other key parasitic life stages would be susceptible, including unhatched eggs encased in cysts, and nematodes in planta.

In this chapter, I investigated the effects of fluensulfone on *G. pallida* hatching and compared this activity to three important classes of nematicides with defined modes of action that are utilized for PPN management (Cabrera et al., 2013; Faske and Hurd, 2015).

3.1.1 Comparisons with nematicides with target-defined modes of action

It has previously been shown that fluensulfone has a distinct mode of action when compared to anticholinesterases and macrocyclic lactones (Kearn et al., 2014). This was evidenced using the free-living model nematode *Caenorhabditis elegans,* where acute and chronic exposure to fluensulfone exhibited distinct effects to the nematicide aldicarb and anthelminthic ivermectin (Kearn et al., 2014). Additionally, aldicarb and ivermectin resistant mutants were shown to be susceptible to fluensulfone treatment, reinforcing a distinct target for fluensulfone relative to the known targets underlying these other chemicals anthelminthic effects (Kearn et al., 2014) (See Chapter 1.5.3). In this chapter I used potato root exudate-induced hatching of *G. pallida* to probe for efficacy of fluensulfone. In parallel, I considered the effects of aldicarb, abamectin, and novel nematicide, fluopyram.

3.1.1.1 Abamectin

Abamectin belongs to the macrocyclic lactone class of compounds that act by impacting glutamate-gated chloride channels that regulate motility and nerve signalling (Cully et al., 1994), although other routes to nematicidal activity have been identified at the level of the mitochondria (Liu et al., 2016). The evidence for this activity is discussed in Chapter 1.4.3.2.

Abamectin has been shown to inhibit hatching of the root-knot nematode, *Meloidogyne incognita,* in addition to causing reduced motility and high mortality of *M. incognita* juveniles, suggesting it is effective across multiple life cycle stages (De Almeida et al., 2017). *Globodera pallida* hatching is also inhibited by abamectin, with a 50% reduction in hatching when using concentrations of ≥9µg/mL for 24 hours. This same reduction in hatching can be achieved with lower concentrations when longer exposure times are used (Sasanelli et al., 2020). This investigation was extended to glasshouse experiments, where it was confirmed that application of aqueous abamectin solution to the soil was able to reduce hatching, observed as a lower number of eggs and J2 per cyst in comparison to the control (Sasanelli et al., 2020).

3.1.1.2 Aldicarb

Aldicarb is a carbamate nematicide that has been shown to impair motility of PPNs in the soil (Opperman and Chang, 1991). This is achieved by inhibiting acetylcholinesterase, preventing hydrolysis of acetylcholine at the neuromuscular synapse and thus resulting in paralysis (Opperman and Chang, 1991). This is discussed in Chapter 1.4.3.1. These paralysing effects on PPN juveniles are, however, reversible (Haydock et al., 2013).

Effects of aldicarb on hatching of PPNs has also been investigated, including effects on potato cyst nematodes, *Globodera rostochiensis* and *G. pallida.* Laboratory bioassays showed that concentrations of aldicarb above 1ppm inhibited potato root diffusate (PRD) -induced *G. rostochiensis* hatch, however, when cysts were transferred to aldicarb-free PRD soltution, hatching was restored (Osborne, 1973). This translates to the effect of aldicarb in the field when used at recommended field rates, where it has been shown to inhibit the early hatch (2-4 weeks post planting) of *G. pallida* when assessed on commercial potato fields in Shropshire, UK (Deliopoulos et al., 2010). This was in contrast to an effect on late hatching (6-8 weeks post planting), where hatching was unaffected (Deliopoulos et al., 2010). This could be due to the short persistence of aldicarb in the soil (Deliopoulos et al., 2007), with hatch of cyst nematodes extending over a prolonged period of time that outstretches the persistence of this class of nematicides (Giannakou et al., 2005).

Hatching of sugar-beet cyst nematodes, *Heterodera schachtii,* is also supressed following aldicarb treatment (Hough and Thomason, 1975; Steele and Hodges, 1975; Steele, 1977) and is also reversible upon removal of chemical treatment (Steele, 1977). In addition to cyst nematodes, egg hatch of root-knot nematodes *Meloidogyne. exigua* and *M. javanica,* is inhibited by aldicarb treatment, (Hough and Thomason, 1975; Huang et al., 1983), although reversibility of this effect was not described.

3.1.1.3 Fluopyram

Fluopyram is a succinate dehydrogenase inhibitor, discussed in Chapter 1.4.3.3. There has been limited investigation of the effects of fluopyram on hatching, with most investigations focusing on its effects on the infective juvenile stage (Faske and Hurd, 2015; Oka and Saroya, 2019). Like abamectin, fluopyram has also been developed as a seed-treatment, marketed as 'ILeVO' (Bayer CropScience, Inc.). The effects of fluopyram seed treatment on *H. glycines* hatching and motility have been investigated and showed that ILeVO significantly reduced *H. glycines* hatching (Beeman and Tylka, 2018). Examining the effects of fluopyram on other species of PPNs will extend understanding of its effects at this life cycle stage. The detailed investigation of fluopyram on *G. pallida* hatching presented in this chapter, including the assessment of recovery from hatching inhibition, is therefore important in understanding the full potential of fluopyram as a nematicide, in addition to providing an important comparison to fluensulfone.

3.1.2 Chapter aims

In this chapter, I aimed to investigate the effect of all three nematicides described above on hatching of *G. pallida* and compare their profile of effects to fluensulfone. This includes a detailed description on the effect of treatment on PRD-induced hatching, recovery from treatment, *in ovo* effect on juvenile motility and a morphological description of unhatched eggs from treated cysts.

3.2 Results

3.2.1 Fluensulfone inhibits *Globodera pallida* hatching

It has previously been shown that fluensulfone has acute effects on *G. pallida* biology, including reduced motility, stylet activity and metabolism (Kearn et al., 2017). Here, I have investigated the time- and concentration- dependent effects of fluensulfone on *G. pallida* hatching and compared these effects to other important classes of nematicide.

All concentrations of fluensulfone tested inhibited hatching from *G. pallida* cysts (Figure 3.1A), with 1, 5, 50 and 500µM fluensulfone inhibiting hatch by 91% , 92%, 99% and 98%, respectively. To investigate recovery from this inhibition, treated cysts were washed with distilled water and subjected to further incubation in PRD only solution (Figure 3.1A). Cysts that were previously treated with the lowest doses of fluensulfone, 1µM and 5µM, recovered and began hatching 7 days after transfer fluensulfone plus PRD to PRD alone. This resulted in a total hatch at the end of the recovery period of 65% and 61%, respectively, in comparison to a control hatch of 78%. 50µM fluensulfone treated cysts also recovered hatching, but this recovery was delayed relative to that seen with low dose treatment, and reached a lower overall recovery. 500µM fluensulfone treated cysts showed no recovery after transfer to PRD alone.

3.2.1.1 *Globodera pallida* hatching from isolated eggs

When assessing hatching from *G. pallida* cysts, the rate of hatch and overall juvenile emergence is variable. Making an egg inoculum, suspending the eggs on mesh inserts in solution and then counting the number of juveniles that passed into the wells was shown to reduce hatching variability (Gaihre et al., 2019).

Thus, hatching was also measured utilizing an assay based on treatment of isolated eggs. This removed the facet of variable hatching between individual cysts. Additionally, the isolated egg hatching assays allow the precise effect of the nematicides on hatching to be investigated, by removing the requirement for the juvenile to emerge from the cyst (Gaihre et al., 2019).

Treatment of eggs with 5, 50 and 500µM fluensulfone resulted in inhibition of hatching by 44%, 88% and 95%, respectively (Figure 3.1 B).

At the end of the treatment period, hatching was not significantly inhibited by 1µM. Fluensulfone did not inhibit hatching from eggs as potently as inhibition of hatching from cysts. This is exemplified by comparing the inhibition of hatching following exposure to 5µM, where hatching is inhibited by 44% when eggs are treated compared to 92% when cysts are treated. A full recovery against the fluensulfone inhibition was seen following treatment of eggs with ≤5µM, relative to control. Treatment of isolated eggs with 5µM fluensulfone appeared to be more reversible than treatment with 1µM fluensulfone, however, hatching at the end of the recovery period following treatment with 5µM was not significantly different to eggs treated with 1µM. In repeated experiments, this pattern of full recovery following treatment of eggs with ≤5µM and no significant difference between the 1µM and 5µM effect was also observed. At higher concentrations, the recovery against inhibition after removal was not as complete in the egg hatching assays. 500µM fluensulfone treated eggs showed no recovery from inhibition after treatment. This pattern of partial and non-recovery was similar to that described in the cyst based hatching assays.

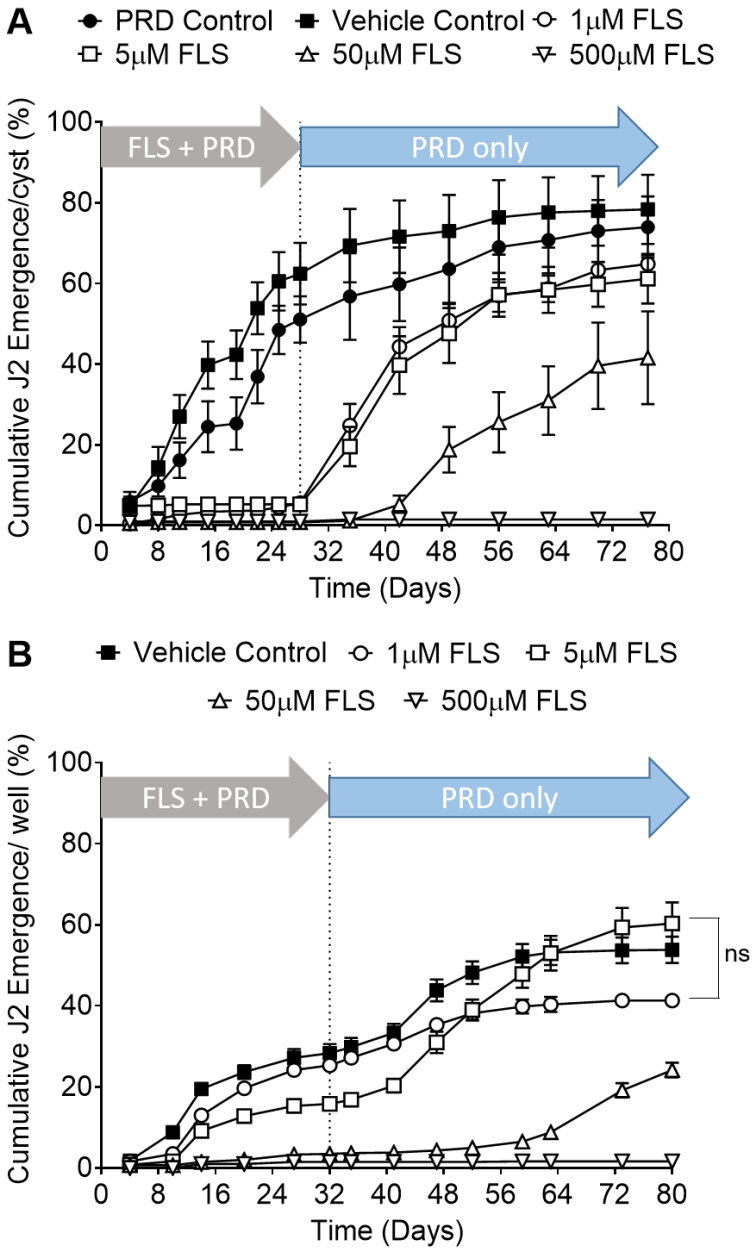

Figure 3.1 Fluensulfone inhibits *G. pallida* hatching. Cysts (A) and isolated eggs (B) were exposed to Vehicle Control (0.5% acetone), PRD Control or PRD containing indicated concentration of fluensulfone (FLS) for 28 days (A) and 32 days (B). All solutions contained 1:3 PRD solution to induce hatch. At 28 days (A) or 32 days (B) (dotted line), the cysts/egg inserts were washed and transferred to PRD alone to assess recovery. N=12 cysts (A) or 6 wells (B) per treatment. Data shown are mean ± S.E.M percentage hatch per cyst/well. Statitical analysis performed by two-way ANOVA with Tukey post-hoc tests ($P<0.05$) comparing 1μM FLS isolated egg recovery with 5μM isolated egg recovery. ns, not significant. Data is representative of four independent experiments.

In addition to investigating the effects of fluensulfone on PRD-induced hatch, I also probed for an effect on artificial hatch. Sodium metavanadate has been shown to induce hatching of *G. pallida* and *G. rostochiensis* (Byrne et al., 2001). Here, treatment with sodium metavanadate induces hatching in *G. pallida* isolated eggs. When treated with fluensulfone in the presence of sodium metavanadate, hatching is inhibited to a similar degree as to when incubated with PRD, and with associated recovery (Figure 3.2).

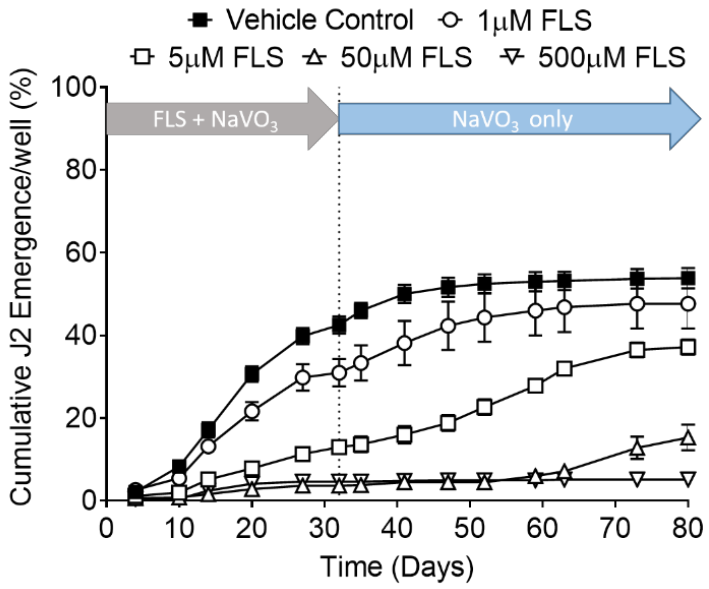

Figure 3.2 Fluensulfone inhibits artificially induced hatch. Isolated eggs were exposed to Vehicle Control (0.5% acetone) or the indicated concentration of fluensulfone (FLS) for 32 days. All solutions contained 300μM Sodium Metavanadate ($NaVO_3$) to induce hatch. At 32 days (dotted line), the egg inserts were washed and transferred to $NaVO_3$ alone to assess recovery from FLS. N= 6 wells per treatment. Data shown are mean ± S.E.M percentage hatch per cyst/well.

3.2.2 Fluensulfone inhibits *Globodera pallida* hatching from cysts where hatching has been initiated

Fluensulfone inhibited *G. pallida* hatching from cysts and eggs at concentrations as low as 1 and 5µM, respectively (Figure 3.1). To investigate whether fluensulfone can inhibit hatching once hatching has been initiated, hatching was initiated by PRD exposure prior to fluensulfone treatment (Figure 3.3).

PRD exposure for 16 days ensured that subsequent fluensulfone treatment was on a population that had established a robust hatching (Figure 3.3). When eggs that had been exposed to PRD were transferred to fluensulfone, hatching was inhibited, resulting in a significantly lower overall juvenile emergence at 50 days (34 days post transfer) after exposure to concentrations of fluensulfone ≥1µM (Figure 3.3B).

At concentrations <1µM, hatching was not significantly inhibited, suggesting a threshold for inhibition of 1µM. Transfer of cysts from PRD solution to fluensulfone also reduced hatching, although this was not significant (Figure 3.3A).

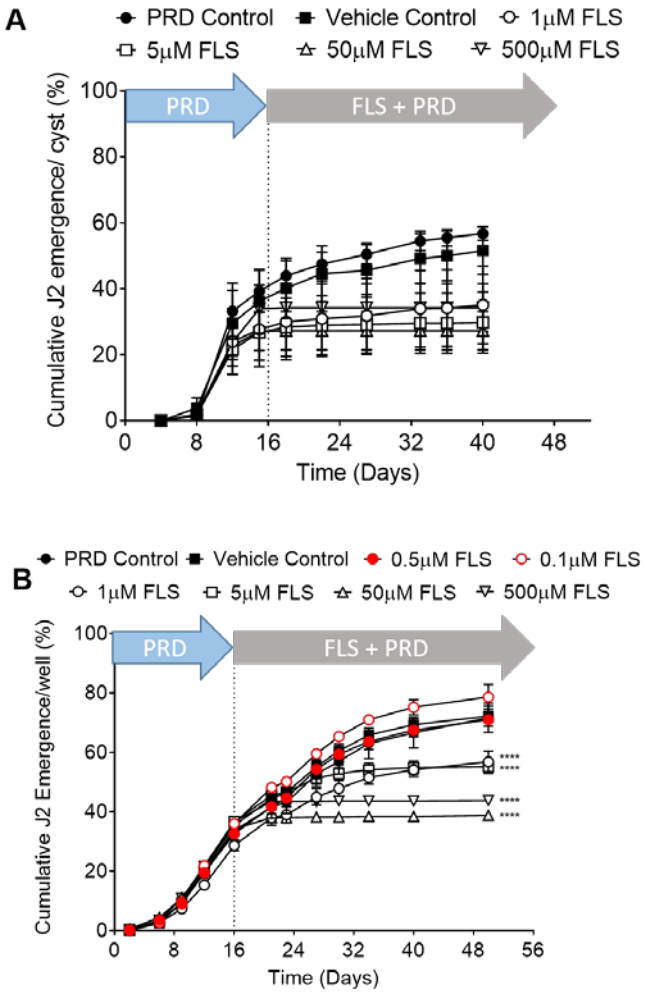

Figure 3.3 Fluensulfone can inhibit hatching post initiation. Cysts (A) or eggs (B) were exposed to PRD solution for 16 days to initiate sustained hatching. Cysts (A) or inserts containing eggs (B) were washed and transferred to PRD Control, Vehicle Control (0.5% acetone) or fluensulfone (FLS) solutions, all containing 1:3 PRD. N = 6 cysts/ wells per treatment. Data shown is ±S.E.M percentage juvenile emergence per cyst/ well. Statistical analysis performed by two-way ANOVA with Tukey post-hoc tests ($P<0.05$) and is in comparison to both PRD and vehicle controls. **** $P<0.0001$. Data is representative of three independent experiments.

3.2.3 Fluensulfone has *in ovo* effects on *Globodera pallida* juveniles

The motility of juveniles that emerged from the cysts during the recovery period, in which fluensulfone had been removed and the cysts or eggs had been washed, was investigated.

This allowed us to assess if the *in ovo* fluensulfone exposure modified subsequent behaviour (Figure 3.4). The motility of juveniles that emerged from cysts previously treated with 1µM fluensulfone were impaired. This is evidenced by a 41% decrease in the percentage of emerged juveniles that were motile in treated preparations relative to vehicle control.

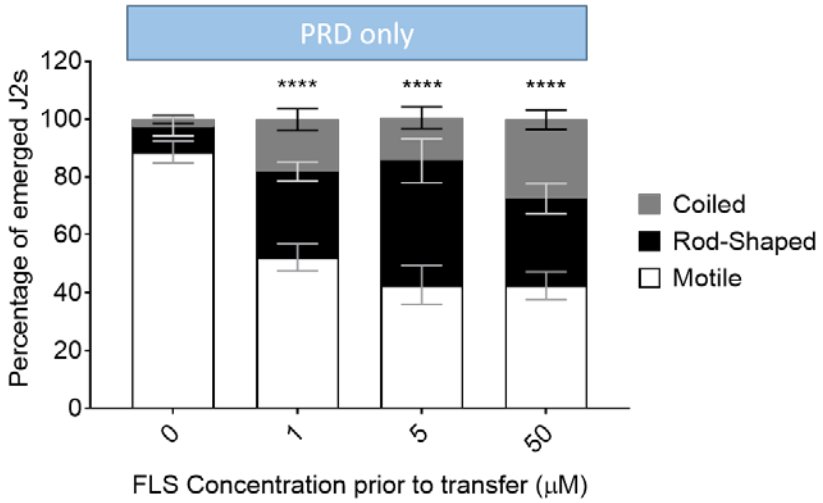

Figure 3.4 J2s exposed to fluensulfone *in ovo* are impaired. J2s that emerged during the recovery period following drug wash out were scored for motility. Visual observation was used to score worms as motile, coiled or rod shaped. A lower percentage of J2s that emerged from fluensulfone treated cysts were motile when compared to J2s that emerged from the vehicle control treated cysts (0µM). No data is shown for cysts that had been treated with 500µM fluensulfone due to no juveniles emerging during the recovery period following treatment with this concentration (see Figure 3.1). Data shown is ± S.E.M percentage of emerged J2s. Statistical analysis performed by two-way ANOVA with Tukey post-hoc tests, comparing the percentage of motile emerged J2s from FLS treated cysts to vehicle control (0µM). **** P<0.0001

3.2.4 Fluensulfone compromises the internal integrity of unhatched juveniles following pre-exposure of cysts

It has previously been shown that after exposure of hatched J2s to fluensulfone juveniles are immotile and appear granular. The granulation made normally ready discrimination of internal organs indistinct (Kearn et al., 2017).

To investigate if a similar phenomenon happened in the egg encapsulated J2 prior to hatching, the effect of fluensulfone on unhatched juveniles was scored. *Globodera pallida* cysts were exposed to fluensulfone for the indicated periods before being broken open. The appearance of cyst contents, including the unhatched eggs, was then scored. J2s were scored as granular when the internal structures of the juvenile could not be identified, as depicted in Figure 3.5.

Exposure to fluensulfone for 10 days resulted in the majority of unhatched eggs from cysts exposed to ≥50µM fluensulfone appearing granular. At lower concentrations of fluensulfone, the morphological integrity of the worms was not impacted, despite these concentrations resulting in clear inhibition of hatching (Figure 3.1).

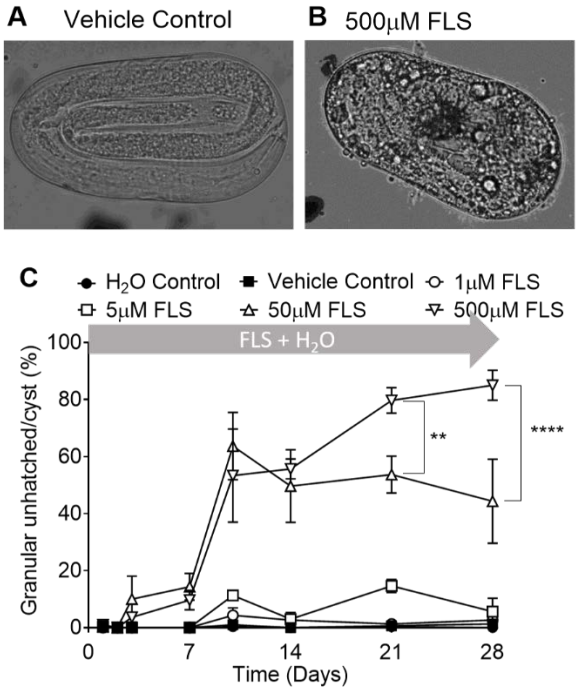

Figure 3.5 Fluensulfone causes morphological changes to the treated unhatched juvenile. When looking at unhatched eggs from control cysts (A) internal structures, such as the stylet and pharynx, are clearly visible. High concentrations of FLS result in unhatched eggs appearing granular (B), with internal structures unidentifiable. (C) *G. pallida* cysts were exposed to ddH_2O, Vehicle (0.5% acetone) or the indicated concentration of fluensulfone (FLS) for up to 28 days. Cysts were broken open at the time points indicated and the proportion of unhatched eggs that appeared granular in comparison to total number of unhatched eggs was scored. N = 3 cysts per time point, per treatment. Data shown are mean ± S.E.M percentage of unhatched eggs that appeared granular, per cyst. Statistical analysis performed by two-way ANOVA with Tukey post-hoc tests ($P<0.05$). ** $P<0.01$, **** $P<0.0001$

3.2.5 Comparing the inhibitory effect of fluensulfone on *Globodera pallida* hatching with other classes of nematicide

I compared the effect of fluensulfone on *G. pallida* hatching with nematicides from three distinct classes; abamectin, aldicarb and fluopyram. I used concentrations that were comparable with those used in studies that were seen to inhibit hatching of other species of plant parasitic nematodes (Osborne, 1973; Greco and Elia, 2000; J. Kim et al., 2016; De Almeida et al., 2017; Beeman and Tylka, 2018).

3.2.5.1 Abamectin irreversibly inhibits *Globodera pallida* hatching

Treatment of cysts with 1µM abamectin for 28 days inhibited hatching by 66%. In contrast, both 10µM and 100µM abamectin exposure for 28 days resulted in a complete inhibition of hatching (Figure 3.6A). Cysts were removed from abamectin solutions and transferred to PRD alone to assess recovery.

Hatching was partially recovered following removal from 1µM abamectin, with total hatch at the end of the recovery 31% lower than controls. In contrast, there was no recovery from the two higher doses that caused complete inhibition of hatching. The juveniles that hatched during the recovery period following treatment with 1µM abamectin were motile (Figure 3.6C).

In similar experiments, there was a strong inhibition with 10 and 100µM abamectin in isolated eggs and again limited recovery. Interestingly when isolated eggs were exposed to 1µM abamectin, hatching was not significantly inhibited (Figure 3.6B). This reduction in potency when eggs are exposed to treatment in comparison to cysts is consistent with what was observed with fluensulfone treatment.

Cyst contents of *G. pallida* cysts that had been treated with abamectin were examined, as was described following fluensulfone treatment. Cysts treated with 1, 10 and 100µM abamectin for 28 days resulted in 59%, 83% and 95% granular unhatched eggs per cyst, respectively (Figure 3.6C).

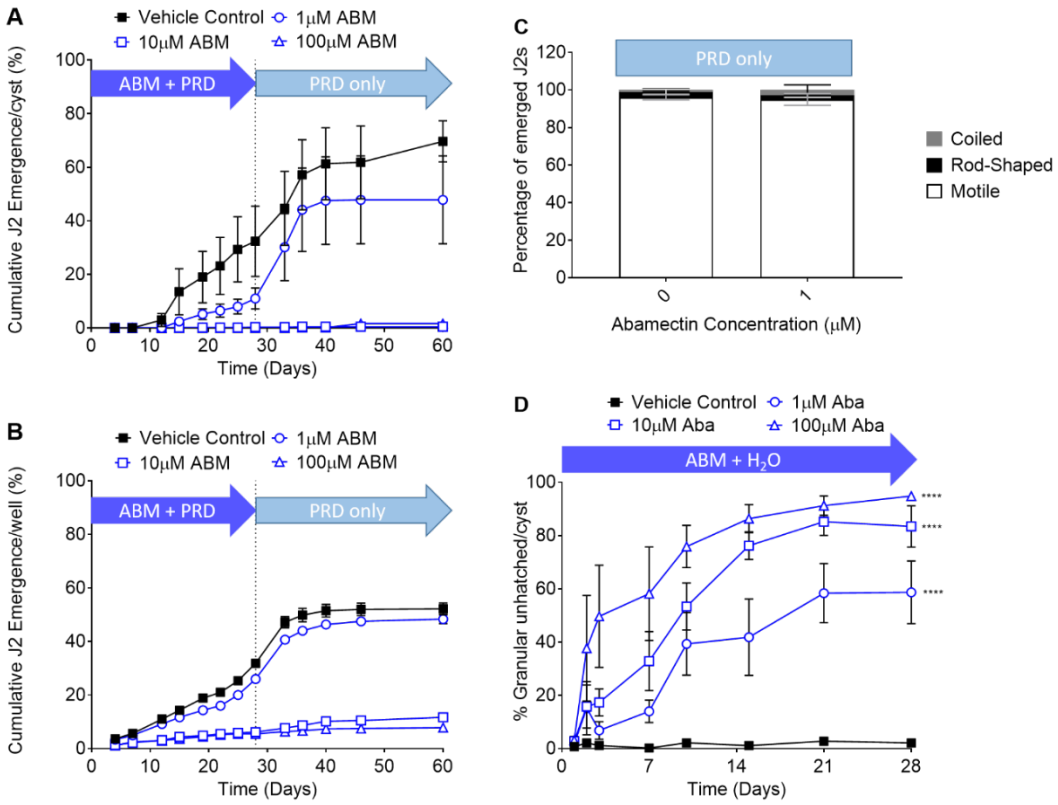

Figure 3.6 Complex effects of abamectin on the hatching efficacy and morphology of *G. pallida* cysts and eggs. Cysts (A) and eggs (B) were exposed to Vehicle Control (0.5% acetone) or the indicated concentration of abamectin (ABM) for 28 days. All solutions contained 1:3 PRD solution to induce hatch. At 28 days (dotted line), the cysts/egg inserts were washed and transferred to PRD alone to assess recovery. N=6 cysts/ wells per treatment. Data shown are mean ± S.E.M percentage hatch per cyst/ well. Data is representative of three independent experiments. (C) Worms that hatched during the recovery period were scored for motility as described for FLS. There was no recovery following cyst exposure to 10 and 100μM ABM and so no data is shown for these concentrations. 1μM ABM in ovo exposure had no effect on juvenile motility. Data shown is ± S.E.M percentage of emerged J2s. (D) Abamectin results in *in ovo* granulation following treatment with all concentrations. N = 6 cysts per time point, per treatment. Data shown are mean ± S.E.M percentage of unhatched eggs that appeared granular, per cyst. Statistical analysis performed by two-way ANOVA with Tukey post-hoc tests (P<0.05). **** P<0.0001.

3.2.5.2 Aldicarb inhibits *Globodera pallida* hatching

Globodera pallida hatching from cysts and eggs is inhibited by aldicarb. 1µM aldicarb did not inhibit hatching but higher concentrations of 10 and 100µM saw significant inhibition of hatching (Figure 3.7). Hatching was recovered partially and completely following removal from 100 and 10µM aldicarb solutions, respectively.

There is a discrepancy between the degree of inhibition between cysts and eggs, with aldicarb having a greater inhibitory effect on hatching from cysts in comparison to eggs, as is the case with abamectin and fluensulfone. At 28 days, 10 and 100µM aldicarb fully inhibited hatching from cysts, with no hatching from cysts treated with these concentrations during the treatment period. In isolated eggs, hatching was inhibited by 61% and 70% following treatment with 10 and 100µM aldicarb, respectively.

Juveniles that hatched during the recovery period from cysts treated with 100µM aldicarb had a small but significantly reduced motility. Treatment with concentrations below 100µM did not result in subsequent impairment of juveniles (Figure 3.7C). Furthermore, aldicarb did not result in *in ovo* granulation at any concentration (Figure 3.7D), consistent with the reversibility of hatching inhibition.

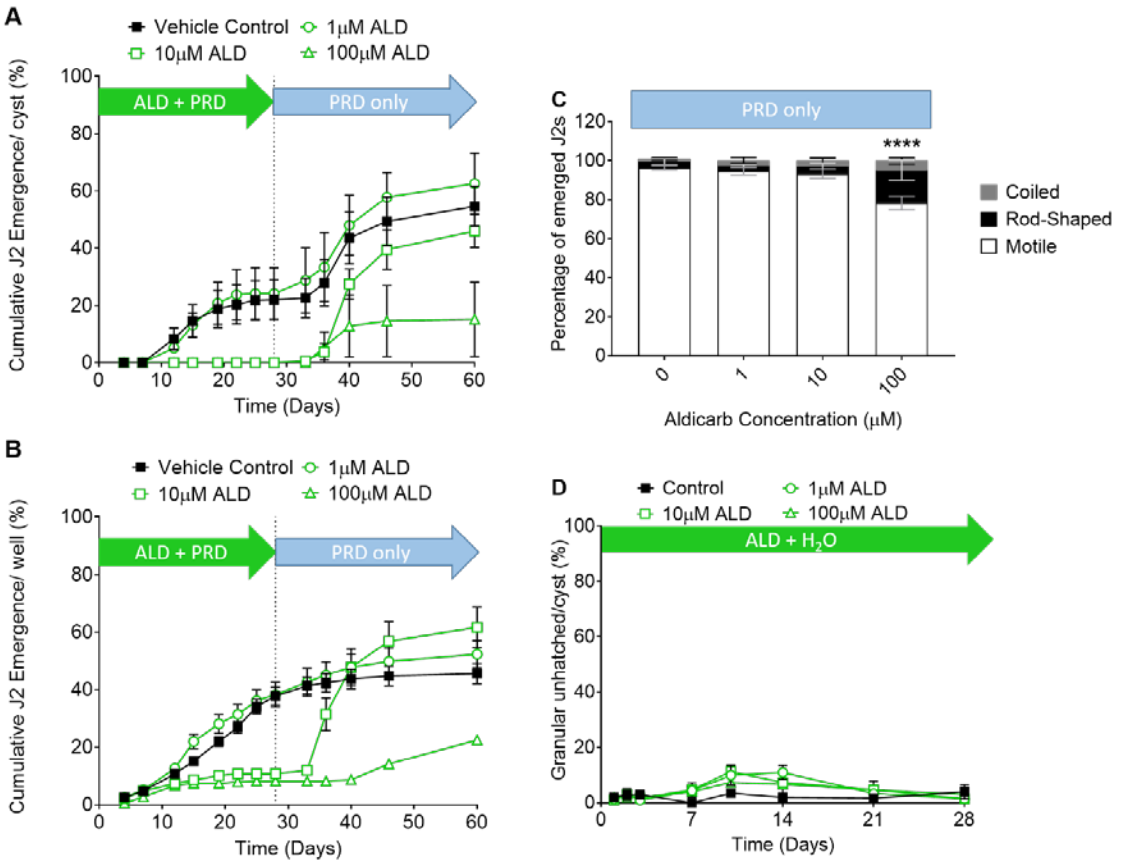

Figure 3.7 Aldicarb reversibly inhibits *G. pallida* hatching ≥10 µM without an effect on egg morphology. Cysts (A) and eggs (B) were exposed to Vehicle Control (0.5% ethanol) or the indicated concentration of aldicarb (ALD) for 28 days. All solutions contained 1:3 PRD solution to induce hatch. At 28 days (dotted line), the cysts/egg inserts were washed and transferred to PRD alone to assess recovery. N=6 cysts/ wells per treatment. Data shown are mean ± S.E.M percentage hatch per cyst/ well. Data is representative of two independent experiments. (C) Worms that hatched during the recovery period were scored for motility as described for FLS. Only in ovo exposure to 100µM ALD resulted in a reduced proportion of motile worms. Data shown is ± S.E.M percentage of emerged J2s. Statistical analysis performed by two-way ANOVA with Tukey post-hoc tests, comparing the percentage of motile emerged J2s from ALD treated cysts to vehicle control (0µM). **** P<0.0001. (D) Aldicarb does not result in granulation of unhatched eggs. N = 3 cysts per time point, per treatment. Data shown are mean ± S.E.M percentage of unhatched eggs that appeared granular, per cyst.

3.2.5.3 Fluopyram irreversibly inhibits *Globodera pallida* hatching

Following treatment with 1µM fluopyram for 32 days, *G. pallida* hatching was inhibited by 82%. Treatment with ≥5µM fluopyram fully inhibited hatching. During the recovery period, some hatching was recorded for cysts that had been treated with 1 and 5µM. At the end of the recovery period total hatch from 1 and 5µM treated cysts was 14% and 8%, respectively, in comparison to 82% hatch from the control group, retaining >80% inhibition. There was no hatching or recovery recorded following treatment with 50 and 500µM fluopyram.

Fluopyram is less effective at inhibiting hatching from isolated eggs. 5µM fluopyram inhibited hatching from eggs by 81%; however, unlike when cysts were treated with fluopyram, this inhibition was partially recovered. 50 and 500µM fluopyram retained complete inhibition of hatching from eggs, with no recovery.

The juveniles that did hatch during the recovery period were impaired, with a significantly lower proportion of juveniles appearing motile in comparison to the control treated cysts (Figure 3.8C). In addition, following 28 days exposure to 50 and 500µM fluopyram, the percentage of eggs that appeared granular was 74% and 83%, respectively (Figure 3.8D).

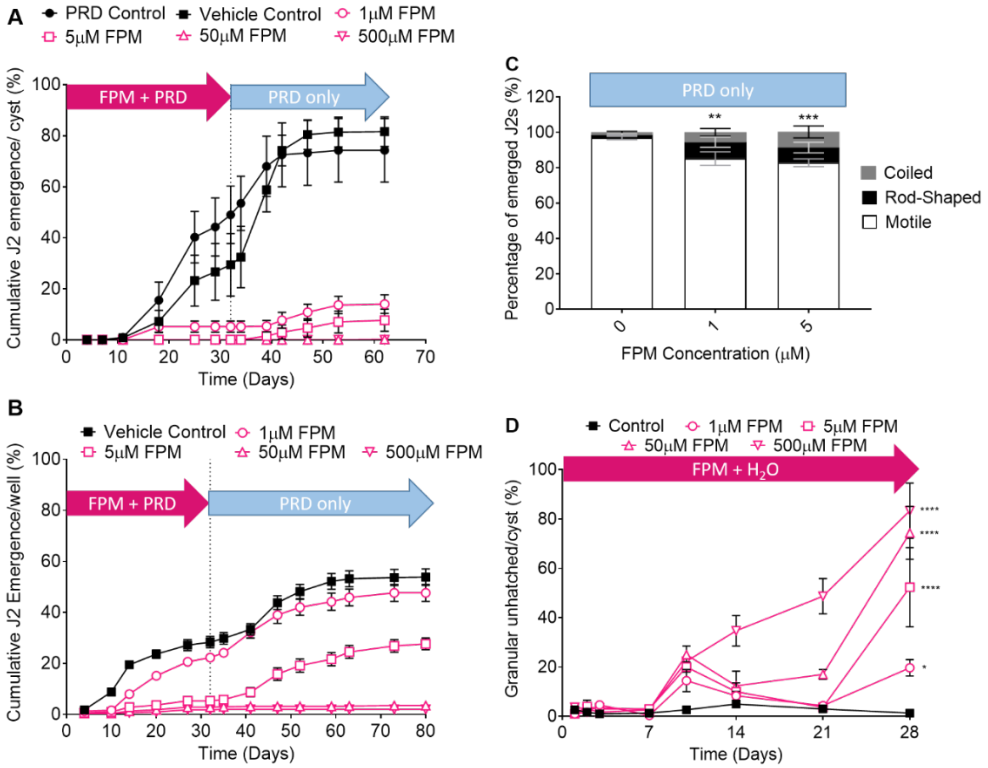

Figure 3.8 Fluopyram inhibits *G. pallida* hatching and has in ovo effects. Cysts (A) and eggs (B) were exposed to Vehicle Control (0.5% acetone) or the indicated concentration of fluopyram (FPM) for 32 days. All solutions contained 1:3 PRD solution to induce hatch. At 32 days (dotted line), the cysts/egg inserts were washed and transferred to PRD alone to assess recovery. N=6 cysts/ wells per treatment. Data shown are mean ± S.E.M percentage hatch per cyst/ well. Data is representative of three independent experiments. (C) Worms that hatched during the recovery period were scored for motility as described for FLS. 1 and 5µM FPM in ovo exposure significantly impair motility of juveniles. No data is shown for 50 and 500µM FPM, as there was no recovery from these concentrations. Data shown is ± S.E.M percentage of emerged J2s. Statistical analysis performed by two-way ANOVA with Tukey post-hoc tests, comparing the percentage of motile emerged J2s from FPM treated cysts to vehicle control (0µM). ** P<0.01, *** P<0.001. (D) Fluopyram results in granulation of unhatched eggs. N = 3 cysts per time point, per treatment. Data shown are mean ± S.E.M percentage of unhatched eggs that appeared granular, per cyst. Statistical analysis performed by two-way ANOVA with Tukey post-hoc tests (P<0.05). * P<0.05, **** P<0.0001.

3.3 Discussion

3.3.1 Irreversible inhibition of hatching is associated with disrupted morphology of encysted eggs

Fluensulfone potently inhibits *G. pallida* hatching. Its effects have been compared against other commonly used nematicides; abamectin, aldicarb and fluopyram, with a view to providing insight into its distinct mode of action. This comparative approach lends further support to the notion that fluensulfone acts as a selective metabolic inhibitor (Kearn et al., 2014; Kearn et al., 2017). Taking the comparative approach allowed a comparison of the ability of each class of nematicide to act on a range of important parameters, including hatching, recovery from hatching after chemical wash out and post hatch motility of emerged J2s that were subjected to chemical exposure when inside the egg. An interesting discriminator between these nematicides is the dual effect of the first three compounds to inhibit hatching and also impact juveniles that emerge from washed chemical-treated cysts into a chemical free solution. This is particularly pertinent for the two metabolic inhibitors fluensulfone and fluopyram.

The concentration dependence of fluensulfone treatment highlighted additional high dose effects of this chemical. Following treatment with 500µM fluensulfone, there is very little juvenile emergence and the morphology of the encysted J2 in these irreversibly inhibited eggs and cysts is consistent with an irreversible inhibition of hatching. The morphological disruption of eggs is indicative of cell death and suggests that the unhatched, egg-protected juvenile is susceptible to fluensulfone treatment. The granulation that I have described is consistent with fluensulfone compromising the internal integrity of hatched *G. pallida* J2s (Kearn et al., 2017). Granular juveniles appeared rod-shaped and were unresponsive when prodded, consistent with the granular appearance providing a visual indication of death (Kearn et al., 2017). The disintegration of internal structures described here for unhatched juveniles is therefore entirely consistent with high concentrations of fluensulfone treatment resulting in mortality. Whether this cell death is apoptotic or necrotic has not been determined. There are morphological differences between apoptotic and necrotic cell death (Edinger and Thompson, 2004), however, these morphological features cannot be distinguished between here. Understanding which cell death pathway fluensulfone induces could lead to important insights into its mode of action.

In a similar way to fluensulfone, both fluopyram and abamectin execute irreversible inhibition of hatching and morphological disruption of eggs. This is seen following treatment with all concentrations of fluopyram and is clear at higher concentrations of abamectin. In contrast, there is no evidence for an irreversible inhibition of hatching to aldicarb and this is not associated with disrupted morphology in any unhatched eggs.

In the case of fluensulfone and fluopyram, distinct metabolic inhibition underlies the mode of action in nematodes (Burns et al., 2015; Kearn et al., 2017). In the former case, the molecular target that leads to metabolic arrest is thought to involve a disruption of lipid metabolism, although the exact target remains to be elucidated (Kearn et al., 2017). In the case of fluopyram, this selective inhibition is via succinate dehydrogenase and block of the electron transport chain (Burns et al., 2015). In the case of abamectin, classically, this class of compound acts on glutamate-gated chloride channels (Cully et al., 1994) and inhibits neuromuscular function. Whether this well-known mode of action, or a less well studied, but reported, secondary metabolic effect drives the morphological change remains to be elucidated. This secondary metabolic effect is achieved by abamectin inhibiting the activity of F_oF_1-ATPase, an inner mitochondrial enzyme that is responsible for ATP synthesis driven by the electron transport chain, and adenine nucleotide translocator (ANT), an important component of the mitochondrial machinery (Maioli et al., 2013). It was shown that treatment of isolated rat mitochondria with abamectin induces mitochondrial dysfunction and reduces cellular ATP levels, leading to necrosis (Maioli et al., 2013). On the other hand, ivermectin was shown to induce apoptosis of human brain microvascular endothelial cells through caspase-dependent pathways (Liu et al., 2016). Granulation achieved by abamectin treatment here could therefore be suggestive of cell death by apoptosis or necrosis. The results presented here are nevertheless consistent with an insult to metabolic activity by fluensulfone, fluopyram or abamectin resulting in mortality of the unhatched juvenile and reflects a core aspect of their modes of action.

3.3.2 Nematicides are less efficacious at inhibiting hatching from isolated eggs

There is a discrepancy in the potency of fluensulfone's inhibition of hatching and recovery when cysts or eggs are exposed. When *G. pallida* cysts are exposed to root diffusate, the juveniles must first emerge from the egg and then emerge from the cyst. In comparison, when juveniles hatch from the eggs that are suspended on mesh inserts, the juveniles are thought to use motility to pass through the mesh and are then counted as hatched juveniles. Fluensulfone treatment of *G. pallida* juveniles results in impairment to motility, which can also be caused because of *in ovo* exposure to fluensulfone.

A possible explanation for the improved efficacy of fluensulfone in inhibiting hatching from cysts could be that it is having an inhibitory effect on motility that selectively impairs emergence from the cyst. Abamectin, aldicarb and fluopyram display a similar difference in efficacy between cysts and eggs, with cysts seeming to be more susceptible than isolated eggs to all nematicides investigated. All of these nematicides have shown to impair motility of hatched juveniles (Huang et al., 1983; De Almeida et al., 2017; Beeman and Tylka, 2018) and so the reduced efficacy of the nematicides ability to inhibit isolated egg hatching is consistent with an impairment to juvenile motility being more perturbing in emergence from the cysts, due to the denser internal matrix of the cyst when compared to movement through mesh.

Furthermore, the ability of these three distinct classes of nematicides to inhibit hatching is consistent with their known modes of action and supports a requirement of neuromuscular junction activity and metabolism for hatching.

3.3.3 Fluensulfone inhibits hatching post hatching initiation

In addition to the effects of fluensulfone on PRD-induced hatching, I investigated approaches that allow sequential investigation of hatching activation and hatching inhibition. Pre-treating with root diffusate ensures robust activation of the hatching mechanism in the context of both the cyst and isolated egg assays.

This will lead to the postulated cascade that underlies the key events of the hatching mechanism, which includes hydration, metabolic activity, *in ovo* motility and stylet thrusting, leading to eclosion (Gaihre et al., 2019). These descriptive hatching sub-steps represent domains that have been identified in hatched juveniles as susceptible to fluensulfone (Kearn et al., 2014; Kearn et al., 2017). The fact that external application of the chemical impacts on the resulting hatching and inhibits its execution supports the notion that fluensulfone is able to access the internal, cyst- and egg-protected J2. This observation shows that fluensulfone can inhibit the cell signalling pathways that are activated by root diffusate initiation of hatching.

Additionally, fluensulfone is able to inhibit the cell signalling pathways that are activated by sodium metavanadate ($NaVO_3$) initiation of hatching. Vanadate is an (Na,K)-ATPase inhibitor, interacting with the high and low affinity ATP sites (Cantley et al., 1978). Structurally, vanadate is a phosphate analog and is commonly used as a general protein-tyrosine phosphatase (PTP) inhibitor (Huyer et al., 1997). Despite this mechanism of vanadate inhibition being well known, its mechanism of action as a hatching factor is not understood. PRD- and $NaVO_3$-induced hatching are differentially sensitive to DMSO and Dafadine-A (*personal communication Gaihre, Y).* Dafadine-A is a selective inhibitor of *C. elegans* DAF-9 cytochrome P450, inhibiting DAF-9 promotion of dauer formation (Luciani et al., 2011). In contrast, PRD- and $NaVO_3$-induced hatching have shared sensitivity to inhibition by reserpine and methiothepin treatment (*personal communication Gaihre, Y).* This suggests that $NaVO_3$ initiation of hatching induces a distinct pathway to that of root-exudate initiation of hatching, prior to the 5-HT dependent steps that lead to eclosion (Figure 3.9). The ability of fluensulfone to inhibit both PRD- and $NaVO_3$-induced hatching suggests that it is acting at a point in the hatching cycle where the two pathways converge. Understanding the mechanism of vanadate-induced hatch would therefore lead to important insight into the mode of action of fluensulfone inhibition of hatching.

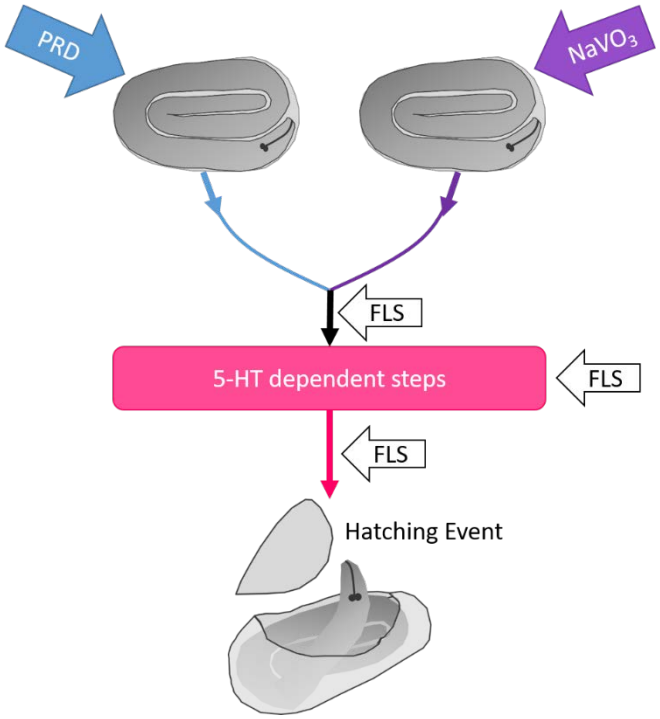

Figure 3.9 PRD and sodium metavanadate act in distinct pathways to induce hatching prior to 5-HT dependent steps. PRD (blue) and sodium metavanadate ($NaVO_3$) (purple) induce hatching of *G. pallida*. The pathways that they induce are not identical, evidenced by their differential sensitivity to inhibitor treatment. They do, however, share sensitivity to methiothepin and reserpine, suggesting convergence of the pathways at (pink), or prior to (black), 5-HT dependent steps of the hatching cycle. The ability of fluensulfone (FLS) to inhibit both PRD- and $NaVO_3$-induced hatching suggests it is acting at a point in the hatching cycle that is shared between both pathways, either prior to, at, or post 5-HT dependent steps.

As the assays developed for this study extend over protracted times *in vitro,* I could also compare the nature of the mode of action with previous studies on free-living J2 metabolism and motility. The kinetics of hatching and the time dependence of the fluensulfone inhibition in the population pre-activated by root diffusate prior to treatment is entirely consistent with fluensulfone resulting in a progressive insult that accumulates its effect. This is consistent with previous observations on free living *G. pallida* J2 (Kearn et al., 2017). Although not well understood, the encysted egg is thought to contain an encapsulated J2 that is in a relatively quiescent metabolic state (see Chapter 1.2.3). Our sequential experiments would suggest that fluensulfone's action is equally efficacious whether executing inhibition on a quiescent J2, one activated for hatching, or subject to inhibition as a free moving J2 (Kearn et al., 2017).

3.3.4 Pre-exposure of cysts to fluensulfone results in impaired juveniles

Exposure to low concentrations of fluensulfone results in a nearly complete, but subsequently slow, reversible inhibition of hatching. Notably, the juveniles that hatch during the recovery period are impaired. This is seen at all concentrations, with a significant decrease in the proportion of juveniles that are motile. Thus, although the nematodes retain or recover sufficient activity to emerge after fluensulfone treatment, the *in ovo* exposed juveniles held within the cysts are impaired. This impairment, scored here as reduced motility, would hinder their ability to locate and invade host roots. This is also seen with doses of fluopyram that result in hatching during recovery, although to a lesser extent, with 1µM fluopyram pre-exposure resulting in a significant 12% decrease in motility, compared to the 1µM effect with fluensulfone, where there is a 41% decrease in motility. In contrast, when comparing the 1µM effect of abamectin and aldicarb, there is no significant decrease in motility following pre-exposure to these chemicals.

In addition, a greater proportion of the nematodes that hatch from cysts pre-treated with fluensulfone appear coiled, which is a phenotype brought about by osmotic stress (Charwat et al., 2002) and could be a form of a stress response in this instance, as is seen when hatched juveniles are exposed to fluensulfone (Kearn et al., 2017). This again highlights a lasting effect of fluensulfone that cannot be overcome by removing the previously exposed cysts from fluensulfone solutions, suggesting that fluensulfone is acting directly on the unhatched juvenile.

Such *in ovo* exposure enhances the nematicidal and crop protective potential of fluensulfone in addition to its targeting of an important life cycle target, through its potent inhibition of hatching.

3.3.5 Field Relevance

In the specific case of fluensulfone and based on the comparative studies, two likely distinct dose dependent effects of different nematicides have been ascribed. Extrapolation between in vitro experiments and the field needs some care, but observations in this study should help inform on field relevant aspects of mode of action. Application method and soil environment, including pH, water table, temperature, soil type and organic matter content of the soil (Jones and Norris, 1998; Faske and Starr, 2007; Arias-Estevez et al., 2008; Chawla et al., 2018), will impact on the concentrations of nematicides in contact with the nematodes in the field. Soil application of fluensulfone (5µM, (Patrick M Norshie et al., 2017)), fluopyram (0.5µM, (Zhang et al., 2014)) and aldicarb (1-20µM, (Hough et al., 1975)) can lead to translatable field concentrations that I have shown here would inhibit hatching of *G. pallida* and so would therefore contribute to their field efficacy. It is clear that identified field relevant doses will impact non-hatching related aspects of the life cycle. Thus my data rather allows one to propose that hatching and its sensitivity to low doses of fluensulfone in vitro suggest it is a key step that may play out in crop protection. In contrast, the exclusive use of abamectin as a seed coat restrict field concentrations to the sub µM range (Faske and Starr, 2007), suggesting levels are largely below those required to execute an inhibition of hatching. The additional high concentration effects of fluensulfone that execute irreversible inhibition and pathological morphology in vitro are less likely to pertain in the field. However, it would be interesting to probe cysts from such field studies for granulation following exposure to fluensulfone and the other nematicides in this study.

3.4 Summary

In this chapter, I have described a high and low concentration effect of fluensulfone on *G. pallida* hatching. Following exposure to fluensulfone, there is a high concentration effect of *in ovo* granulation suggestive of cell death, resulting in complete inhibition of hatching with no recovery. At lower concentrations, fluensulfone inhibits hatching, and although reversible, leaves a trace of effect, with the juveniles that hatch following exposure displaying impaired motility, which is an important aspect of the fluensulfone insult and suggests a lasting effect of treatment on juveniles that cannot be overcome by removal from fluensulfone.

This profile of effects overlaps with, but is distinct, to other nematicides of target-defined modes of action that have been described here. The variation in execution and recovery of hatching inhibition supports the novel mode of action of fluensulfone and suggests that the low concentration inhibition of hatching may contribute to its efficacy in crop protection.

Chapter 4 Targeting Key Metabolic Fluxes to Determine the Effect of their Inhibition on *Globodera pallida* hatching

4.1 Introduction

The previous chapter identified the potent inhibition of *Globodera pallida* hatching by fluensulfone. This displays key potency at the hatching stage of the PPN life cycle, in addition to the reported efficacy of fluensulfone on the free-living, hatched J2 stage of species occurring within the *Meloidogyne* and *Globodera* genera (Oka et al., 2009; Oka et al., 2012; Oka, 2014; Norshie et al., 2016; Kearn et al., 2017; Oka and Saroya, 2019).

It has previously been shown that fluensulfone treatment elicits an insult that is consistent with a progressive metabolic impairment. The evidence for metabolic inhibition is primarily based on a progressive loss of motility and metabolic activity, observed through loss of MTT (2-(4,5-dimethyl-2-thiazolyl)-3,5-diphenyl-2H-tetrazolium bromide) staining (Kearn et al., 2017). An important facet of the fluensulfone signature is its selective effect on PPNs (Kearn et al., 2014) and the preservation of lipid stores in the face of ensuing toxicity (Kearn et al., 2017). A key factor to consider is the changing metabolism between distinct developmental and functional stages, such as quiescence versus the PRD-activated, unhatched J2 through to the active, hatched J2 (Chapter 1.2.3). Here, I employ a comparative approach, using inhibitors with defined selectivity for distinct steps of key metabolic fluxes, to define if selective inhibition of energy mobilizing pathways prevents hatching. This will be benchmarked against the effects of fluensulfone identified in Chapter 3 to determine whether the action of fluensulfone on hatching is underpinned by a common progressive metabolic impairment that is observed on the hatched J2 stage.

4.1.1 Evidence for impairment to lipid utilization by treatment with fluensulfone

Previously, the major lipid storage component of *G. pallida* was investigated in freshly hatched and starved (14 days post-hatch) juveniles. To investigate lipid stores in *G. pallida* J2s, Nile red fluorescence was used, which is a fixation stain that selectively stains intracellular lipid droplets (Phillip Greenspan et al., 1985) (Chapter 1.5.5.1). The intensity of Nile red fluorescence reduced by over 60% in starved worms relative to freshly hatched J2s, consistent with the notion that lipid stores are depleted post-hatch. Treatment with 10µM fluensulfone arrested this reduction in fluorescence, suggesting that lipid consumption is reduced in the presence of fluensulfone (Kearn et al., 2017). This suggests that disruption in utilizing lipids causes impaired motility that translates to fluensulfone's nematicidal mitigation against PPN infectivity.

The steps of the *G. pallida* hatching cycle are mapped out in the general introduction (Chapter 1.3). There is limited evidence that during the hatching cycle, utilization of lipids accompanies the metabolic activation of the juvenile prior to eclosion, forming a vital step of the hatching process (Holz et al., 1997; Perry et al., 2013). This would therefore be consistent with fluensulfone inhibiting access to stored lipid in hatched J2s and could provide an explanation for the inhibition of hatching by fluensulfone that I describe in the previous chapter.

To investigate whether access to lipid stores are critical to the hatching cycle in *G. pallida,* I used the carnitine palmitoyltransferase (CPT) inhibitor, perhexiline (Kennedy et al., 1996). Inhibition of CPT prevents the transfer of long-chain fatty acids into the mitochondria for β-oxidation (Figure 4.1). Perhexiline treatment yields deleterious effects in parasitic nematodes *Haemonchus contortus* and *Onchocerca lienalis,* with selective inhibition between 20-50µM, and the free-living nematode *C. elegans* (Taylor et al., 2013).

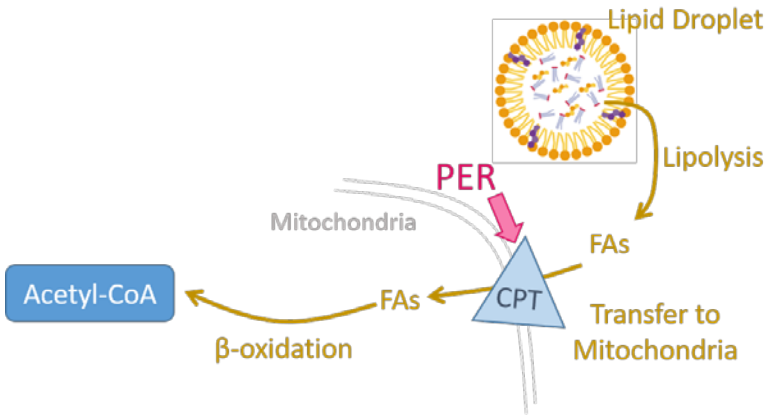

Figure 4.1 Perhexiline mode of action. Perhexiline (PER; pink) inhibits carnitine palmitoyltransferase (CPT), which prevents the transfer of fatty acids (FAs), which are generated by lipolysis of lipid droplets from the cytoplasm into the mitochondria for β-oxidation. This inhibition prevents the mobilization of energy from stored lipids, which is speculated to play a key role in energy provision when J2s emerge form hatching (Holz et al., 1997).

Taylor et al. demonstrated that treatment of *C. elegans* with perhexiline resulted in a decrease in motility, with an EC_{50} of 47.3µM. This coincided with a decrease in oxygen consumption rate (OCR), indicating reduced metabolic activity. The effect of perhexiline on OCR was equivalent to that of CPT-1 inhibitor, etomoxir. Furthermore, using RNAseq to measure the transcriptional response to perhexiline and etomoxir, it was shown that the two compounds clustered together, disrupting similar pathways, including peroxisome and fatty acid β-oxidation, suggesting common mode of actions and that perhexiline was acting at its predicted target of CPT in *C. elegans* (Taylor et al., 2013).

In a separate study, treatment of *C. elegans* with 100µM perhexiline resulted in increased lipid accumulation. Interestingly, lipid accumulation was coordinated to a mitochondrial-to-cytoslic stress response (MCSR) (H.E. Kim et al., 2016). Inhibition of CPT by perhexiline results in a decrease in fatty acid oxidation and an increase in lipid accumulation. This results in metabolic restructuring where there is a shift from the lipid metabolism pathway to the lipid storage pathway. These changes in lipid balance may serve as a cytosolic signal, which results in induction of the cytosolic response and improved cytosolic protein homeostasis (H.E. Kim et al., 2016).

Comparing the effects of fluensulfone and perhexiline on *G. pallida* hatching will therefore provide an important comparison to assess whether fluensulfone is acting on lipid fluxes to inhibit hatching. It will also provide important insight as to whether perhexiline is efficacious at this PPN life cycle stage and determine the importance of mobilizing stored lipid during hatching.

4.1.2 TCA cycle activity for energy mobilization

Acetyl-CoA plays a central role in energy metabolism (Fuchs and Berg, 2014) and flux to and from acetyl-CoA is dependent on the metabolic state of the nematode. For many nematodes, the TCA cycle and electron transport chain (ETC) are utilized to generate energy, with the main input of acetyl-CoA from carbohydrate (Behm, 2002). The TCA cycle involves a series of oxidation reactions to generate NADH, $FADH_2$ and CO_2, which are utilized in the ETC to generate ATP (Berg et al., 2002). The carbohydrate input to acetyl-CoA can be in the form of trehalose, via its breakdown into glucose. Indeed it has been shown that stored trehalose can be readily utilized in this way by parasitic and entomopathogenic nematodes (Behm, 1997; Grewal et al., 2006). It is well documented that trehalose is a protective agent during dessication in anhydrobiotic organisms, including nematodes (Madin and Crowe, 1975; Erkut et al., 2011; Erkut and Kurzchalia, 2015) and is present in high concentrations in the perivitelline fluid surrounding the unhatched J2 of PPNS (Perry and Clarke, 1981). However, the utilization of ATP is not well characterised and many models imply that trehalose is simply transported out of the egg, leading to a water exchange that co-ordinates with rehydration of the juvenile and swelling of the egg that follows activation of hatching (Chapter 1.3.3).

To investigate the importance of the TCA cycle in hatching, I used aconitase inhibitor, fluroacetic acid (Figure 4.2). Fluoroacetate combines with coenzyme-A to form fluoroacetyl-CoA, which subsequently combines with oxaloacetate in place of acetyl-CoA to form fluorocitrate. Fluorocitrate is subsequently able to bind with aconitase, causing depletion of TCA cycle metabolites downstream of citrate (Proudfoot et al., 2006).

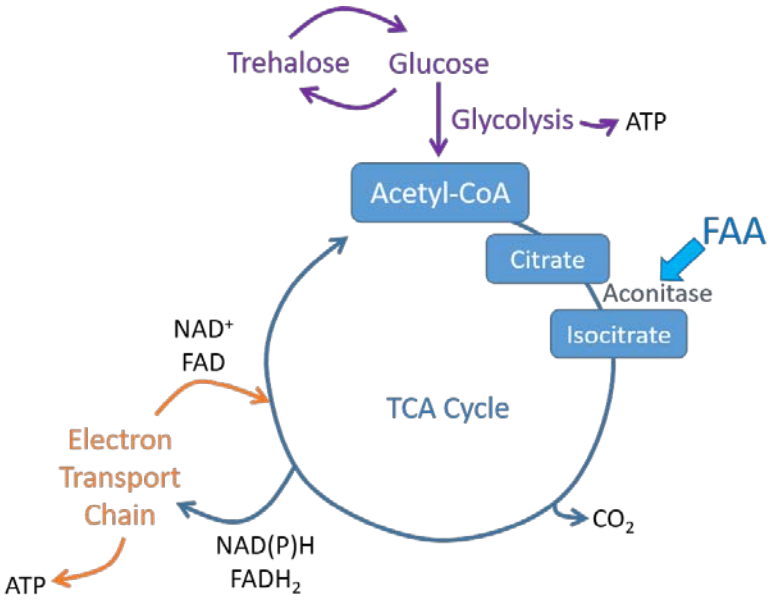

Figure 4.2 Targeting the TCA cycle with Fluoroacetic Acid. Fluoroacetic acid (FAA; blue) inhibits TCA cycle enzyme aconitase. This prevents the isomerization of citrate to isocitrate.

4.1.3 Glyoxylate shunt activity and its role in nematodes

It has been described for several nematode species that during non-feeding stages, acetyl-CoA input can be from the β-oxidation of fatty acids, which are liberated from lipid stores, and subsequent flux from acetyl-CoA can be via the TCA cycle to generate energy. Alternatively this input can flux via the glyoxylate shunt to produce carbohydrates (Khan and McFadden, 1982; Wandsworth and Riddle, 1989; Liu et al., 1995; Siddiqui et al., 2000; Kondrashov et al., 2006; Lourenço-Tessutti et al., 2015). The glyoxylate shunt allows the generation of carbohydrates from stored lipid, bypassing the requirement for uptake of carbohydrates from external sources (Barrett et al., 1970) (Figure 4.3) and there is evidence for the employment of this pathway to enable lipid utilization during infective, non-feeding juvenile stages of PPNs (Lourenço-Tessutti et al., 2015).

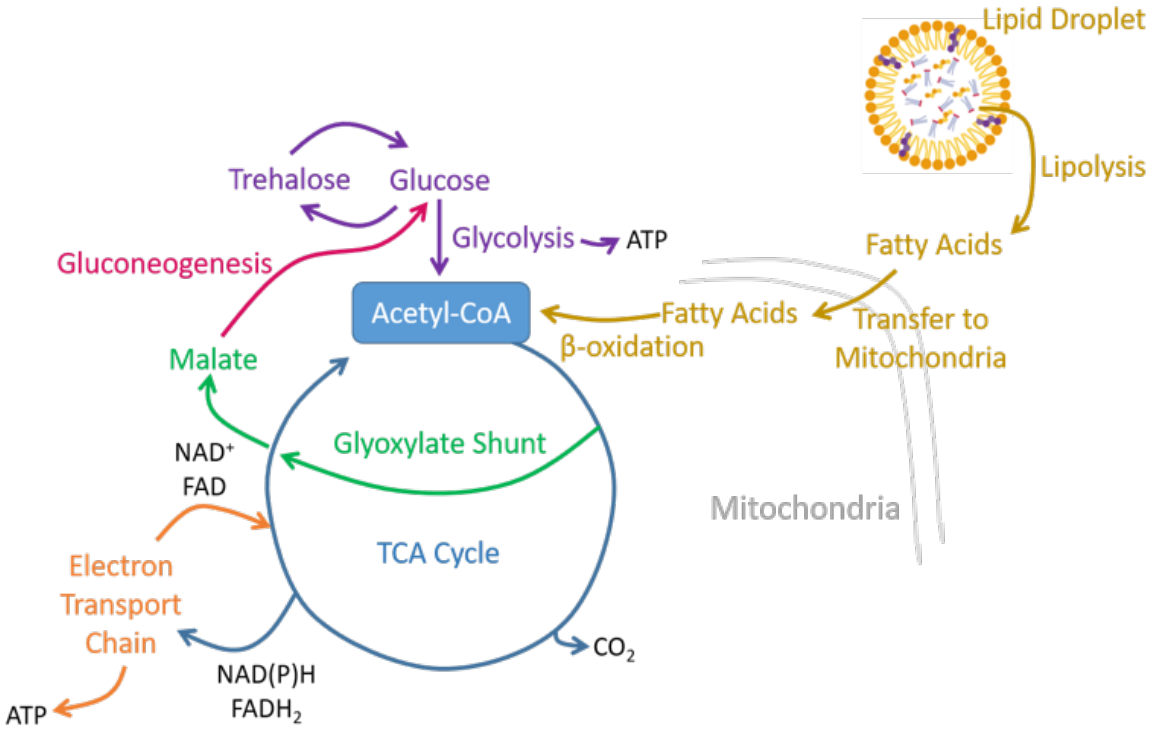

Figure 4.3 Key metabolic fluxes for the mobilization of energy stores. The pathways highlighted here are utilized by nematodes to allow the generation of ATP from stored lipid and carbohydrate. Carbohydrate flux to acetyl-CoA is via glycolysis (purple) with subsequent employment of the TCA cycle (blue) and ETC (orange). Acetyl-CoA input can also be from the β-oxidation of fatty acids (gold), which are liberated from lipid droplets via lipolysis. Flux is then via the glyoxylate shunt (green), providing a route to generate carbohydrate from stored lipid via gluconeogenesis (pink).

In the free-living nematode *C. elegans,* the activities of glyoxylate shunt enzymes are maximal at the time of egg hatching and decline during development as the larvae begin to feed on bacteria. In the absence of bacteria, activity of these enzymes in *C. elegans* does not decline, suggesting a requirement for glyoxylate shunt activity during non-feeding stages of the life cycle and to prepare for entry into these non-feeding stages (Khan and McFadden, 1982). This is further supported by the up- regulation of the gene encoding glyoxylate shunt enzymes in *C. elegans* dauer larvae and the *daf-2* mutant that consistently expresses dauer-like physiology (McElwee et al., 2006). The control of carbon flow through the glyoxylate shunt allows unhatched larvae and dauer larvae to utilize stored lipids and generate carbohydrates, switching to the use of the TCA cycle when food intake and energy demands are increased (Wandsworth and Riddle, 1989). Determination of which pathway is employed is context dependent and will shift between states of growth and quiescence (Burnell et al., 2005; Erkut and Kurzchalia, 2015; Penkov et al., 2015; Erkut et al., 2016), regulated by the tight control of the molar ratios of competing enzymes present in the TCA cycle and glyoxylate shunt (Penkov et al., 2020). In addition to the absolute molar ratios of the enzymes, information on post-translational modifications would be beneficial in evidencing post-translational control.

4.1.4 Selective inhibition of energy mobilizing pathways

To dissect the importance of the activities of energy mobilizing pathways during *G. pallida* hatching, I looked to intervene with selective inhibitors to differentially target the glyoxylate shunt and TCA cycle routes (Figure 4.4). In addition to fluoroacetic acid, which inhibits activity of both the glyoxylate shunt and TCA cycle activity, I investigated the effects of itaconic acid and malonic acid. Itaconic acid inhibits isocitrate lyase (Middendorf and Dusenbery, 1993) and succinate dehydrogenase (also known as mitochondrial complex II) (Lampropoulou et al., 2017). In the latter case, this is a competitive inhibition mediated by binding to the succinate-binding pocket of succinate dehydrogenase (SDH). Malonic acid also acts at the succinate-binding pocket in order to inhibit SDH (Sierotzki and Scalliet, 2013). This is in contrast to the SDH inhibitor fluopyram, which binds to the ubiquinone binding site, preventing the reduction of quinone to quinol and further cycling of succinate oxidation (Horsefield et al., 2006; Avenot and Michailides, 2010; Burns et al., 2015).

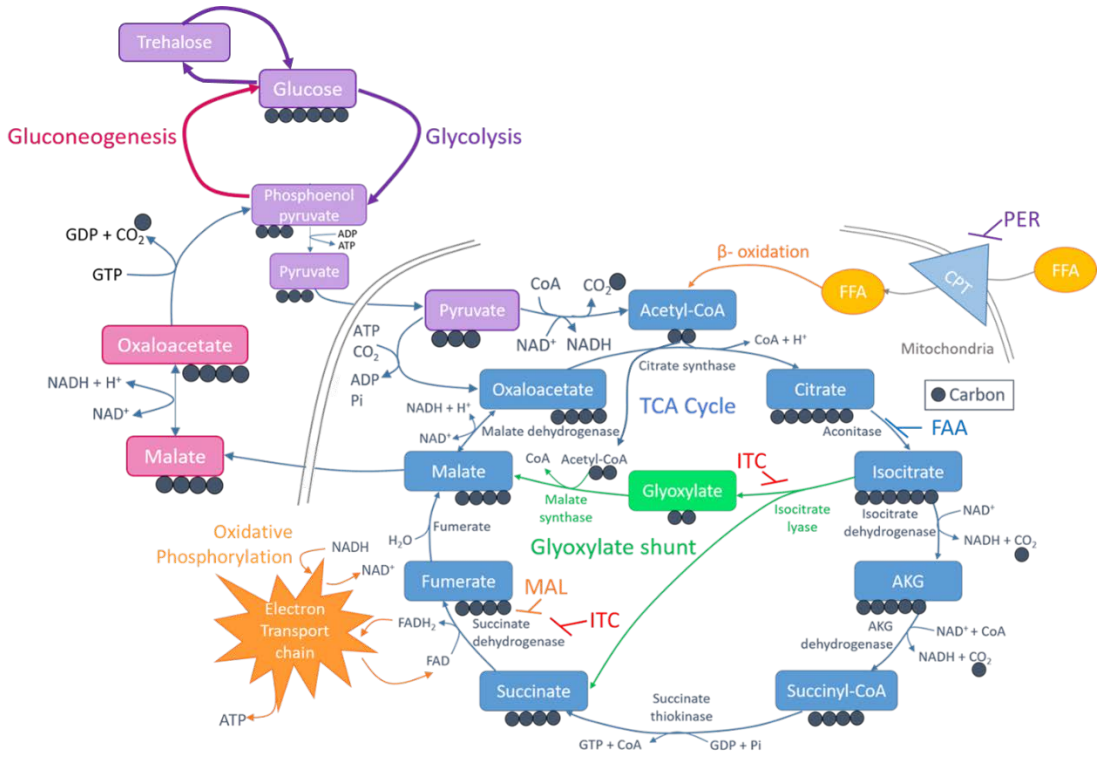

Figure 4.4 Targets in the TCA cycle (blue) and glyoxylate shunt (green) of metabolic inhibitors. Fluoroacetic acid (FAA) inhibits aconitase; Itaconic acid (ITC) inhibits isocitrate lyase and succinate dehydrogenase; Malonic acid (MAL) inhibits succinate dehydrogenase; Perhexiline (PER) inhibits carnitine-palmitoyltransferase (CPT) to inhibit the transfer of free fatty acids (FFA) into the mitochondria for β-oxidation.

The effects of itaconic, malonic and fluoroacetic acid on the free-living nematode, *C. elegans,* have been reported. Acute and long term effects of each inhibitor were investigated by determining 24-hour survival rates and second-generation reproduction, respectively. This allowed the calculation of LC_{50} values based on 24-hour survival and EC_{50} values for second-generation reproduction.

Inhibitor	Site of action	Reported Ki Value	Experimental evidence in nematodes
Perhexiline	Carnitine palmitoyl-transferase: inhibits transfer of fatty acids into the mitochondria for β-oxidation	74-99µM (rat heart) (Kennedy et al., 1996)	EC_{50} 47.3µM (motility phenotype, *C. elegans*) (Taylor et al., 2013). 100µM treatment increases fat accumulation (*C. elegans*) (H.E. Kim et al., 2016)
Fluoroacetate	Aconitase: Inhibits the conversion of citrate to isocitrate in the TCA cycle	290µM* (pig heart) (Villafranca, 1974)	LC_{50} 76mM (24-hour survival, *C. elegans*) EC_{50} 23µM (second-generation reproduction, *C. elegans)* (Middendorf and Dusenbery, 1993)
Itaconate	Isocitrate lyase: Inhibits the conversion of isocitrate to glyoxylate + succinate, which is the first step of the glyoxylate shunt	19µM (*C. elegans)* (Patel and McFadden, 1978)	LC_{50} 21mM (24-hour survival, *C. elegans*) EC_{50} 4.3mM (second-generation reproduction, *C. elegans)* (Middendorf and Dusenbery, 1993)
Malonate	Succinate dehydrogenase: inhibits oxidation of succinate to fumerate in TCA cycle, preventing electron transfer to ETC	5.4 - 9.8µM (pig heart) (Thorn, 1953)	LC_{50} 9.9mM (24-hour survival, *C. elegans*) EC_{50} 3.3mM (second-generation reproduction, *C. elegans)* (Middendorf and Dusenbery, 1993)

Table 4.1 Ki values of Glyoxylate shunt and TCA cycle inhibitors and the experimental evidence for these acting in nematodes. The inhibitors used in this study with their site of action and Ki value. Experimental evidence for the use of these inhibitors in nematodes is described along with EC50 values generated from these studies. * The Ki value for fluoroacetate is for its active metabolite, fluorocitrate, which binds to aconitase.

The LC_{50} and EC_{50} values for each inhibitor are shown in Table 4.1. For fluoroacetic acid, the LC_{50} was calculated as 76mM and EC_{50} as 23µM, resulting in an LC_{50}/ EC_{50} ratio of 3474. This discrepancy in potency between the effect of fluoroacetic acid on lethality and on reproduction, indicated by a large ratio, was not common to itaconic and malonic acid, suggesting a specific, long-term effect of fluoroacetic acid on reproduction. The combination of malonic acid and itaconic acid did not produce results similar to those obtained with fluoroacetic acid, suggesting that the specific potent effect of fluoroacetic acid on *C. elegans* reproduction is not caused by inhibiting the TCA and glyoxylate cycles, but that fluoroacetic acid acts on an alternative pathway (Middendorf and Dusenbery, 1993).

4.1.5 Chapter Aims

Investigating the action of the aforementioned inhibitors will extend the understanding of the involvement of the metabolic pathways that they target in *G. pallida* hatching. This will provide us with a clearer view of the metabolic fluxes that are important during this life cycle stage and how impacting on these fluxes can be exploited for nematicidal activity. This will help inform on whether the progressive metabolic impairment that is reported for the effect of fluensulfone on hatched J2s (Kearn et al., 2017) is underpinned by the same mechanism as the inhibitory effect of fluensulfone on hatching.

4.2 Results

4.2.1 Treatment with perhexiline does not inhibit *Globodera pallida* hatching

Mobilization of lipids for energy production generates free fatty acids which are then transferred into the mitochondria for β- oxidation. Failure to do this prevents β-oxidation and results in the build-up of cellular free fatty acids and if not regulated, the generation of toxic intermediates. Thus, I treated cysts and eggs with perhexiline, which inhibits the transfer of fatty acids into the mitochondria for β-oxidation through inhibition of CPT, to probe for a role on *G. pallida* hatching.

There was no significant inhibition of *G. pallida* hatching following treatment with 5µM or 50µM perhexiline to cysts or isolated egg preparations (Figure 4.5A). Due to perhexiline's insolubility, I was unable to investigate concentrations above 50µM without using a concentration of DMSO vehicle that would impact on hatching (Gaihre et al., 2019).

Consistent with the approach taken when comparing the profile of effects of fluensulfone with nematicides on hatching, I also scored the motility of juveniles that hatched during the recovery period from cysts that had been treated with perhexiline and then washed and transferred to PRD. There were no significant effects observed on J2 motility following *in ovo* perhexiline treatment (Figure 4.5B). In addition, no granulation to unhatched eggs was recorded.

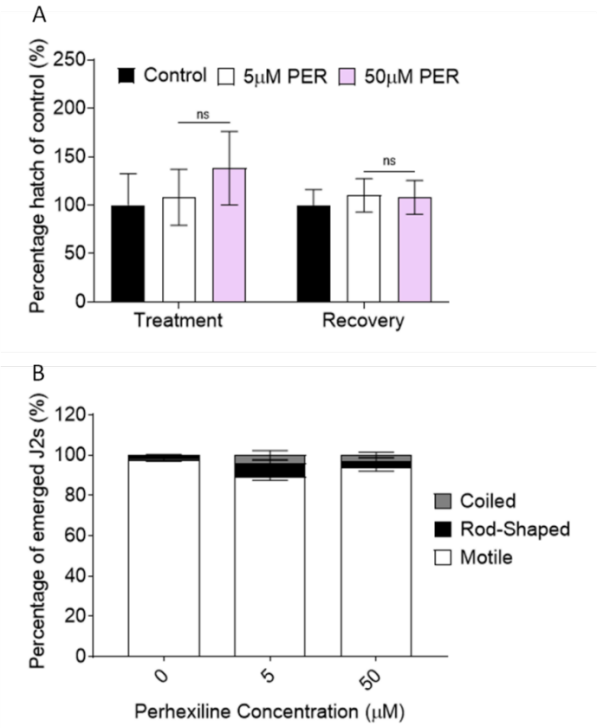

Figure 4.5 Perhexiline has no effect on *G. pallida* hatching. (A) Cysts and eggs were exposed to 5µM and 50µM perhexiline with a final vehicle concentration of 0.5% ethanol (control). All solutions contained PRD to stimulate hatch. At the end of the treatment period of 28 days, cysts and eggs were washed and transferred to PRD alone to assess subsequent hatch during the recovery period (days 28-80). Data is combined hatching from cysts and eggs, with N=6 cysts and N=6 wells per treatment group, with each experiment performed independently. Data shown is ± S.E.M percentage hatch of control. Statistical analysis performed by two-way ANOVA with Tukey post-hoc tests ($P<0.05$) and is in comparison to PRD control. (B) During the recovery period, motility of hatched juveniles was assessed, and juveniles were visually scored as motile, rod-shaped or coiled.

4.2.2 Fluoroacetic acid inhibits *Globodera pallida* hatching

Fluoroacetic acid inhibits aconitase, resulting in the disruption of both the TCA cycle and glyoxylate shunt. Treatment with 500µM fluoroacetic acid inhibits *G. pallida* hatching from cysts and isolated eggs (Figure 4.6). To assess recovery, cysts or eggs were washed and transferred to chemical free PRD. When removed from fluoroacetic acid incubation, the subsequent hatching, although significantly increased relative to cysts and eggs during treatment, does not reach control hatch, indicating that there is partial recovery of hatching inhibition.

To extend this investigation, juveniles that were exposed to 50µM and 500µM fluoroacetic acid *in ovo* and subsequently emerged upon washout were scored for motility. Concentrations of fluoroacetic acid ≤50µM are insufficient to bring about inhibition of hatching. Additionally, whilst 500µM fluoroacetic acid significantly inhibits hatching, there are no significant differences to the motility of juveniles that hatch during the recovery period from treated cysts when compared to controls (Figure 4.7A). This is in contrast to fluensulfone, which has *in ovo* effects at concentrations that inhibit hatching, observed as disrupted motility to juveniles that hatch during the recovery period.

The contents of *G. pallida* cysts treated with fluoroacetic acid were examined, as was described when comparing nematicides with fluensulfone. Exposure of cysts to 50µM fluoroacetic acid did not result in *in ovo* necrosis and is consistent with this concentration not impacting on hatching (Figure 4.7A). There was, however, a significant increase in the proportion of eggs that appeared granular following exposure to 500µM FAA when compared to H_2O controls (Figure 4.7C).

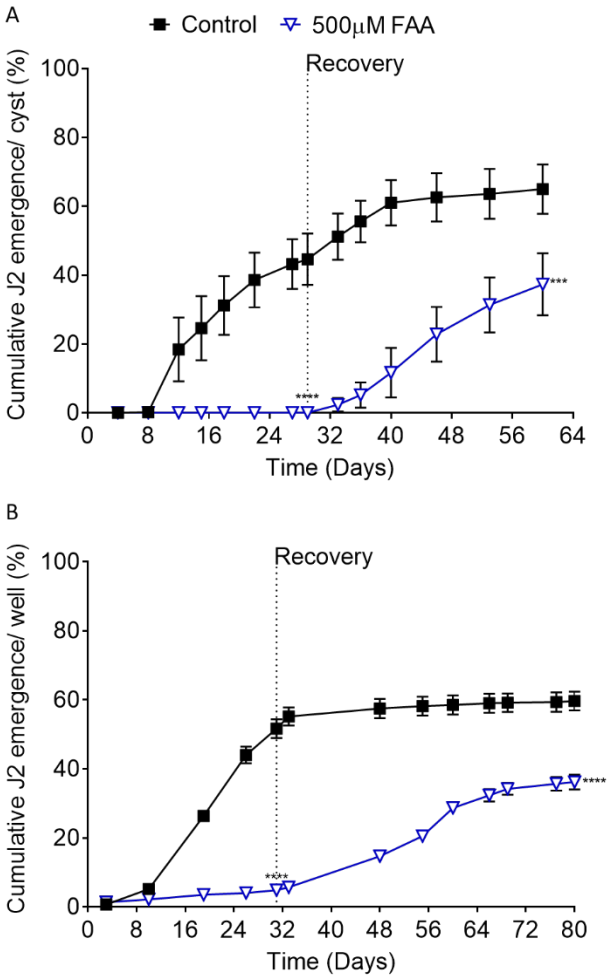

Figure 4.6 Aconitase inhibitor, fluoroacetic acid, reversibly inhibits G. pallida hatching. Cysts (A) and eggs (B) were exposed to PRD control and 500µM Fluoroacetic acid (FAA) for 28 days. At 28 days (dotted line), the cysts/ eggs were washed and transferred to PRD alone to assess recovery. N=6 cysts/wells per treatment. Data shown are mean ± S.E.M percentage hatch per cyst (A) or well (B). Statistical analysis performed by two-way ANOVA with Tukey post-hoc tests ($P<0.05$) and is in comparison to PRD control.

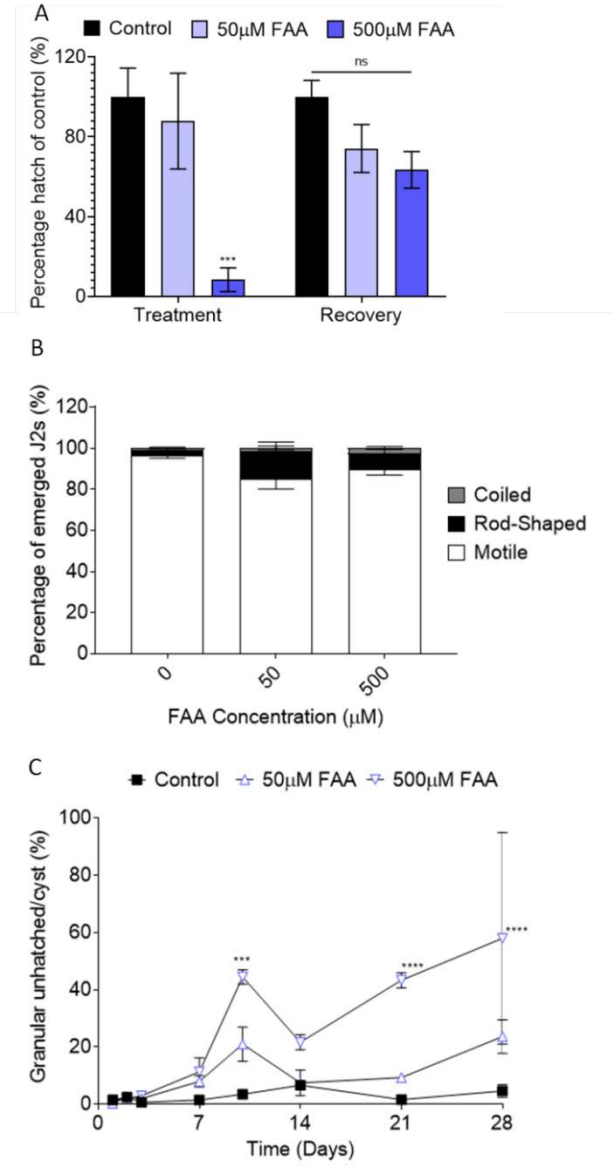

Figure 4.7 Effects of fluoroacetic acid on the hatching efficacy and morphology of unhatched eggs. (A) Cysts were exposed to 50µM and 500µM FAA for 28 days. Cysts were then washed and transferred to PRD alone and subsequent hatching assessed. Data shown is ± S.E.M percentage hatch of control and is pooled from three independent experiments. (B) During the recovery period, motility of hatched juveniles was assessed, and juveniles were scored as motile, rod-shaped or coiled. There were no significant differences between the percentages of J2s that appeared motile when compared to the control. (C) Cyst contents were examined and the proportion of eggs that appeared granular was scored. N = 3 cysts per time point, per treatment. Data shown are mean ± S.E.M percentage of unhatched eggs that appeared granular, per cyst. Statistical analysis performed by two-way ANOVA with Tukey post-hoc tests ($P<0.05$).

4.2.3 Inhibition of glyoxylate shunt activity does not contribute to inhibition of *Globodera pallida* hatching

Fluoroacetic acid treatment results in a partially reversible inhibition of *G. pallida* hatching. Treatment with fluoroacetic acid will impact on both the TCA cycle and glyoxylate shunt, due to it inhibiting the production of isocitrate, which is a metabolite involved in steps of both pathways. To unpick the involvement of TCA cycle and glyoxylate shunt activity in the fluoroacetic acid insult, I used itaconic acid and malonic acid, which inhibit the glyoxylate shunt and TCA cycle, respectively.

Cysts were exposed to PRD or PRD containing 1mM and 500µM itaconic and malonic acid for 28 days. In keeping with previous observations, PRD exposure resulted in a progressive hatch that led to 44.6% juvenile emergence after 28 days. In contrast, hatching was enhanced following 1mM itaconic and malonic acid treatment in PRD, with a final hatch after 28 days of 70.8% and 69.3%, respectively (Figure 4.8A). This suggests that itaconic and malonic acid enhance PRD-induced hatching of *G. pallida.* These results were also seen in the isolated egg set-up, although only significant ($P < 0.0001$) for 1mM itaconic acid treatment.

Cysts treated with itaconic acid and malonic acid were washed and transferred to PRD alone and the juveniles that hatched into PRD solution during this phase were probed for an *in ovo* effect of inhibitor on juvenile motility. Treatment with 500µM and 1mM itaconic acid and 1mM malonic acid significantly enhanced PRD-induced hatching. Hatching from cysts that were removed from treatment conditions during the recovery phase was not significantly different to control hatch (Figure 4.9A). The motility of juveniles that hatched during this phase was not significantly different to controls (Figure 4.9B).

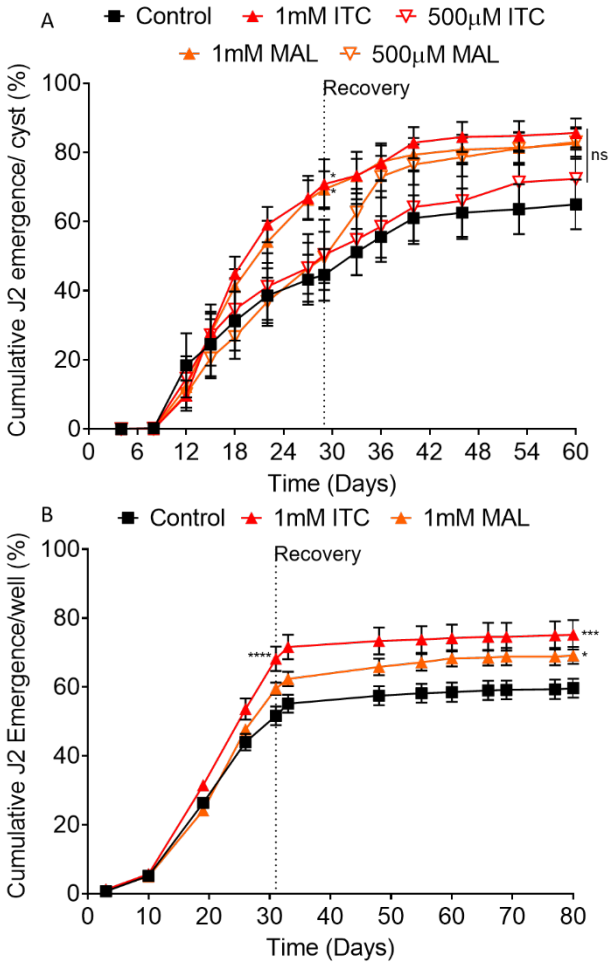

Figure 4.8 Treatment of *G. pallida* cysts with itaconic acid and malonic acid enhances PRD-induced hatching. Cysts (A) and eggs (B) were exposed to PRD control and PRD in the presence of 1mM or 500µM Itaconic acid (ITC) or malonic acid (MAL) for 28 days (A) or 31 days (B). At the point of recovery, indicated by the dotted line, cysts/eggs were washed and transferred to PRD alone. N=6 cysts/ wells per treatment. Data shown are mean ± S.E.M percentage hatch per cyst (A) or well (B). Statistical analysis performed by two-way ANOVA with Tukey post-hoc tests ($P<0.05$) and is in comparison to PRD control.

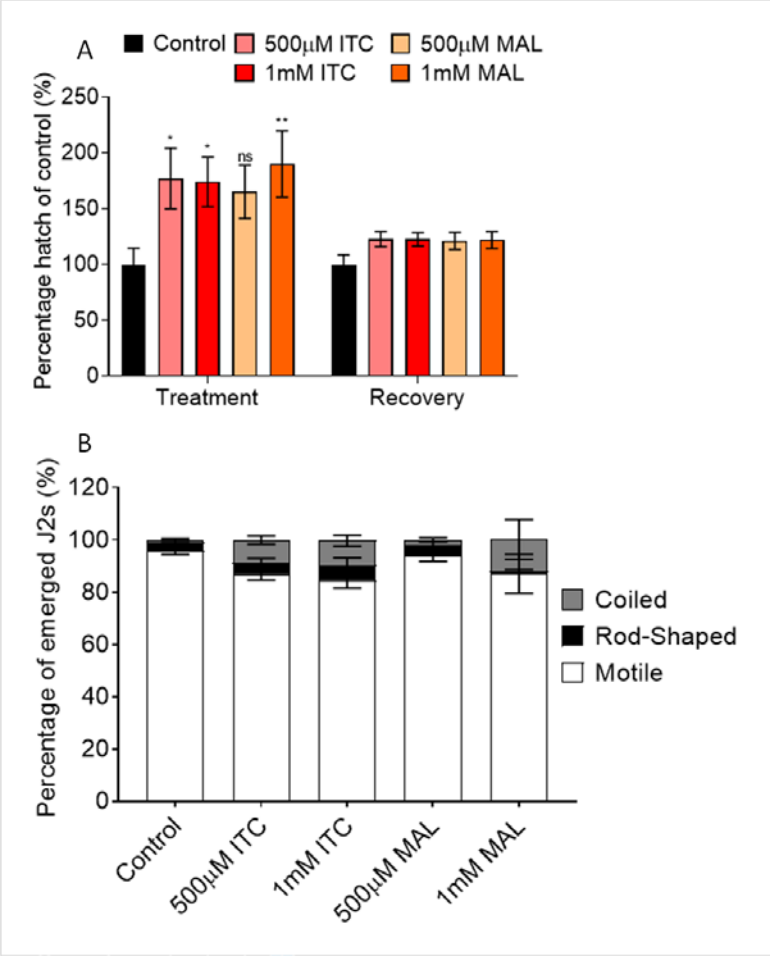

Figure 4.9 Itaconic and malonic acid have no *in ovo* effect on juvenile motility. (A) Cysts were exposed to 500µM and 1mM itaconic acid (ITC) or malonic acid (MAL) for 28 days. Cysts were then washed and transferred to PRD alone and the subsequent hatch during the recovery period (days 28-60) assessed. Data shown is ± S.E.M percentage hatch of control and is pooled from three independent experiments. Statistical analysis performed by two-way ANOVA with Tukey post-hoc tests ($P<0.05$) and is in comparison to PRD control.*$P<0.05$, **$P<0.01$ (B) J2s that emerged during the recovery period following drug wash out were scored for motility and were scored as motile, rod-shaped or coiled. There were no significant differences between the percentages of J2s that appeared motile when compared to the control.

4.2.4 Itaconic acid and malonic acid treatment do not induce hatching in the absence of PRD

Given the enhancement of hatching observed when cysts are co-treated with PRD and itaconic or malonic acid, the hatching assay was performed with the inhibitors alone, in the absence of PRD (Figure 4.10). Itaconic and malonic acid per se did not stimulate hatching. When the cysts were transferred to PRD alone, hatching was initiated but no enhancement of hatching was observed by pre-treatment. The overall yield at the end of the experiment (57 days, 29 days post transfer to PRD) is reduced in cysts that have been pre-treated with itaconic and malonic acid, although not significant in comparison to the H_2O control.

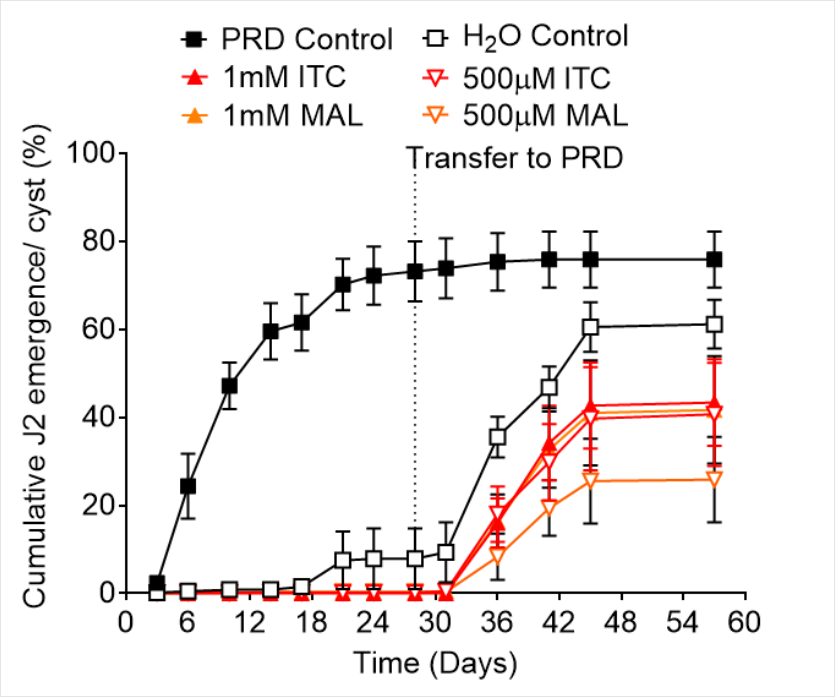

Figure 4.10 Itaconic acid and malonic acid are unable to stimulate *G. pallida* hatching in the absence of PRD. Treatments of 500µM and 1mM itaconic acid (ITC) and malonic acid (MAL) were performed in the absence of PRD. PRD and H_2O controls were performed in parallel. Cysts were exposed to the treatment groups for up to 28 days, washed and then transferred to PRD alone (dotted line). N=6 cysts/ treatment. Data shown is ± S.E.M percentage juvenile emergence/ cyst.

4.2.5 Inhibition of the glyoxylate shunt and TCA cycle by co-treatment with itaconic acid and malonic acid does not result in hatching inhibition

Here I have shown that fluoroacetic acid treatment inhibits *G. pallida* hatching. Fluoroacetic acid inhibits aconitase, which as described, would impact on both the glyoxylate shunt and TCA cycle (Figure 4.11). Inhibiting each of these metabolic routes independently with itaconic acid and malonic acid had no inhibitory effect on hatching. Conversely, enhancement of PRD-induced hatching was observed (Figure 4.8). To further investigate the contribution of these pathways to *G. pallida* hatching, combinations of itaconic, malonic and fluoroacetic acid were applied to *G. pallida* eggs and hatching was recorded (Figure 4.12). All solutions contained PRD to induce hatching and a PRD control was performed in parallel.

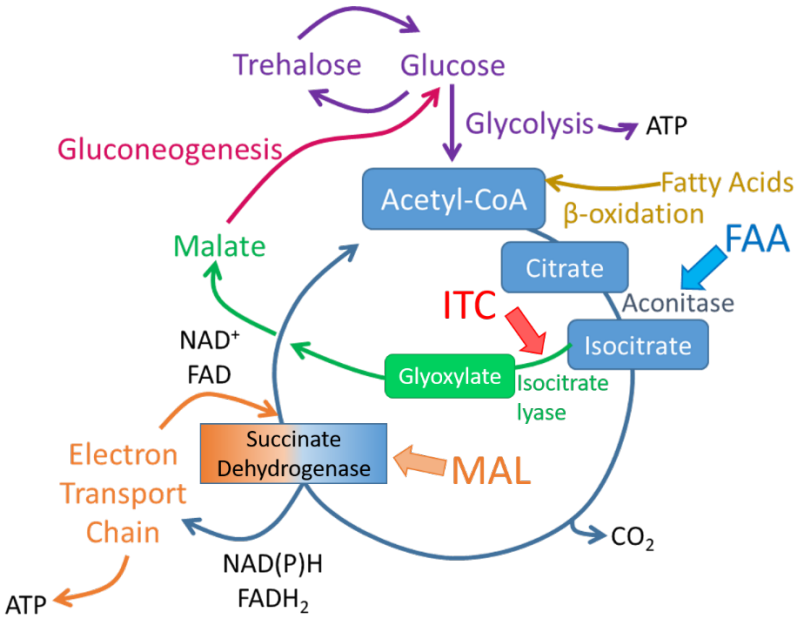

Figure 4.11 Sites of action of fluoroacetic acid, itaconic acid and malonic acid and how the pathways interconnect. Fluoroacetic acid inhibits aconitase, preventing the formation of isocitrate, which is a metabolite in both the TCA cycle and glyoxylate shunt. Itaconic acid inhibits isocitrate lyase, inhibiting the production of glyoxylate in the glyoxylate shunt. Malonic acid inhibits succinate dehydrogenase, which is a key enzyme in both the TCA cycle and ETC.

All solutions containing fluoroacetic acid inhibited hatching, as described when fluoroacetic acid was applied alone (Figure 4.6). The reported limited recovery was also observed. When itaconic acid and malonic acid were applied in combination, hatching was not significantly different from controls, with hatching at the end of the treatment period reaching 48% in comparison to a control hatch of 51%.

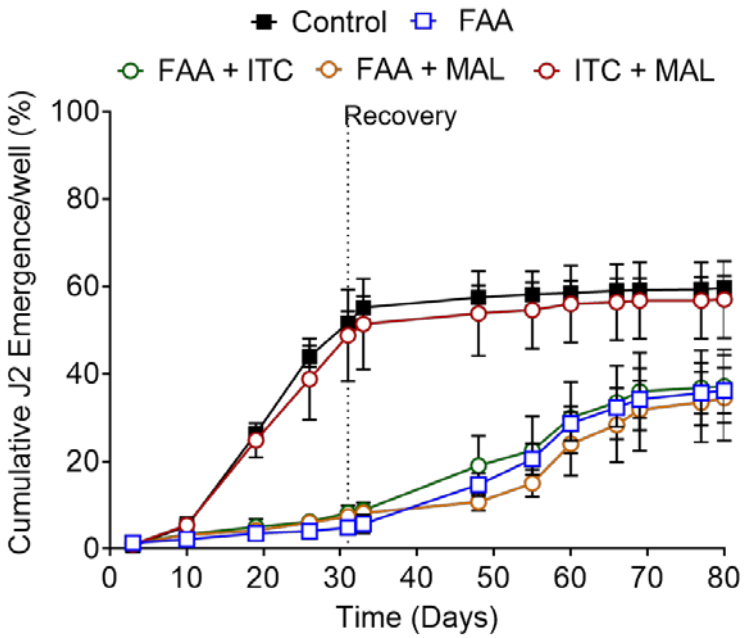

Figure 4.12 Comparison of combined effect of metabolic inhibitors on *G. pallida* hatching. Eggs were exposed to PRD control, 500µM FAA, 500µM ITC + 500µM MAL, 500µM FAA + 500µM ITC and 500µM FAA + 500µM MAL. All solutions contained PRD to stimulate hatch. At 31 days (dotted line) eggs were washed and transferred to PRD alone to assess recovery. N=6 wells per treatment. Data shown are mean ± S.E.M percentage hatch per well.

4.3 Discussion

4.3.1 Effects of perhexiline on *Globodera pallida* hatching

As described in the chapter introduction, acetyl-CoA plays a central role in metabolism (Figure 4.3). In nematodes, it has been described that during non-feeding stages of their life cycle, acetyl-coA is primarily derived from the β-oxidation of fatty acids. Acetyl-CoA is then utilized via the TCA cycle and ETC to generate ATP. Alternatively, there is evidence for the employment of the glyoxylate shunt to utilize lipid-derived acetyl-CoA, which provides a route to generate carbohydrates from stored lipid. Perhexiline inhibits carnitine palmitoyltransferase (CPT) (Kennedy et al., 1996) which was identified by Taylor et al. as a chokepoint enzyme in nematodes. Metabolic chokepoints are reactions defined as consuming or producing a unique substrate or product, and have been shown to be successful anthelmintic targets (Taylor et al., 2013). Inhibition by perhexiline blocks transfer of fatty acids into the mitochondria, preventing sustained metabolic flux from stored lipid and its subsequent provision of carbon for carbohydrate biosynthesis, or its direct utilization in ATP generation via the TCA and ETC. Perhexiline has a reported effect on motility and oxygen consumption rates in *C. elegans, Haemonchus contortus* and *Onchocerca lienalis,* suggesting it is able to target CPT in nematodes (Taylor et al., 2013). It also has reported effects on increasing lipid accumulation in *C. elegans,* further supporting that it is acting at its known target and is resulting in the inhibition of fatty acid oxidation (Kim et al., 2016). Furthermore, in Chapter 5 I provide evidence that perhexiline is able to act on the PPN *G. pallida,* inhibiting juvenile motility following treatment with ≥25µM.

Targeting lipid utilization presents an attractive route to impose disruption to this critical life cycle stage and impart nematotoxic activity. I do not see any inhibition of hatching following treatment with perhexiline. Furthermore, juveniles from treated eggs/cysts emerge without impairment, which would suggest that mobilizing energy from lipids during hatching is not essential to the ability of the juvenile to hatch, or sustain locomotion following *in ovo* exposure. It is important to note that the motility of juveniles was assessed during the recovery period and so the juveniles are hatching into perhexiline-free solution, allowing the effect of *in ovo* exposure to be investigated rather than a direct effect of perhexiline on the hatched juvenile, which is considered in the next chapter.

These results would suggest that juveniles emerge from eggs by employing carbohydrate catabolism to generate ATP. There is evidence for *G. rostochiensis* juveniles utilizing both lipids and carbohydrates post-activation by PRD, with both glycogen and lipid stores significantly depleted in contrast to juveniles not exposed to PRD (Clarke and Hennessy, 1984). Additionally, when comparing the lipid content of *G. rostochiensis* juveniles across different developmental stages, the greatest lipid content was found in hatched J2, with the suggestion that carbohydrates may be converted to lipids during hatching (Holz et al., 1998a). This would be in contrast to *A. avenae,* where glycogen is anabolized from neutral lipids (Cooper and Van Gundy, 1970) and *M. incognita* and *M. arenaria* where lipids are utilized and depleted during hatching (Krusberg et al., 1973).

β-oxidation can be mitochondrial and peroxisomal, with the relative proportions of lipid oxidation activity between each organelle unknown in *C. elegans* (Watts and Ristow, 2017). There is an indication from genetic screens in *C. elegans* that peroxisomal oxidation is important for the breakdown of fats from large lipid droplets (Zhang et al., 2010; Li et al., 2016). CPT is not required for the transfer of fatty acids into the peroxisome, and so therefore, lipid oxidation yielding acetyl-CoA would be able to take place in the peroxisome. As a result, the lack of inhibition that I describe here for perhexiline could be attributable to peroxisomal β-oxidation providing a sufficient input of acetyl-CoA to drive energy producing fluxes necessary for hatching.

The concentration of perhexiline used is consistent with the concentration that was seen to impair *C. elegans* motility and oxygen consumption rate (Taylor et al., 2013). One possibility to consider is that perhexiline is unable to reach the egg- and cyst-protected juvenile at concentrations that result in inhibition of the intended target. Testing higher concentrations was not possible due to the lack of solubility in ethanol and the adverse effects of increasing DMSO vehicle concentration on *G. pallida* hatching (Gaihre et al., 2019). The nematode eggshell, which is described in Chapter 1.3.2, and cyst casing present a barrier to chemical access, which can result in differential ability of chemicals to permeate the lipid bilayers. Perhexiline (Figure 4.13) consists of three six-membered rings, two of which are saturated cyclohexane rings and one a pyridine group. The cyclohexane rings are strongly hydrophobic (Ashrafian et al., 2007), which could result in poor diffusion across the cyst and eggshell barriers.

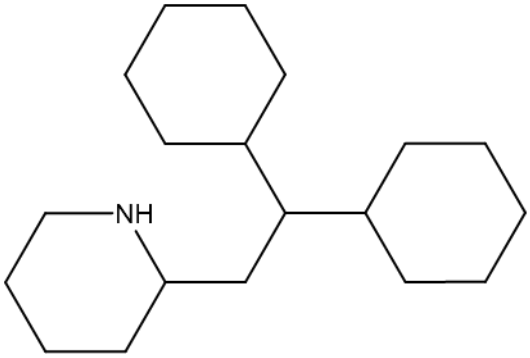

Figure 4.13 The chemical structure of perhexiline. 2-(2,2-dicyclohexylethyl)piperidine

4.3.2 Fluoroacetic acid treatment results in inhibition of *Globodera pallida* hatching

My results suggest that by inhibiting aconitase and preventing the conversion of citrate to isocitrate, which is a key substrate of both the glyoxylate shunt and TCA cycle, fluoroacetic acid is able to inhibit *G. pallida* hatching. By looking at the effects of fluoroacetic acid treatment independently of the effects of itaconic acid and malonic acid, I am unable to determine whether it is the prevention of one or both of these pathways that results in inhibition of hatching. However, it does suggest that flux through acetyl-CoA preceding the TCA cycle or the gloxylate shunt is essential to hatching.

I have shown that at a concentration of 500µM, fluoroacetic acid inhibits hatching from both cysts and isolated eggs, with limited recovery. This is accompanied by a proportion of unhatched eggs appearing granular following treatment. Irreversible inhibition of hatching is associated with necrotic morphology of encysted eggs (Chapter 3.3.1) and is seen following exposure to high concentrations of fluensulfone. The limited recovery that is observed following fluoroacetic acid treatment here, accompanied with a proportion of eggs appearing granular, is consistent with a lack of recovery from compromised eggs. Interestingly, juveniles that were able to hatch during the recovery period behaved like controls, suggesting that a sub-population of juveniles are able to escape the insult and emerge and behave as expected. This hints at fluoroacetic acid being toxic *in ovo* and thus resulting in granulation to only a proportion of unhatched juveniles and not the total population.

The limited recovery that I observe could be explained by a process that makes sub-populations of unhatched juveniles more susceptible to fluoroacetic acid than others. In order for fluoroacetic acid to inhibit aconitase, it combines with coenzyme-A to form fluoroacetyl-CoA, which subsequently combines with oxaloacetate in place of acetyl-CoA to form fluorocitrate (Figure 4.14).

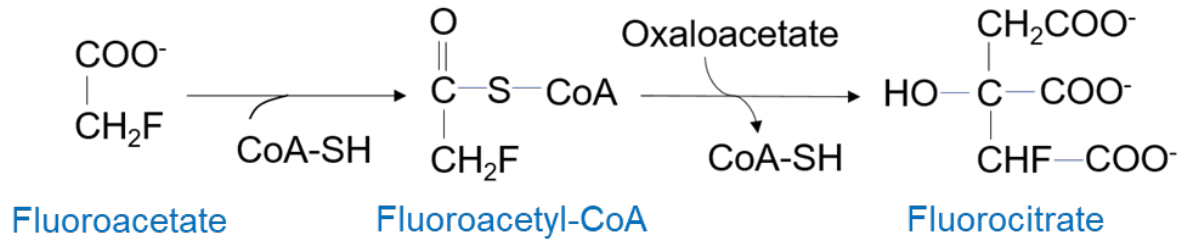

Figure 4.14 Fluoroacetate to fluorocitrate conversion

Fluorocitrate is then able to bind with and inhibit aconitase. This means that for fluoroacetic acid to be inhibitory, there must be accessibility to coenzyme-A and oxaloacetate (Proudfoot et al., 2006). If the unhatched juvenile is not metabolically active, metabolism of fluoroacetate may not occur and so the toxic metabolite that binds to aconitase may not be produced. The removal of these unhatched juveniles and then subsequent activation by PRD may therefore allow a subset of juveniles to hatch that are unaffected by the treatment. To probe this further, it would be interesting to directly look at the effects of fluorocitric acid treatment.

A similar phenomenon has been described following treatment of *H. schachtii* and *C. elegans* with Spirotetramat (SPT)-enol, an insecticide targeting acetyl-CoA carboxylase (ACC) of pest insects and mites that has been developed for use as a nematicide. Non-developing larval stages of both nematode species were unaffected by SPT-enol treatment. This was described to be due to low ATP levels at non-developing stages being insufficient to support inhibition of ACC activity by SPT-enol (Gutbrod et al., 2020). The metabolic state of the nematode is thus an important consideration in assessing these compounds on hatching and other life-cycle stages.

The results reported here have some similarity with the results presented in Chapter 3 with respect to fluensulfone. In these earlier studies, 50µM fluensulfone treatment inhibited hatching and was also followed by limited recovery. This was also associated with a proportion of unhatched eggs becoming granular in appearance. This limited recovery could be indicative of a subset of juveniles being susceptible and an irreversible nematicidal insult. This speculation may have important consequence as fluxes in metabolism are not as detrimental to inactivated juveniles that are then able to escape the insult when drug is removed.

In addition, it has previously been reported that the rapidity of fluoroacetic acid toxicity does not correlate with enzyme activity, suggesting that there is a build-up of toxic metabolites that result in toxicity independently of aconitase inhibition (Lauble et al., 1996). Experiments in *C. elegans* support evidence that fluoroacetic acid can act independently of aconitase inhibition, evidencing that there is a specific effect of fluoroacetic acid on reproduction that is not achieved with co-treatment of itaconic and malonic acid. This suggests that the effect on reproduction is not due to an effect on TCA cycle or glyoxylate shunt activity (Middendorf and Dusenbery, 1993) and should be a consideration when interpreting these results. Co-treatment with itaconic acid and malonic acid in these experiments does not result in inhibition of hatching, which is achieved with fluoroacetic acid treatment. My results could therefore support an effect of fluoroacetic acid that is independent of aconitase inhibition.

4.3.3 Metabolic shifts in the nematode life cycle and the role of the glyoxylate shunt

During an organism's life cycle, it will alternate between states of high and low metabolic activity. This will allow shifts in metabolism to support the distinct demands of the different developmental stages (Penkov et al., 2020). In *C. elegans,* nematodes enter a dauer stage in response to unfavourable environmental conditions (Chapter 1.2.3.1). Dauer larvae are described to be quiescent and entry into this stage is associated with a metabolic shift away from oxidative phosphorylation and towards gluconeogenesis (Penkov et al., 2020). This metabolic transition is regulated by dauer formation genes (*daf*), specifically the FoxO member DAF-16 and nuclear hormone receptor DAF-12. Together with the AMP-activated protein kinase α subunit, AAK-2, which regulates lifespan in response to environmental cues and insulin-signalling (Apfeld et al., 2004), DAF-16 and DAF-12 maintain low catabolism and act in parallel with the steroid hormone pathway to inhibit TCA cycle activity and promote gluconeogenesis, via the employment of the glyoxylate shunt (Erkut et al., 2016; Penkov et al., 2020).

In PCNs, unhatched juveniles exist in a dormant state and exhibit limited metabolic activity. Indeed, there are two distinct stages; diapause and quiescence (Perry and Moens, 2011). These life cycle stages are described in Chapter 1.2.3.

The *G. pallida* life cycle includes both diapause and quiescent stages. For hatching assays with PRD, eggs in diapause will not hatch despite being in the presence of PRD and will have the potential to hatch at later time points when diapause is broken (Kroese et al., 2011). Whilst efforts are made to use cysts that are not in diapause, there are populations of eggs within cysts that will not hatch. This is reflected in the control hatch with PRD where there is less than 100% hatch (Chapter 3 and results presented here). With this in mind, it is not possible to identify how many eggs within a cyst are in diapause or quiescence. In these inhibitor studies, it is therefore important to appreciate the different metabolic requirements at each life cycle stage and how inhibition of the pathways being targeted may differentially effect the juveniles at the different stages.

Despite similarities between *C. elegans* dauer and dormant (diapause and quiescent) *G. pallida* unhatched juveniles, there is a lack of conservation of dauer-associated genes in *G. pallida*, including DAF-12 and DAF-16 (Palomares Ruiz et al 2013, Cotton et al 2014). The glyoxylate shunt, however, which is one of the critical branch points for the determination of lipid-derived acetyl-coA and enables the utilization of stored lipid for the generation of carbohydrates via gluconeogenesis, is employed by *C. elegans* dauer (Erkut et al., 2016). There is evidence of its conservation among PPN species (Mccarter et al., 2003; Kondrashov et al., 2006; Opperman et al., 2008; Lourenço-Tessutti et al., 2015). The evidence in *C. elegans* suggests that in quiescent animals, metabolic networks remain intact and switches between states occur as a result of adjustments to key enzyme ratios, regulated by insulin-like peptides, AMP-activated protein kinase (AMPK) activity and the steroid hormone pathway (Penkov et al., 2020). Although the conservation of key genetic determinants that regulate metabolic transitions in *C. elegans* are not well understood in PPNs, the presence of the glyoxylate shunt could suggest that dormant juveniles exhibit a similar metabolic state to that of dauer larvae, with the promotion of gluconeogenesis achieved by the employment of the glyoxylate shunt.

4.3.3.1 Inhibition of glyoxylate shunt enzyme stimulates PRD-induced hatch

Here, I probed for a role of the glyoxylate shunt during *G. pallida* hatching by treating cysts and eggs with itaconic acid, which inhibits the glyoxylate pathway enzyme, isocitrate lyase. My observations suggest a modest, but significant, stimulatory effect on PRD-induced hatching.

Prior to a hatching stimulus, unhatched juveniles, whether in diapause or quiescence, exhibit a low catabolic rate in order to permit long-term survival (Palomares-Rius et al., 2013). In *C. elegans* dauer*,* a switch to a low catabolic rate is associated with the accumulation of trehalose (Penkov et al., 2020). High concentrations of trehalose can be achieved by the conversion of stored lipids to carbohydrates via the glyoxylate shunt. The glyoxylate shunt is therefore essential in *C. elegans* to prepare for entry into dauer (Erkut et al., 2016). In PPNs, the unhatched juvenile requires a high concentration of trehalose in order to survive harsh environmental conditions (Crowe and Madin, 1975). There is evidence in *G. pallida* that long-term storage of cysts will result in a reduction in juvenile lipids (Holz et al., 1998b) supporting the notion that turnover of lipids to trehalose may be active during dormancy. There is evidence of up-regulated expression of a *trehalose 6-phosphate synthase* gene in PCN dry cysts in comparison to hydrated cysts, reflecting accumulation of trehalose to enable dessication survival (Duceppe et al., 2017). Long-term storage of cysts results in up-regulation of *trehalase*, which converts trehalose to glucose (Duceppe et al., 2017). Up-regulation of these opposing genes prior to rehydration and exposure to a hatching stimulus could therefore reflect the dynamics of trehalose turnover, with its accumulation apparent during early anhydrobiosis and use as an energy source for longer survival.

The importance and function of the glyoxylate shunt in PPNs is therefore less well understood than in *C. elegans*. Relative expression of isocitrate lyase (*ICL)* transcripts during *M. incognita* developmental stages shows that *ICL* levels are highest in pre-parasitic juveniles (non-feeding juveniles prior to root invasion) in comparison to eggs or parasitic stages (Lourenço-Tessutti et al., 2015), suggesting employment of the glyoxylate shunt by juveniles prior to the establishment of a feeding site. Given the relatively low expression of *ICL* in the egg (Lourenço-Tessutti et al., 2015), glyoxylate shunt activity does not seem to be an essential pathway during the unhatched juvenile stage.

The results presented in this chapter suggest that glyoxylate shunt activity is not required for *G. pallida* hatching. Prior to *G. pallida* hatching, metabolic activation of the unhatched juvenile, evidenced by an increase in cyclic AMP (Atkinson et al., 1987; Atkinson and Fowler, 1990) occurs. This suggests that there is a metabolic switch that occurs between the quiescent, unhatched juvenile and one that is activated for hatching. In *C. elegans,* the metabolic switch that controls the transition between growth and diapause is regulated by enzyme ratios at metabolic branch points. For the determination of entry into the TCA cycle or glyoxylate shunt, the branch point is at isocitrate, which can be converted to glyoxylate by isocitrate lyase, or α-Ketoglutarate by isocitrate dehydrogenase (Penkov et al., 2020) (Figure 4.4). In *G. pallida,* the stimulatory effect on PRD-induced hatching as a result of glyoxylate shunt inhibition that I report could reflect changes at this metabolic branch point that promote flux via the TCA cycle. Measuring metabolite and enzyme concentrations in the context of these hatching assays would be a practical next step in providing more clarity to these results. Given that application of itaconic acid in the absence of PRD does not initiate hatching, the results are consistent with a shift in metabolic fluxes stimulating hatch rather than an activation of flux that is non-functional until one triggers hatching.

Interestingly, malonate, which shares its target with fluopyram as a succinate dehydrogenase inhibitor, is unable to inhibit *G. pallida* hatching and also displays a modest stimulatory effect when co-applied with PRD, again suggesting that a shift in metabolic flux can result in an increase in hatching yield. This is in contrast to the results that I reported in the previous chapter for fluopyram, which inhibited *G. pallida* hatching at a concentration of 5µM. The disparity of these results could arise from malonate binding to the succinate-binding pocket (Sierotzki and Scalliet, 2013) and fluopyram binding to the ubiquinone binding site of SDH, which subsequently prevents the reduction of quinone to quinol and the coupled oxidation of succinate. This non-competitive binding of fluopyram would therefore not be overcome by an increase in succinate concentration. It has previously been shown that fluopyram is able to kill *C. elegans,* with an LD_{100} (dose lethal to 100% of the nematodes tested) of 0.469µM in contrast to malonate which was shown to have an LD_{100} of >120µM, which was the highest concentration tested (Burns et al., 2015). This is reflected in my observations here, where fluopyram is able to potently inhibit *G. pallida* hatching, whereas malonate is not, despite both acting to inhibit SDH.

4.4 Summary

The controlled regulation of metabolic shifts are critical in the transition from one developmental stage to another, such as the transition from a quiescent, unhatched juvenile to an activated, hatched juvenile (Atkinson et al., 1987; Atkinson and Fowler, 1990). Here, I have investigated key metabolic fluxes that were hypothesised to be important in *G. pallida* hatching through application of specific inhibitors, with a view to better understanding the metabolic requirements for *G. pallida* hatching and subsequently how fluensulfone may be acting to disrupt these. Interestingly, perhexiline treatment did not inhibit hatching. This could suggest that *G. pallida* are able to utilize an alternative substrate other than lipids to provide energy during the hatching process or that breakdown of lipids in the peroxisome is sufficient to drive hatching. However, it must also be considered that perhexiline is unable to act on the unhatched juvenile. Other inhibitors of β-oxidation, including peroxisomal β-oxidation, should therefore be considered to determine the importance of lipid fluxes on *G. pallida* hatching.

I have demonstrated that by inhibiting ATP producing flux through acetyl-coA, via inhibition of aconitase, hatching is irreversibly inhibited and juveniles that hatch upon drug removal are able to hatch without impairment. In contrast, I have shown that interfering with the glyoxylate shunt augments PRD-inducement of hatching, suggesting that glyoxylate shunt activity is not required for the transition from quiescence to eclosion. My results here suggest that by inhibiting flux via the glyoxylate shunt, increased stimulation of hatching can be achieved, and that this is likely linked to the increase in flux via alternative, energy-producing pathways that will be more favourable for hatching, such as the TCA cycle and ETC. As discussed, measuring metabolite and enzyme concentrations and how these are impacted by inhibitor treatment will be critical in understanding these pathways further.

Chapter 5 Investigations of the Metabolic Basis for Inhibited Lipid Depletion by Fluensulfone

5.1 Introduction

During the juvenile's life cycle, it will undergo numerous metabolic transitions, from states of quiescence through to activation and more energy demanding developmental stages (Chapter 1.2.3). Understanding shifting metabolic flux that supports energy production at each life cycle stage, and how fluensulfone might interfere with these fluxes, will provide important insight into mode of action. This will define or provide a better platform to resolve the discrete targets that underpin fluensulfone's mode of action.

I have so far discussed the effects of fluensulfone on *G. pallida* eggs and have used comparative nematicide and inhibitor studies to probe for the mechanism of action that underpins fluensulfone's inhibitory effect on hatching. In this chapter, I investigate the effects of fluensulfone on the hatched, non-feeding J2. Most investigations assessing the action of fluensulfone as a nematicide have focused on its effects on the pre-parasitic, infective juvenile stage (Oka et al., 2009; Oka et al., 2012; Oka, 2014; Norshie et al., 2016; Oka and Saroya, 2019). Whilst these studies have been paramount in confirming fluensulfone's nematicidal potential, they have not addressed the mechanism by which fluensulfone acts to bring about its effects.

5.1.1 Fluensulfone elicits a progressive metabolic insult

As was described in Chapter 4.1, there is evidence for fluensulfone eliciting a progressive metabolic impairment that is associated with an impairment to lipid utilization (Kearn et al., 2017). The evidence for metabolic inhibition is based on the progressive loss of MTT staining that is accompanied with loss of motility (Kearn et al., 2017). MTT staining acts as a measure of the NADH/NADPH levels that are sustained by metabolic fluxes. When MTT is reduced, it yields a water insoluble violet-blue formazan precipitate and thus is used as a metabolic stain for cell viability (Mosmann, 1983). Modifications of the MTT assay have been successfully applied to assess the viability of free-living larvae, with living *C. elegans* able to take up and reduce MTT, providing a visual assessment of viability (James and Davey, 2007) (Chapter 1.5.4.1). Loss of this reducing potential can arise through disruption at several steps. In the experiments described in this chapter, I use MTT staining to probe for an organismal overview of metabolism.

Most nematodes are able to generate energy in the form of ATP, by oxidising substrates via oxidative pathways; glycolysis, the citric acid (TCA) cycle and the electron transport chain (ETC). Glycolysis and the TCA cycle convert NAD^+ and FAD to their reduced forms, NADH and $FADH_2$. These are then re-oxidised by mitochondrial membrane enzyme complexes of the ETC. Oxidation of NADH and $FADH_2$ is exergonic, providing the energy required to drive the synthesis of ATP. In contrast, anabolic pathways are largely associated with $NADP^+$/NADPH oxidation/reduction reactions.

It was previously observed in *G. pallida* that treatment with the succinate dehydrogenase inhibitor, fluopyram, results in a rapid loss of MTT staining, in contrast to the progressive loss of MTT staining that is observed with a range of fluensulfone concentrations (Figure 5.1). This exemplifies how interference with the oxidative pathways described can lead to nematotoxicity.

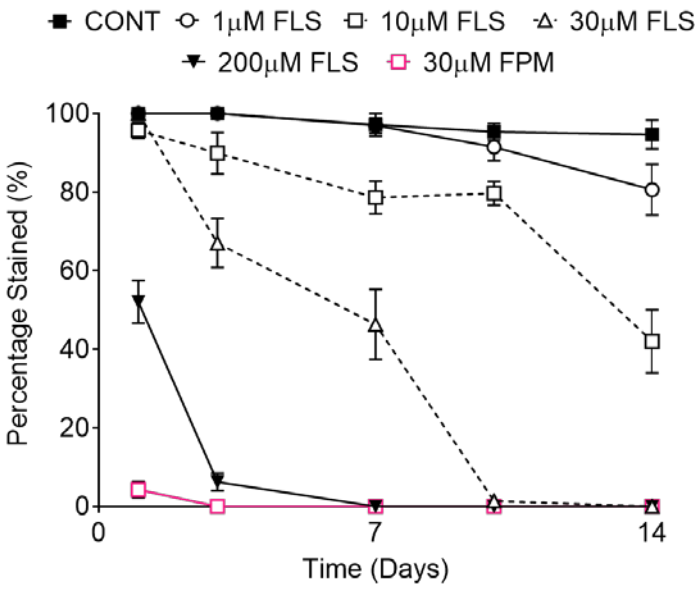

Figure 5.1 Fluopyram treatment results in a rapid loss of metabolic activity. *G. pallida* J2s were exposed to the indicated concentrations of fluensulfone (FLS) and 30μM fluopyram (FPM) for up to 14 days. At each time point, >10 J2s were removed from solution and soaked in 5mg/ml MTT solution for 24 hours in order to assess metabolic activity. At 24-hours post-staining, the number of J2s that were stained were recorded. Data shown are ± S.E.M percentage of J2s that were stained. N= 7 wells per treatment group. Statistical analysis performed by two-way ANOVA with Tukey post-hoc tests ($P<0.05$) in comparison to the control. Data summarised from (Kearn, 2015).

Metabolic flux from acetyl-CoA, which plays a central role in metabolism (Fuchs and Berg, 2014), is dependent on the metabolic requirements of the nematode dependent on developmental stage (Chapter 1.2.3). As shown in Figure 5.1, inhibiting flux via the ETC results in a rapid loss of MTT staining, indicating that inhibition of the ETC is nematicidal. In this chapter, I extend the comparative approach taken in the previous chapter to the hatched juvenile, comparing the effects of selective inhibitors of distinct steps of essential metabolic fluxes with fluensulfone. Here, I use fluoroacetic acid to inhibit TCA cycle activity (Chapter 4, Figure 4.2), which will generate the substrates used in the ETC to generate ATP, and evaluate the time-dependent effect of metabolic inhibition.

Acetyl-CoA is the key entry point into the TCA cycle which drives subsequent associated oxidative phosphorylation. Acetyl-CoA can be carbohydrate or lipid derived (See Chapter 4, Figure 4.4) and the initial source is context dependent. Carbohydrate and lipid metabolism pathways converge, with routes to generate carbohydrate from stored lipid (See Chapter 4.1.3) and carbons from dietary carbohydrates converted to acetyl- CoA, where they can be diverted into fatty acid synthesis (Watts and Ristow, 2017). Lipid-derived acetyl-CoA is particularly important during non-feeding stages associated with the life cycle of PPNs, as lipids are their predominant long-term energy stores (Holz et al., 1997). Given the dependence of non-feeding PPN juveniles on their lipid stores, and the indication from Nile red staining that fluensulfone prevents access to stored lipid (Kearn et al., 2017) (Chapter 4.1.1), I have used inhibitor studies to directly compare the effects of fluensulfone with perhexiline (Chapter 4, Figure 4.1). Inhibitor studies benchmarking against the effects of fluensulfone on the hatched juvenile are important in dissecting the involvement of metabolic pathways at this life cycle stage, due to the inability to use other mechanisms to probe at these pathways, for example RNAi. Lipid utilization is a vital pathway to investigate due to the reliance of the juvenile on its lipid stores prior to establishing a feeding site. Interestingly, my results described in the previous chapter suggest that perhexiline is unable to inhibit hatching, which could suggest that the energy producing fluxes used for hatching are not lipid-derived. However, it must also be considered that fat oxidation can be peroxisomal, which would not be inhibited by perhexiline, and so flux from lipid-derived acetyl-coA could remain intact. Perhexiline has a reported effect on motility and oxygen consumption rates in *C. elegans* (Taylor et al., 2013), and acts to increase lipid accumulation (H.E. Kim et al., 2016) (See Chapter 4.3.1). It is therefore interesting to probe for an effect on metabolism and lipid droplet stores in the PPN *G. pallida.*

5.1.2 Investigating lipid metabolism as a route to fluensulfone's nematicidal action

Fatty acids are liberated from lipid storage organelles known as lipid droplets. These structures are monolayer lipid ensheathing structures defined by a number of organelle associated proteins that encapsulate neutral lipids (Olzmann and Carvalho, 2019) (Figure 5.2). Lipid droplets are dynamic organelles with a vital function in lipid and energy homeostasis. This is regulated through alternating phases of lipolysis and lipophagy, reflecting changes in cellular metabolism and nutrient availability, where they are able to deliver fatty acids to the mitochondria for their consumption as an alternative energy source during nutrient depletion (Rambold et al., 2015). Their control extends to buffering cellular amounts of potentially toxic free fatty acids, which if left unregulated will result in lipotoxicity and oxidative stress (Nguyen et al., 2011; Olzmann and Carvalho, 2019). Activated lipases are used to liberate the stored neutral lipid and provide the substrate for the 2-carbon catabolism that generates acetyl-CoA for utilization by the TCA cycle (Rambold et al., 2015).

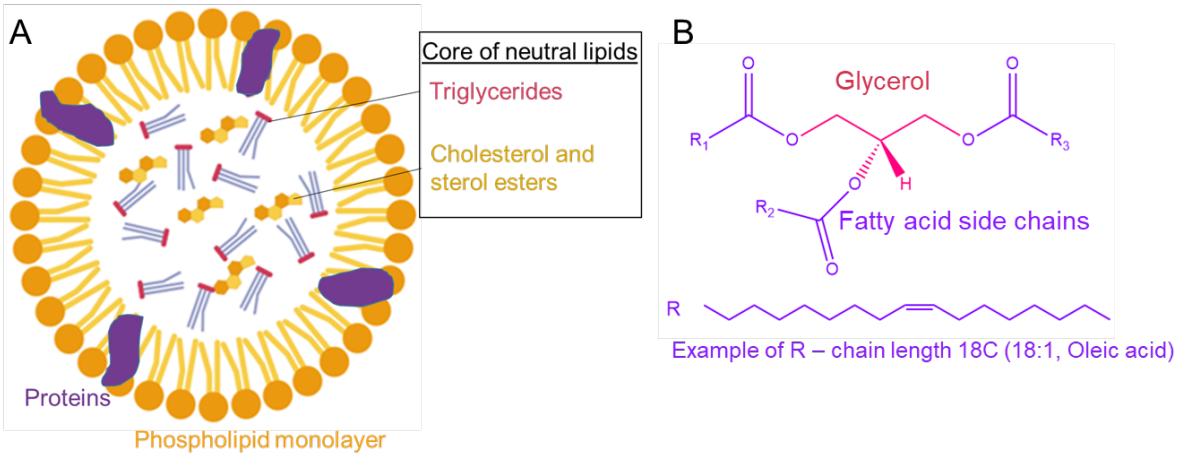

Figure 5.2 Lipid droplet organisation consists of a core of neutral lipids. (A) Lipid droplets consist of a phospholipid monolayer studded with specific proteins to regulate lipid droplet dynamics and a core of neutral lipids, which include triglycerides and sterols. (B) Triglycerides are the predominant storage lipid. Their structure consists of a glycerol backbone esterified to three fatty acid side chains. Fatty acids are characterized by repeating methylene groups, which can vary in length and degree of saturation.

In the free-living, non-feeding *G. pallida* juvenile, neutral lipids constitute approximately 70% of the lipid content (Holz et al., 1997). This observation is based largely on chromatographic studies of extracted lipids, but is also supported by varying imaging approaches, including vital dyes and electron microscopy.

This has recently been reinforced by label free interrogation of lipid droplet stores using CARS spectroscopy (Smus et al., 2017). CARS spectroscopy has the ability to resolve stereotypical chemical signatures with anatomical localization that overcomes limits of previous approaches. In the case of lipid droplets, the abundant signal is from the numerous C-H bonds associated with the fatty acid side chains of triglycerides (Figure 5.2). Previous optimization in *G. pallida* has enabled semi quantitative measurement of depleting lipids at increasing times post hatching, consistent with lipid stores being required during the infective J2 stage as the nematode locates and invades host roots (Wright et al., 1989; Smus et al., 2017).

5.1.3 Chapter Aims

In this chapter I compare fluensulfone with fluoroacetic acid and perhexiline for their effect on motility and metabolism, building on the previously reported effects of fluensulfone on *G. pallida* juveniles (Kearn et al., 2017). These behavioural assays of nematicidal potency are combined with the dynamics of histological staining and cross referenced to CARS spectroscopy to assess metabolic activity and its consequence for the integrity of the critical lipid droplet stores.

5.2 Results

5.2.1 Fluensulfone results in a time- and dose-dependent decrease in motility and metabolic activity

G. pallida J2s were treated with fluensulfone for up to 14 days. J2s were assessed for motility and MTT staining at indicated time points during this optimized treatment period. I observed a time- and dose-dependent decrease in motility (Figure 5.3). As dose increases from 5µM to 500µM, the absolute inhibition in comparison to controls at 14 days increases from 59% to 92%. Similarly, the onset and speed of inhibition is dose dependent. Fluensulfone significantly inhibits motility as early as day 3, with 5µM FLS treatment resulting in 14% inhibition compared to 87% inhibition with 500µM (Figure 5.3A).

These dose dependent effects on motility are accompanied by a dose-dependent loss of MTT (Figure 5.3B). Following treatment with 5µM FLS for 14 days, there is a 59% inhibition of staining. This increases to 97% inhibition following treatment with 500µM.

In addition to a loss of MTT staining, I noted a redistribution of predominant staining following fluensulfone exposure that has previously been reported (Kearn et al. 2017). Prior to a complete non-staining, there is a loss of anterior staining and a shift to discernible posterior staining that is not evident in the control worms (Kearn et al. 2017) (Figure 5.4).

The observed description of redistribution of staining was quantified by visually scoring the region of predominant staining as anterior or posterior. Juveniles were also noted as being stained throughout if there was no distinction between predominant anterior or posterior staining, weakly stained or unstained. This analysis showed a shift in staining from day 1, with a greater proportion of J2s appearing predominantly posterior stained following treatment with all concentrations of fluensulfone relative to controls. This shift in staining is more marked as the experiment progressed across the treatment period (Figure 5.5).

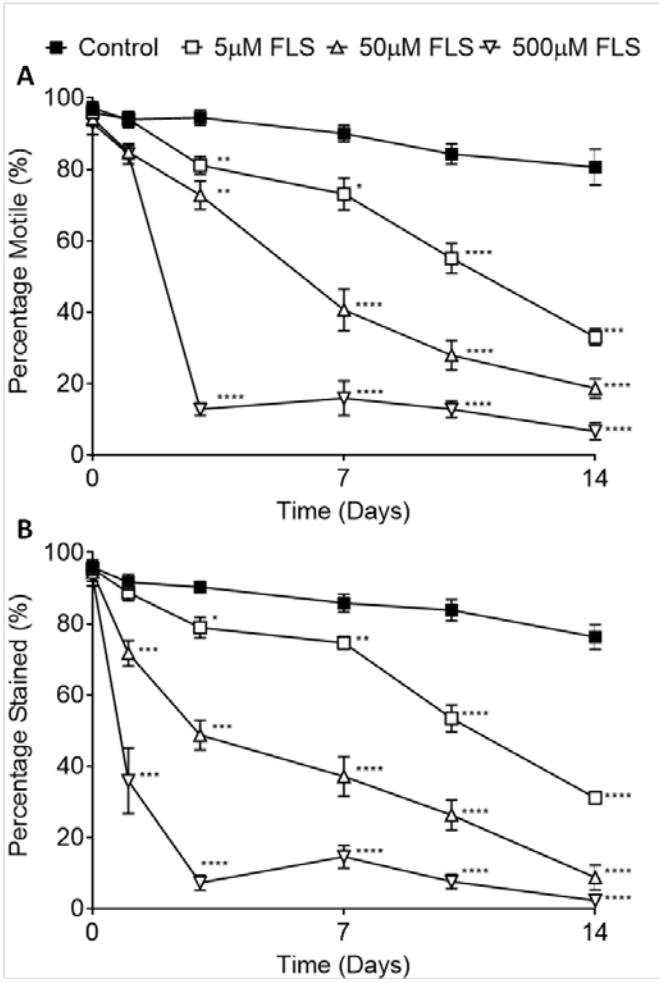

Figure 5.3 Prolonged fluensulfone exposure results in a time- and dose-dependent decrease in motility and metabolic activity of *G. pallida* J2s. (A) *G. pallida* J2s were exposed to the indicated concentrations of fluensulfone (FLS) for up to 14 days. At each time point, >10 J2s per well were removed from solution and juvenile motility was recorded. (B) J2s were then soaked in 5mg/ml MTT solution for 24 hours. 24-hours post-staining, the number of J2s stained was recorded. Data shown are ± S.E.M percentage of J2s that appear motile (A)/ were stained (B). N=6 wells per treatment group, with >10 J2s assayed per well. Data is pooled from two independent experiments, resulting in >120 J2s assayed per treatment. Statistical analysis performed by two-way ANOVA with Tukey post-hoc tests ($P<0.05$) in comparison to the control.

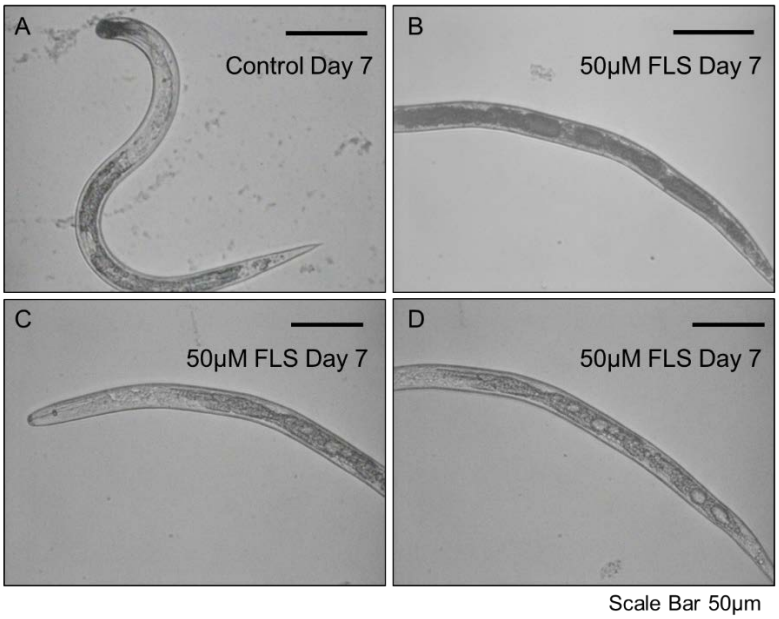

Figure 5.4 Fluensulfone results in shift of MTT staining to posterior. Representative images to show the distribution of MTT staining in control (A) and fluensulfone treated (B, C, D) *G. pallida* juveniles. (A) At 7 days post-hatch, control juveniles exhibit predominant anterior staining. At day 7, a proportion of 50µM fluensulfone treated juveniles are stained, however, stain predominantly in the posterior (B). The majority of juveniles are unstained in the anterior (C) and posterior (D).

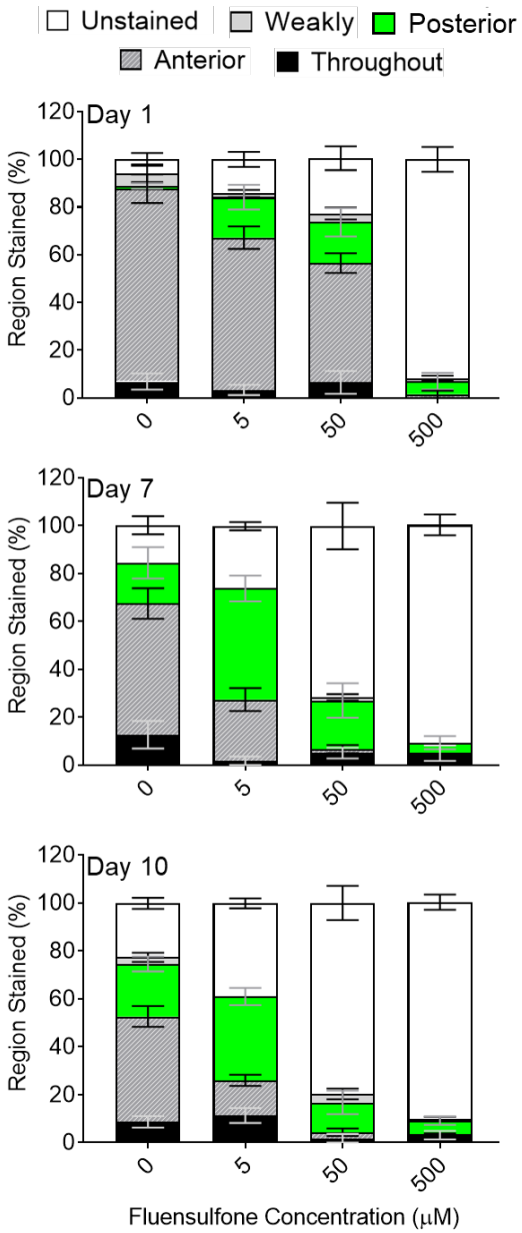

Figure 5.5 Fluensulfone treatment of J2s results in redistributed MTT staining prior to death. *G. pallida* J2s were exposed to the indicated concentrations of fluensulfone for up to 14 days. At indicated time points, J2s were removed from treatment solutions, washed and incubated with 5mg/ml MTT for 24-hours. 24-hours post-staining, the number of J2s stained was recorded. The distribution of observed staining was also recorded as unstained, weakly, posterior, anterior or stained throughout. This data is shown above for days 1, 7 and 10. Data shown are ± S.E.M percentage of region stained. N= 6 wells per treatment, with >10 J2s per well.

5.2.2 Perhexiline is nematicidal to free-living *Globodera pallida* juveniles and leads to re-distributed MTT staining

Lipid-derived acetyl-CoA is critical for oxidative phosphorylation during non-feeding life cycle stages. This is controlled by fatty acid transfer into the mitochondria by carnitine palmitoyltransferase (CPT), which is inhibited by perhexiline (PER) (Kennedy et al., 1996) (see Chapter 4).

Perhexiline treatment results in a dose-dependent decrease in motility and metabolic activity (Figure 5.6). The phenomenon of shifted staining to the posterior observed with fluensulfone treatment is also noted during perhexiline treatment (Figure 5.7).

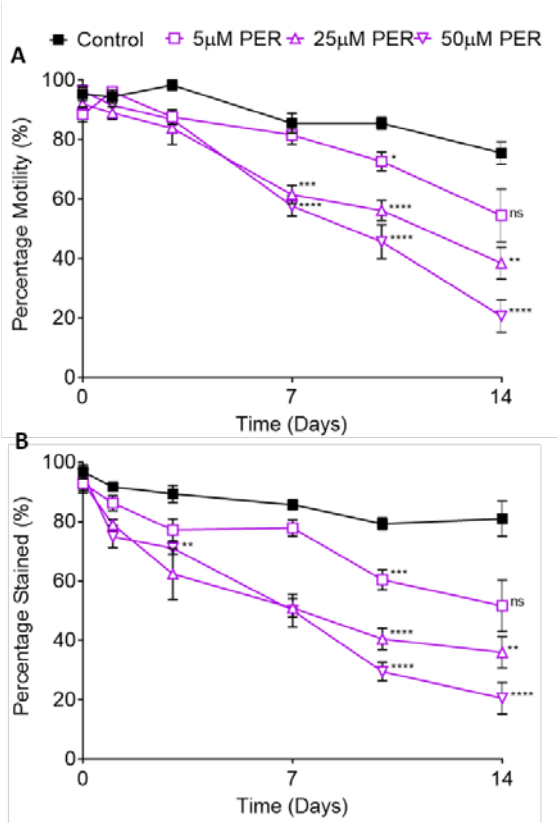

Figure 5.6 Prolonged perhexiline treatment impairs motility and metabolism of *G. pallida* J2s. (A) *G. pallida* J2s were exposed to the indicated concentrations of perhexiline (PER) for up to 14 days. J2s were removed from solution and the proportion immotile recorded. (B) J2s were then soaked in 5mg/ml MTT solution for 24 hours. Data shown are ± S.E.M percentage of J2s that appear motile (A)/ were stained (B). N=6 wells per treatment group, with >10 J2s assayed per well. Data is pooled from two independent experiments, resulting in >120 J2s assayed per treatment. Statistical analysis performed by two-way ANOVA with Tukey post-hoc tests (P<0.05) in comparison to the control.

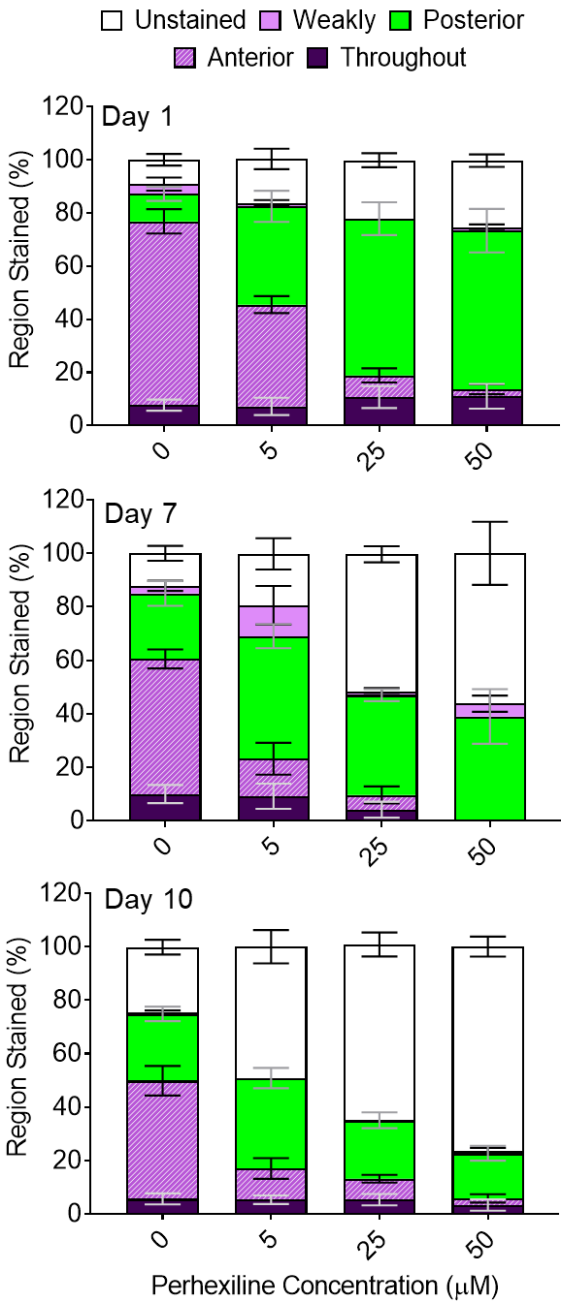

Figure 5.7 Perhexiline re-distributes MTT staining akin to fluensulfone treatment. *G. pallida* J2s were exposed to the indicated concentrations of perhexiline for up to 14 days. J2s were removed from treatment solutions, washed and incubated with 5mg/ml MTT for 24-hours. At 24-hours post-staining, the number of J2s stained was recorded. The distribution of predominant staining was also recorded as unstained, weakly, posterior, anterior or stained throughout. This data is shown above for days 1, 7 and 10. Data shown are ± S.E.M percentage of region stained. N= 6 wells per treatment, with >10 J2s per well.

5.2.3 Fluoroacetic acid is nematicidal to *Globodera pallida* juveniles

Treatment with fluoroacetic acid results in a loss of motility and an associated change in MTT staining in *G. pallida* J2s (Figure 5.8). Like fluensulfone and perhexiline, treatment results in a progressive decrease in the proportion of J2s that appear motile and this is accompanied by a loss of MTT staining.

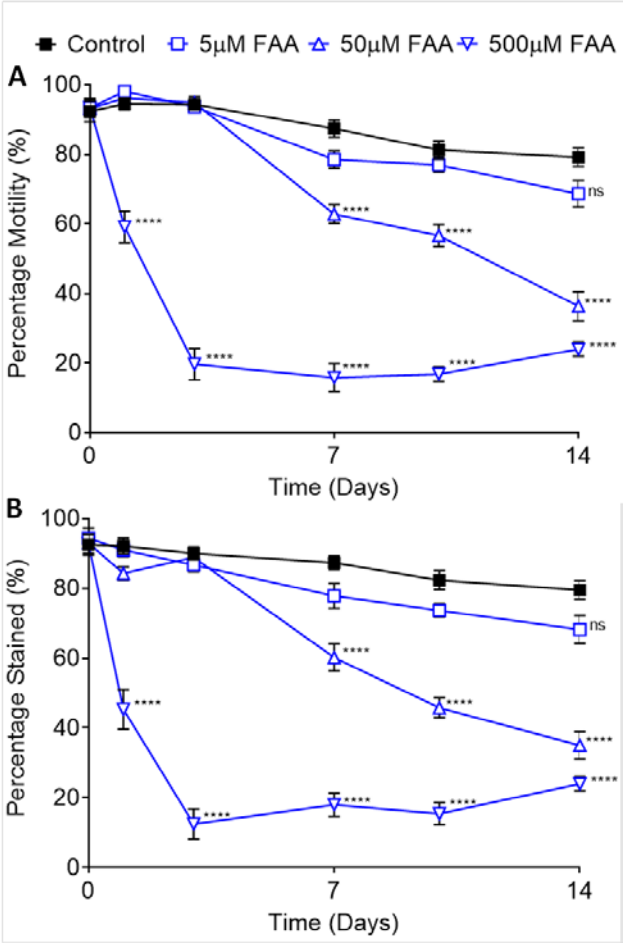

Figure 5.8 Prolonged fluoroacetic acid exposure results in the immotility and death of *G. pallida* J2s. (A) *G. pallida* J2s were exposed to the indicated concentrations of fluoroacetic acid (FAA) for up to 14 days. At each time point, >10 J2s were removed from FAA solution and the number of immotile J2s was recorded. (B) At each time point, the J2s were then soaked in 5mg/ml MTT solution for 24 hours. At 24-hours post-staining, the number of J2s that were stained were recorded. Data shown are ± S.E.M percentage of J2s that appear motile (A)/ were stained (B). N=6 wells per treatment group, with >10 J2s assayed per well. Data is pooled from two independent experiments, resulting in >120 J2s assayed per treatment. Statistical analysis performed by two-way ANOVA with Tukey post-hoc tests ($P<0.05$) in comparison to the control.

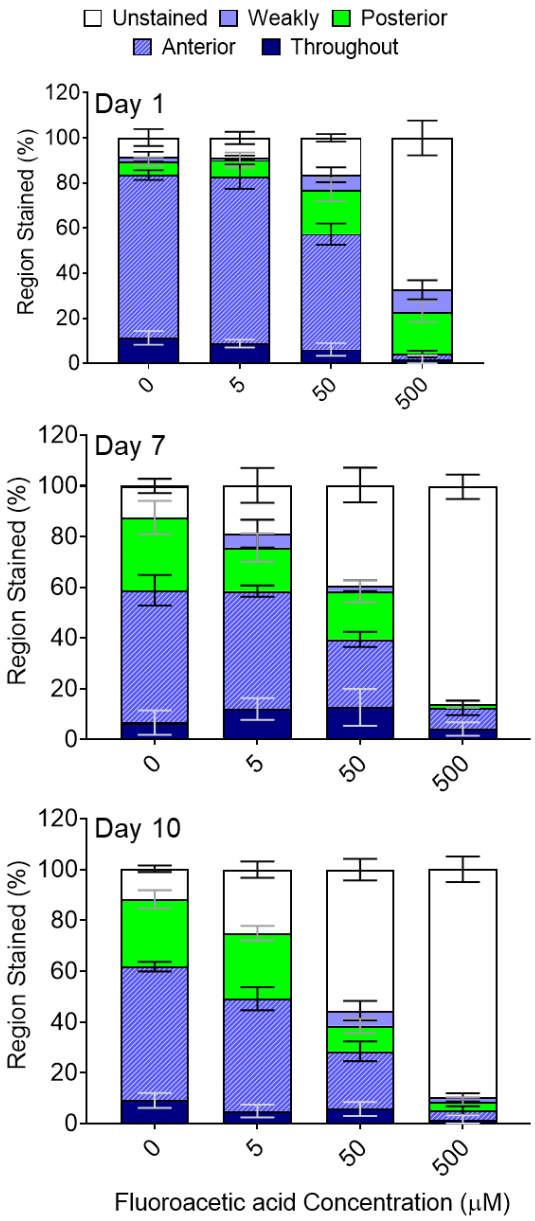

Figure 5.9 Fluoroacetic acid treatment of J2s reduces, but does not redistribute, MTT staining during the progressive intoxication. *G. pallida* J2s were exposed to the indicated concentrations of fluoroacetic acid for up to 14 days. At set time points, J2s were removed from treatment solutions, washed and incubated with 5mg/ml MTT for 24-hours. At 24-hours post-staining, the number of J2s stained was recorded. The distribution of predominant staining was also recorded as unstained, weakly, posterior, anterior or throughout. This data is shown above for days 1, 7 and 10. Data shown are ± S.E.M percentage of region stained. N= 6 wells per treatment with >10 J2s per well.

In contrast, and different to fluensulfone and perhexiline treatment, FAA did not result in a shift in predominant staining. As staining was lost, juveniles that remained stained did so by expressing histochemical responses from the anterior region (Figure 5.9).

5.2.4 Direct comparisons of chemical treatment

In order to directly compare the potency of each inhibitor on motility and metabolic activity, I quantified percentage inhibition for motility and MTT staining at day 7 (Table 5.1). A dose-dependent increase in percentage inhibition for motility and MTT staining was seen for each inhibitor tested. At later time points, it is difficult to distinguish between the range of concentrations tested, with the higher concentrations of 50 and 500µM fluensulfone converging at 100% inhibition of motility and MTT staining. This suggests that prolonged exposure to lower concentrations can result in the same effect as treatment with higher concentrations, eluding to accumulating action.

Inhibitor	Concentration (µM)	Percentage inhibition motility (%)	Percentage inhibition MTT staining (%)
Fluensulfone	5	18.5	20.5
	50	55.0	56.8
	500	81.9	83.1
Perhexiline	5	12.3	16.8
	25	28.0	40.4
	50	37.7	45.6
Fluoroacetic acid	5	10.3	10.9
	50	28.2	31.1
	500	81.9	79.6

Table 5.1 Percentage inhibition at day 7 for effects on *G. pallida* juvenile motility and MTT staining. Comparison of the effects of fluensulfone, perhexiline and fluoroacetic acid on *G. pallida* juvenile motility and MTT staining following 7 days treatment. Percentage inhibition calculated from figures Figure 5.3, Figure 5.6 and Figure 5.8 in comparison to paired controls.

To determine the relative potency of the compounds tested I estimated EC_{50} values for effects on motility and MTT staining at day 7. This resulted in an order of potency based on estimated EC_{50} values of fluensulfone (41 µM)> perhexiline (87 µM)> fluoroacetic acid (117 µM) for motility and fluensulfone (42 µM)> perhexiline (52 µM)> fluoroacetic acid (112 µM) for MTT staining.

In view of the distinct dynamics of the MTT staining following the different metabolic inhibitions, I made a direct comparison of the distribution of the stain between the anterior and posterior regions (Figure 5.10). This comparison highlights that fluensulfone and perhexiline exhibit similar loss and redistribution of histological stains during toxicity that are not observed with a generalised metabolic insult achieved with fluoroacetic acid treatment. This supports the notion that fluensulfone and perhexiline may act in a common or overlapping mode of action pathway. The loss of staining suggests that both exhibit a slow accumulating insult, in which MTT formazan precipitates in the posterior during intermediate toxicity.

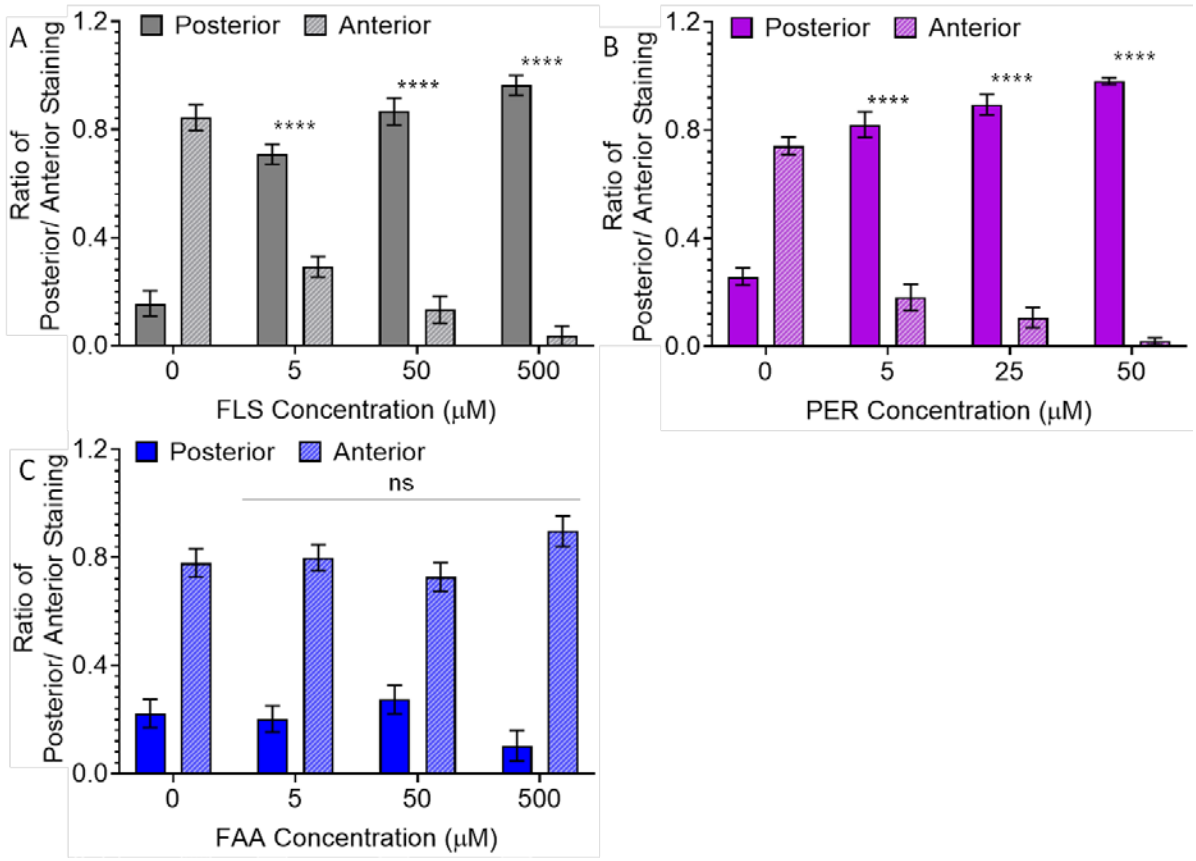

Figure 5.10 Comparison of the relative distribution of MTT formazan during fluensulfone, perhexiline and fluoroacetic acid treatment 7 days post-hatch. Combined data from Figures 5.4, 5.6 and 5.8. Data is normalised to show the relative proportions of posterior and anterior staining for juveniles that stained; unstained juveniles are excluded. Data is pooled from two independent experiments. Statistical analysis performed by two-way ANOVA with Tukey post-hoc tests ($P<0.05$) in comparison to the vehicle control (0µM).

5.2.4.1 MTT formazan partitions into hydrophobic environments

The MTT-formazan assay is based on the reduction of MTT, a pale yellow, water-soluble compound, by cellular dehydrogenases, yielding a water insoluble violet-blue formazan (Mosmann, 1983). In this way, it can be used to evaluate cell viability (Mosmann, 1983) and has been adapted to assess *C. elegans* (James and Davey, 2007) and *G. pallida* (Kearn et al., 2017). Many studies utilizing the MTT-formazan assay have assumed that it is an indicator of mitochondrial function. Although the reduction of MTT can be achieved by mitochondrial NADH, the use of the assay as a direct measure of mitochondrial activity is inaccurate, given that there are other reducing intracellular agents that will reduce MTT (Stockert et al., 2012).

MTT formazan will accumulate in lipid droplets, due to the high lipophilicity of the formazan precipitate (Stockert et al., 2012). As lipids are selectively stored in the posterior region in *G. pallida* J2s (Smus et al., 2017), I hypothesised that the shared staining following fluensulfone and perhexiline treatment represented MTT formazan partitioning into lipid stores that are failing to be depleted, due to an impairment to lipid utilization. This idea was investigated using CARS to visually detect neutral lipid stores in control, fluensulfone and perhexiline treated worms.

5.2.5 CARS data supports an impairment to lipid utilization in *Globodera pallida* J2s following fluensulfone and perhexiline exposure

Coherent anti-Stokes Raman spectroscopy (Chapter 1.5.5.1.1) was used to image lipids in live *G. pallida* juveniles. To do this, juveniles were subjected to designated treatment, washed and mounted onto an agarose pad on a glass slide. The samples were then subjected to CARS analysis by using two lasers; a pump and Stokes beam, where the anti-Stokes signal was tuned to the symmetrical stretching vibration at 2845 cm^{-1}. This allows the selective resolution of the CH_2 stretching vibration that is abundant to triglycerides, the most abundant single lipid constituent of J2 PPN and the predominant component of lipid droplets, where it constitutes up to 70% of their composition (Holz et al., 1997). The juveniles were imaged in two parts; anterior (head−abdomen) and posterior (abdomen−tail). Imaging of freshly hatched untreated worms displayed weak CARS signal from the anterior region, apart from a bright signal corresponding to the stylet knob. The CARS signal tuned to the vibrational frequency of neutral lipid was strongest from the posterior region of the juvenile. This is consistent with previous CARS analysis, highlighting that storage lipids in the form of lipid droplets are selectively stored in the posterior region of J2s (Smus et al., 2017). Subsequent imaging of juveniles at increasing times post-hatch indicate a decreasing CARS signal in the posterior region (Figure 5.11), which is consistent with previous reports of an essential post-hatch utilization of stored lipids (Storey, 1984).

Juveniles were treated with 30µM fluensulfone for 7 and 14 days. In comparison to the control, there were no significant differences between the CARS signal tuned to the vibrational frequency of neutral lipid from the anterior region (data not shown). In contrast, the CARS signal from the posterior regions relative to the parallel untreated controls is significantly higher Figure 5.11. This is consistent with the neutral lipids stored in lipid droplets, from which the signal is derived, being retained relative to controls. Treatment with 50µM perhexiline also resulted in a relatively higher CARS signal from the posterior region when compared to controls. This indicates that both treatments result in J2s being less able to draw on their lipid stores that would otherwise be important in maintaining the free-living, non-feeding J2 stage. This is entirely consistent with the known mode of action for perhexiline, which has been shown to result in lipid accumulation in *C. elegans* (Kim et al., 2016).

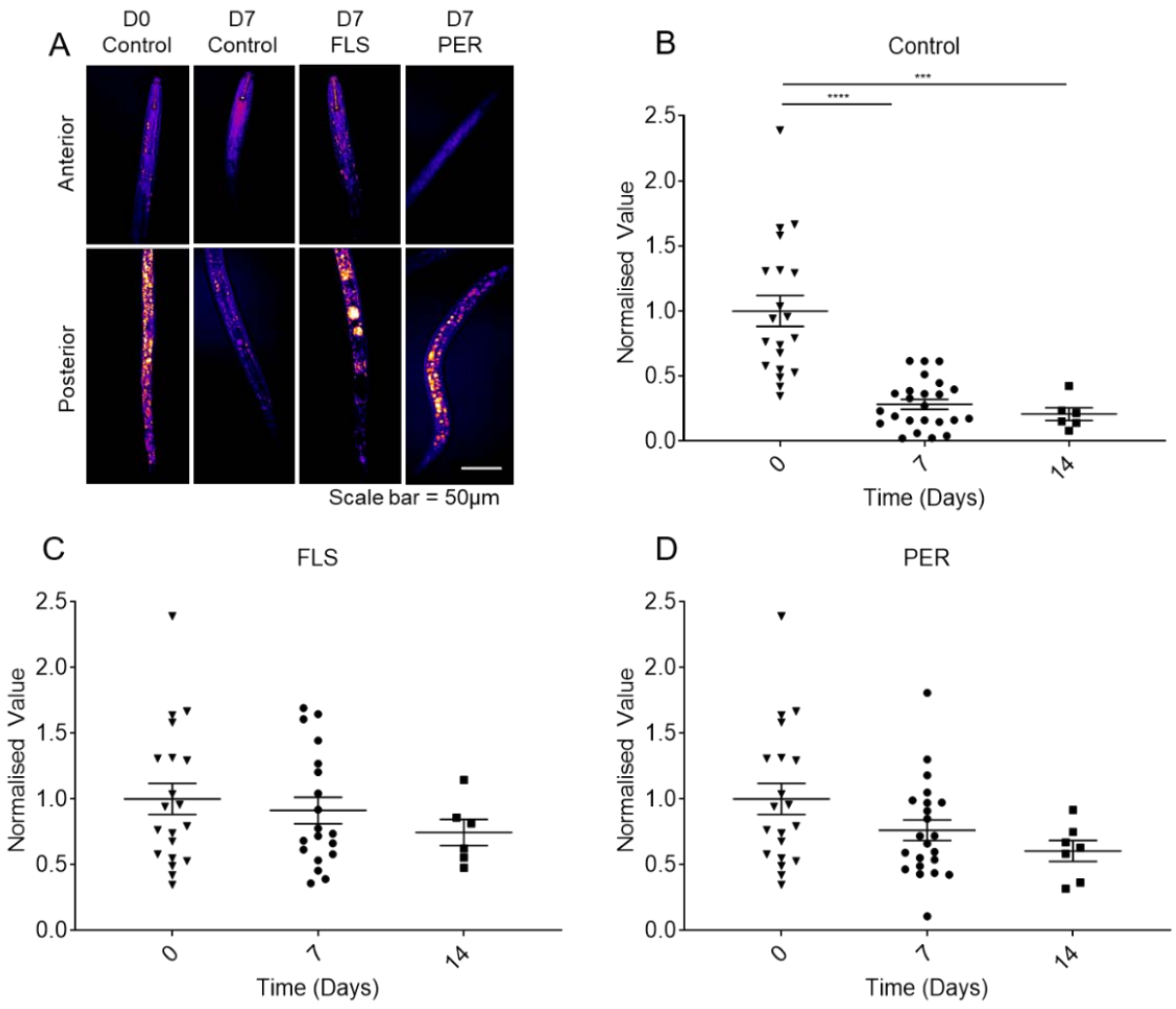

Figure 5.11 Fluensulfone and perhexiline treatment prevent reduction in CARS signal. CARS images (A) show associated super-threshold signal from both the anterior and posterior regions of representative control, fluensulfone (FLS) and perhexiline (PER) treated J2s. CARS signal generated from the posterior region was analysed by using a threshold to select signal that related to lipid area and calculating the intensity from this region. Light microscopy was used to define the tail boundary and integrated density was normalised to the total tail area imaged for each sample (See methods). Data shown is normalised CARS signal relative to Control day 0. (B) In controls, CARS signal is significantly depleted after 7 and 14 days. (C) J2s treated with FLS (30µM). (D) J2s treated with PER (50µM). Data shown are ± S.E.M normalised IntDensity/ tail area. For Day 0 and 7, data pooled from 3 independent experiments with ≥6 J2s per treatment group. For Day 14, N= ≥6 J2s per treatment group. Statistical analysis performed by one-way ANOVA with Tukey post-hoc tests ($P<0.05$).

5.3 Discussion

5.3.1 Fluensulfone, fluoroacetic acid and perhexiline are nematicidal to *Globodera pallida* juveniles

These results show that treatment of *G. pallida* J2s with fluensulfone, perhexiline or fluoroacetic acid results in their death. This is seen by observing motility and posture and is reinforced by the histological stain MTT. The loss of MTT staining suggests a lack of metabolic activity and is consistent with chemical inhibition disrupting essential steps of critical metabolic fluxes.

As described in the Chapter introduction (5.1.1) and General Introduction (Chapter 1.6), activity via the TCA cycle generates the key substrates, NADH and $FADH_2$, for generation of ATP via the ETC. Here, I have investigated inhibiting the TCA cycle via block of aconitase with fluoroacetic acid. Input to the TCA cycle can be carbohydrate or lipid-derived. To probe for an effect on lipid catabolism, due to the inference that *G. pallida* juveniles utilize stored lipids post-hatch (Storey, 1984; Holz et al., 1997; Smus et al., 2017), I used the CPT inhibitor, perhexiline.

Metabolic flux to generate energy from stored carbohydrate or lipid will require the activity of succinate dehydrogenase, an enzyme that is crucial to both the TCA cycle and electron transport chain, coupling the oxidation of succinate to fumerate in the mitochondrial matrix with the reduction of ubiquinone, and thus driving the generation of ATP via the electron transport chain (Horsefield 2006 and Avenot 2010). Fluopyram blocks the ubiquinone binding site, preventing the reduction of quinone to quinol and further cycling of succinate oxidation (Avenot and Michailides, 2010; Burns et al., 2015; Horsefield et al., 2006). Treatment of *G. pallida* with fluopyram has been shown to result in a rapid loss of metabolic activity (Figure 5.1) (Kearn, 2015), suggesting that metabolic flux through the electron transport chain is critical to life. Fluopyram is a nematicide, suggesting that targeting metabolism can be a successful route to nematicidal activity.

Treatments with fluensulfone, perhexiline and fluoroacetic acid, result in a relatively slow progressive loss of motility and metabolic activity. EC_{50} values estimated for perhexiline and fluoroacetic acid (Table 5.1) are comparable to the K_i values reported for each drug (Chapter 4, Table 4.1). Due to the progressive nature of these compounds, the estimated EC_{50} values change over time. One of the confounding factors of investigating drug effects in nematodes is that the concentration that is applied to the nematode, in this case to the solution the juveniles are suspended in, is not an accurate indicator of the concentration acting at the enzyme it is selective for. Therefore, these results may reflect a build-up of drug that is able to reach a threshold concentration to have an effect, or maybe indicative of a slowly accumulating insult that is as a result of continued drug exposure. The behavioural outputs measured in this study are indirect measures of drug activity, and so the EC_{50} values presented here are for the purpose of comparing drug potency.

At the non-feeding juvenile stage, utilizing stored lipids and their subsequent breakdown provides the energy required for the juvenile to locate and migrate towards host roots. A readout of this behaviour that can be scored in vitro is motility. Blocking access to stored lipids would by hypothesised to impair motility, through blocking the essential energy source available to the juvenile. Inhibition of CPT by perhexiline prevents the transfer of fatty acids into the mitochondria for β-oxidation and thus would impair the breakdown of stored lipids required to generate ATP. Here, I show that perhexiline is efficacious against the plant parasitic nematode *G. pallida,* impairing motility. I also show with MTT staining that impairment to motility is accompanied by a loss of metabolic activity, suggesting that perhexiline is nematicidal to *G. pallida* juveniles. It has previously been shown that treatment of *C. elegans* with perhexiline also results in impaired metabolism, with *C. elegans* exposed to perhexiline resulting in a dose-dependent decrease in basal oxygen consumption rates, consistent with its important role in controlling catabolic lipid flux (Taylor et al., 2013). This suggests that perhexiline is likely acting via its known mode of action on CPT in both *C. elegans,* and by extension, in *G. pallida.*

In addition to the effects of fluroacetic acid on *G. pallida* hatching described in Chapter 4, here I show that prevention of flux through the TCA cycle and/or glyoxylate shunt by fluoroacetic acid results in loss of MTT staining of *G. pallida* J2s. However, the effects on metabolic activity are not as rapid by interfering at this point in the metabolic pathway as inhibiting the electron transport chain, as is seen with fluopyram treatment (Figure 5.1). The speed of effect is therefore an important discriminator as to where the inhibitor is acting to impair ATP generating flux. Inhibition of TCA cycle activity would reduce the amount of coenzymes generated, which are shuttled to the ETC for oxidative phosphorylation. Indeed, it has been shown that a depletion of NADH/NADPH can result in cell death (Petrat et al., 2003). The effects of limiting the available reducing agents through impaired TCA cycle activity may however result in a progressive insult, due to already available coenzymes being utilized. Inhibition of a single enzyme in the electron transport chain, such as inhibition of succinate dehydrogenase by fluopyram, will halt the rest of the process and subsequently inhibit ATP formation.

Fluensulfone treatment results in a progressive loss of motility and metabolic activity, suggesting that fluensulfone is targeting a pathway that is not immediately critical to life. The progressive nature of the fluensulfone insult is consistent with a mode of action that results in the accumulation of intermediary toxic products, which lead to the block of ATP generating flux, rather than a direct effect on the flux that ultimately forms ATP.

5.3.2 Re-distribution of MTT staining to the posterior may be indicative of impaired lipid utilization

Intracellular reduction of MTT is primarily provided by nicotinamide coenzymes, which are mainly produced in the mitochondria and endoplasmic reticulum (Stockert et al., 2012). Our results support previous observations that in control J2s, MTT staining is predominantly detected as precipitations concentrated in the anterior portion of the worm. In *C. elegans*, the cationic, mitochondria-targeted, fluorescent dye, MitoSOX, predominantly localizes to mitochondria- rich pharyngeal bulbs in the anterior region of *C. elegans* (Dingley et al., 2010). DiS-C3(3) is a fluorescent dye that also stains mitochondria. Staining of *C. elegans* and *G. pallida* with DiS-C3(3) results in intense fluorescence from the anterior region of both nematode species (Kearn, 2015). The MTT staining in the control non-feeding J2 is therefore consistent with a high concentration of mitochondrial activity leading to NADH production in the anterior region. Upon fluensulfone treatment, there is a loss of anterior staining and a shift to predominant posterior staining, prior to a complete loss of staining. Whilst this shift in MTT staining pattern has been observed and reported by our group previously (Kearn et al 2017) the underpinning reason was not addressed. Here, I provide evidence that this staining pattern could be indicative of an impairment to lipid catabolism.

It has been shown that MTT formazan preferentially partitions and accumulates in lipid droplets. This is related to the hydrophobic nature of the MTT formazan precipitate (Stockert et al., 2012). In *G. pallida* J2s, lipids are predominantly stored in the posterior region and are depleted post hatch (Smus et al. 2017). MTT staining in healthy juveniles is diffuse in the posterior, with predominant staining observed in the anterior region across all time points. This is representative of continued relatively high metabolic activity in the anterior region of healthy J2s post-hatch. Treatment with fluensulfone inhibits the predominant source of metabolic activity and causes a loss of staining relative to the untreated controls. This shift in staining away from the anterior could reflect a change in the source of MTT reducing agents. Oxidative stress generates a rapid decrease of mitochondrial NADH and so as mitochondrial activity is disrupted during the earlier stages of intoxication, the fluensulfone insult may leave other sources of intracellular reducing agents intact, which are able to reduce MTT to the water insoluble MTT formazan. In this situation, if lipid utilization is disrupted, this background lower level generation of MTT formazan can decorate residual and retained lipid droplet stores. This results in the apparent shift to predominant posterior staining following treatment with metabolic inhibitors that primarily prevent lipid utilization. This is exemplified by treatment with the CPT inhibitor perhexiline, which will prevent the transfer of fatty acids into the mitochondria for β-oxidation. The shift to posterior staining is therefore consistent with MTT formazan localizing and accumulating in lipid droplets that are not being depleted.

It can also be speculated that the MTT staining in the tail region is not as apparent in the posterior of control nematodes because NADH and mitochondrial activity are not the principle drivers of MTT formazan production in this region. NADPH is also able to reduce MTT formazan and so staining in the tail could reflect cytosolic NADPH levels. The prominent staining seen in fluensulfone treated J2s could therefore reflect a block of NADPH consumption, which would otherwise be consumed via the process of lipolysis (Issa et al., 2018). Assessing the ability of fluensulfone to directly block NADPH oxidase activity would be attractive to explore. Nevertheless, a block to lipolysis would result in retainment of lipid droplets, which is entirely consistent with MTT formazan preferentially partitioning into lipid stores that have not been depleted.

Fluoroacetic acid treatment should prevent activity through the TCA cycle and/or glyoxylate shunt. The EC_{50} value I report here is consistent with inhibition of aconitase, resulting in loss of motility and metabolic activity. However, this inhibition does not result in the described redistribution of the deposited MTT formazan to the posterior in face of the ongoing intoxication. This suggests that unlike perhexiline, the perturbing inhibition of metabolism does not prevent lipid droplet depletion. This also indicates that lipid droplets are not generated upon fluoroacetic acid treatment and supports that it's mechanism of action is distinct from perhexiline and fluensulfone. This argument is consistent with this inhibitor acting down-stream of the critical β-oxidation of fatty acids that facilitates lipid depletion (Chapter 4, Figure 4.4). To investigate this effect further, it would be beneficial to perform CARS analysis on fluoroacetic acid treated juveniles.

5.3.3 CARS analysis suggests access to lipid stores is prevented by fluensulfone and perhexiline treatment

To independently address the ideas mapped out above, CARS imaging was used to analyse the lipid droplet stores in *G. pallida* juveniles. CARS signal tuned to the vibrational stretching mode at 2845 cm^{-1} was used to image neutral lipids in anterior and posterior regions of treated and untreated J2s post hatch. This approach, benchmarked by previously reported depletion of signal with increasing time post hatching, was used to analyse the effects of perhexiline and fluensulfone on the critical lipid stores. This analysis showed that CARS signal tuned to neutral lipids is maintained in drug treated juveniles, in contrast to their depletion in controls post-hatch. This further supports the evidence for perhexiline acting via its intended target on CPT in *G. pallida* juveniles. Fluensulfone, whose molecular target has not yet been defined, also prevents the depletion of lipid associated signal.

5.3.4 Spatial resolution of CARS imaging

CARS spectroscopy is designed to extract chemical signatures from the storage organelle that harbour neutral lipids, predominantly triglyceride (Zhang et al., 2010). In *C. elegans,* lipid droplet structures range in size from <3µm to approximately 8µM in diameter. It was however observed that *C. elegans* mutants that accumulate high levels of triglyceride, due to peroxisomal dysfunction, had lipid droplets of >10µm in diameter (Zhang et al., 2010). Due to the abundance of triglyceride stored in the core of lipid droplets, the assumption is that when tuning to the CH_2 stretching vibration, the CARS signal provides visualisation of the lipid droplet stores (Figure 5.2). Whilst the CARS signal acquired relates to regions of interest, the methodology is unable to resolve the in situ finer organization of the storage deposits due to the resolution of the system employed in these investigations limiting lipid droplet size analysis, with signal relating to merged signal and not reflective of 3 dimensional area. Although dynamics of these structures are clear, one cannot address changes in individual size and precise localization of lipid droplets within cells.

5.3.5 Comparative investigations with nematicides of known modes of action

One caveat of this investigation is that lipid depletion is associated with compounds that reduce motility, opening the possibility that a decrease in lipid utilization is due to the juvenile not moving. This highlights the importance of investigating lipid stores of fluoroacetic acid treated juveniles. When staining with MTT, MTT formazan does not precipitate into the posterior regions of fluroacetic acid treated juveniles, suggesting that the formazan precipitate is not partitioning into reserved lipid droplet stores as is suggested with fluensulfone and perhexiline. Following this investigation up with CARS analysis would provide an important assurance that the MTT staining hypothesis I describe is reflective of sustained lipid stores.

It has previously been shown that ivermectin treatment, which targets glutamate-gated chloride channels (See Chapter 3.1.1.1), results in the loss of motility of *G. pallida* juveniles, however, in contrast to the prevention of lipid utilization following fluensulfone and perhexiline treatment, results in the acceleration of lipid depletion, as evidenced by CARS (Smus et al., 2017). This suggests that inhibition of motility does not underpin prevention of lipid depletion.

Furthermore, spirotetramat, a nematicide that inhibits acetyl-coA carboxylase, suppresses development of *H. schachtii* and *C. elegans* whilst resulting in lipid droplet depletion (Gutbrod et al., 2020). It is therefore apparent that targeting lipid metabolism pathways, whether it be via impairing fatty acid synthesis, as is the case with spirotetramet, or preventing β-oxidation through inhibition of CPT with perhexiline, is an attractive route to nematicidal activity.

Although the molecular target of fluensulfone is currently unknown, I have shown here that treatment with fluensulfone results in an impaired ability to access stored lipid. Our results suggest that an impairment to lipid utilization, either with fluensulfone or perhexiline treatment, will result in a slow, progressive death.

Disruption of metabolic fluxes is an established nematicidal route (Chapter 1.7). What is intriguing about published observations of fluensulfone is that it exhibits a selective nematicidal inhibition by potentially targeting a metabolic flux that is particularly important in PPNs (Kearn et al., 2014; Kearn et al., 2017). If impairment to accessing stored lipid by fluensulfone is the point at which it is impacting metabolic flux, it is important to understand how this mechanism might work. That such a disruption can be nematicidal is highlighted by perhexiline treatment.

The process of liberating lipid substrates for catabolic energy production is a complex, multi-step process. One of these steps is the transfer of liberated fatty acids into the mitochondria for β-oxidation, which is inhibited by perhexiline. It is possible that fluensulfone is also acting to inhibit CPT, however, there is some evidence that perhexiline and fluensulfone are acting at distinct targets. This includes the data described in Chapter 4, where fluensulfone has a potent inhibitory effect on *G. pallida* hatching in contrast to perhexiline, which has no effect on hatching. Additionally, fluensulfone has been shown to display PPN specificity, with fluensulfone concentrations in the mM range required to impact on the free-living nematode *C. elegans* (Kearn et al., 2014) in contrast to the µM doses I describe here for *G. pallida*. This is in contrast to perhexiline, which has a comparable EC50 for effect on motility in both *C. elegans* (Taylor et al 2013) and *G. pallida*, suggesting a common target. However to provide more clarity on this, developing an assay to measure CPT activity in nematodes would be beneficial.

This leaves several other distinct steps at which fluensulfone could be acting (Figure 5.12), including liberation of triglycerides from lipid droplets and subsequent breakdown of fatty acids to yield acetyl-CoA. Additionally, lipid oxidation can be both mitochondrial and peroxisomal, with different enzymes involved in the individual routes. In order to understand the mechanism by which fluensulfone results in sustained CARS signal, the nature of the lipids the signal is corresponding to needs resolution. This involved biochemical analysis to identify lipid class and further, lipid species, to better elucidate the role of fluensulfone on lipid catabolism.

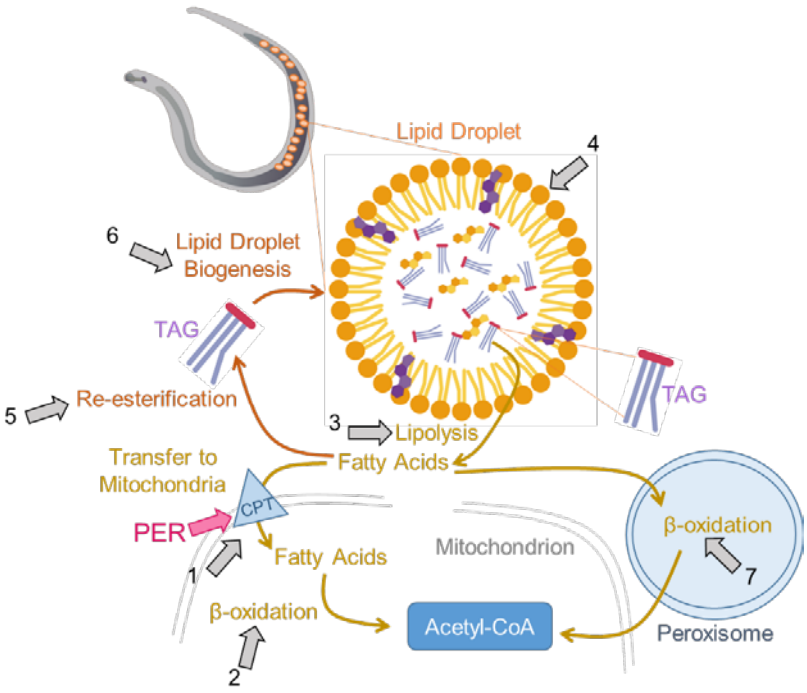

Figure 5.12 Cartoon summarizing critical steps in model for the potential mode of action of fluensulfone in the context of deficient lipid droplet utilization. Perhexiline (PER) targets carnitine palmitoyltransferase (CPT) to prevent the transfer of fatty acids into the mitochondria for β-oxidation. We have identified that fluensulfone shares a similar profile of effects with perhexiline, resulting in impairment to the utilization of lipids. It remains unknown as to where fluensulfone is acting to impair utilization; acting at the same site as perhexiline to prevent the transfer of fatty acids to the mitochondria (1); a direct effect on mitochondrial β-oxidation (2); impairment to lipolysis and thus the mobilization of fatty acids from lipid droplets (3); interference with lipid droplet dynamics, such as disrupting lipid droplet-organelle contacts (4); preventing the sequestering of free fatty acids, resulting in lipotoxicity (5); acting on mechanisms of lipid droplet biogenesis (6); acting to disrupt peroxisomal β-oxidation (7). Schematic not to scale.

5.4 Summary

I have provided evidence that fluensulfone treatment of *G. pallida* J2s disrupts access to stored lipid, supporting previous observations made with Nile red staining. It has a comparable, accumulating behavioural disruption and effect on utilization of lipids to an established inhibitor of mitochondrial β-oxidation, perhexiline. This is consistent with the important role of accessing and metabolising stored lipid that is released from lipid droplets in the non-feeding J2. The overlapping behavioural and histological description of fluensulfone and perhexiline might suggest a shared molecular target.

The histological staining and CARS signatures that I have described here provide evidence that fluensulfone prevents the depletion of lipid droplets. Lipid catabolism is known to be a complex multi-step process. While not pinpointing the molecular target, this comparative inhibitor study highlights that investigation of lipid biology in PPNs will be an important route to define the selective toxicity of fluensulfone.

Chapter 6 Biochemical Investigation of Lipid Composition in Fluensulfone Treated *Globodera pallida*

6.1 Introduction

I have described an effect of fluensulfone on the motility and metabolic activity of *G. pallida* juveniles (Chapter 5.2.1). This progressive metabolic impairment supports previous reported observations (Kearn et al., 2017). I also describe a pattern of MTT staining that is consistent with MTT formazan partitioning into lipid droplets. CARS analysis of fluensulfone treated juveniles supports this hypothesis (Chapter 5.2.4). This is consistent with a mechanism of action for fluensulfone on preventing the depletion of lipids in the tail region of *G. pallida* juveniles post-hatch, in face of decreasing metabolic activity prior to death. This highlights a potential explanation through which fluensulfone may be acting, consistent with the important pre-storage and depletion of lipid stores post hatching. Here, I aimed to optimize and benchmark methods that allow a direct biochemical investigation of lipids to establish parallel investigations that help cross reference the hypothesis mapped out above and further mode of action.

6.1.1 Lipid classes and their role in nematodes

Lipids are hydrophobic or amphipathic small molecules. Amphipathic lipids contain both hydrophilic and hydrophobic ends, whish is key to them forming components of cellular and organelle membranes, with their hydrophilic ends on the outside, in contact with water, and their hydrophobic ends on the inside, away from water (Fahy et al., 2011).

Fatty acids are one of the major building blocks of complex lipids, acting as precursors for storage lipids (GLs), membrane lipids (GPs and SPs), and signalling lipids (e.g. fatty acyl amides, eicosanoids) (Watts and Ristow, 2017). Fatty acids can be in the form of saturated, mono- and polyunsaturated, and mono methyl branched fatty acids (Witting and Schmitt-Kopplin, 2016) (Figure 6.1).

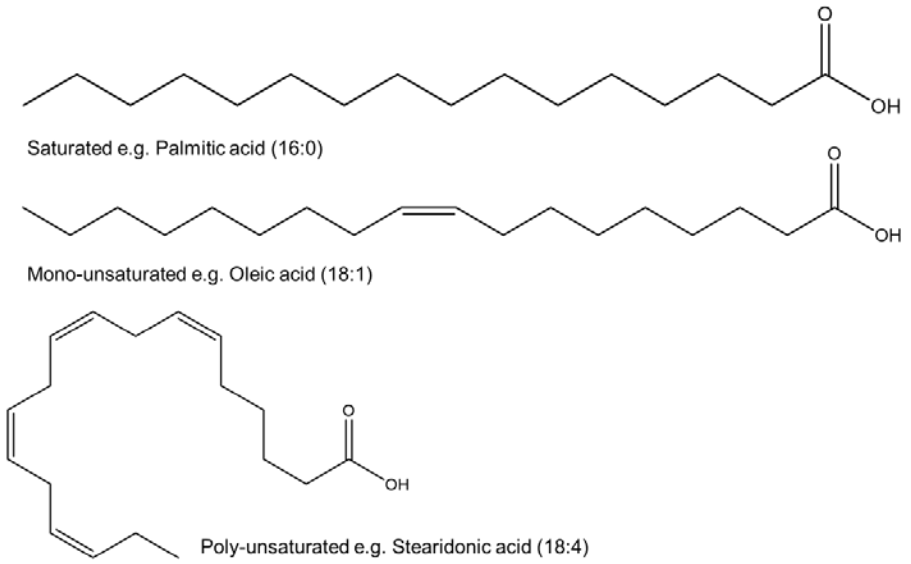

Figure 6.1 Fatty acids are the major lipid building blocks of complex lipids. The fatty acyl group in the fatty acids class is characterized by repeating methylene groups. Straight-chain saturated fatty acids contain a terminal carboxylic acid. Variations on this basic structure include fatty acids with one (mono-unsaturated) or more (poly-unsaturated) double bonds.

Lipids are divided into eight categories: fatty acids (FA), glycerolipids (GL), glycerophospholipids (GP), sphingolipids (SP), saccharolipids (SL), polyketides (PK) sterol lipids (ST) and prenol lipids (PL). Representative lipids from these classes are tabulated in Table 6.1 and summarised in Figure 6.2.

Lipid Class	Representative Lipids
Fatty acyls (Figure 6.)	Fatty acids
Glycerolipids (GL)	Monoacylglycerol Diacylglycerol Triacylglycerol
Glycerophospholipids (GP)	Phosphatidic acid Phosphatidylcholine Phosphatidylethanolamine Phosphatidylserine Phosphatidylglycerol Phosphatidylinositol Cardiolipin
Sphingolipids (SP)	Sphingosine Ceramide Sphingomyelin Galactosyl-/Glucosylceramide Ganglioside
Sterol lipids (ST)	Cholesterol Cholesterolester
Prenol lipids (PL)	Isoprenoids Quinones and hydroquinones Polyprenols Hopanoids
Saccharolipids (SL)	UDP-3-(3R-hydroxy-tetradecanoyl)-αD-glucosamine
Polyketides (PK)	Erythromycin

Table 6.1 Lipid classifications based on the LIPID MAPS classification system. The LIPID MAPS classification system for lipids is available online at (lipidmaps.org) (Fahy et al., 2009).

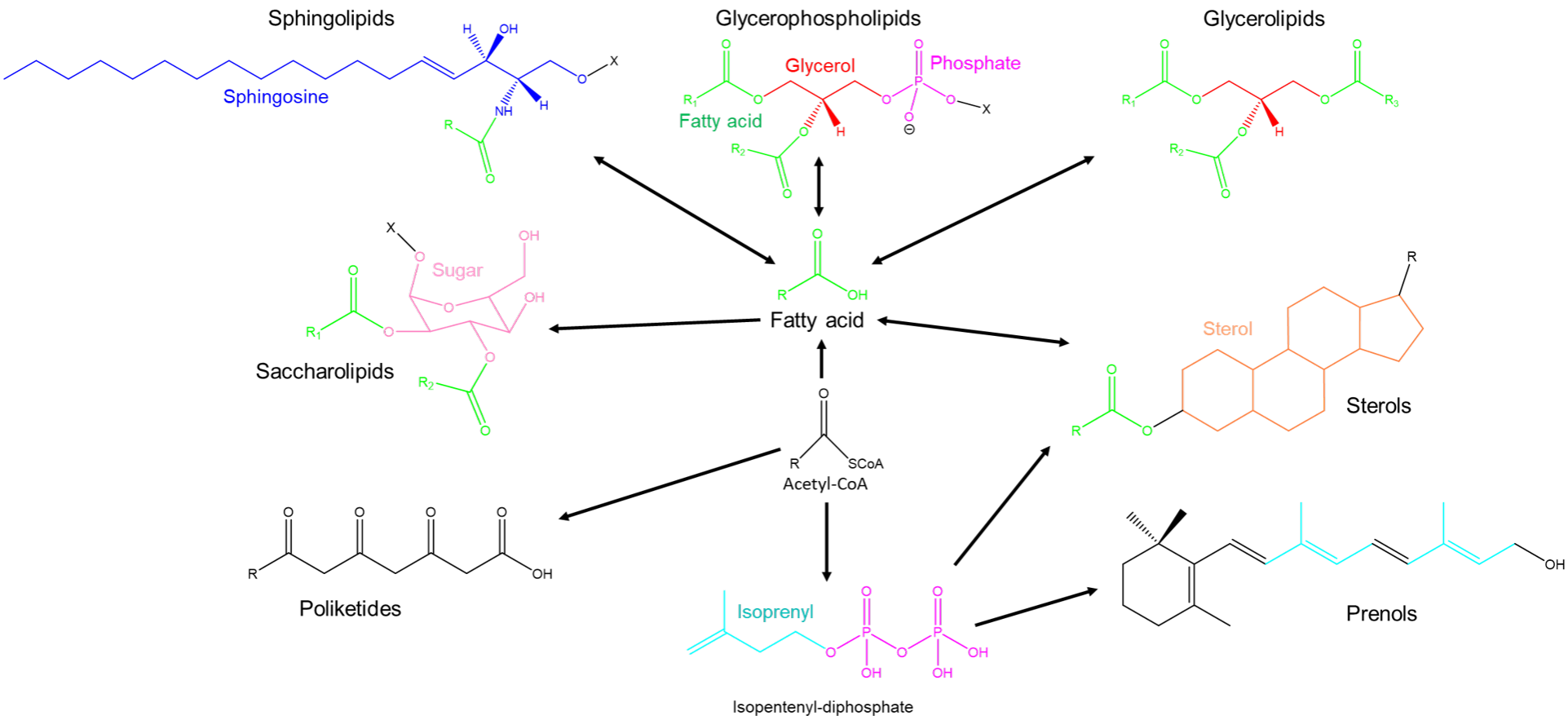

Figure 6.2 Major lipid classes and representative structures. Fatty acids (FA) are synthesised by chain elongation of an acetyl-CoA primer with malonyl-CoA groups. FAs (green) are the major building blocks of most lipid classes; glycerolipids and glycerophospholipids, which both have a glycerol backbone (red), sphingolipids and saccharolipids. In addition to FAs, acetyl units are used to generate the polyketide lipids and isopentenyl diphosphate molecule, through the mevalonate pathway. Isoprenyl units (turquoise) are substrates for the prenols and sterols.

The core organization of lipid classes described in Figure 6.2 show diversity in structure, due to variation in chain length, biochemical transformations and modifications of sugar residues and functional groups that form the backbones of the lipid structures (Fahy et al., 2011). Lipids function in a multitude of ways, acting as structural components of cell membranes, participating in signalling pathways and form important energy stores (Fahy et al., 2011).

The *C. elegans* lipidome has been reviewed (Witting and Schmitt-Kopplin, 2016; Watts and Ristow, 2017), describing lipid classes and species that are present in the free-living nematode and providing an overview of methods available for their analysis. *C. elegans* are an emerging model organism for studying the biological functions of lipids, due to their adaptability for genetic manipulation that modulate key enzymatic activities and the ability to visualize lipid droplets at an organismal level (Zhang et al., 2013). In contrast, there is more limited investigation in PPNs, although as highlighted, it is evident that lipids are important metabolic stores in these organisms.

6.1.1.1 Glycerolipids

The glycerolipids class is composed of mainly mono-, di- and tri-substituted glycerols, the most common being the fatty acid esters of glycerol, known as triglycerides (Figure 6.3).

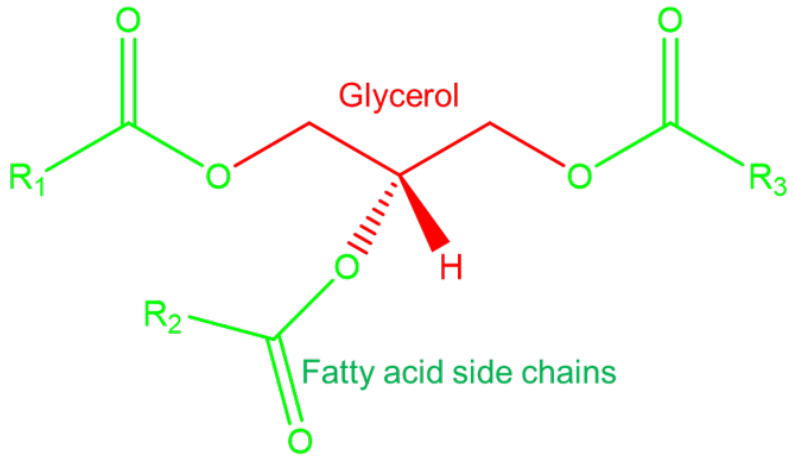

Figure 6.3 Triglyceride chemical structure. Triglycerides consist of a glycerol backbone (red) esterified to three fatty acid side chains (green). These can differ in chain length and saturation, resulting in diverse triglyceride molecules. The fatty acid side chains consist of multiple CH_2 moieties. The most abundant fatty acids making up triglycerides in *Globodera* spp. are C20:4, C20:1 and C18:1 (Holz et al., 1997)

Neutral lipids have been identified as the major component of total lipid in PCN juveniles, the predominant lipid class attributed to triglycerides (Gibson et al., 1995). It was described in the previous chapter that non-feeding PPN juveniles rely on the mobilisation of triglycerides from lipid droplets prior to locating and invading a host. The main principles of lipid droplet organisation and function are introduced in Chapter 5.1.2. Here, I provide further detail on lipid droplet dynamics and their critical role in lipid and energy homeostasis.

6.1.1.1.1 Lipid droplet dynamics

Lipid droplets consist of a phospholipid monolayer enclosing a core of neutral lipids (triglycerides and sterols). The phospholipid monolayer is studded with proteins, which interact with other organelles and are responsible for controlling diverse aspects of lipid droplet dynamics (Olzmann and Carvalho, 2019).

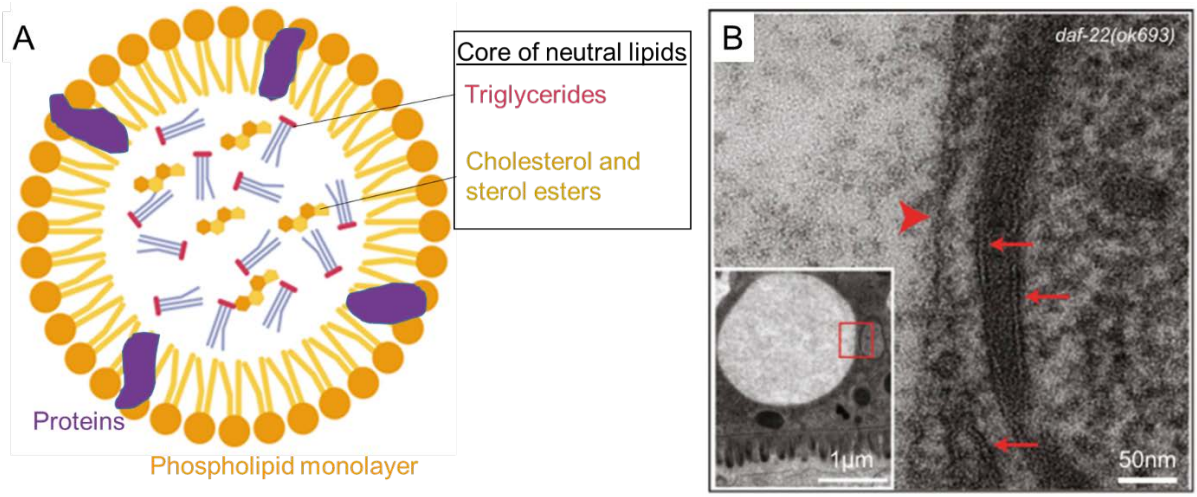

Figure 6.4 Lipid droplet structure. (A) Lipid droplets are organelles that store neutral lipids, surrounded by a phospholipid monolayer, which is studded with proteins that are involved in coordination of lipid droplet-organelle contacts and regulation of lipid droplet dynamics. (B) Electron micrograph from (Zhang et al., 2010) showed that lipid droplets (boxed area in Inset) consist of a phospholipid monolayer (arrowhead) as opposed to a phospholipid bilayer (arrows) of nearby organelles. Image from *daf-22* mutant *C. elegans.*

Lipid droplet-associated proteins include enzymes involved in lipid metabolism, membrane trafficking and protein degradation. Class I proteins partition between lipid droplets and the endoplasmic reticulum (ER). Class II proteins are directly recruited from the cytosol to the lipid droplet surface (Olzmann and Carvalho, 2019). Lipid droplets associate with most cellular organelles, including the ER, golgi, mitochondria, lysosomes and peroxisomes, reflecting their highly dynamic nature (Valm et al., 2017). Lipid-droplet contacts allow the coordination of lipid metabolism across distinct organelles (Valm et al., 2017). Processes include lipid synthesis at the ER (Phillips and Voeltz, 2016), lipid droplets for storage and energy homeostasis (Beller et al., 2010), mitochondria and peroxisomes for β-oxidation of fatty acids (Tatsuta et al., 2014; Shai et al., 2016), and lysosomes for hydrolysis and recycling of cellular waste (Settembre et al., 2013) (Figure 6.5). Contacts facilitate the exchange of material between organelles, such as lipids, metabolites and ions (Olzmann and Carvalho, 2019).

The identification of lipid droplet- associated proteins and lipid droplet interactions with cell organelles demonstrates that lipid droplets are far more dynamic than static storage deposits and are in fact central to the regulation of lipid metabolism (Beller et al., 2010).

Lipid droplets vary in size, reflecting changes in TAG concentration and lipid metabolism. In *C. elegans,* mutants that accumulate high levels of TAG due to peroxisomal dysfunction, result in lipid droplet expansion. Furthermore, lipid droplet size can be influenced by diet (Zhang et al., 2010). Enlarged lipid droplets were also shown to be resistant to lipolysis; TAG hydrolysis is induced during fasting, however this process is severely impaired when peroxisomal β-oxidation is defective. Indeed, peroxisomal β-oxidation was shown to modulate lipid droplet size, with peroxisomes clustering adjacent to the surface of enlarged lipid droplets, suggesting a physical interaction between these organelles (Zhang et al., 2010).

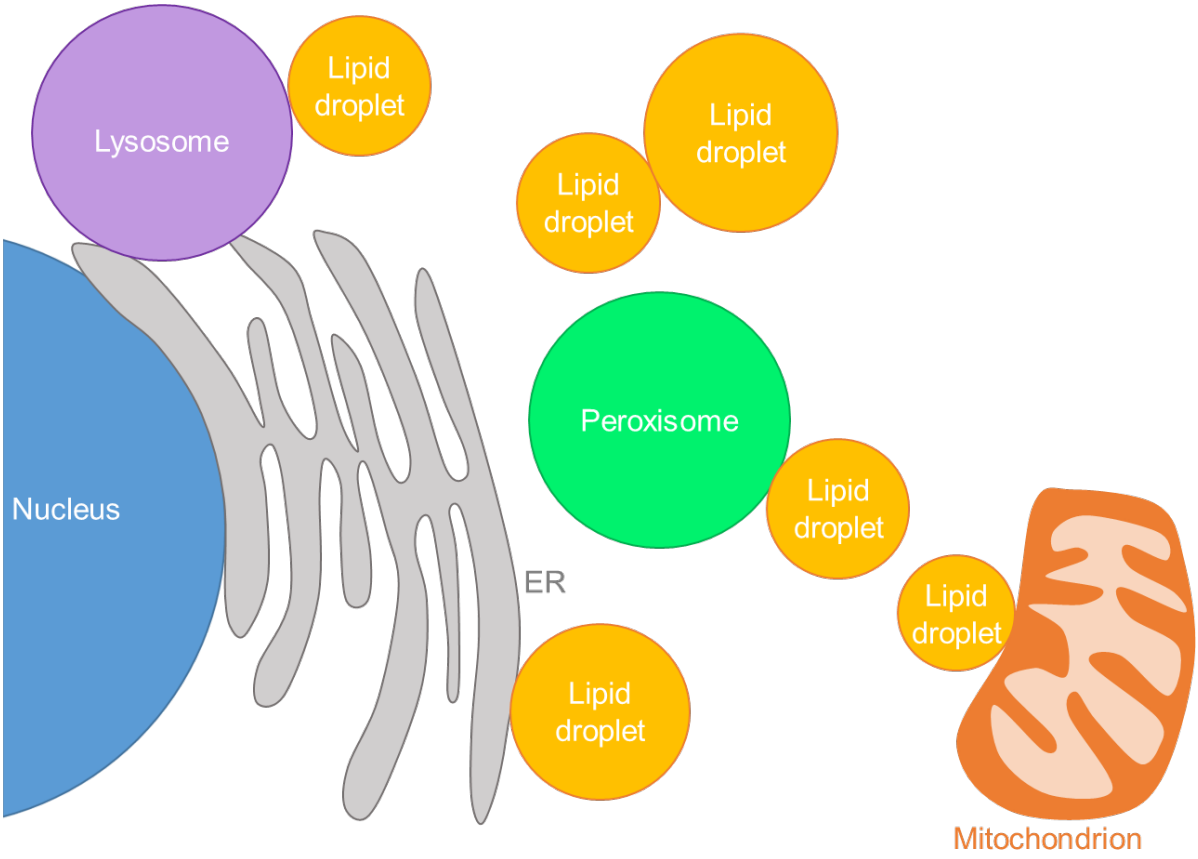

Figure 6.5 Lipid droplet dynamics. Lipid droplets make contacts with organelles throughout the cell and with each other. Whilst the molecular basis for some of these interactions are not completely understood, the proteins that are involved in the lipid droplet-organelle interactions are reviewed by (Olzmann and Carvalho, 2019). This diagram represents individual lipid droplet-organelle contacts, however, it is likely that a single lipid droplet will make contact with multiple organelles at the same time. Figure adapted from (Olzmann and Carvalho, 2019).

Phospholipid composition is able to influence TAG concentration, which will ultimately influence lipid droplet size and abundance (Guo et al., 2008). Disruption of phosphatidylcholine (PC) synthesis in *C. elegans* leads to increased TAG and enlarged lipid droplets (Walker et al., 2011). This was shown to be regulated by the sterol regulatory element-binding protein, SREBP-1, where blocking PC synthesis leads to increased SREBP-1-dependent transcription and lipid droplet accumulation (Walker et al., 2011). It has since been shown in *C. elegans* that in mutants with impaired stearoyl-CoA desaturases (SCDs), there is a reduction in fat stores and a decrease in lipid droplet size (Shi et al., 2013). This was also linked to phospholipid composition, with SCD activity required for normal ratios of PC to phosphatidylethanolamine (PE) (Shi et al., 2013).

6.1.1.2 Glycerophospholipids

Glycerophospholipids (GPs) are the building blocks of membranes, built from two fatty acids esterified to a glycerol backbone. *C. elegans* can synthesize a large variety of head groups, resulting in many classes of GPs. These include phosphatidic acids (PA), phosphatidylcholines (PC), phosphatidylethanolamines (PE), phosphatidylserines (PS), phosphatidylglycerols (PG) and phosphatidylinositols (PI) (Figure 6.6). Additionally, cardiolipins (CL), which consist of two molecules of PG, also make up constituents of *C. elegans* mitochondrial membranes (Witting and Schmitt-Kopplin, 2016). To achieve structural diversity, *C. elegans* are able to synthesize a vast amount of different fatty acids with different chain lengths and degree of saturation, however, also directly utilize fatty acids derived from bacterial diet (Witting and Schmitt-Kopplin, 2016). For example, palmitic acid (16:0) can be synthesised de novo or obtained from the *E. coli* diet in *C. elegans* and is subsequently converted to palmitoleic acid (16:1) by SCD activity, specifically by the desaturase FAT-5 (Brock et al., 2007). Palmitoleic acid can then be elongated to the most abundant fatty acid in phospholipids and TAG, cis-vaccenic acid (18:1), or elongated to stearic acid (18:0), which is desaturated to oleic acid (18:1). Oleic acid can then be further desaturated or elongated to form other polyunsaturated fatty acids (PUFAs) (Brock et al., 2007).

Glycerophospholipids are the major constituent of membranes. Due to their major role in membrane structure, GPs strongly influence membrane fluidity and the mechanical properties of cells (Witting and Schmitt-Kopplin, 2016).

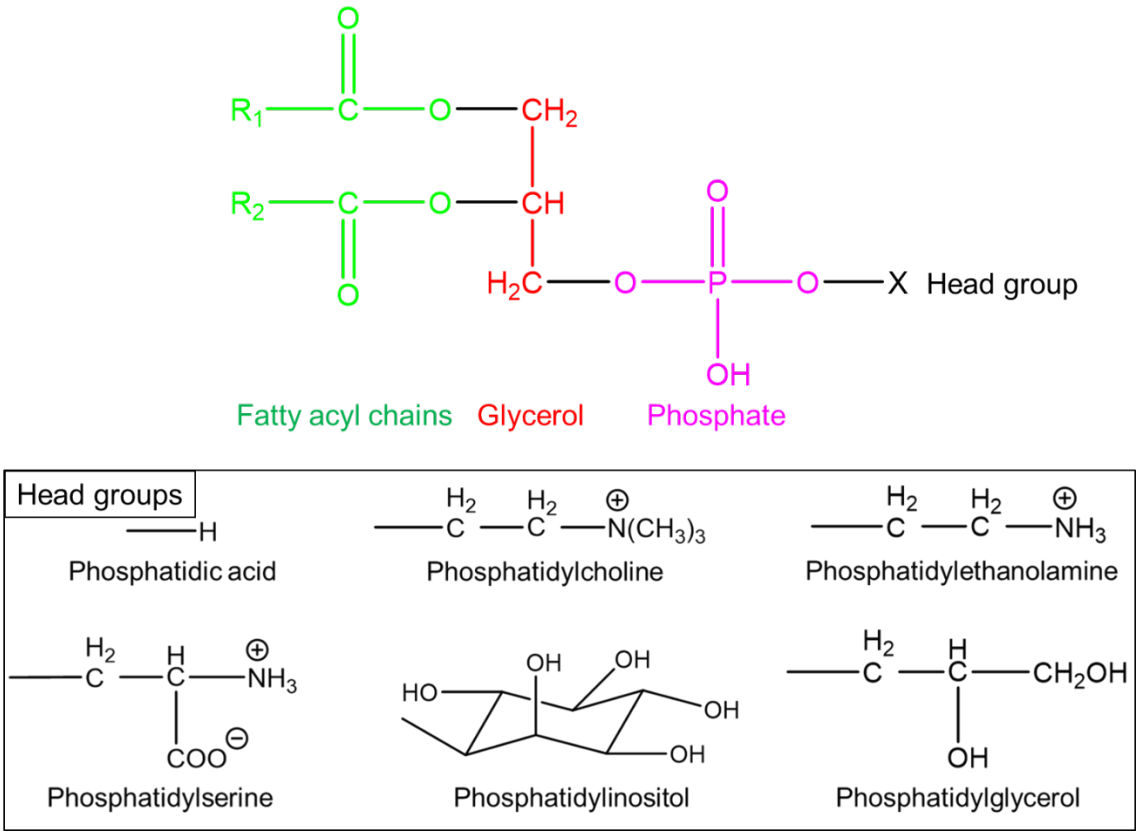

Figure 6.6 Glycerophospholipids class and structure. Glycerophospholipids consist of a hydrophobic tail of two fatty acyl chains (green) and a hydrophobic head of glycerol (red), phosphate (purple) and corresponding head group (black). X corresponds to class head group which are shown for the major classes of phospholipids.

6.1.1.2.1 Phospholipids are important signalling molecules

Phospholipids are not only important in membrane structure, but also have vital roles in cell signalling. For example, phosphatidylserines act as signals at the surface of apoptotic cells to allow recognition by phagocytic cells, allowing efficient clearance of cell corpses. Surface exposure of PSs has been described in *C. elegans* (Jenzer et al., 2019). Phosphatidylinositol signalling impacts a diverse number of cellular processe, such as proliferation, survival and glucose homeostasis (Lundquist et al., 2018). Phosphatidylcholine signalling has also shown to be important for regulation of glucose homeostasis (Lee et al., 2011), in addition to playing an important role during oxidative stress (Mateos et al., 2008).

6.1.1.3 Sphingolipids

Sphingolipids differ from glycerophospholipids in that they consist of a sphingosine base (Figure 6.7).

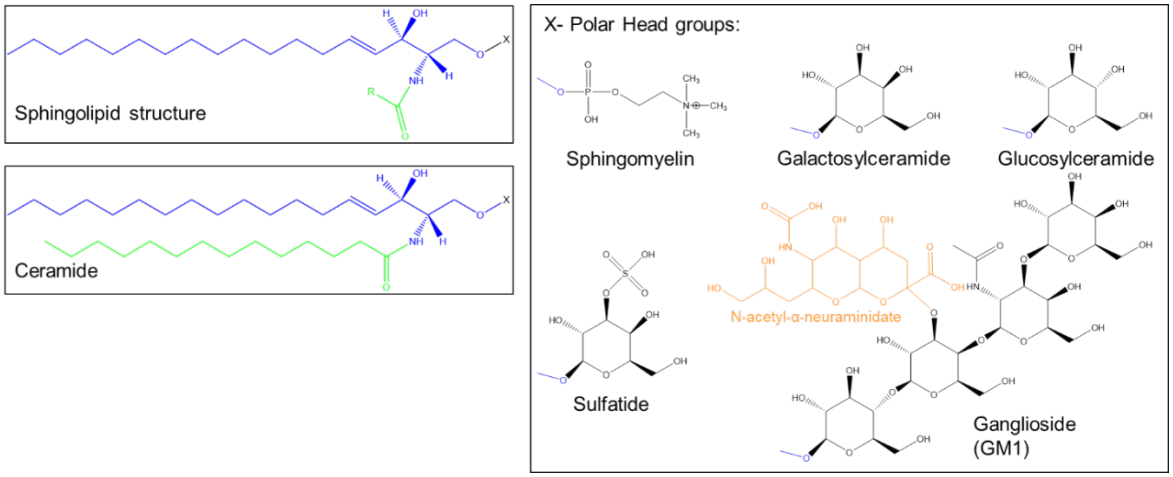

Figure 6.7 Sphingolipid chemical structure. Sphingolipids consist of a sphingosine base (blue) and fatty acid tail (green). The polar head group can contain a phosphate group (sphingomyelin)

The sphingosine base that makes up *C. elegans* sphingolipids differs from the basic chemical structure that is displayed in Figure 6.7. In *C. elegans,* sphingolipids are based on an iso-branched C_{17} compound, 15-methyl-2-aminohexadec-4-en-l,3-diol (Chitwood et al., 1995) (Figure 6.8).

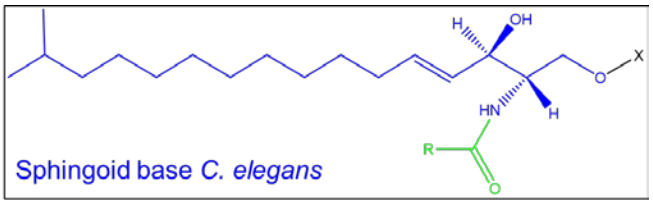

Figure 6.8 Sphingoid base structure of *C. elegans* sphingolipids. The only sphingoid base detected from *C. elegans* lipid extracts is 15-methyl-2-aminohexadec-4-en-l,3-diol.

Sphingolipids are integral members of membranes, where they form small micro-domains within the membrane called lipid rafts. Lipid rafts are made up of sphingolipid, cholesterol and proteins, and function in membrane signalling and trafficking (Lingwood and Simons, 2010). In contrast to mammals, *C. elegans* membranes contain low amounts of cholesterol, and so the specific role of sphingolipids in *C. elegans* lipid raft formation is not fully understood, given that a detailed analysis of the lipid composition of lipid rafts has not been performed (Hänel et al., 2019).

Glucosylceramides, a lipid species within the sphingolipid class (Figure 6.7), are important for *C. elegans* development, acting with the TORC1 signalling pathway to coordinate nutrient and metabolic status during growth (Zhu et al., 2013). Furthermore, ceramides, gangliosides and spingomyelins also influence development rate and lifespan in *C. elegans* (Cutler et al., 2014).

6.1.1.4 Sterol and prenol lipids

Sterol lipids, specifically cholesterol (Figure 6.9), are important components of membrane lipids, along with the glycerophospholipids and sphingolipids, crucial for the function of most eukaryotic cells (Kurzchalia and Ward, 2003). However, *C. elegans* are sterol auxotrophs, meaning that cholesterol has to be supplied exogenously through diet.

C. elegans requires too little cholesterol for it to play a significant structural role in membranes (Hänel et al., 2019), however, sterols are required for the synthesis of steroid signalling molecules (Kurzchalia and Ward, 2003).

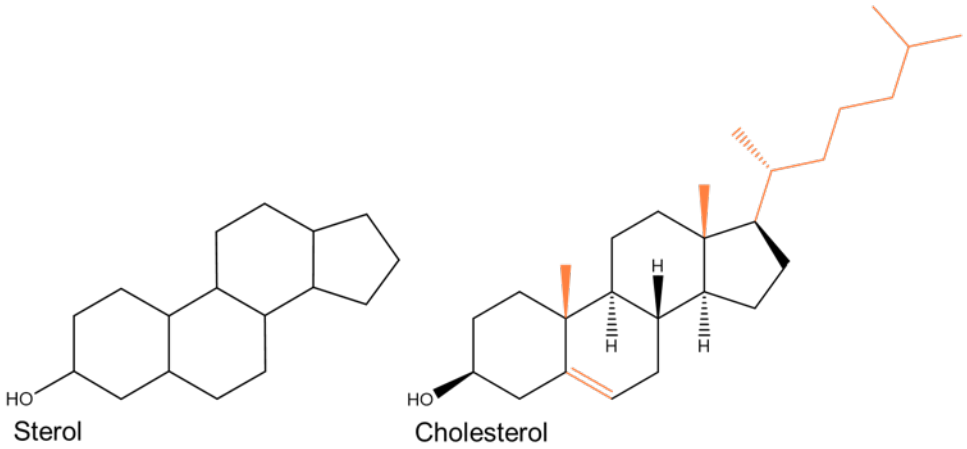

Figure 6.9 Chemical structure of Sterol lipids. Cholesterol is a sterol lipid, sharing the common steroid base. Additional structural changes that differ from the basic structure are shown in orange.

For example, dafachronic acid is a bile acid like steroid hormone that is involved in the regulation of development. Dafachronic acids are ligands for a *C. elegans* orphan nuclear receptor, DAF-12 (Motola et al., 2006). DAF-12 is a member of the dauer formation (daf) genes that regulate dauer diapause, reproductive development, fat metabolism and longevity (Antebi et al., 2000). This dafachronic acid-DAF-12 system has also been discovered in the free-living nematode *Pristionchus pacificus* (Ogawa et al., 2009) and parasitic nematodes *Ancylostoma ceylanicum, Strongyloides stercoralis* (Wang et al., 2009) and *Haemonchus contortus,* (Ma et al., 2019).

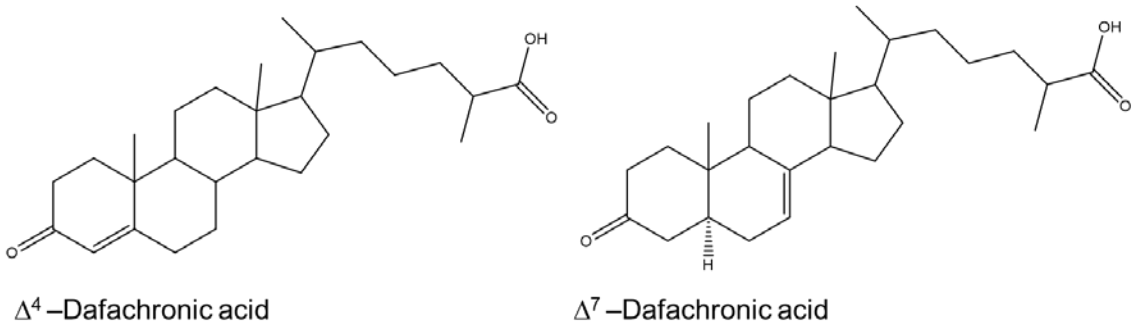

Figure 6.10 Structure of bile acid like steroid hormones, dafachronic acids. Structures of dafachronic acids adapted from (Motola et al., 2006). Both compounds are 3-keto, C-26 oxidized derivatives of cholesterol that differ in the position of an unsaturated double bond at C-4 (Δ^4 – Dafachronic acid) or C-7 (Δ^7 – Dafachronic acid) of the steroid nucleus.

The mevalonate pathway in mammals is responsible for the conversion of acetyl-CoA into cholesterol and other important molecules, including the prenol lipids. The mevalonate pathway is conserved in *C. elegans*, however without the cholesterol synthesis branch (Witting and Schmitt-Kopplin, 2016). Subclasses of prenol lipids include isoprenoids, polyprenols, quinones, and hydroquinones (Fahy et al., 2011). One important function of prenol lipids is the formation of coenzyme Q (ubiquinone) (Witting and Schmitt-Kopplin, 2016). Coenzyme Q functions as an electron acceptor in the mitochondrial electron transport chain and is essential for the development and survival of *C. elegans* (Rauthan and Pilon, 2011).

6.1.2 Lipid class distribution in nematodes at distinct developmental stages

6.1.2.1 Caernohabditis elegans

In young adult *C. elegans,* lipid composition is largely dominated by triglycerides (TAGs) and phospholipids (PLs). TAGs contribute to approximately 50% of total lipid, whilst the main PL species are from the phosphatidylcholine (~54% of PLs) and phosphatidylethanolamine (~36% of PLs) subclasses (Shi et al., 2013). Predominant fatty acid species are derivatives of C16, C18 and C20 (Watts and Browse, 2002). In *C. elegans,* polyunsaturated fatty acids (PUFAs), such as C20:4, can be synthesised from dietary or de novo synthesised C16:0 (See 6.1.1.3). This is in contrast to mammals, which are unable to convert oleic acid (C18:1n-9) to linoleic acid (C18:2n-6) or convert omega-6 fatty acids to omega-3 fatty acids, because they lack the required desaturases (Watts, 2009). The role of PUFAs in *C. elegans* is vast, including roles in determining growth, neurotransmission, sensory signalling, germ-cell maintenance, sperm attraction to oocytes, and innate immune response (reviewed by Watts, 2009).

In dauer larvae, there is an excessive accumulation of endogenous PUFAs, which enable extended longevity. Dauer larvae also exhibit enriched PUFAs in their membrane phospholipids, displaying accumulation of esterified PUFAs throughout the course of dauer endurance. This is thought to minimize the oxidative stress that is induced by the excessive accumulation of endogenous PUFAs (Lam et al., 2017). Furthermore, there is a distinct accumulation of branched-chain fatty acids in PC species during early dauer phases, which will prevent the formation of branched-chain glucosylceramides and subsequent resumption of normal development (Lam et al., 2017).

There is also evidence for maradolipids, a special class of glycolipid, performing a structural role in *C. elegans* dauer larvae that is not identified in other developmental stages (Penkov et al., 2010). This highlights specific lipid classes and species that can be identified as key indicators of developmental stage.

6.1.2.2 *Globodera* spp.

The neutral lipid fraction of *G. pallida* and *G. rostochiensis* juveniles dominates total lipids to a greater extent than *C. elegans,* contributing ~73%, of which ~95% is triglyceride. The remaining neutral lipid fraction is comprised of species from the diacylglycerol, monoacylglycerol and cholesterol ester subclasses (Holz et al., 1997). The two other predominant lipid classes are phospholipids and free fatty acids, which contribute comparably, however, the authors describe that the large free fatty acid fraction could be due to technical factors in which free fatty acids are generated during lipid extraction and analysis (Holz et al., 1997).

The fatty acid composition of the free fatty acid fraction in *G. rostochiensis* has shown to be influenced by hydration of cysts and PRD exposure, where cysts exposed to PRD show an increase in monounsaturated fatty acids. In contrast, hatched juveniles show a decrease in monounsaturated fatty acids and an increase in polyunsaturated fatty acids (Holz et al., 1998a). Fatty acids identified from total lipid range from carbon lengths of 14 to 22, the predominant species being C20:4, C20:1, and C18:1 (Holz et al., 1997; Holz et al., 1998a). C20:4 (arachidonic acid) is the major fatty acid in hatched juveniles, displaying ≥30 fold increase in comparison to lipids extracted from cysts activated by PRD, suggesting a significant role of C20:4 for the hatched J2 stage (Holz et al., 1997). This could be reflective of C20:4 being involved in the parasite/host plant interaction, due to it being identified as a phytoalexin elicitor, stimulating de novo synthesis of phytoalexin by the plant, which is a toxin to invading parasites (Creamer and Bostock, 1988).

6.1.3 Analytical methods for describing lipid species

Nile red staining (Kearn et al., 2017) and CARS analysis are imaging techniques (Chapter 1.5.5.1.1) that allow the direct analysis of lipids, providing information on localization and amount of detectable lipid. To investigate lipid classes and individual species, other biochemical approaches are required.

6.1.3.1 Lipid extraction

To analyse individual lipids or lipid classes, they must first be extracted from the sample. Lipid extraction protocols published by Folch and Bligh and Dyer (Bligh and Dyer, 1959) are widely employed for rapid extraction of total lipids (Witting and Schmitt-Kopplin, 2016). Tissue is homogenized with a mixture of chloroform and methanol, yielding a monophasic solution when mixed with the water that is present in the tissue. The subsequent homogenate can then be diluted with water and chloroform to result in a biphasic system. The chloroform layer will contain the lipids and the methanol-water layer will contain the non-lipids. The chloroform layer provides a purified lipid extract (Bligh and Dyer, 1959). Chloroform extraction protocols have been replaced by MTBE extractions, which build a two phase system with the organic solvent on top and the cell debris on the bottom (Sostare et al., 2018). This modified Matyash method was shown to be more reproducible and have higher extraction yield when compared to the more traditional extraction method (Sostare et al., 2018).

6.1.3.2 Chromatography

Solid phase chromatography and gas chromatography can be employed to separate lipid extracts post extraction. Solid phase chromatography uses solvents with different polarities to separate the sample into specific lipid classes, such as neutral lipids, free fatty acids and non-acetic phospholipids (Holz et al., 1997). Fatty acids from nematode populations are commonly analysed using acidic methylation to produce fatty acid methyl esters, which are separated from each other by gas chromatography (GC), and detected with either mass spectrometry (MS) or flame ionization detection (FID) (Watts and Browse 2002). Solid phase and gas chromatography have been used to compare the total lipid, free fatty acid and non-acetic phospholipid contents of *G. rostochiensis* and *G. pallida* (Holz et al., 1997; Holz et al., 1998a). The studies by Holz et al. identified that the major fatty acids in both *G. rostochiensis* and *G. pallida* were C18:1, C20:1 and C20:4, the three fatty acids predominant in all classes (Holz et al., 1997; Holz et al., 1998a).

Following extraction, a simple way to separate and assign lipids is by thin layer chromatography (TLC). TLC assesses lipid composition at a class level. A two-phase solvent system can be used to separate lipids from *C. elegans* extracts, distinguishing between phospholipids and neutral lipids (Shi et al., 2013).

TLC is unable to identify lipid species below the level of lipid classes (Watts and Ristow, 2017). TLC methods can be used to separate and enrich specific lipid classes and then combined with more sensitive methods, such as mass spectrometry based techniques, for more detailed analysis.

6.1.3.3 Mass Spectrometry

Mass spectrometry (MS) is used for qualitative and quantitative lipidomic analysis (Kofeler et al 2012). Mass spectrometers can add or remove an electron to/from the molecule or add or remove an ion to/from the molecule. In this way, the mass spectrometer is able to provide information on the mass of the ion of interest, as well as information on other properties, such as the reactivity of the ion. This is particularly important when needing to distinguish between ions that have the same mass but different chemical properties.

The mass spectrometer consists of an ionisator, a desolvator, 2 mass filters, a collision cell and a detector. For a molecule to be detected, it must pass through all of these parts; the molecule is charged in the ionisator, solvents are removed in the desolvator, the mass of the ion is checked in mass filter 1, the selected ion will then be broken down in the collision cell, its fragments are checked in mass filter 2 and only charged fragments with the correct mass are let through and detected. To achieve a mass spectrum of the whole ion, the collision cell is not used and once checked by mass filter 1, all ions that pass the first mass filter will be detected.

There are numerous mass spectrometric platforms for lipidomic analysis, including shotgun lipidomics, liquid chromatography-mass spectrometry (LC-MS) and matrix assisted laser desorption ionization-time of flight (MALDI-TOF) (Köfeler et al., 2012).

Shotgun lipidomics is based on neutral loss scans of readily ionisable phophoslipid headgroups, resulting in specific lipid fragments being detected. This platform can utilize HPLC apparatus to automatically inject samples into the flow (Köfeler et al., 2012).

LC-MS allows analysis of lipids by chromatography which is coupled to mass spectrometry. This method has enabled increased specificity for identifying lipid species. However, due to variable ionization during a gradient LC run, can complicate absolute quantification (Brandsma et al., 2017). Electrospray ionisation mass spectrometry (ESI-MS) can be used with LC-MS to allow the measurement of stable isotope-labelled precursor molecules into complex lipid species (Brandsma et al., 2017).

MALDI-TOF analysis can assign molecular ions of lipid species, allowing good sensitivity. However, this platform shares the drawbacks of LC-MS, in that issues arise in quantification (Köfeler et al., 2012). This platform can be combined with TLC, allowing identification of spots that have been resolved by TLC (Köfeler et al., 2012). MALDI can also be combined with imaging mass spectrometry (IMS) and has been used to profile the phospholipid composition of adult *C. elegans* (Hameed et al., 2015). This technique allows analysis of lipid composition of whole-body nematodes without requiring lipid extraction. MALDI-IMS allows spatial information of lipid species and as shown with *C. elegans,* enables analysis of lipids in individual nematodes (Hameed et al., 2015).

Shotgun lipidomics is the most employed platform for the analysis of the *C. elegans* lipidome, however, chromatographic separation is required to differentiate between isomeric lipids (Witting and Schmitt-Kopplin, 2016). To my knowledge, mass spectrometry has not been employed to analyse the lipidome of any plant parasitic nematode.

6.1.4 Targeting lipid metabolism as a route to nematicidal activity

One of the distinct aspects of fluensulfone is its selective toxicity toward PPNs, including a favourable toxicity profile towards non-target nematodes (Waldo et al., 2019). This could be due to it acting at a specific target in PPNs that is not present in other nematode species. An alternative is that it is targeting a pathway that is of a greater significance to the PPNs than other nematode species. It is attractive to speculate that targeting lipid metabolism could provide a selective route to targeting PPNs due to their reliance on lipids for energy prior to establishing a feeding site.

The insecticide resistance action committee (IRAC) use a classification system based on mode of action to organize nematicides into groups. Currently, fluensulfone is in 'Group N-UN: Unknown.' Other groups include the acetylcholinesterase inhibitors, GluCl allosteric modulators and mitochondrial complex II electron transport inhibitors. Spirotetramat is the sole occupier of 'Group N-4: Lipid synthesis, growth regulation' due to its action as an inhibitor of acetyl CoA carboxylase (Gutbrod et al., 2020). Spirotetramat demonstrates that the inhibition of de novo lipid biosynthesis has nematicidal potency, reinforcing the targeting of lipid metabolism as a potential route to nematicidal action.

6.1.5 Chapter Aims

The aim of this chapter is to provide a detailed description of biochemical analysis that has been performed and the optimized protocols that have been designed to investigate lipids in *G. pallida*¸ specifically for the identification of changes to lipid content and profiles following treatment with fluensulfone. Comparative behavioural studies have provided a comprehensive profile of effects of fluensulfone on both the unhatched and hatched juvenile. This analysis has provided evidence for its action as a nematicide as well as providing insight into its mode of action, however without describing the pathway it is acting in or more specifically, its molecular target.

Analysing the lipid profiles of treated and untreated juveniles will improve the understanding of how fluensulfone acts to impair utilization of lipids. This will enable more targeted investigation into the mechanism of action of fluensulfone, highlighting specific aspects of lipid metabolism that may be compromised by fluensulfone treatment.

6.2 Results

In the process of initial extraction using favoured approaches, I identified that variation in extraction had a confounding effect on subsequent biochemical analysis (data not shown). A significant hurdle is the quantity of worm input material that is required to perform biochemical analysis. This is compounded by the cuticular body structure that is resistant to non-mechanical organic extraction. Optimization of the extraction protocol became an important priority in early experiments.

6.2.1 Optimization of lipid extraction from *Globodera pallida* juveniles

I employed a similar protocol to the Bligh and Dyer method (Bligh and Dyer, 1959) based on chloroform/methanol extraction, which yields a biphasic system, in which the chloroform layer that contains the lipids can be isolated.

It is recommended that for efficient extraction of lipids, tissue should be homogenized with a mixture of chloroform and methanol (Bligh and Dyer, 1959). Homogenization can be performed with a Dounce homogenizer (glass-glass), allowing relatively small volumes (<2ml) to be homogenized. In my case, inputs of up to 3,000 juveniles in volumes ≤100 µl resulted in smearing of sample over apparatus that lead to unacceptable losses and variability in sample recovery. In addition, even with high yields (10,000 juveniles), visual inspection of samples following Dounce homogenization resulted in modest disruption, with many juveniles remaining intact.

To improve physical disruption, I investigated the use of an electric homogenizer (Ika T-10 basic ultra-turrax with an SN10 N5G dispersing element), where the small rotor diameter enabled homogenization in a 2ml Eppendorf, preventing the need to transfer the sample to a specific tube prior to homogenization. However, homogenizing in chloroform resulted in the juveniles sticking to the metal apparatus. Interestingly, self-organization of the juveniles in solvent solution results in solution encapsulated, undisrupted sample, where the hydrophobicity of the cuticle acted against homogenisation (data not shown). In the free-living nematode *Pristionchus pacificus,* dauer larvae synthesize a long-chain polyunsaturated wax ester, termed nematoil, that has been shown to cover the surface of the nematode, promoting congregation of dauer larvae (Penkov et al., 2014). A similar wax ester on the surface of *G. pallida* juveniles would be consistent with the encapsulation of juveniles in solvent that I describe.

In view of the protective effect of solvent via organism interaction, likely driven by the oil wax of the cuticle, I took a two-step process in which firstly, cup sonication was employed to drive the breakdown of the worms and secondly, organic extraction. Cup sonication (FisherBrand Q700 sonicator) was optimized to run at an amplitude of 50%, for a total process time of six minutes, with 10 seconds on, 30 seconds off. This resulted in an energy input of approximately 30,000 J. Observation of the samples concluded that approximately 90% physical disruption, based on intact versus ghost cuticles, was achieved with these parameters (Figure 6.1).

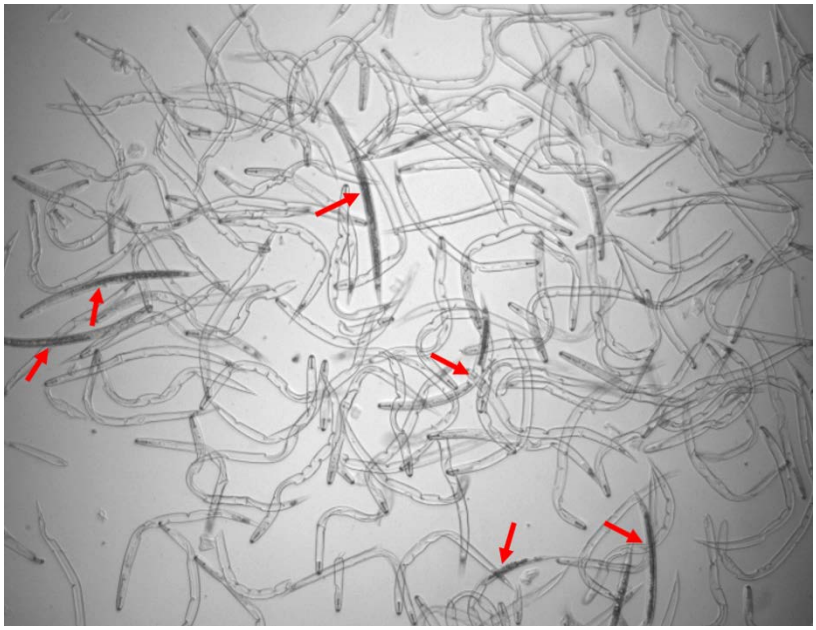

Figure 6.11 *Globodera pallida* juveniles post-sonication. *Globodera pallida* juveniles were suspended in 60µl M9 buffer. Samples were sonicated using a FisherBrand Q700 sonicator, with CL-334 converter and cup horn accessory. The following parameters were used: 50 amplitude, 6 minute process time, 10 seconds on, 30 seconds off. The system was controlled at 4°C. The image above shows successful disruption of juveniles, observed as 'ghost-like' cuticular structures. Worms that are not disrupted are indicated (red arrows).

Following sonication, the samples were then subjected to chloroform-methanol extraction. It was found that an overnight incubation in the chloroform-methanol mixture prior to biphasic separation improved juvenile disruption. Juveniles post-sonication but pre-solvent exposure were observed as having intact stylets, despite disruption of their intestinal regions. Post-chloroform-methanol incubation, the juveniles stylets were observed as being disrupted (Figure 6.2). Visual inspection of samples was performed at each stage of the extraction protocol to ensure robust disruption of the juveniles had occurred.

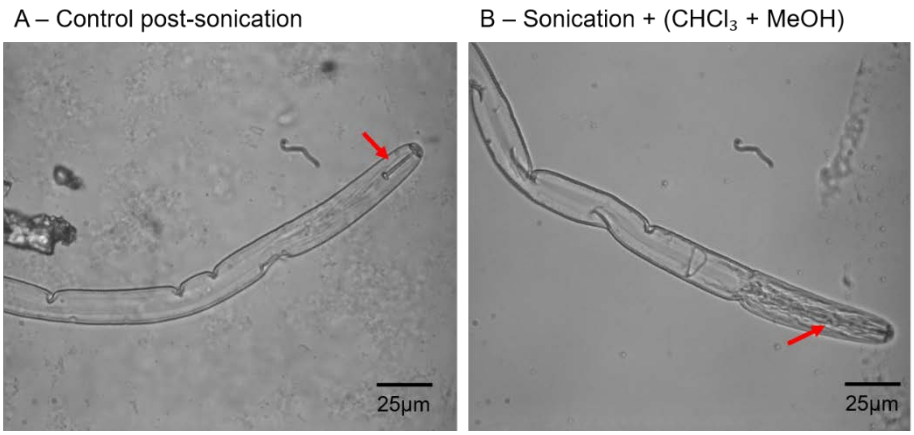

Figure 6.12 Stylet disruption following sonication and incubation with chloroform-methanol. Freshly hatched *Globodera pallida* juveniles post-sonication (A) and post-sonication with subsequent 24-h incubation in Chloroform ($CHCl_3$) + Methanol (MeOH) (B). Stylet is visible in A, however is disrupted following 24-h incubation in solvents (B) (red arrows highlight stylet position).

The optimized extraction procedure was therefore as follows:

1. Collect *Globodera pallida* juveniles from PRD exposed cysts. For each treatment group, carefully match population numbers to ensure accurate comparisons. A minimum of 6,000 J2s per treatment group is recommended, however, ≥10,000 J2s is preferable.
2. Pellet juveniles using a table-top centrifuge. Spin at 1000 x g for 3 minutes at room temperature. Remove supernatant and repeat wash 3 times.
3. Re-suspend juvenile pellet in 60µl M9 solution and transfer pellet to polystyrene sonication tubes – keep on ice. Sonication tubes provide more efficient energy transfer during sonication.
4. Equilibrate cup sonicator to 4°C, ensuring anti-freeze solution is topped up. Set up sonicator with the parameters 50 amplitude, 6 minute process time, 10 seconds on, 30 seconds off.
5. Following sonication, transfer sample (total tube contents) into a clean glass tube. Rinse out sonication tube with 1000µl methanol (100%) and add to tube.
6. To each tube add 2000µl chloroform (100%) and a further 1000µl methanol. Vortex well. Neutral lipids will be extracted with chloroform, while membrane lipids are extracted by methanol (Barros et al., 2012). Add 800µl Saline solution (0.9% sodium chloride made in dd.H_2O) and vortex to a single phase. If required, add a drop of methanol and vortex - repeat until a single phase is achieved. Add 1000µl chloroform and 1000µl dd.H_2O and vortex. Seal tubes and incubate at -20°C overnight.

7. Using a Pasteur pipette, transfer bottom lipid layer into a clean Eppendorf and dry sample – this can be achieved by drying under nitrogen flow at 37°C or spinning at 30°C under vacuum.

For lipid analysis, re-suspend sample in required volume of solvent (for TLC, use 10µl methanol (100%)). Store samples at -20°C if not analysed immediately.

6.2.2 Thin Layer Chromatography optimization

I used Thin Layer Chromatography (TLC) to provide an overview of lipid extraction efficiency and the proportion of significant lipid classes present in *G. pallida* juveniles, informing on the quantities and ratios of the major lipid classes and how these might change over time and following drug treatment.

TLC has been used to analyse lipid classes from *C. elegans* lipid extracts using a single phase system of hexane: diethyl ether: acetic acid at 75 mL: 25 mL: 2 mL (vol/vol/vol) ratio (Zhang et al., 2010). The same single phase system was used here, in addition to a two phase system, which allowed clearer fractionation of neutral (TAG) and polar lipids e.g. phosphatidylcholine (Figure 6.6).

6.2.2.1 Single phase separation

The optimized extraction protocol was used to extract total lipids from nematode samples. Prior to *G. pallida* analysis, extraction of 1,000 L4 *C. elegans* was performed and compared to published observations. This allowed identification of major lipid classes and provided a benchmark for the quantities of *G. pallida* sample required to visualise the major storage lipid, triglyceride.

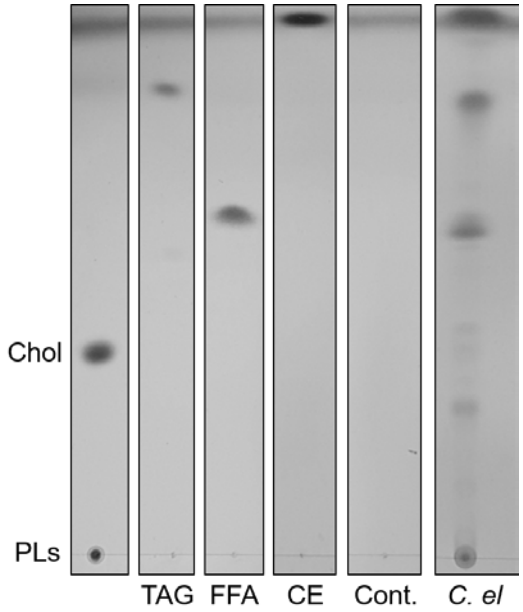

Figure 6.13 Single phase separation of lipids. 1,000 *C. elegans* L4 extracted according to optimized extraction protocol. Extracted lipids were suspended in 10µl methanol and full sample was spotted on to plate (*C. el,* lane 6). Standards used: Polar lipids (PLs), which includes phosphatidylcholine, phosphatidylethaolamine and sphingomyelin, and Cholesterol (Chol) 10µg (Lane 1). Triglyceride (TAG; triolein 18:1) (Lane 2), free fatty acids (FFA; oleic acid) (Lane 3) and Cholesterol ester (CE) (Lane 4) 20 µg. A blank methanol sample (Cont.) was run in lane 5 to ensure bands that were visualized were not due to contamination. Solvent system for separation was hexane: diethyl ether: acetic acid at 75 mL: 25 mL: 2 mL (vol/vol/vol) ratio. For lipid visualisation, plate was sprayed with 10% phosphomolybdic acid and heated at 100°C for 10 minutes.

Single phase separation of *C. elegans* lipid extract displays clear fractionation of polar and neutral lipids (Figure 6.13). Predominant bands relating to CE, TAG, FFA and polar lipids are observed. Subsequent repeats showed a similar profile, however, the FFA band is not always visualised. This could be due to the generation of FFAs during the extraction and analysis procedure. Lipid extraction from *G. rostochiensis* and *G. pallida* revealed that a predominant fraction of total lipids was assigned to the FFA fraction, however the authors noted that this could be due to generation of FFAs during lipid extraction (Holz et al., 1997).

The cholesterol ester (CE) band was interesting to us given that it was such a prominent band. It was considered that this band could correspond to a wax ester, consistent with the long-chain polyunsaturated wax ester that has been described to coat the cuticle in the free-living nematode *P. pacificus* (Penkov et al., 2014). However, further investigation concluded that this band was in fact due to contamination from plastic, where plastic falcon tubes were used during the extraction protocol. Subsequently, the lipid extraction protocol described here should be performed with glass and exclude the use of plastic where possible. Additionally, the solvent front interferes with the visualisation of the cholesterol ester band. To investigate this lipid species, it is therefore advised that different solvents and ratios of solvents should be optimized for separation of cholesterol esters. Cholesterol esters were not a focus in the investigations here and so this was not performed.

Lipid extraction performed with 10,000 *G. pallida* juveniles was shown to give comparable levels of polar lipids extracted from 1,000 *C. elegans* L4 larvae (Figure 6.14). The TAG fraction visualised from *G. pallida* juveniles was of a greater intensity when compared to the TAG band from *C. elegans,* which would be consistent with TAG contributing to a greater proportion of total lipids in *G. pallida* than its contribution in *C. elegans* (Section 6.1.3). Furthermore, distinct species could be identified from *G. pallida* extraction. To investigate this further and compare subclasses of polar lipids, two-phase separation was employed.

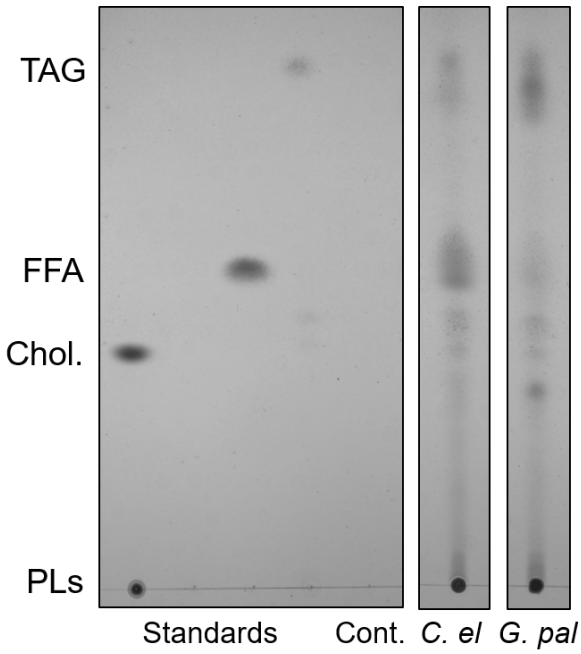

Figure 6.14 Comparison of *C. elegans* and *G. pallida* lipid extracts using single phase separation. 1,000 *C. elegans* L4 and 10,000 *G. pallida* J2 extracted according to optimized extraction protocol. Extracted lipids were suspended in 10µl methanol and full sample was spotted on to plate. Standards used: Polar lipids (PLs: phosphatidylcholine, phosphatidylethaolamine and sphingomyelin) and Cholesterol (Chol) 10µg. Triglyceride (TAG; triolein 18:1) and free fatty acids (FFA; oleic acid) 20µg. A blank methanol sample (Cont.) was run in parallel. Solvent system for separation was hexane: diethyl ether: acetic acid at 75 mL: 25 mL: 2 mL (vol/vol/vol) ratio. For lipid visualisation, plate was sprayed with 10% phosphomolybdic acid and heated at 100°C for 10 minutes.

6.2.2.2 Two-phase separation

Two phase separation was used in which the first solvent system used is chloroform: methanol: H_2O at 32.5 mL: 12.5 mL: 2 mL (vol/vol/vol) ratio, followed by the second solvent system of hexane: diethyl ether at 4 mL: 1mL (vol/vol) ratio. Lipid extraction was performed on 1,000 *C. elegans* L4 that after rinsing from *E. coli* seeded NGM plates and washed 3 times to remove bacteria, were immediately pelleted and stored at -80°C (*C. elegans* fed) or were re-suspended in M9 solution for 24 hours prior to extraction (*C. elegans* starved). Freshly hatched *G. pallida* juveniles were collected from PRD exposed cysts, washed, pelleted and stored at -80°C (*G. pallida* Day 0) or were re-suspended in M9 solution and stored at room temperature for seven days prior to extraction (*G. pallida* Day 7). The starvation experiments performed allow direct comparison with previously reported CARS data for *C. elegans* that show that lipids are depleted after 24 hours in the absence of food (Smus et al., 2017) and the data that I report in Chapter 5 for *G. pallida* juveniles 7 days post hatch. Here, I probed to see whether the reduction in CARS signal is supported by biochemical analysis and visualisation of lipids by TLC.

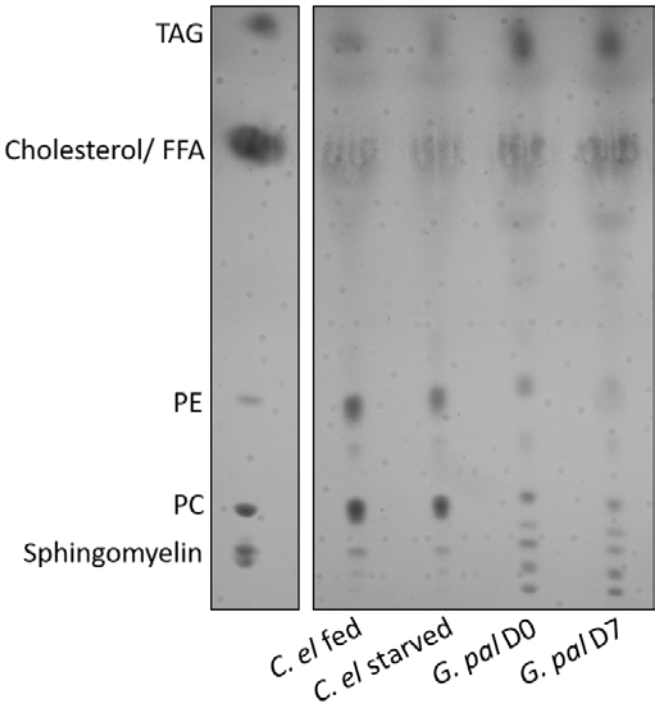

Figure 6.15 Two-phase separation of lipid species from *C. elegans* and *G. pallida* lipid extracts.
C. elegans L4 larvae were washed from NGM plates and pelleted (*C. el* fed) or washed and incubated in M9 solution for 24-h (*C. el* starved). Each sample consists of 1,000 L4s. *Globodera pallida* juveniles were collected at day 0 (*G. pal* D0) or washed and incubated in M9 solution for seven days (*G. pal* D7). Each sample consists of 10,000 juveniles. Lipids were extracted and separated on TLC plate using a two-phase separation system. Standards: sphingomyelin (10 µg), phosphotidylcholine (PC; 10µg), phosphotidylethanolamine (PE; 10 µg), Cholesterol (10µg), free fatty acid (FFA; Oleic acid; 20 µg) and triglyceride (TAG; Triolein 18:1; 20 µg).

Similarly to the single-phase separation of lipids, it was observed that the predominant lipid fraction in *G. pallida* samples was TAG. In *C. elegans,* the phospholipid classes were more dominant than TAG. Lipid species can be compared to standards for quantification purposes. This was performed here by using imaging software analysis (ImageJ). The area and greyscale profile of the lipid region can be determined for each standard and compared to each lipid species detected in samples to give an estimate of lipid quantity (Figure 6.16).

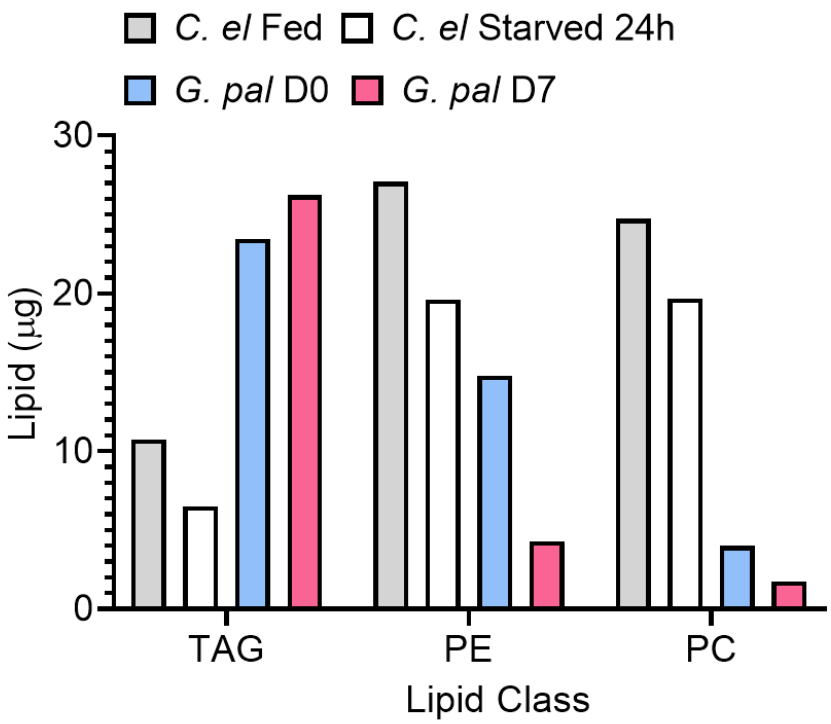

Figure 6.16 TLC quantification of major lipid classes in *C. elegans* L4 and *G. pallida* J2. Quantification of major lipid classes visualised by TLC (Figure 6.15). Triglyceride (TAG), phosphatidylethanolamine (PE) and phosphatidylcholine (PC).

Lipid samples loaded onto TLC plates can be adjusted to reflect similar protein concentrations for the purpose of normalization. Due to limited input material, this was not done here. Alternative methods for normalization include normalizing to PCs, assuming that these remain unchanged. Whilst every effort is made to ensure population numbers are equivalent across samples, I cannot conclude whether a reduction in PEs and PCs is of biological significance or whether it reflects a reduction in total lipid extraction. Subsequently, it is not appropriate to normalize the TAG concentration to the PCs.

When analysing the TAG band from *G. pallida* samples, there were no clear differences in TAG amount between the freshly hatched and seven days post-hatch juveniles. This was surprising, given that CARS analysis showed a clear depletion in lipids from the tail region of *G. pallida* J2s at seven days post-hatch (See Chapter 5.2.4). There was however a decrease in phosphatidylethanolamines.

TLC-based quantification of lipids was repeated with *G. pallida* juvenile samples to include seven day treatment with 30µM fluensulfone and 50µM perhexiline. Two-phase separation was performed in order to facilitate revelation of any changes in specific phospholipids species.

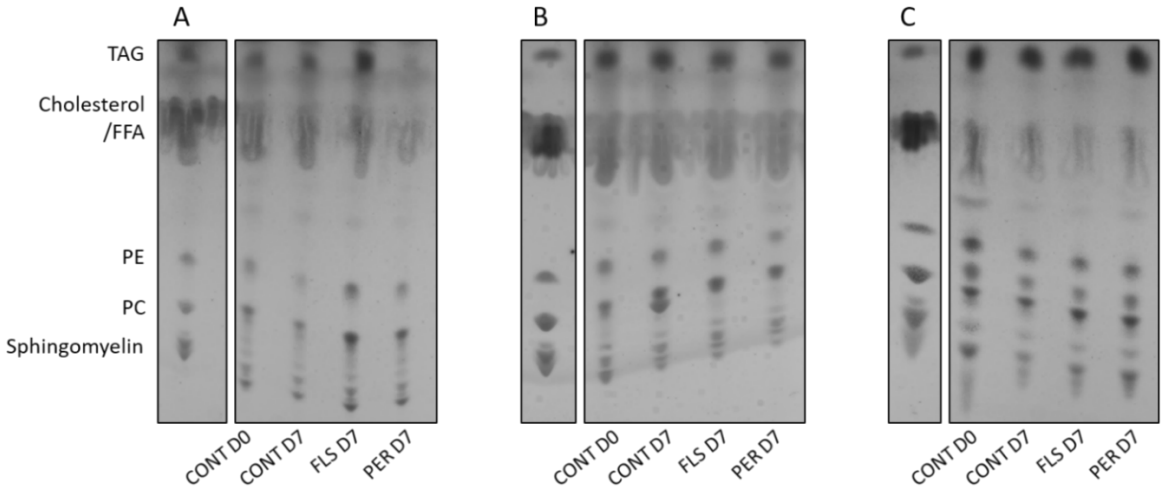

Figure 6.17 Composition of major lipids extracted from fluensulfone and perhexiline treated *Globodera pallida* juveniles. Juveniles were collected at day 0 (CONT D0), washed and frozen at -80°C. For day 7 treatment, juveniles were washed and transferred to M9 solution for 7 days (CONT D7), M9 + 30µM fluensulfone (FLS D7) or M9 + 50µM perhexiline (PER D7). At the end of the treatment period, juveniles were washed and then frozen at -80°C. For lipid extraction, samples were pooled from multiple collections to give a total of 10,000 *G. pallida* juveniles per treatment group. Lipids were extracted according to optimized extraction protocol and then separated on TLC plate using a two-phase separation system. Standards: sphingomyelin, phosphotidylcholine (PC), phosphotidylethanolamine (PE), Cholesterol, free fatty acid (FFA; Oleic acid) and triglyceride (TAG; Triolein 18:1), all at 20µg. Representative images from 3 independent experiments, extracted and resolved on 3 different days.

Quantification of lipids was performed by scanning density and subjecting it to analysis with ImageJ. There were no significant differences between any treatment groups for any lipid class (Figure 6.18A). Because phosphatidylcholines were not significantly different between groups, TAG and PE were normalized to PCs (Figure 6.18B). Despite there being a reduction in PEs in all treatments when compared with control day 0, these reductions were not significant.

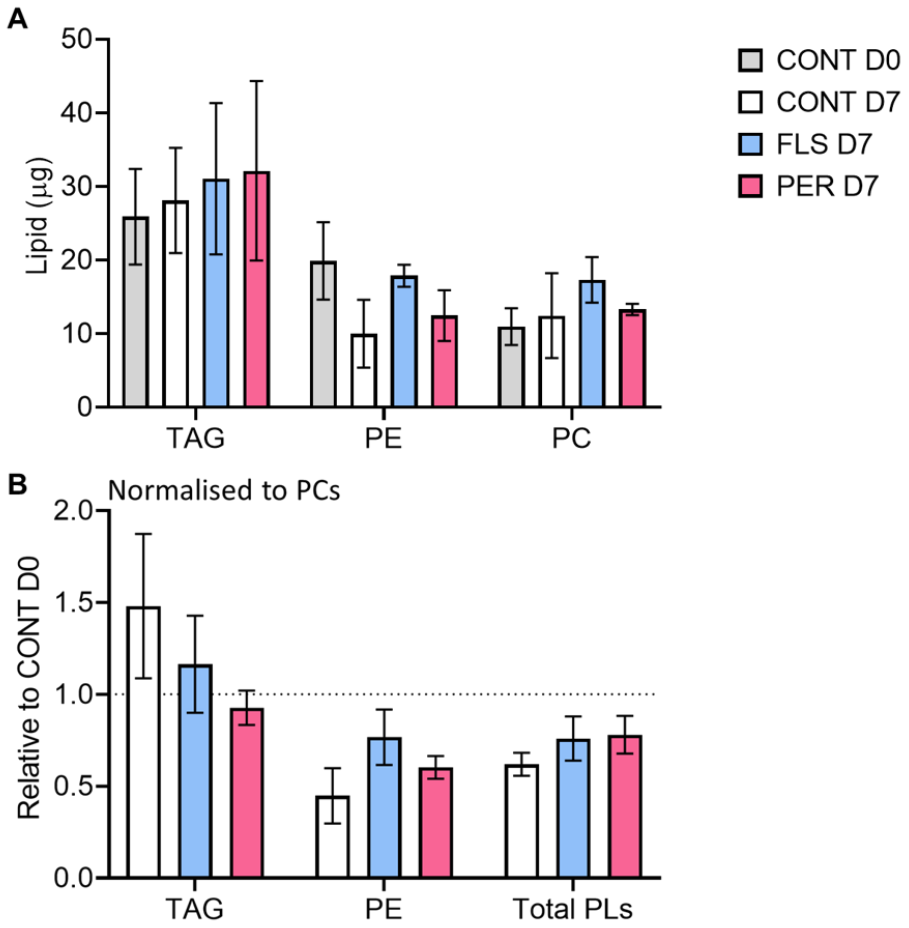

Figure 6.18 TLC-based quantification of lipids extracted from fluensulfone and perhexiline treated *Globodera pallida* juveniles. Quantification of major lipid classes visualised by TLC (Figure 6.17). (A) Triglyceride (TAG), phosphatidylethanolamine (PE) and phosphatidylcholine (PC) quantities for control day 0 (CONT D0), seven days post hatch (CONT D7), seven days fluensulfone treatment (FLS D7) and seven days perhexiline treatment (PER D7). (B) Data normalized to PC quantification and expressed relative to control day 0 (dotted line). Data plotted are mean ± S.E.M. No significant differences were observed. Statistical analysis performed by two-way ANOVA with Tukey post-hoc test.

6.2.3 Mass spectrometry of lipid extracts from *Globodera pallida* juveniles

TLC provides a relatively cheap and simple way of assessing lipid profiles. It is, however, unable to provide detail on the individual lipid species that may differ within each class. Mass spectrometry enables investigation of structure by employing ionization to produce fragments that can subsequently be detected.

Initial mass spectrometry analysis was performed using lipid extracts from 8,000 *G. pallida* juveniles. To detect all whole ions according to their mass/charge (M/z), a full positive (full +) scan was performed. In addition to the full + scan, I ran parent scans, allowing the selection of ions with a specific head group that is formed as the charged fragment and thus provides information on the class of lipid. Furthermore, neutral loss scans were used to provide structural information on each lipid species, specifically the fatty acid profile of particular lipids.

The major lipid class detected was triglycerides, consistent with this being the predominant lipid class detected by GC/MS in *Globodera* spp. (Holz et al., 1997) (Figure 6.19). Diacylglycerols (DAGs), PCs and sphingomyelins were also detected, with other lipid classes too low to be analysed or lost due to contamination effects. For example, a parent scan of mass 153 (P153), which will show the species that lose a charged fragment mass of 153 and thus correlate to phosphatidylserines, showed no informative data due to a high level of contaminant signal (data not shown).

The main triglyceride species are assigned in Table 6.2. Predominant fatty acids were 18:0>20:4>18:1. C20:4 and C18:1 have been previously described to be predominant fatty acid species in *G. pallida* (Holz et al., 1997). This data would suggest that C18:0 fatty acids are also prevalent in *G. pallida* triglyceride species.

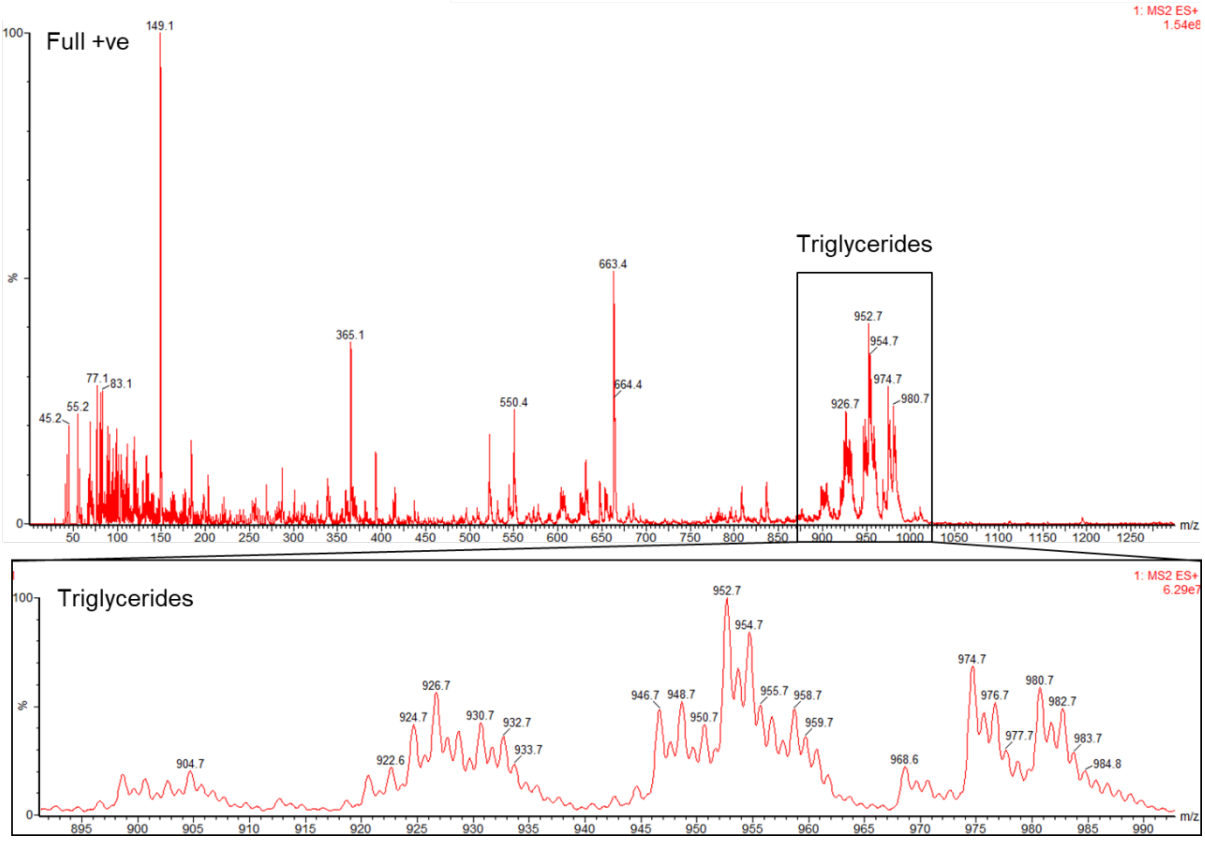

Figure 6.19 Mass spectrum highlighting triglyceride lipid species extracted from *Globodera pallida* juveniles. 8,000 freshly hatched *G. pallida* juveniles were used for lipid extraction and subsequent mass spectrometry analysis. Data acquired from Xevo TQD Triple Quadrupole Mass Spec from Waters. Spectrum shown is in the full positive, with region relating to triglyceride species highlighted. Triglyceride fraction is the predominant lipid class observed in the full positive. Mass/charge (M/z) is displayed on the x-axis against relative intensity (%).

M/z	Lipid Species	M/z	Lipid Species
904	TAG 18:0/18:1/18:1	952	TAG 18:0/18:0/22:6
922	TAG 18:1/20:4/18:2	954	TAG 18:0/22:5/18:0
924	TAG 18:0/20:4/18:2	958	TAG 18:0/18:0/22:3
926	TAG 18:0/18:1/20:4	968	TAG 22:5/20:5/18:2
932	TAG 18:0/20:2/18:0	974	TAG 18:0/22:5/20:4
946	TAG 22:5/16:0/20:4	976	TAG 18:0/20:4/22:4
948	TAG 20:4/18:0/20:4	980	TAG 20:4/18:0/22:2
950	TAG 22:5/18:1/18:1	982	TAG 20:3/18:0/22:2

Table 6.2 Lipid assignments for triglyceride species. Using neutral loss scans, the fatty acids comprising each lipid species could be assigned. Data was extracted from MassLynx spectrums using analyser software. Only the major lipid species are shown, correlating to the spectrum shown in Figure 6.19.

Phosphatidylcholine species can be easily seen in the full positive spectrum, with the major PCs detected in the *G. pallida* total lipid extract being PC 18:1/20:4 (M/z 808) and PC 18:0/22:5 (M/z 836) (Figure 6.20 & Table 6.3).

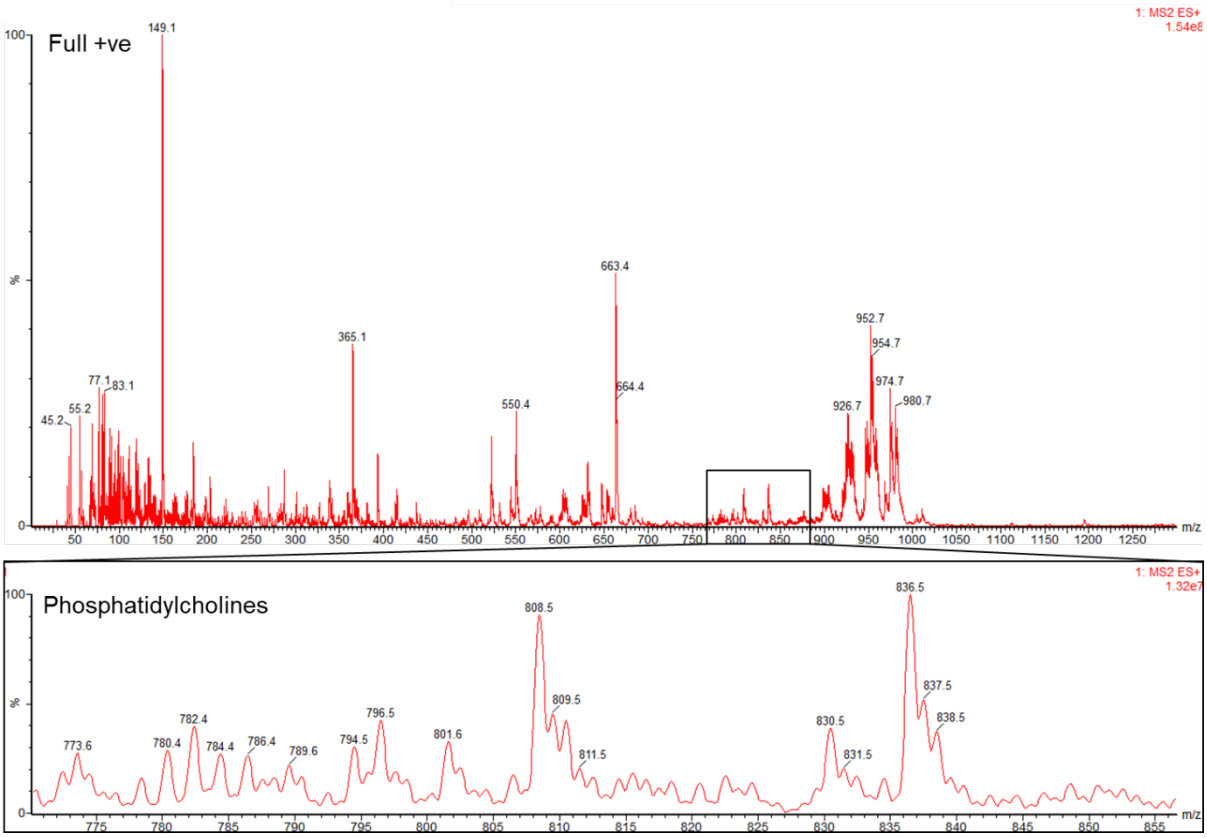

Figure 6.20 Mass spectrum highlighting phosphatidylcholine lipid species extracted from *Globodera pallida* juveniles. 8,000 freshly hatched *G. pallida* juveniles were used for lipid extraction and subsequent mass spectrometry analysis. Data acquired from Xevo TQD Triple Quadrupole Mass Spec from Waters. Spectrum shown is in the full positive, with region relating to phosphatidylcholine species highlighted. Mass/charge (M/z) is displayed on the x-axis against relative intensity (%).

M/z	Lipid Species
796	PC18:0a/20:4
808	PC18:1/20:4
830	PC20:4/20:4
836	PC18:0/22:5
838	PC18:0/22:4

Table 6.3 Lipid assignments for main PC species from Figure 6.20.

Phosphatidylcholine species are confirmed by using a parent loss scan of mass 184 (P184), which relates to the phosphatidylcholine head group. However, as this head group is common between sphingomyelin and phosphatidylcholine (Figure 6.6 and Figure 6.7) both will give a charged fragment mass of 184. When assigning the spectrum of P184, sphingomyelins will show up as an odd mass because of containing two nitrogen atoms in their structure, and phosphatidylcholines will show up as an even mass, because there is only one nitrogen. When looking at the P184 spectrum from the *G. pallida* sample, the main PCs with M/z 808 and 836 are clearly visible. LysoPCs are also detected, the main species at M/z 496, 522 and 550. The sphingomyelins are at very low concentrations.

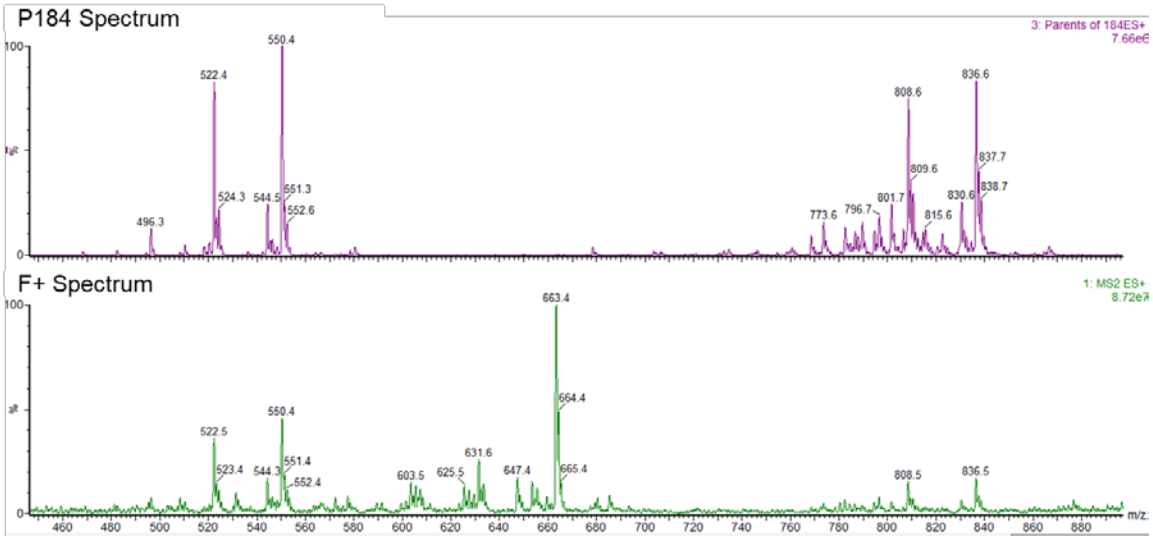

Figure 6.21 Parent loss scan mass 184 (P184) taken under Electro Spray positive condition. P184 scan (top) highlights PC species observed in the full + spectrum (bottom). Both spectrums are taken under electro spray positive condition (ES+). LysoPCs, PCs and sphingomyelins are observed in the P184 spectrum.

M/z	Lipid Species
496	LPC 16:0
522	LPC 18:1
550	LPC 20:1
808	PC18:1/20:4
836	PC18:0/22:5

Table 6.4 Lipid assignments for main lipid species detected in P184 scan.

6.2.3.1 Mass spectrometry of lipid extracts from fluensulfone treated *Globodera pallida* juveniles (Experiment 1)

Triglyceride species were readily detected in the full positive spectrum in early experiments with 8,000 *G. pallida* juveniles (Figure 6.19). This was encouraging and given that the triglyceride species are assumed to be the predominant origin of the CARS signal, which was shown to deplete over time in controls and was sustained following fluensulfone treatment (Chapter 5), was the focus of subsequent mass spectrometry analysis.

Treatment groups comprised of 2,500 *G. pallida* juveniles and were as follows: Control day 0, 1, 3, 5, 7, 10 and 14 and 30µM fluensulfone treated day 1, 3, 5, 7, 10 and 14. Full positive scans, parent scans and neutral loss scans were performed as before. The control day 0 full positive spectrum for the triglyceride species is shown in Figure 6.22. The triglyceride species that were detected are comparable between both samples.

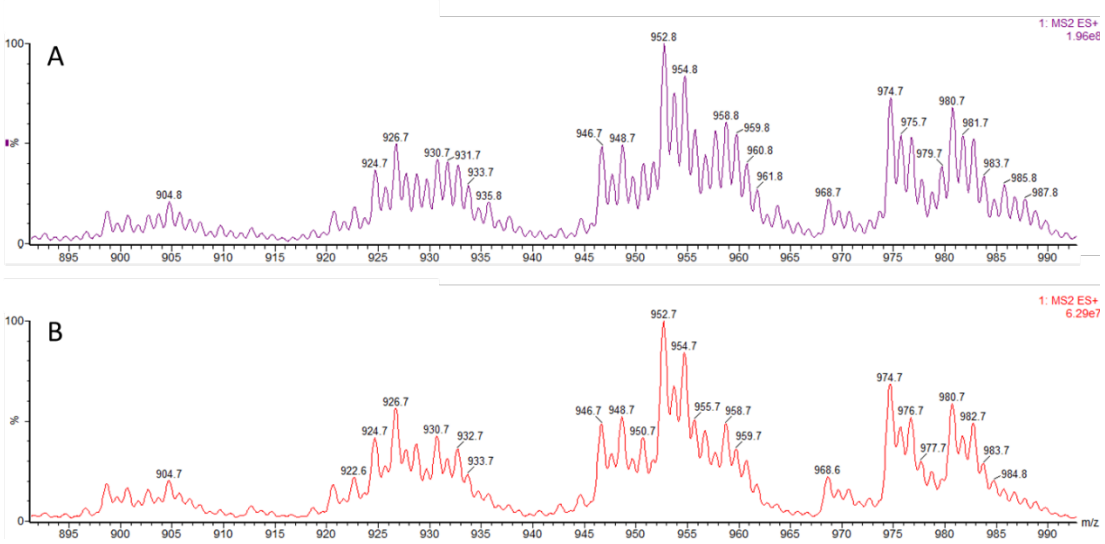

Figure 6.22 Full positive spectrum of triglyceride species extracted from *G. pallida* juveniles. Triglyceride species detected in the full + are consistent for control day 0 samples. (A) Total lipids extracted from 2,500 *G. pallida* juveniles. (B) Total lipids extracted from 8,000 *G. pallida* juveniles (Figure 6.19).

Triglyceride species can be compared to control day 0 samples to determine any changes over time post hatch and how fluensulfone treatment may interfere with the regular lipid profile. When looking at the full positive spectrum, there are no clear differences in lipid profiles between 7 day fluensulfone treated, 7 day untreated and control day 0 samples (Figure 6.23).

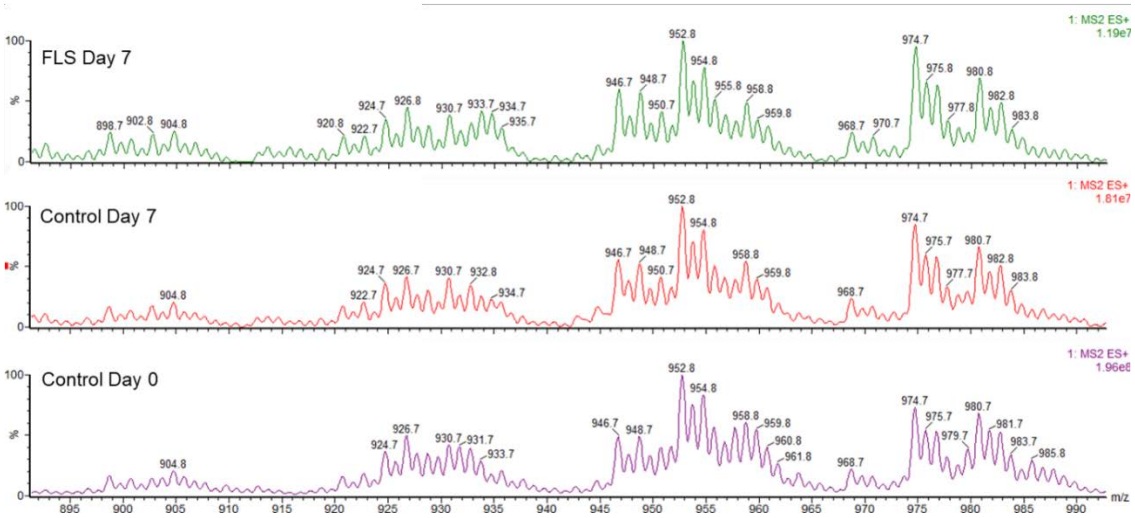

Figure 6.23 Triglyceride species do not change 7 days post hatch or following fluensulfone treatment. Total lipid extraction was performed for 2,500 *G. pallida* juveniles per treatment group. Full positive spectrum is shown for detection of major triglyceride species. Main triglycerides do not differ between treatment groups. Assignments are equivalent to those described in Table 6.2.

Mass spectrometry can also indicate lipid concentration based on normalization to standards that are added to the samples during lipid extraction. The highest peak intensity can then be matched across different spectrums to allow for direct comparisons between treatment groups. Performing this analysis suggests that triglyceride species are depleted in both control day 7 and fluensulfone day 7 juveniles, relative to control day 0 (Figure 6.24).

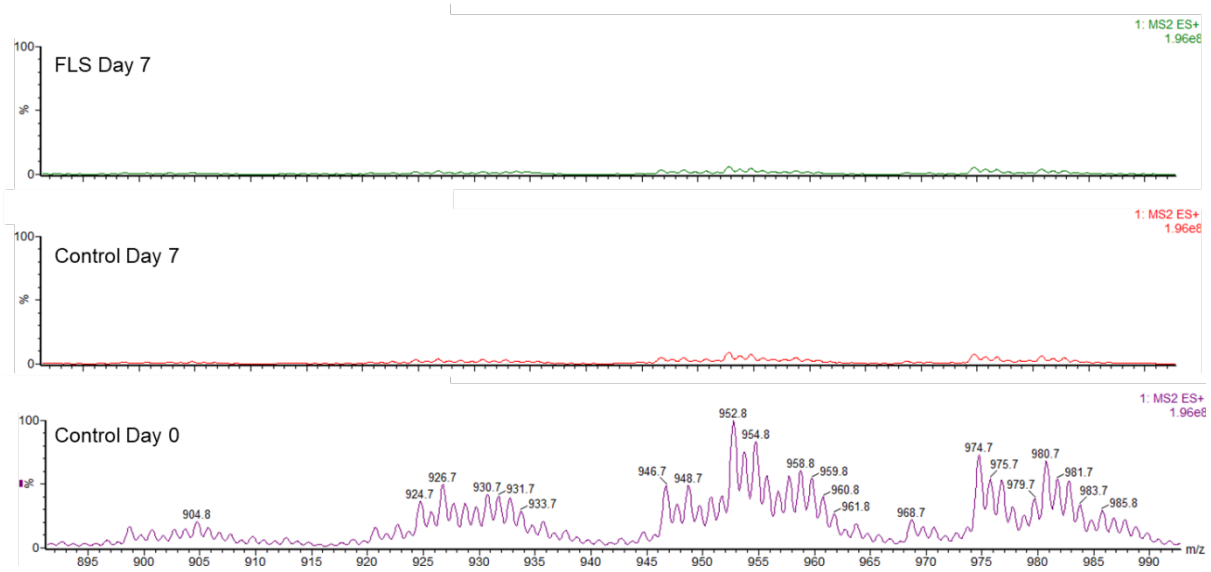

Figure 6.24 Normalized spectrum shows depleted triglyceride species seven days post hatch and following fluensulfone treatment. Peak intensity normalized to TAG lipid standard and linked on the y-axis to allow comparisons between control Day 0 (bottom), control day 7 (middle) and fluensulfone treated day 7 (top). Mass spectrum in full positive. Normalized data from Figure 6.23.

Data is also shown for day 14 treatment groups. Main triglyceride species remain unchanged in comparison to control day 0 (Figure 6.25).

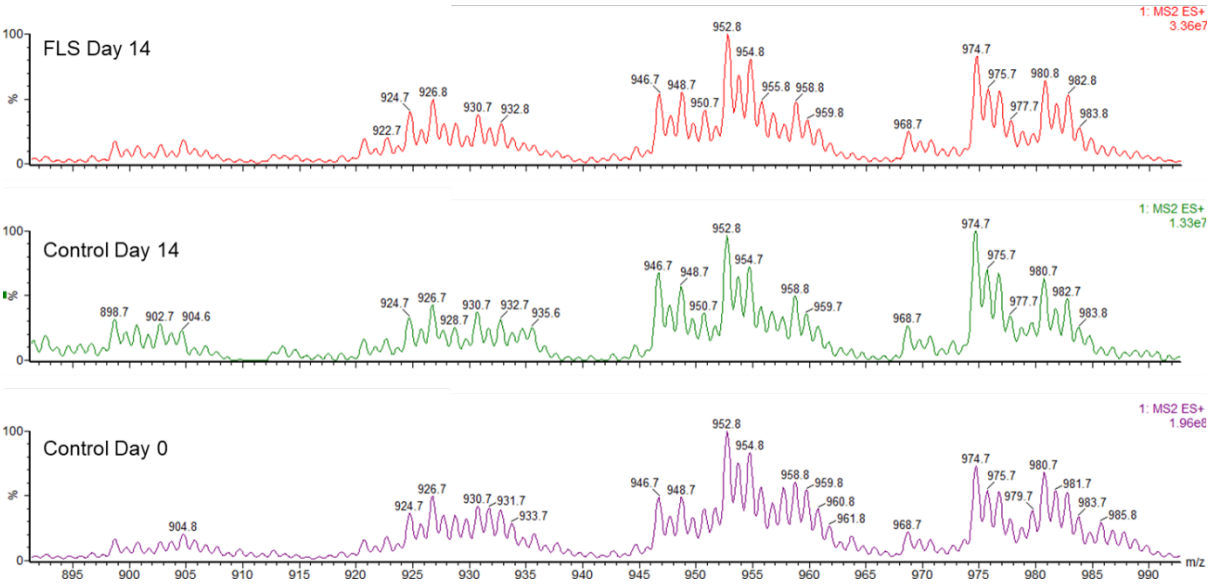

Figure 6.25 Triglyceride species identified by full positive spectrum 14 days post hatch. Total lipid extraction was performed for 2,500 *G. pallida* juveniles per treatment group. Full positive spectrum is shown for detection of major triglyceride species. Main triglycerides do not differ between treatment groups. Assignments are equivalent to those described in Table 6.2

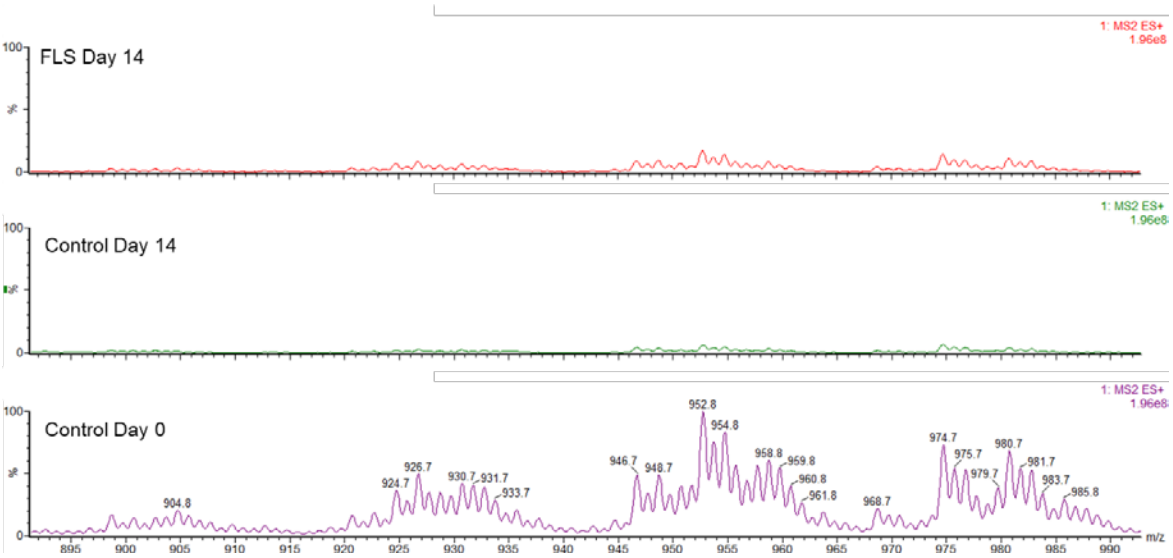

Figure 6.26 Normalized data from Figure 6.25.

Normalized signal from lipid extractions 14 days post hatch also indicate that triglyceride species are depleted in controls and in fluensulfone treated juveniles. The signal from fluensulfone treated juveniles is more evident than in parallel controls, however is clearly reduced in comparison to freshly hatched juveniles.

Signal from phosphatidylcholine species was not readily detected in this set of experiments, including the extraction from control day 0 samples. Indeed, phospholipid species generally were not well detected. This was apparent across all treatment groups and in contrast to the phospholipid species detected in initial experiments (Figure 6.21). There is however some indication that following fluensulfone treatment there is a decrease in PC species M/z 808 and 836. These species were assigned as PC18:1//20:4 and PC 19:0/22:5 and were the two main PCs identified in initial scans (Figure 6.27).

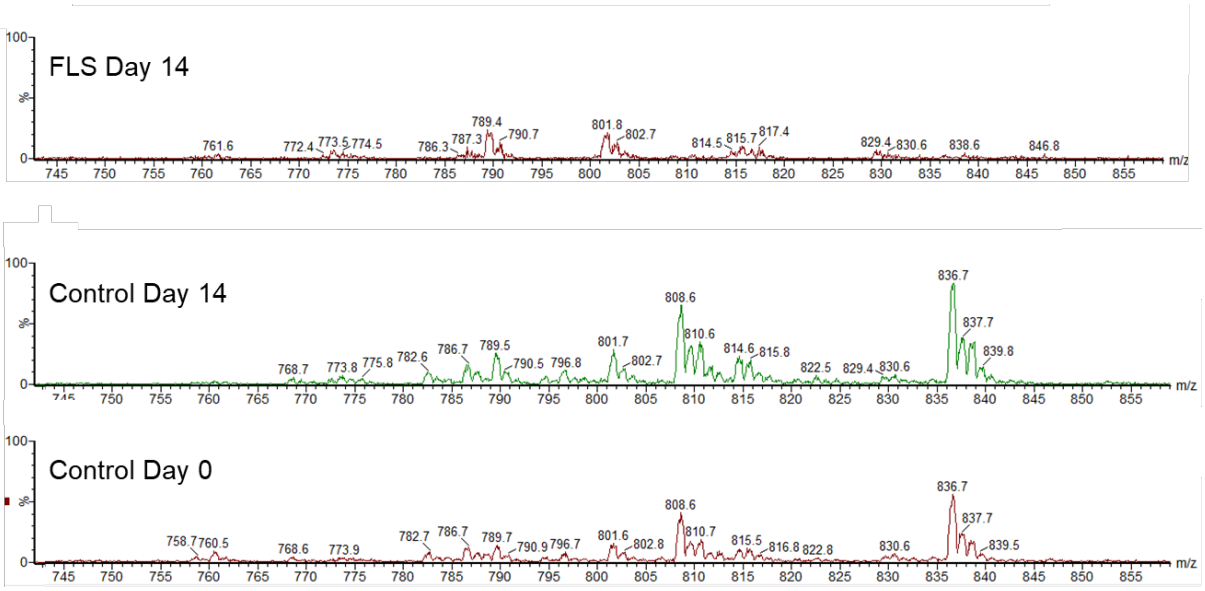

Figure 6.27 Fluensulfone treatment results in reduction of PC species at M/z 808 and 836. Parent loss scan mass 184 (P184) taken under Electro Spray positive condition. Total lipid extraction was performed for 2,500 *G. pallida* juveniles per treatment group. Results are shown for control Day 0 (bottom), control 14 days post-hatch (middle), and fluensulfone treated 14 days post-hatch (top).

6.2.3.2 Mass spectrometry of lipid extracts from fluensulfone and perhexiline treated *G. pallida* juveniles (Experiment 2)

Triglyceride species comparisons were made following treatment with 50µM perhexiline in parallel to fluensulfone treatment. The majority of the lipid profile for the TAG region was consistent with previous observations, however in addition to the lipid species described in Table 6.2, a prominent species at M/z 902 was observed in all samples. This was given the assignment TAG 18:1/18:1/18:1.

The TAG lipid profile of fluensulfone treated juveniles remained unchanged at day 7 and day 14. In contrast, perhexiline treatment resulted in the generation of a unique species that was not detected in any other samples. This was at M/z 940 and was given the assignment TAG18:0a/18:0/22:5. This is highlighted in the spectrums at both day 7 and to a greater intensity at day 14, suggesting the increase of this lipid species with prolonged perhexiline treatment.

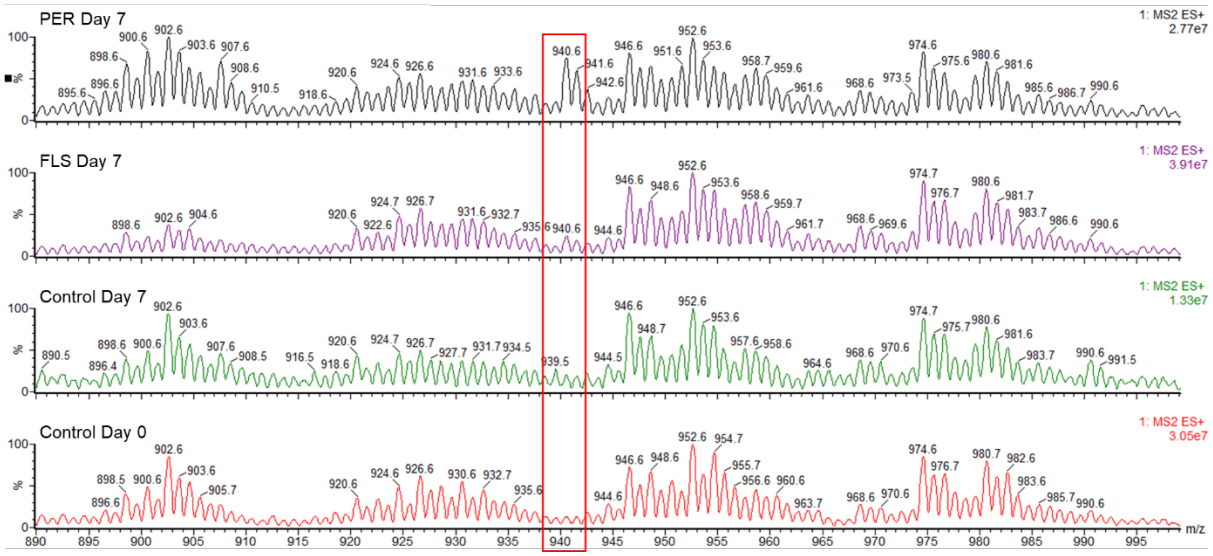

Figure 6.28 Triglyceride species in full positive spectrum for fluensulfone and perhexiline treated juveniles. Total lipid extraction was performed for 2,500 *G. pallida* juveniles per treatment group. Full positive spectrum is shown for detection of major triglyceride species at day 0 (bottom), control day 7 (second from bottom), fluensulfone day 7 (second from top) and perhexiline day 7 (top). Region of unique TAG species detected in perhexiline samples is highlighted across all spectra.

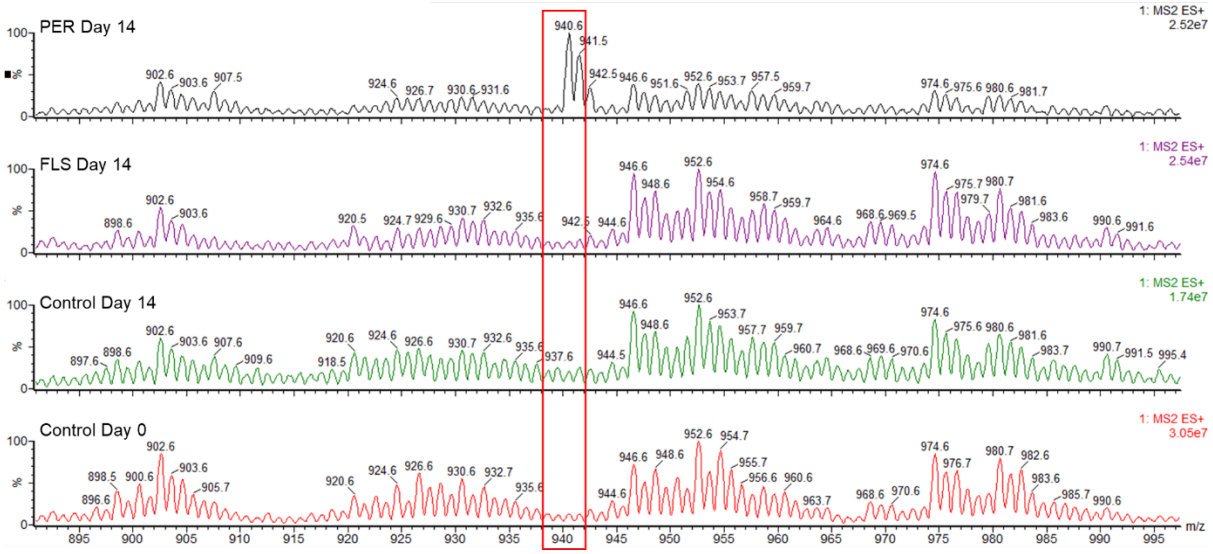

Figure 6.29 Unique TAG species identified following perhexiline treatment. Full positive scan showing TAG species following 14 days treatment with fluensulfone and perhexiline. M/z 940 peak unique to perhexiline treatment (highlighted).

Analysis of other lipid species was complicated by sample contaminants weakening signal. Running blank samples through the mass spectrometer identified that these same contaminants were present in the absence of any sample (data not shown), suggesting that the interference was not due to error introduced whilst extracting, but a more substantial problem with cross-contamination on the machine.

6.3 Discussion

6.3.1 Efficient lipid extraction is vital for lipid class analysis

Here I analysed lipids using two biochemical approaches that involved first extracting lipids from the sample. As discussed in section 6.2.1, this in itself can raise substantial issues. It became apparent that efficient disruption of the juveniles was vital for efficient extraction. Initial extraction protocols relied on exposure to chloroform and methanol solvents to effectively homogenize the animals, without mechanical input. Through observing juveniles after solvent exposure, it was noticeable that disruption was varied and limited. The starting point for lipid extraction is utilizing whole animal homogenates and so it is vital that homogenization is consistent across all samples. Mechanical homogenization improved disruption, however was variable, and due to introducing additional apparatus, increased the likelihood of loss of sample. In already limited sample sizes, it is critical to minimize variables that may greatly influence the parameter of interest that is being investigated.

Sonication provided a way of effectively breaking up the juveniles that could be controlled from sample to sample and between experiments. Subsequent chloroform-based extraction successfully liberated total lipids that could be visualised on a TLC plate.

6.3.2 TLC provides a platform to analyse lipid extraction efficiencies and identify major lipid classes

Thin layer chromatography provides a relatively fast and simple way of monitoring lipid extraction, as well as providing information on lipid classes contained in the sample. Single-phase separation of lipids from *C. elegans* L4 was comparable to published observations (Figure 6.30) including a prominent free fatty acid (FFA) band. It is important to note that this band was not always observed and could be as a result of liberated FFAs from other lipid classes during the extraction.

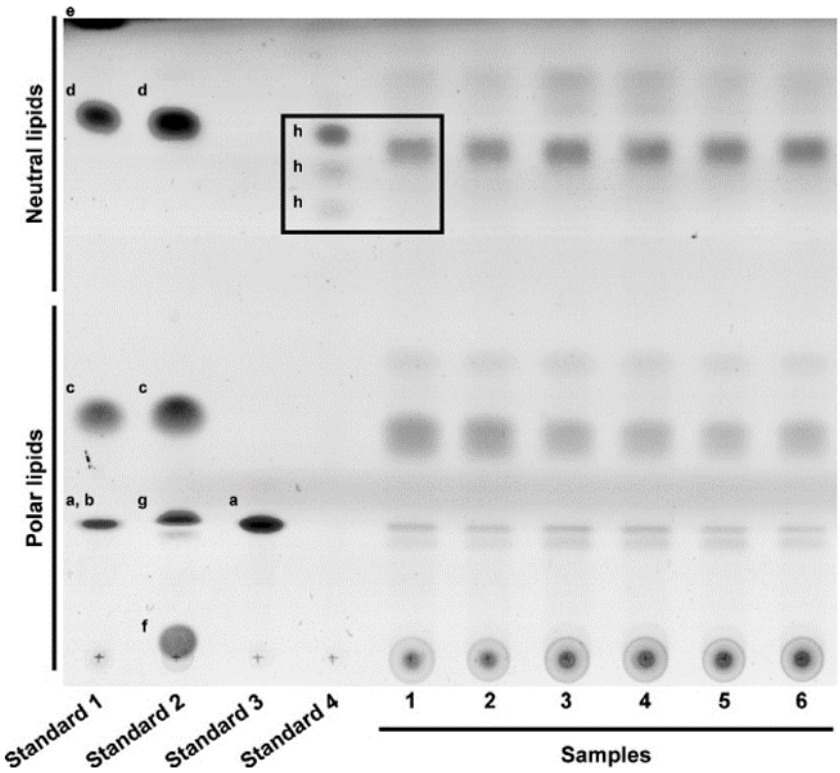

Figure 6.30 Thin Layer Chromatography example gel. Image of gel taken from (Barros et al., 2012). Standards used: (a) cholesterol; (b) lecithin; (c) oleic acid; (d) triolein; (e) cholesteryl oleate; (f) monoolein; (g) diolein; and (h) mixture of different triglycerides (C16:0 (4%); C18:0 (2%); C18:1 (61%); C18:2 (21%); C18:3 (9%); C20:0 (1%) C20:1 (1%); C2e2:1 (1%)). Samples are 10,000 L4-stage wild type *C. elegans* from 3 separate growths, in duplicate (1&2, 3&4, 5&6). Single-phase separation with hexane, diethyl ether, and acetic acid. Following fractionation, plate was sprayed with 20% phosphomolybdic acid and heated at 100°C for 10 minutes.

Two-phase separation allowed more information to be extracted on phospholipid species (Section 6.1.1.3). Comparisons of *C. elegans* and *G. pallida* samples support previous observations for a greater proportion of TAG in PPN species. It also clearly shows that the polar lipid profiles of each nematode species are distinct. Information relating to the *C. elegans* lipidome may therefore not wholly relate to PPNs and care should be taken when interpreting PPN results. Identifying the distinct species shown here for *G. pallida* could provide important information that reflects key aspects of the PPN life cycle.

6.3.3 Discrepancies between experimental platforms — are TAGs depleted?

Surprisingly, there was no decrease in the amount of TAG detected between freshly hatched *G. pallida* juveniles and juveniles seven days post-hatch in the TLC experiments. This is in contrast to the conclusion drawn from images of the anti-Stokes signal tuned to 2845cm^{-1} generated by CARS data. The CARS data identified a defined reduction in CARS signal against which it was argued that neutral lipid is depleted over time post-hatch. The neutral lipid fraction of *G. pallida* juveniles is dominated by TAG (Holz et al., 1997) and I relayed a similar observation based on both TLC and mass spectrometry scans. This implies that the input is capable of being detected by TLC and if a 50% or greater reduction, then this would be readily resolved.

One consideration is that lipid metabolism and TAG content are dynamically regulated and that utilizing whole animal homogenates may fail to detect changes in one region or tissue that are offset by opposing changes elsewhere. For example, in *C. elegans,* in addition to stored TAG, intestinal yolk and developing embryos will contribute substantial amounts of TAG in a whole animal extraction (Barros et al., 2012). In the CARS analysis, we are measuring signal from neutral lipid in the tail region of individual worms, in contrast to TLC where total lipid extraction is performed on 10,000 juveniles. Dynamic changes to stored TAGs that are identified on an individual basis in CARS may therefore be lost upon total lipid extraction across a population of juveniles.

Given that populations of juveniles are used for total lipid extractions, TAG measurements should be normalized to an independent measure of the parameter of interest. TAG measurements are routinely normalized to protein concentration (Barros et al., 2012), where extractions of protein are performed on separate aliquots of nematodes. In the experiments performed here, due to working with limited material, it was not feasible to perform a separate extraction for protein quantification without initially increasing the quantity of input material. Furthermore, protein extraction can introduce more potential for random variability in measurements. Indeed, measuring protein concentrations for paired samples of ~3,000 *G. pallida* juveniles resulted in protein quantification estimates ranging from 30µg to 55µg (data not shown). TAG levels can therefore be normalized to phospholipid levels, where both species are extracted together in the same process, minimizing error due to sample loss. However, this assumes that phospholipids are invariant and given that we do not know how fluensulfone acts, may not be appropriate here.

Without effective normalization, it is difficult to determine whether changes seen in lipid classes are of biological significance or due to variation in extraction. Identifying a class that remains unchanged by treatment would enable effective normalization of data. This would be useful for both TLC and mass spectrometry approaches. Furthermore, here I describe using 10,000 juveniles per treatment group. In the literature it is reported that >10,000 *C. elegans* are routinely used in this kind of biochemical analysis (Watts and Ristow, 2017). In my experiments, I identify a 10-fold difference between phospholipid detection between nematode species. This would therefore suggest that >100,000 *G. pallida* juveniles should be used for biochemical approaches. Increasing the material input would likely limit the effects of sample loss and variability in extraction.

Lastly, Barros et al., comment that phosphomolybdic acid, which is the lipid-staining dye that I used in developing the TLC plates, is most effective in revealing triglycerides in a range from 0.001 to 10 µg. It may therefore be that the detection of TAGs is saturated and subtle differences between treatment groups are unable to be visualised using this approach. Dilutions of TAG standards were performed and resolved by TLC, whereby differences were apparent in a range from 0.25–20µg. Higher concentrations of TAG were not tested and would be required to observe whether differences can be seen at concentrations ≥20µg.

6.3.3.1 Depletion of TAG species indicated by mass spectrometry

When comparing the TAG species from freshly hatched *G. pallida* juveniles and juveniles post hatch (Figure 6.24), there is a decrease in signal over time. This would be consistent with utilization of and depletion of TAG post hatch. However, the TAG species are also seen to be depleted following fluensulfone treatment, which would not support the CARS data that is reported in the previous Chapter. The same considerations must be applied to mass spectrometry as to the ones for TLC above, where both platforms utilize whole animal homogenates, and so any variation in extraction will be reflected in analysis.

This being said, on repetition of the mass spectrometry analysis, using the same parameters and juvenile numbers, very low lipid signal was detected, not allowing analysis of species from any of the treatment groups. Furthermore, a much larger problem across all analysis was contamination from unknown sources, likely plastic. Large peaks from contaminants skew the data interpretation, as ionisation that occurs will be influenced by everything in the sample. The ions that are formed will depend on what is present and the process of selecting which ion is formed is known as preferential ionisation. Preferential ionisation means that there is a limit to the amount of ions that can be produced and molecules that are too difficult to be ionised, in comparison to the rest of the sample, will be suppressed and therefore not seen in the spectrum. This means that the presence of a contaminant can suppress detection of molecules of interest.

Furthermore, when there is less material present (i.e. the sample is diluted), it is possible to detect species that are lower on the ionisation ladder, due to preferential ionisation. This means that when comparing signals between samples, ions may respond stronger or weaker due to the presence of other ions, such as those generated from contaminants. When contaminants are present, intensities cannot be compared reliably and thus conclusions on absolute amounts cannot be drawn.

The mass spectrometry analysis performed here, therefore, is unable to provide us with information relating to the absolute quantities of lipid in the samples. Despite the apparent loss of TAG signal in comparison to control day 0 samples in initial analysis, this effect was not repeated, in fact in experiment two (section 6.2.3.1), TAG signal was low across all samples, including the freshly hatched juveniles. Data is not shown for additional experiments where lipid signal was too low to be analysed.

6.3.4 Analysing lipid species from *G. pallida* samples using mass spectrometry

I have shown here mass spectrometry's power in describing the lipid species that are present in *G. pallida* samples. The juvenile numbers that were used for the mass spectrometry analysis (2,500) were very low in comparison to the numbers required for visualisation of lipids in TLC (10,000), yet information on individual lipid species can be extracted. For understanding lipid dynamics in the PPN, mass spectrometry can provide a vital tool.

6.3.4.1 Changes in lipid species indicative of drug treatment

There were no differences between the TAG species between control and fluensulfone treated juveniles. However, it was observed across experiment one and experiment two that PC species decreased with fluensulfone treatment and sphingomyelin species increased. Both lipid classes are involved in membrane structure and implicated in various signalling pathways (Sections 6.1.1.3 and 6.1.1.4), however, their explicit role in PPNs is not described. It may reflect a breakdown of membrane structure following fluensulfone treatment, resulting in the granular appearance of juveniles that has been previously reported (Kearn et al., 2017).

Preliminary mass spectrometry analysis with perhexiline treated juveniles suggests that perhexiline treatment results in the generation of a triglyceride species that is not observed to detectable levels in other samples (M/z 940). The TAG assignment for this species was determined as TAG18:0a/18:0/22:5. This may reflect changes in triglyceride organisation as a consequence of β-oxidation inhibition and should be supported by analysis with other inhibitors of β-oxidation. Nevertheless, the change in profile demonstrates the ability of this platform to be utilized to provide signatures based on drug treatment. The absence of the peak at M/z 940 in fluensulfone treated juveniles could suggest that the two drugs do not share a common mode of action.

6.3.5 Extracting data from mass spectrum

A major bottleneck in mass spectrometry based lipidomics is the lack of robust and readily available data analysis software (Brandsma et al., 2017). There are a number of open source software packages available, which are able to process information on precursor and fragment masses and compare to internal databases that allow the assignment of lipid species in a sample (Köfeler et al., 2012). These programmes can be adjusted by the user, however, this requires a lot of time and expertise to employ effectively. The subsequent volume of data generated further adds to the complexity of analysing mass spectrometry data and gaining meaningful insight (Köfeler et al., 2012; Brandsma et al., 2017).

The analysing software used to assign peaks identified by mass spectrometry in this study was written in Excel by Grielof Koster. It is written to extract data from MassLynx, the software application that is used to configure and control the mass spectrometer and process the data acquired. By selecting the spectra that were taken for each sample, the analyser software will then assign species to each peak.

Until recently, there has been no centralized database for *C. elegans* lipids (Witting and Schmitt-Kopplin, 2016). For lipidomics to be a useful tool to researchers working with nematodes, a comprehensive in silico library is required. Lipid profiling of *C. elegans* strains has been performed, specifically, describing triacylglycerol (TAG), phosphatidylcholine (PC) and phosphatidylethanolamine (PE) species and how the profiles of these classes change following drug administration (Admasu et al., 2018). This data is available for download and provides a necessary resource for lipidomic research in *C. elegans.* Additionally, the sphingolipidome of *C. elegans* has recently been published (Hänel et al., 2019). Given that this information has only just been made available for the model organism *C. elegans,* it highlights the difficulty in effectively analysing data produced from mass spectrometry analysis of PPNs.

6.3.6 Summary

This chapter has provided a detailed protocol for extracting lipids from the plant parasitic nematode *G. pallida.* Furthermore, the TLC protocol has been optimized and I demonstrate its use as an effective way to monitor extraction efficiencies. I have determined that for biochemical analysis, a minimum of 10,000 *G. pallida* juveniles should be used, however, if feasible, a greater number should be attempted to enable multiple platforms to be employed in parallel.

Mass spectrometry has enabled a detailed description of the lipid species present in the *G. pallida* juvenile. Having optimized lipid extraction, it would be beneficial to repeat this analysis and confirm whether the changes described to the PCs and sphingomyelins have any significance to fluensulfone's mode of action.

Chapter 7 General Discussion

7.1 Advances into understanding the mode of action of fluensulfone

Fluensulfone is a novel nematicide belonging to the heterocyclic fluoroalkenyl sulfones group (Oka et al., 2009; Oka, 2020a). In field studies, fluensulfone has shown efficacy against a number of plant parasitic nematode species (Chapter 1.5.2). Fluensulfone has a favourable toxicity profile in comparison to other nematicides (Chapter 1.5) and importantly, has minimal reported impact on non-target nematodes (Waldo et al., 2019). This gives it a significant selective toxicity, helping overcome the drawbacks that are associated with non-selective nematicides, many of which have been banned or under restricted use (Chapter 1.4.3).

Currently, fluensulfone has an IRAC nematicide mode of action classification as unknown (See Chapter 1.4.3). Initial studies focused on its efficacy in the field and provided descriptive analysis on its profile of effects on PPNs (Oka et al., 2009; Oka et al., 2012; Oka, 2014; Norshie et al., 2016), where it was suggested that fluensulfone exhibited a novel mode of action in comparison to acetylcholinesterase inhibitors, cadusafos and fenamiphos (Oka et al., 2009). Morphologically, immobile *M. incognita* juveniles in fluensulfone were straight and rod-shaped in comparison to the shrunken posture that was induced by acetylcholinesterase inhibitors (Oka et al., 2009). Detailed investigations into its effects on the model organism, *C. elegans* (Kearn et al., 2014; Kearn, 2015), reinforced that fluensulfone has a distinct mode of action in comparison to anticholinesterases and additionally, macrocyclic lactones (Chapter 1.5.3).

Additional advances were made investigating its action on the PPN, *G. pallida* (Kearn et al., 2017), providing insight into the mode of action of fluensulfone, which formed the starting point for this project. The central aim of this project was therefore to more precisely define the mode of action of fluensulfone.

7.1.1 High concentration, non-selective effects of fluensulfone on *C. elegans* and *G. pallida:* insights into mode of action

C. elegans is a useful model organism for anthelmintic and nematicide discovery and has previously been utilized as a platform to investigate the mode of action of fluensulfone (Kearn et al., 2014). At high concentrations (≥300µM), fluensulfone effects the *C. elegans* pharyngeal system, consistent with its effects on the *G. pallida* stylet (See Chapter 1.5.3). Fluensulfone was found to stimulate pumping and stylet thrusting in respective species, and block 5-HT-stimulated activity, to suggest that fluensulfone might interact with the serotonergic system (Kearn, 2015; Kearn et al., 2017). Methiothepin, a 5-HT receptor antagonist, was shown to inhibit fluensulfone-induced stylet activity (Kearn, 2015) to suggest at high concentrations of fluensulfone (≥300µM), there may be direct agonist activity at 5-HT receptors. Alternatively, fluensulfone may act to stimulate 5-HT release at the synapse or prevent re-uptake of 5-HT.

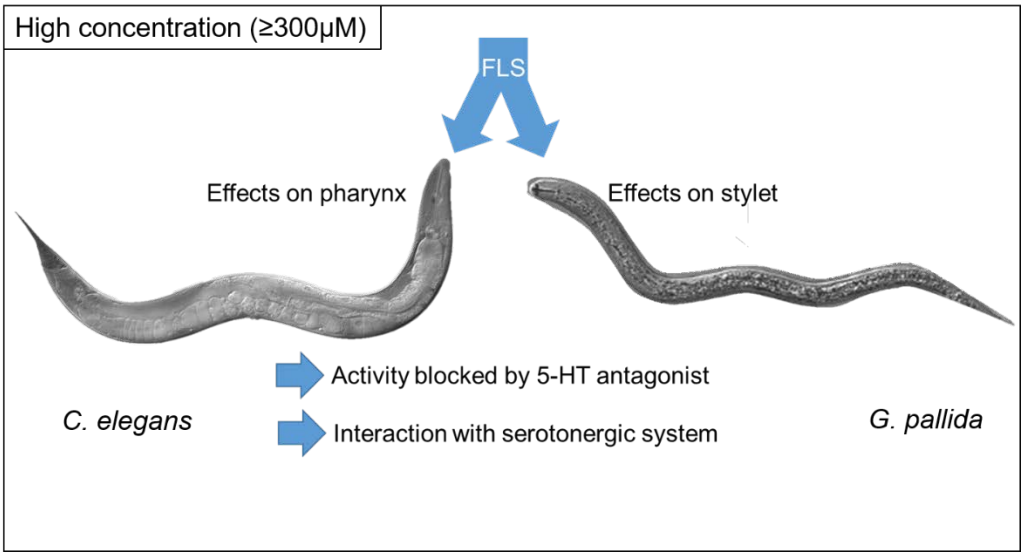

Figure 7.1 High concentration effects of fluensulfone on *C. elegans* and *G. pallida.* Fluensulfone stimulates pharyngeal pumping in *C. elegans* and stylet thrusting in *G. pallida* (Kearn et al., 2017). Fluensulfone blocks the stimulatory effects of 5-HT on both the pharynx and stylet to suggest that fluensulfone can interact with the serotonergic system (Kearn, 2015).

Fluensulfone displays some phytotoxicity in the field (Oka et al., 2012; Morris et al., 2016) which is likely attributable to a high concentration, non-selective toxicity on plants. Investigations into the mode of action of fluensulfone using the model organism *Arabidopsis thaliana* suggest that at concentrations above 200µM, fluensulfone induces effects in the plant consistent with a perturbation in auxin signalling (*personal communication Eleanor Kirby).* Auxin and 5-HT are tryptophan-derived compounds and share related chemical structures (Figure 7.2). In the plant, diverse physiological roles of 5-HT have been postulated, including germination (Roshchina, 2001), seed development and root growth (Csaba and Pál, 1982), and defence responses (Ishihara et al., 2008). Pharmacologically, exogenously applied 5-HT can alter auxin-regulated development, potentially acting as an auxin inhibitor (Pelagio-Flores et al., 2011).

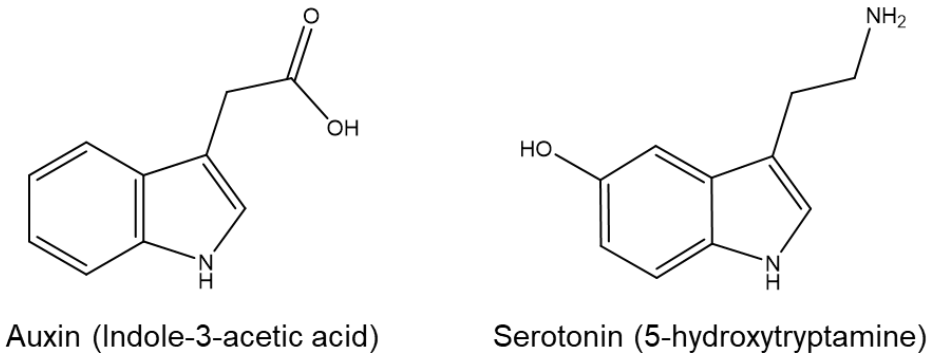

Figure 7.2 Chemical structures of auxin and 5-HT. Tryptophan-derived auxin and 5-HT share structural similarity.

The high-concentration effects of fluensulfone on *G. pallida, C. elegans* and *A. thaliana* could therefore be as a result of an interaction with 5-HT receptors and/or auxin receptors. This activity is, however, unlikely to account for the low concentration, selective effects that are observed in PPNs.

7.1.2 Investigating the low concentration, selective effects of fluensulfone on PPN, *Globodera pallida*

This thesis used the plant parasitic nematode *G. pallida* to resolve the relatively low concentration effects on nematodes. In particular, I focussed on life cycle stages that might reflect perturbation that are field relevant. Previous studies in *G. pallida* indicated that fluensulfone elicits impaired metabolic activity, with a hint at fluensulfone preventing lipid depletion (Kearn et al., 2017) (See Chapter 1.5.4 and 1.5.5). These effects are summarized in Figure 7.3 below.

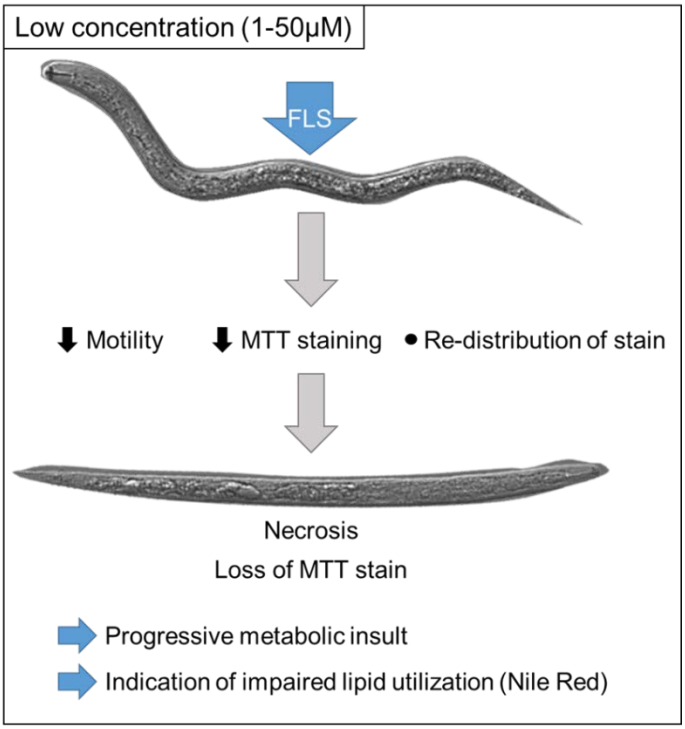

Figure 7.3 Low concentration effects of fluensulfone on *G. pallida.* Fluensulfone induces selective effects on the PPN *G. pallida* that result in a progressive decrease in motility and MTT staining. The latter is indicative of a loss of metabolic activity. Prolonged fluensulfone exposure leads to irreversible paralysis and granulation of the juvenile's internal structures, consistent with necrosis. Staining with Nile red suggested that prior to death, there was a decrease in lipid utilization (Kearn et al., 2017).

As highlighted in the general introduction, the *G. pallida* hatching cycle (Chapter 1.3) requires metabolic activation of the quiescent juvenile, in which lipid utilization prior to eclosion has been suggested (See Chapter 1.3.4). Investigating the effects of fluensulfone on *G. pallida* hatching therefore provides a platform to investigate fluensulfone and compare its effects to inhibitors with selective effects on distinct steps of metabolic pathways.

7.2 *Globodera pallida* hatching as a platform to investigate the mode of action of fluensulfone

The first aim of this project was to build a profile of effects of fluensulfone in a detailed analysis on hatching. This included assessing inhibition of hatching from cysts and isolated eggs, in ovo effects on the unhatched juvenile and recovery from fluensulfone exposure (Chapter 3). This identified a high and low concentration effect of fluensulfone on *G. pallida* hatching. Following exposure to fluensulfone, there is a high concentration effect of in ovo necrosis, resulting in complete inhibition of hatching with no recovery. At lower concentrations, fluensulfone inhibits hatching, and although reversible, leaves a trace of effect, with the juveniles that hatch following exposure displaying impaired motility (Figure 7.4).

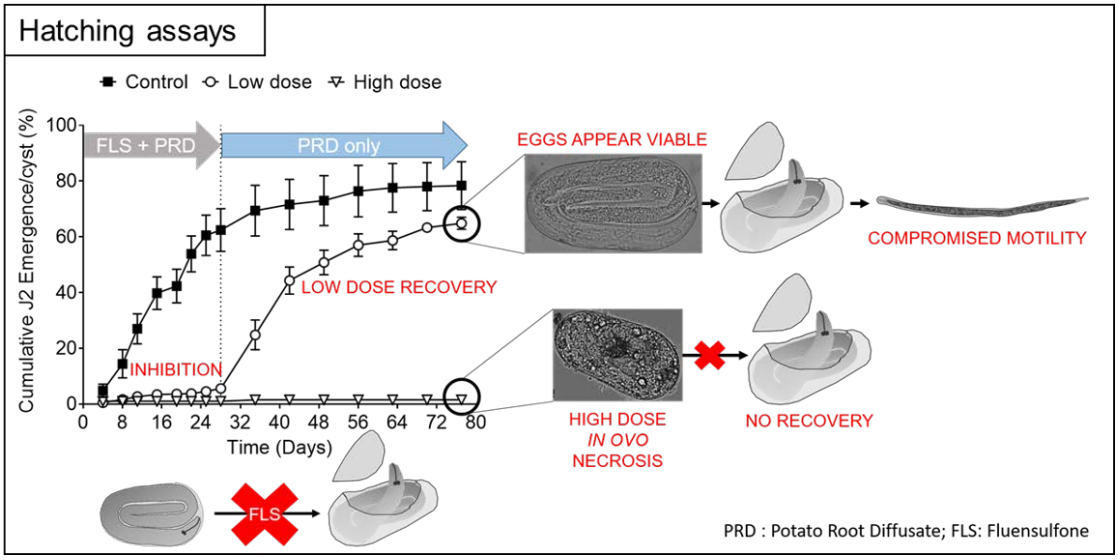

Figure 7.4 High and low concentration effects of fluensulfone on *G. pallida* hatching. Concentrations of 1–500µM fluensulfone inhibited PRD induced *G. pallida* hatching. Following removal from FLS, there was low dose recovery, however, juveniles were compromised. Hatching inhibition was irreversible following high dose exposure, resulting in granulation of unhatched juveniles (Feist et al., 2020).

The hatching assays provided a platform to compare fluensulfone with nematicides with defined modes of action, including fluopyram, which targets metabolic flux by inhibiting complex II of the mitochondrial electron transport chain. This is an essential step in the efficient generation of ATP. Nematicide comparisons identified that fluensulfone has a phenotypic profile that overlaps with, but is distinct, to the nematicides of target-defined modes of action that were investigated, including fluopyram.

The distinct effects of fluensulfone on *G. pallida* hatching were also compared against metabolic inhibitors with target-defined modes of action (Chapter 4). These comparative assays conducted with different inhibitors stressed the importance of energy generating fluxes in *G. pallida* hatching. This highlighted that inhibition of the TCA cycle via application of aconitase inhibitor, fluoroacetic acid, could partially mimic the effects of fluensulfone, with high dose irreversible inhibition of hatching and low dose recovery. Surprisingly, the β-oxidation inhibitor, perhexiline, failed to inhibit hatching, however, as discussed in Chapter 4, could be confounded by an inability to access the internal, cyst-protected juvenile (Chapter 4.3.1.1). Treating with other compounds that inhibit fatty acid oxidation would determine whether the results reported here for perhexiline are due to an inability of the compound to access the egg-protected juvenile, or reflect the use of energy-generating fluxes that do not rely on mitochondrial β-oxidation during hatching. As described in Chapter 4.3.1, energy generated from carbohydrate catabolism or peroxisomal β-oxidation may be utilized during hatching. Indeed, targeting the TCA cycle with fluoroacetic acid, which is utilised for carbohydrate breakdown, inhibits *G. pallida* hatching (Chapter 4.3.2). Fluoroacetic acid and perhexiline investigations were extended to the hatched juvenile.

7.3 Effects of fluensulfone on *G. pallida* juveniles

As summarized in Figure 7.3, there is an indication that fluensulfone inhibits metabolic activity and lipid utilization. The assays to assess motility and metabolic activity using MTT staining were repeated in this project, and as reported in Chapter 5, confirmed previous published observations (Kearn et al., 2017).

7.3.1 Indications from MTT staining following fluensulfone exposure

Reports of reduced metabolic activity were based on histological staining, relying on the conversion of MTT to MTT formazan in the presence of NADH or other reducing agents (See Chapter 5). More sensitive techniques, such as measuring oxygen consumption rates (OCRs), are available to assess metabolic activity and have been used in *C. elegans* to evaluate the effects of perhexiline (Taylor et al., 2013; H.E. Kim et al., 2016). Analysers that measure OCRs have the capacity to provide real-time data, with a function to apply drug whilst continuing to measure OCR, providing a quantitative readout of metabolic activity. This technique could be considered to provide more clarity on the effects of short exposure of PPNs to fluensulfone and the impact it has on metabolic activity.

In addition to a loss of MTT staining, precluding complete loss of staining, fluensulfone induced an interesting re-distribution of staining that manifest as a loss of anterior staining and a shift to predominant posterior staining (Chapter 5.3.2). This phenomenon has been previously identified (Kearn et al., 2017), with the suggestion that a shift in staining to the posterior reflects a shift in metabolic activity to the posterior, or alterations to metabolism occurring in this region (Kearn et al., 2017).

Treatment with perhexiline, described in Chapter 5.2.2, induced the same pattern of re-distributed staining, whilst treatment with fluoroacetic acid, described in Chapter 5.2.3, did not, suggesting that the re-distribution of staining to the posterior may be indicative of impaired lipid utilization. Furthermore, there is evidence that MTT-formazan preferentially precipitates into lipid droplets (Stockert et al., 2012), which could suggest that the re-distribution of predominant staining to the posterior reflects MTT-formazan precipitating into lipid droplets that are not depleted following fluensulfone and perhexiline treatment (Chapter 5.3.2). In contrast to a prevention of lipid utilization, lipid droplet accumulation of MTT formazan could be indicative of an increase in lipid droplets that are generated in response to an increase in cellular free fatty acids, buffering against lipotoxicity. Failure to sequester free fatty acids can result in lipotoxicity and oxidative stress (Ioannou et al., 2019), which has been linked to necrotic cell death, coinciding with an accumulation of reactive oxygen species (ROS) (Rockenfeller et al., 2010). Measuring lipid peroxidation would therefore be interesting in the face of fluensulfone toxicity (Salgueiro et al., 2017).

7.3.2 CARS analysis of fluensulfone treated juveniles

Juveniles were treated with fluensulfone and subjected to CARS analysis to analyse the lipid droplet stores in *G. pallida* juveniles (Chapter 5.2.4). The CARS analysis that was performed looked at signal generated from both the anterior and the posterior regions of individual worms. CARS signal was in agreement with previous reports of lipid distribution in *G, pallida,* where CARS signal appears to be highly concentrated in the posterior, consistent with lipid storage in the tail region (Smus et al., 2017). The relatively slow depletion of lipids over time was also consistent with previous reports (Smus et al., 2017). Analysis of lipid droplets using CARS reinforced previous observations with Nile red staining (Kearn et al., 2017) that lipids are not depleted following fluensulfone treatment in comparison to the reduction of lipids in controls. This supports the ability of fluensulfone to disrupt lipid utilization that coincides with reduced motility (Figure 7.5).

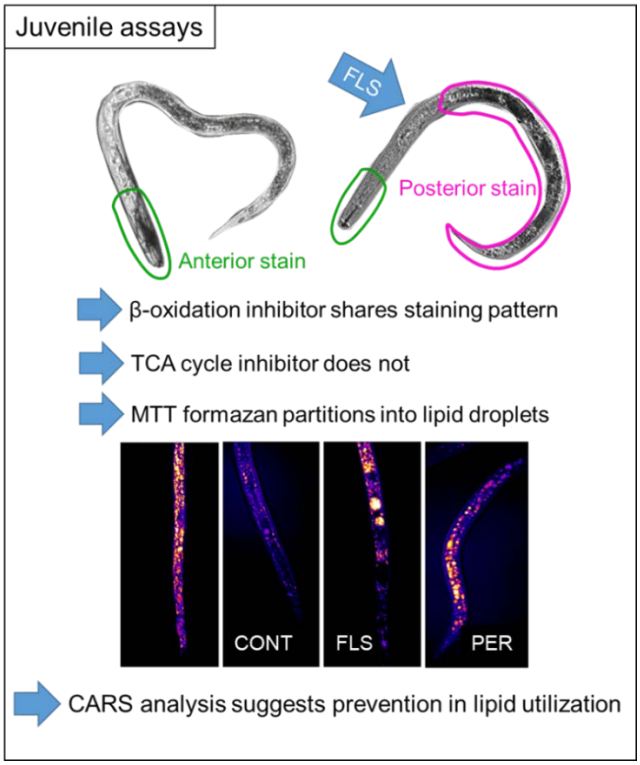

Figure 7.5 Fluensulfone effects on motility, metabolic activity and lipid utilization. The loss and concomitant re-distribution of MTT staining is interpreted as MTT formazan partitioning into lipid droplets following fluensulfone (FLS) treatment. This phenomenon is shared by β-oxidation inhibitor perhexiline (PER). CARS analysis following fluensulfone and perhexiline treatment suggests that lipid stores are sustained relative to the depletion of lipids in controls.

The observations described here following MTT staining and CARS analysis of fluensulfone treated juveniles highlight an important disruption to metabolism that is mediated by preventing access to the essential energy store that fuels the post hatching and infection steps of the PPN life cycle. However, as demonstrated by perhexiline, inhibition blocking a single step can starve the organism of energy-producing substrates but also disrupt fluxes such that they allow un-physiological accumulation of toxic intermediates (Chapter 4.2.1).

CARS analysis provides information on relative quantity and localization of lipid droplets, but lacks information on class and species. A number of distinct biochemical approaches were therefore modified for use in the PPN to investigate lipid content.

7.4 Biochemical analysis of fluensulfone treated juveniles

Biochemical approaches were developed and optimized for use in *G. pallida* (Chapter 6). Thin layer chromatography (TLC) was used to provide an overview of the major lipid classes present in *G. pallida* juveniles. This showed that the major lipid class present in *G. pallida* juveniles was triglycerides (TAG) (Chapter 6.2.2), consistent with TAGs dominating the neutral lipid fraction of this species (Holz et al., 1997). However, surprisingly, the TLC data did not reflect changes in TAGs that are interpreted as being the major signal detected by CARS analysis, which is tuned to detect the abundant CH_2 bonds in neutral lipids. CARS analysis on single worms seven days post hatch suggested >50% reduction in CARS signal relating to neutral lipid in comparison to freshly hatched juveniles. Lipid extractions from 10,000 juveniles seven days post hatch showed no change when analysed using TLC. This is discussed in Chapter 6.3.3, highlighting the differences in measuring signal from neutral lipid in the tail region of an individual worm (CARS analysis) in contrast to utilizing whole animal homogenates and total lipid extraction followed by solvent separation (TLC), which may be confounded by sample loss and variability in extraction.

One explanation for this disparity is that the threshold for detections are limited in the respective techniques. For example, if the CARS signal is not representative of the total neutral lipid fraction, subtle differences in TAG amount may be more apparent as it depletes, such as the depletion of storage lipids that are specifically stored in the tail and utilized post-hatch. On the other hand, if the TAG band is saturated in the TLC, small differences that are identified in CARS may not be resolved.

CARS analysis has previously been used for a kinetic analysis of lipid depletion using *C. elegans*, where CARS signal was localised to the intestine and hypodermis (Smus et al., 2017). CARS resolved discrete aspects of lipid homeostasis that were not readily detected by histological methods, evidencing the depletion of lipid content in *C. elegans* within 30 minutes of the onset of food deprivation (Smus et al., 2017), in contrast to histological methods that suggested no significant lipid depletion within three hours of starvation (Pang et al., 2014; Garcia-Segura et al., 2015). This exemplifies the sensitivity of CARS as a method to resolve lipid dynamics that are not detected by other techniques.

7.5 Morphological changes following fluensulfone treatment

Discrepancies between the CARS analysis of individual worms and analysis of total lipid extract by TLC and mass spectrometry prompted a more careful interrogation of the imaging that the CARS signal was being generated from. CARS has the capacity to resolve individual lipid droplets in nematodes (Hellerer et al., 2007), dependent on the resolution of the CARS microscope that is used. However, in the experimental set up that was used here, the resolution of the CARS system did not allow for analysis of individual droplets. The signal detected is therefore indicative of summed signal from multiple droplets rather than signal generated from single organelle. There were, however, regions in the juvenile tail that attributed large areas of high intensity, observed as concentrated pockets of signal up to ~10µM in diameter. These were most apparent in perhexiline and fluensulfone treated juveniles (Figure 7.6).

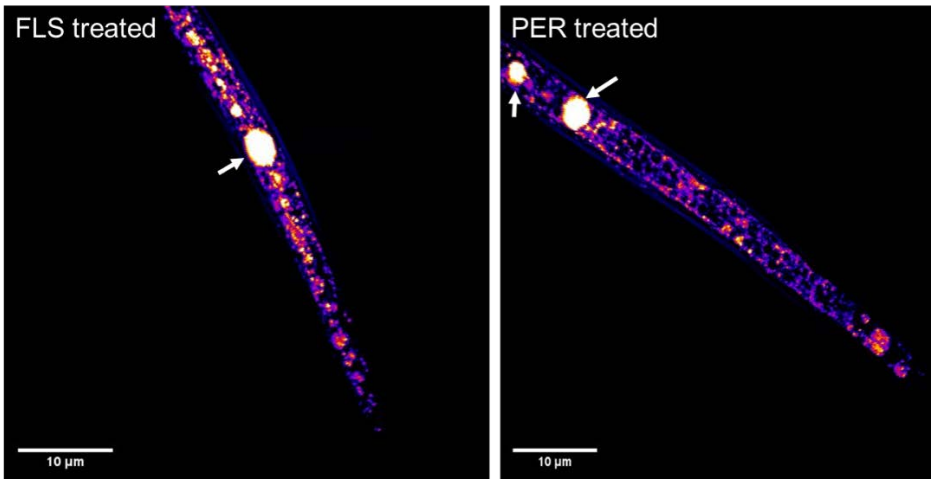

Figure 7.6 Representative CARS images of fluensulfone and perhexiline treated juveniles. Regions of concentrated CARS signal indicated by arrows. Scale bars 10µm.

Juveniles treated with fluensulfone for prolonged periods have been described to display granulation of internal structures that is consistent with tissue necrosis and death of the juvenile (Kearn et al., 2017). This is comparable with the high concentration effects of fluensulfone on unhatched juveniles, described in Chapter 3. Prior to complete disruption of juvenile integrity, I observed structures that were distinct from the granulation described previously (Kearn et al., 2017) and were apparent at earlier time points, where the stylet remained intact (Figure 7.7). These structures were not observed in control juveniles. Higher resolution images with x40 magnification were generated to inspect these structures more closely (Figure 7.8).

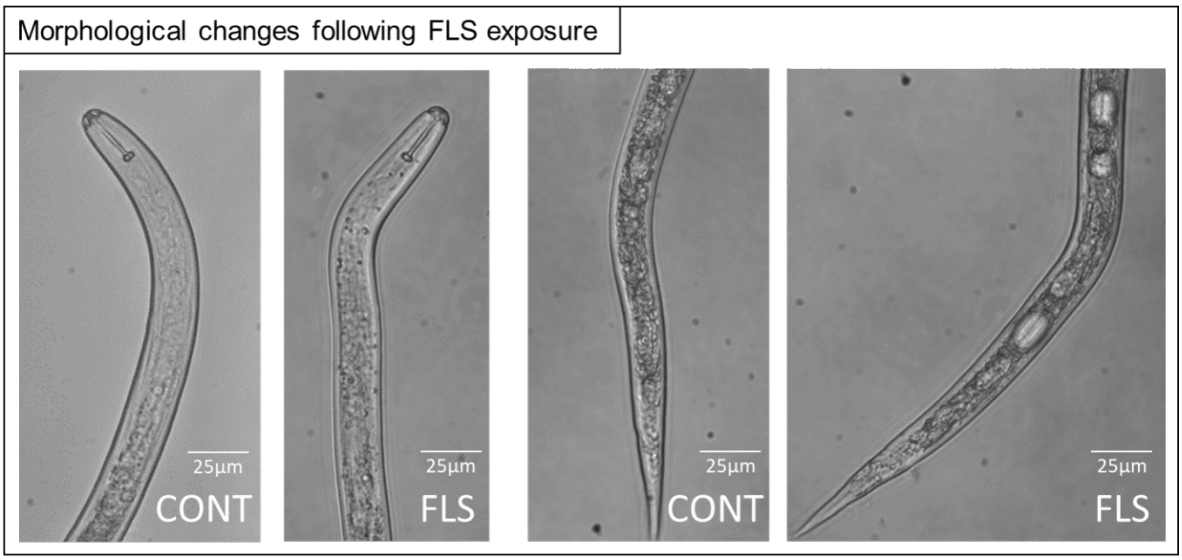

Figure 7.7 Morphological changes following fluensulfone exposure. Control (CONT) and fluensulfone (FLS) treated juveniles seven days post hatch. Vacuole-like structures observed in the tail region of 30µM treated *G. pallida* juveniles. Scale bars 25µm.

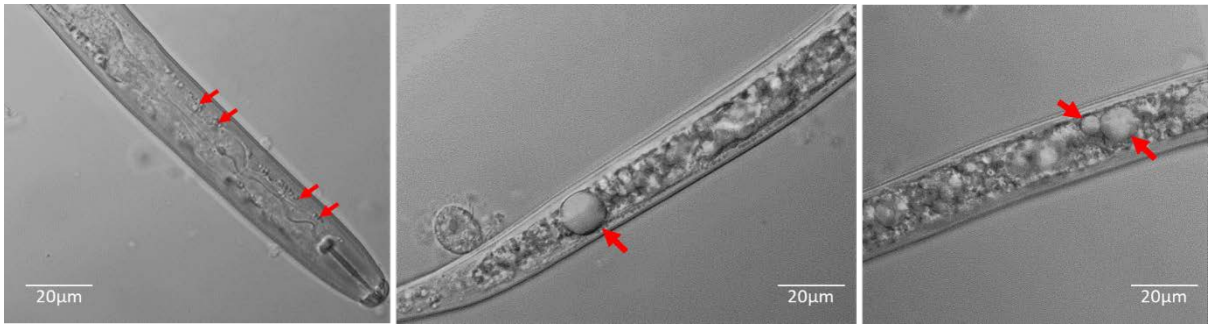

Figure 7.8 High resolution images of vacuole-like structures in fluensulfone treated juveniles. Juveniles were treated with 30µM fluensulfone for seven days. DIC images were taken with a Zeiss Axioplan microscope fitted with an x40 oil immersion objective. Scale bars 20µm.

The structures identified in the tail were apparent after seven days treatment with fluensulfone and were vacuole-like in appearance. Earlier time points were not investigated and should be looked at to determine when these structures appear. The vacuole-like structures in the tail were not observed in the anterior region of the juvenile and were distinct from small spherical structures (Figure 7.8) that were observed in this region. Localisation to the tail may inform on how these structures are formed.

Vacuole-like structures in nematodes have been linked to a specific type of cell death termed methuosis. Cells that are undergoing methuosis are characterized by the formation of large cytoplasmic vacuoles. In nematodes, these vacuoles are distinctly visible and can lead to tissue damage and death (Rajasekharan and Lee, 2020). Vacuolization is thought to be driven by abnormal cell hydrodynamics, leading to giant vacuoles that contain water, lipids and glycogen. Raman spectroscopy of these structures exhibit typical features for lipids, with the lipid profile dominated by unsaturated fatty acids (Bogner et al., 2017). Furthermore, chemicals that trigger this phenomenon in parasitic nematodes have been described and termed hydropic anthelmintics (Rajasekharan and Lee, 2020).

The appearance of vacuole-like structures in fluensulfone treated *G. pallida* juveniles could be indicative of methuosis. Understanding this phenomenon further and comparing fluensulfone to chemicals that have been described as hydropic anthelmintics could provide vital insight into the mechanism of action of fluensulfone. Interestingly, perhexiline treatment was shown to induce formation of similar structures (Figure 7.9). Careful analysis of this phenomenon is required to determine if this is a specific effect of targeting a common pathway.

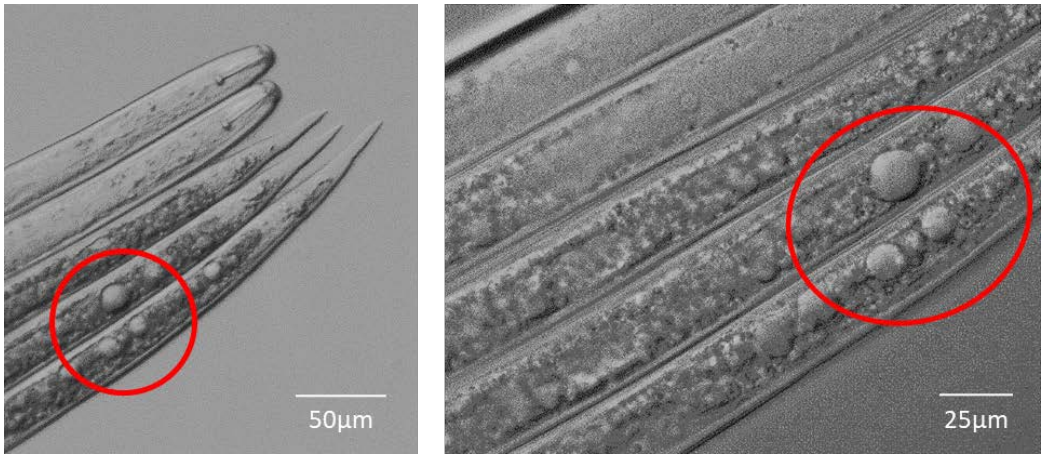

Figure 7.9 Perhexiline treatment induces vacuole formation. Juveniles were treated with 50µM perhexiline for seven days. DIC images were taken with a Zeiss Axioplan microscope fitted with an x20 air objective (image 1) and an x40 oil immersion objective (image 2). Area of higher magnification imaged is indicated with red circle.

The mechanism of vacuolization in parasitic nematodes is not fully determined, however, it could provide an endpoint marker for methuotic death. *M. incognita* juveniles treated with indole-3-acetic acid or 4-hydroxybenzoic acid displayed vacuole-like droplets in their central and tail regions, prior to death (Bogner et al., 2017). 5-iodindole treatment also induced vacuole formation in *M. incognita* juveniles, leading to methuosis to induce nematode death (Rajasekharan et al., 2019). It was proposed that these compounds might interact with the Na+/K+ antiporter pump or decrease ATP production by compromising mitochondrial function, which leads to disrupted osmoregulation and influx of water, leading to the formation of vacuoles (Rajasekharan and Lee, 2020). These could be potential avenues to explore for understanding the mechanism of action of fluensulfone.

7.6 Biochemical measurements of metabolic rates in the nematode

In this project, I have largely taken a comparative approach with chemicals of defined modes of actions to identify similarities in their effects with fluensulfone (Chapter 4 and 5). This approach is suggestive, rather than conclusive, of primary targets underpinning mode of action for fluensulfone. Previous work with fluensulfone showed the drug imposed a progressive metabolic insult, with an indication that lipid utilization may be impaired. Comparisons with perhexiline have further supported these suggestions, with CARS analysis providing evidence for an impairment to lipid utilization. Here, I have optimized protocols to allow efficient extraction of lipids from *G. pallida* juveniles and careful cataloguing of lipid and fatty acid composition. Re-visiting the biochemical techniques that have been described in this thesis could be a promising route to provide more clarity to the effect of fluensulfone on lipid metabolism.

Additional biochemical assays to identify changes in metabolite levels were also explored, however the quantity of juveniles required for sensitivity prevented use of such techniques. These are summarised in Table 7.1.

Assay	Purpose	Requirements	Reference
PicoProbe Acetyl CoA Assay Kit (abcam)	Measurement of acetyl-CoA levels	>10,000 J2s per treatment group, per replicate	Not performed in nematodes; used in isolated mitochondria from mouse livers (Zhang et al., 2016)
Triglyceride Quantification Colorometric/Fluorometric kit (Merck)	Measurement of triglyceride concentration	>10,000 J2s per treatment group, per replicate	
Fatty Acid Oxidation Assay Kit (bmrservice, University at Buffalo)	Measure rate of β-oxidation	> 6,000 J2s per treatment group, per replicate.	Cell culture (Kwong et al., 2019)
Labelled isotopes/oleate	Determining rates of *de novo* lipid synthesis and breakdown by β-oxidation	N/a, relies on nematode feeding and so not suitable for use in non-feeding *G. pallida*	Performed in *C. elegans* (Perez and Van Gilst, 2008; Barros et al., 2012; Elle et al., 2012)

Table 7.1 Biochemical assays to detect changes in metabolism. A summary of the biochemical assays that were considered for use in this project, with the input of *G. pallida* required based on optimization and assay thresholds.

7.7 Implications for mode of action of fluensulfone

This thesis has shown that two distinct life cycle stages of the PPN *G. pallida* are sensitive to low doses of fluensulfone. The doses investigated are relevant, as it is possible to envisage these scaling with the soil concentrations that may pertain during nematicide treatment in the field, which are reported to be ~5µM (Norshie et al., 2017).

The investigations described in this thesis highlight that hatching and the free-living juvenile present platforms to identify the primary target of fluensulfone. The nature of the observed intoxication shows clearly that fluensulfone executes a slow, irreversible insult, which distinguishes fluensulfone from the old generation organophosphates and fluopyram (Oka, 2020a). This time-course of effects opens the potential that fluensulfone acts as a pro-drug.

It had been determined prior to the start of this project that fluensulfone elicits a progressive metabolic insult that may be underpinned by an impairment to lipid utilization. Comparisons with β-oxidation inhibitor, perhexiline, and direct analysis of neutral lipids with CARS, supports an action on lipid utilization.

The selective toxicity that fluensulfone exhibits is one of its favourable qualities as a nematicide, however, this makes investigating its mode of action more challenging, with the model organism *C. elegans* only susceptible at higher concentrations. For example, many techniques that have been used in *C. elegans* for investigating changes in metabolites (Vergano et al., 2014; Gao et al., 2017; Hastings et al., 2019) have not been optimized for use in PPNs. Furthermore, techniques that exploit genome analysis in *C. elegans,* such as forward and reverse genetics, cannot be conducted in *G. pallida.* Nevertheless, the distinct action of fluensulfone on PPNs offers a selective target, and perhaps mode of action, acting on a pathway that is selectively expressed or used in the PPN. This favours an action of fluensulfone on lipid metabolism, given that PPNs have a strong reliance on liberating stored lipid due to their non-feeding life cycle stages.

The platforms for investigating lipids outlined in Chapter 6 were explored to detail fluensulfone's impact on lipid metabolism. I detail significant developments I have made to be able to utilize these techniques in PPN research. Mass spectrometry has the capability to identify changes in the lipidome as a result of fluensulfone treatment. This is a platform that should be revisited, however with careful consideration of treatment group size to ensure meaningful data can be generated and subsequently replicated. Furthermore, a challenging aspect of the mass spectrometry work is the analysis of the data. As interest in lipid dynamics extends and grows in the research community, analysis of data generated from mass spectrometry will be greatly improved with the availability of more resources to process large lipid databases.

Finally, the morphological descriptions for fluensulfone treated juveniles present an interesting avenue that should be interrogated to discern the nature of fluensulfone-induced death. The vacuole-like structures that were observed following fluensulfone treatment are comparable to previous reports of vacuolization in drug-treated PPNs. The lipid nature of these structures is interesting, given the indication that fluensulfone prevents lipid depletion. Appearance of these structures is therefore entirely consistent with increased CARS signal relative to controls and the re-distribution of MTT staining, where MTT formazan precipitates into hydrophobic environments. The appearance of these structures prior to granulation suggests that they proceed cell death and may be a marker for impaired metabolism leading to death. Understanding how these structures are formed, and subsequently how fluensulfone acts to induce their generation, provides a promising route to extending fluensulfone mode of action studies.

7.8 Conclusion

The data presented in this thesis enables an increased understanding of the mode of action of fluensulfone, supporting a model in which fluensulfone elicits a slowly developing metabolic insult that is nematicidal to PPNs, and an ability of fluensulfone to act on multiple life-cycle stages, which is critical when considering its use in the field. There is evidence that fluensulfone acts to disrupt lipid utilization and experiments building on the optimized techniques that have been described here could better explain this insult. CARS imaging identified the generation of puncta in the posterior region of *G. pallida* juveniles following treatment with fluensulfone, consistent with the precipitation of MTT formazan in the posterior. Combining microscopy techniques to clarify the nature of these puncta would be beneficial to understanding how fluensulfone exerts its toxicity and there is value in exploring this avenue for future mode of action studies.

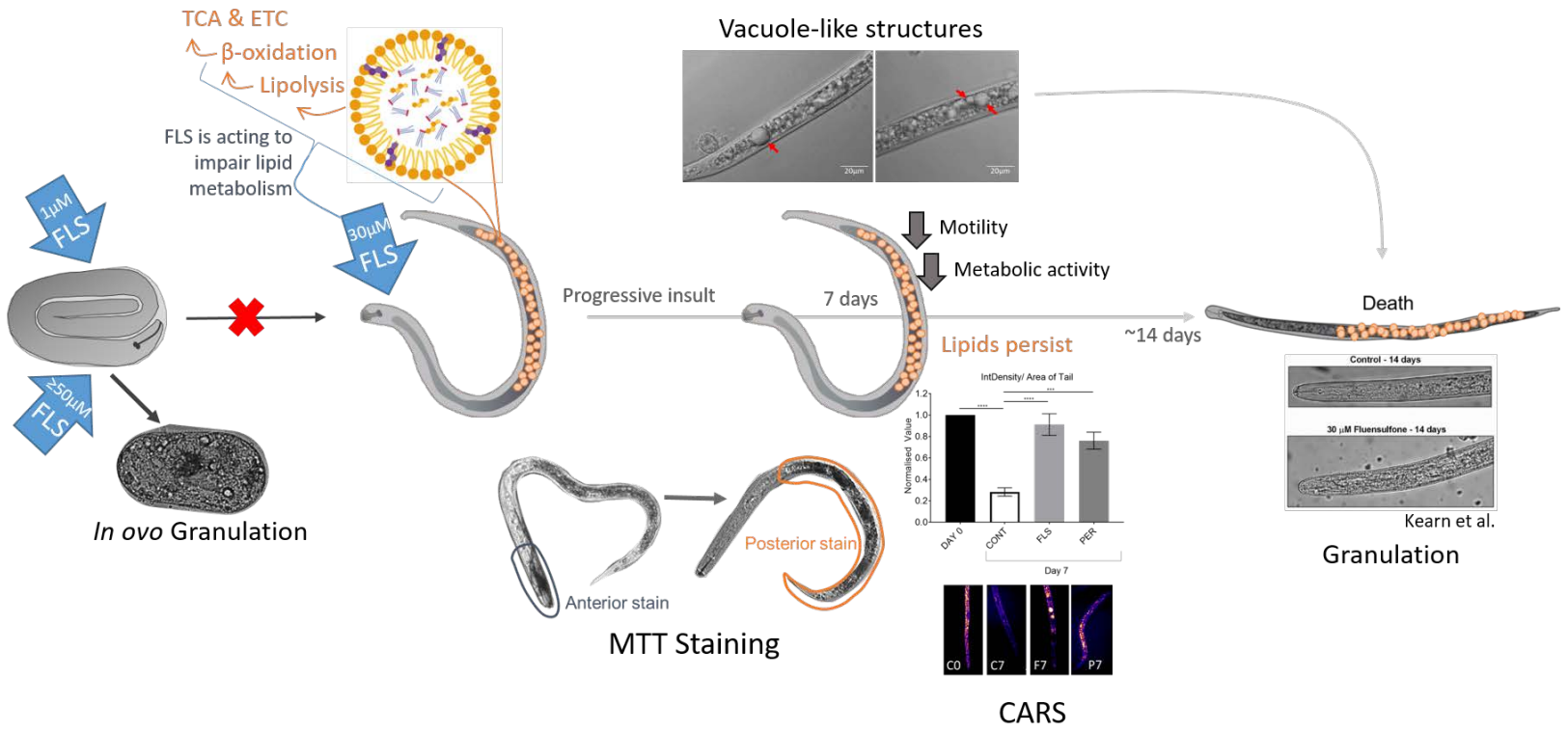

Figure 7.10 Refined model for the mode of action of fluensulfone. Fluensulfone inhibits *G. pallida* hatching and has nematicidal activity against the infective juvenile stage, eliciting a progressive, accumulating insult. Prior to death, juveniles become immotile and exhibit reduced metabolic activity, coinciding with the persistence of stored lipid and the appearance of vacuole-like structures in the posterior. It can therefore be suggested that fluensulfone acts to impair lipid utilization. Building on the optimized biochemical techniques that have been described in this thesis will further understanding of fluensulfone's mode of action.

List of References

Abusharkh, S.E., Erkut, C., Oertel, J., Kurzchalia, T. V. and Fahmy, K. 2014. The role of phospholipid headgroup composition and trehalose in the desiccation tolerance of *Caenorhabditis elegans*. *Langmuir*. (30), pp.12897–12906.

Admasu, T.D., Batchu, K.C., Ng, L.F., Cazenave-Gassiot, A., Wenk, M.R. and Gruber, J. 2018. Lipid profiling of *C. elegans* strains administered pro-longevity drugs and drug combinations. *Scientific Data*. **5**, pp.1–12.

De Almeida, A.A., Abe, V.H.F., Gonçalves, R.M., Balbi-Peña, M.I. and Santiago, D.C. 2017. Seed treatment for management of *Meloidogyne javanica* in soybean. *Semina:Ciencias Agrarias*. **38**(5), pp.2995–3006.

Antebi, A., Yeh, W.H., Tait, D., Hedgecock, E.M. and Riddle, D.L. 2000. daf-12 encodes a nuclear receptor that regulates the dauer diapause and developmental age in *C. elegans*. *Genes and Development*. **14**(12), pp.1512–1527.

Apfeld, J., O'Connor, G., McDonagh, T., DiStefano, P.S. and Curtis, R. 2004. The AMP-activated protein kinase AAK-2 links energy levels and insulin-like signals to lifespan in *C. elegans*. *Genes and Development*. **18**(24), pp.3004–3009.

Arias-Estevez, M., Lopez-Periago, E., Martinez-Carballo, E., Simal-Gandara, J., Mejuto, J.-C. and Garcia-Rio, L. 2008. The mobility and degradation of pesticides in soils and the pollution of groundwater resources. *Agriculture Ecosystems and Environment*. **123**, pp.247–260.

Ashrafian, H., Horowitz, J.D. and Frenneaux, M.P. 2007. Perhexiline. **25**(1), pp.76–97.

Atkinson, H.J. and Fowler, M. 1990. Changes in polyphosphoinositide metabolism in *Globodera Rostochiensis* following stimulation to hatch by potato root diffusate. *Nematologica*. **36**, pp.417–423.

Atkinson, H.J., Taylor, J.D. and Fowler, M. 1987. Changes in the second stage juveniles of *Globodera rostochiensis* prior to hatching in response to potato root diffusate. *Annals of Applied Biology*. **110**(1), pp.105–114.

Avenot, H.F. and Michailides, T.J. 2010. Progress in understanding molecular mechanisms and evolution of resistance to succinate dehydrogenase inhibiting (SDHI) fungicides in phytopathogenic fungi. *Crop Protection*. **29**(7), pp.643–651.

Barrett, J., Ward, C.W. and Fairbairn, D. 1970. The glyoxylate cycle and the conversion of triglycerides to carbohydrates in developing eggs of *Ascaris lumbricoides*. *Comparative Biochemistry and Physiology*. **35**(3), pp.577–586.

Barros, A.G. de A., Liu, J., Lemieux, G.A., Mullaney, B.C. and Ashrafi, K. 2012. Analyses of *C. elegans* Fat Metabolic Pathways. *Methods in Cell Biology*. **107**, pp.383–407.

Becker, J.O., Ploeg, A. and Nuñez, J.J. 2019. Multi-Year Field Evaluation of Fluorinated Nematicides Against *Meloidogyne incognita* in Carrots. *Plant disease*. **103**(9), pp.2392–2396.

Beeman, A.Q. and Tylka, G.L. 2018. Assessing the Effects of ILeVO and VOTiVO Seed Treatments on Reproduction, Hatching, Motility, and Root Penetration of the Soybean Cyst Nematode, *Heterodera glycines*. *Plant Disease*. **102**(1), pp.107–113.

Behm, C.A. 2002. Metabolism *In*: D. Lee, ed. *The Biology of Nematodes*. Taylor and Francis, pp.261–290.

Behm, C.A. 1997. The role of trehalose in the physiology of nematodes. *International Journal for Parasitology*. **27**(2), p.215.

Bell, C., Lilley, C.J., McCarthy, J., Atkinson, H.J. and Urwin, P.E. 2019. Plant-parasitic nematodes respond to root exudate signals with host-specific gene expression patterns. *PLoS Pathogens*. **15**(2), pp.1–19.

Beller, M., Thiel, K., Thul, P.J. and Jäckle, H. 2010. Lipid droplets: A dynamic organelle moves into focus. *FEBS Letters*. **584**(11), pp.2176–2182.

Berg, J., Tymoczko, J. and Stryer, L. 2002. *Biochemistry* 5th ed. New York: W. H. Freeman.

Bernard, G.C., Egnin, M. and Bonsi, C. 2017. The Impact of Plant-Parasitic Nematodes on Agriculture and Methods of Control *In*: M. M. Shah and M. Mahamood, eds. *Nematology - Concepts, Diagnosis and Control*., pp.121–151.

Bird, D. and Bird, A. 2001. Plant-parasitic nematodes *In*: M. Kennedy and W. Harnett, eds. *Parasitic nematodes: molecular biology, biochemistry and immunology*. CABI, p.139.

Blaxter, M.L., De Ley, P., Gareys, J.R., Liu, L.X., Scheldeman, P., Vierstraete, A., Vanfleteren, J.R., Mackey, L.Y., Dorris, M., Frisse, L.M., Vida, J.T. and Thomas, W.K. 1998. A molecular evolutionary framework for the phylum nematoda. *Nature*. **392**(March), pp.71–75.

Bligh, E.G. and Dyer, W.J. 1959. A rapid method of total lipid extraction and purification. *Canadian Journal of Biochemistry and Physiology*. **37**(8), pp.911–917.

Bloemberg, G. V. and Lugtenberg, B.J.J. 2001. Molecular basis of plant growth promotion and biocontrol by rhizobacteria. *Current Opinion in Plant Biology*. **4**(4), pp.343–350.

Bogner, C.W., Kamdem, R.S.T., Sichtermann, G., Matthäus, C., Hölscher, D., Popp, J., Proksch, P., Grundler, F.M.W. and Schouten, A. 2017. Bioactive secondary metabolites with multiple activities from a fungal endophyte. *Microbial Biotechnology*. **10**(1), pp.175–188.

Brandsma, J., Bailey, A.P., Koster, G., Gould, A.P. and Postle, A.D. 2017. Stable isotope analysis of dynamic lipidomics. *Biochimica et Biophysica Acta (BBA) - Molecular and Cell Biology of Lipids*. **1862**(8), pp.792–796.

Brenner, S. 1974. The genetics of *Caenorhabditis elegans*. *Genetics*. **77**(1), pp.71–94.

Bridge, J. 1996. Nematode Management in Sustainable and Subsistence Agriculture. *Annual Review of Phytopathology*. **34**(1), pp.201–225.

Brock, T.J., Browse, J. and Watts, J.L. 2007. Fatty acid desaturation and the regulation of adiposity in *Caenorhabditis elegans*. *Genetics*. **176**(2), pp.865–875.

Burnell, A.M., Houthoofd, K., O'Hanlon, K. and Vanfleteren, J.R. 2005. Alternate metabolism during the dauer stage of the nematode *Caenorhabditis elegans*. *Experimental Gerontology*. **40**(11), pp.850–856.

Burns, A.R., Luciani, G.M., Musso, G., Bagg, R., Yeo, M., Zhang, Y., Rajendran, L., Glavin, J., Hunter, R., Redman, E., Stasiuk, S., Schertzberg, M., Angus McQuibban, G., Caffrey, C.R., Cutler, S.R., Tyers, M., Giaever, G., Nislow, C., Fraser, A.G., MacRae, C.A., Gilleard, J. and Roy, P.J. 2015. *Caenorhabditis elegans* is a useful model for anthelmintic discovery. *Nature Communications*. **6**(May), pp.1–11.

Butler, D.M., Kokalis-Burelle, N., Albano, J.P., McCollum, T.G., Muramoto, J., Shennan, C. and Rosskopf, E.N. 2014. Anaerobic Soil Disinfestation (ASD) Combined with Soil Solarization as a Methyl Bromide Alternative: Vegetable Crop Performance and Soil Nutrient Dynamics. *Plant and Soil*. **378**(1–2), pp.365–381.

Byrne, J., Twomey, U., Maher, N., Devine, K.J. and Jones, P.W. 1998. Detection of hatching inhibitors and hatching factor stimulants for golden potato cyst nematode, *Globodera rostochiensis*, in potato root leachate. *Annals of Applied Biology*. **132**(3), pp.463–472.

Byrne, J.T., Maher, N.J. and Jones, A.P.W. 2001. Comparative Responses of *Globodera rostochiensis* and *G. pallida* to Hatching Chemicals. *Journal of Nematology*. **33**(4), pp.195–202.

Cabrera, J.A., Menjivar, R.D., Dababat, A. el F.A. and Sikora, R.A. 2013. Properties and Nematicide Performance of Avermectins. *Journal of Phytopathology*. **161**, pp.65–69.

Cantley, L.C., Cantley, L.G. and Josephson, L. 1978. A characterization of vanadate interactions with the (Na,K)-ATPase. Mechanistic and regulatory implications. *Journal of Biological Chemistry*. **253**(20), pp.7361–7368.

Cao, J., Guenther, R.H., Sit, T.L., Lommel, S.A., Opperman, C.H. and Willoughby, J.A. 2015. Development of abamectin loaded plant virus nanoparticles for efficacious plant parasitic nematode control. *ACS Applied Materials and Interfaces*. **7**, pp.9546–9553.

Charlson, D. V and Tylka, G.L. 2003. Heterodera glycines Cyst Components and Surface Disinfestants Affect *H. glycines* Hatching. *Journal of nematology*. **35**(4), pp.458–64.

Charwat, S., Fisher, J. and Wyss, U. 2002. The effect of osmotic stress on desiccation survival and water content of four nematode species. *Nematology*. **4**(1), pp.89–97.

Chawla, S., Patel, D.J., Patel, S.H., Kalasariya, R.L. and Shah, P.G. 2018. Behaviour and risk assessment of fluopyram and its metabolite in cucumber (*Cucumis sativus*) fruit and in soil. *Environmental Science and Pollution Research*. **25**, pp.11626–11634.

Cheng, J.X. and Xie, X.S. 2004. Coherent anti-Stokes Raman scattering microscopy: Instrumentation, theory, and applications. *Journal of Physical Chemistry B*. **108**(3), pp.827–840.

Chet, I., Ordentlich, a, Shapira, R. and Oppenheim, a 1990. Mechanisms of biocontrol of soil-borne plant-pathogens by rhizobacteria. *Plant and Soil*. **129**(1), pp.85–92.

Chitwood, D.J. 2003. Research on plant-parasitic nematode biology conducted by the United States Department of Agriculture-Agricultural Research Service. *Pest Management Science*. **59**(6–7), pp.748–753.

Chitwood, D.J., Lusby, W.R., Thompson, M.J., Kochansky, J.P. and Howarth, O.W. 1995. The glycosylceramides of the nematode *Caenorhabditis elegans* contain an unusual, branched-chain sphingoid base. *Lipids*. **30**(6), pp.567–573.

Clarke, A.J. and Hennessy, J. 1984. Movement of *Globodera Rostochiensis* (Wollenweber) juveniles stimulates by potato-root exudate. *Nematologica*. **30**, pp.206–212.

Cooper, A.F. and Van Gundy, S.D. 1970. Metabolism of Glycogen and Neutral Lipids by *Aphelenchus avenae* and *Caenorhabditis* sp. in Aerobic, Microaerobic and Anaerobic Environments. *Journal of nematology*. **2**(4), pp.305–30515.

Cotton, J.A., Lilley, C.J., Jones, L.M., Kikuchi, T., Reid, A.J., Thorpe, P., Tsai, I.J., Beasley, H., Blok, V., Cock, P.J.A., Eves-Van Den Akker, S., Holroyd, N., Hunt, M., Mantelin, S., Naghra, H., Pain, A., Palomares-Rius, J.E., Zarowiecki, M., Berriman, M., Jones, J.T. and Urwin, P.E. 2014. The genome and life-stage specific transcriptomes of *Globodera pallida* elucidate key aspects of plant parasitism by a cyst nematode. *Genome Biology*. **15**:R43.

Creamer, J.R. and Bostock, R.M. 1988. Contribution of eicosapolyenoic fatty acids to the sesquiterpenoid phytoalexin elicitor activities of *Phytophthora infestans* spores. *Physiological and Molecular Plant Pathology*. **32**(1), pp.49–59.

Crook, M. 2014. The dauer hypothesis and the evolution of parasitism: 20 years on and still going strong. *International Journal for Parasitology*. **44**(1), pp.1–8.

Crowe, J.H. and Madin, K.A.C. 1975. Anhydrobiosis in nematodes: Evaporative water loss and survival. *Journal of Experimental Zoology*. **193**(3), pp.323–333.

Csaba, G. and Pál, K. 1982. Effects of insulin, triiodothyronine, and serotonin on plant seed development. *Protoplasma*. **110**(1), pp.20–22.

Cully, D.F., Vassilatis, D.K., Liu, K.K., Paress, P.S., Van der Ploeg, L.H.T., Schaeffer, J.M. and Arena, J.P. 1994. Cloning of an avermectin-sensitive glutamate-gated chloride channel from *Caenorhabditis elegans. Nature*. **371**, pp.707–711.

Cutler, R.G., Thompson, K.W., Camandola, S., Mack, K.T. and Mattson, M.P. 2014. Sphingolipid metabolism regulates development and lifespan in *Caenorhabditis elegans*. *Mechanisms of Ageing and Development*. **143**–**144**, pp.9–18.

Davis, E.L., Hussey, R.S., Mitchum, M.G. and Thomas, J. 2008. Parasitism proteins in nematode – plant interactions. *Current Opinion in Cell Biology*. **11**, pp.360–366.

Decraemer, W. and Hunt, D. 2013. Structure and classification *In*: R. Perry and M. Moens, eds. *Plant Nematology*. CABI, pp.3–39.

Deliopoulos, T., Devine, K.J., Haydock, P.P.J. and Jones, P.W. 2007. Studies on the effect of mycorrhization of potato roots on the hatching activity of potato root leachate towards the potato cyst nematodes, *Globodera pallida* and *G. rostochiensis*. *Nematology*. **9**(5), pp.719–729.

Deliopoulos, T., Minnis, S.T., Jones, P.W. and Haydock, P.P.J. 2010. Enhancement of the efficacy of a carbamate nematicide against the potato cyst nematode, *Globodera pallida*, through mycorrhization in commercial potato fields. *Journal of Nematology*. **42**(1), pp.22–32.

Desaeger, J.A. and Watson, T.T. 2019. Evaluation of new chemical and biological nematicides for managing *Meloidogyne javanic*a in tomato production and associated double-crops in Florida. *Pest Management Science*. **75**(12), pp.3363–3370.

Devine, K.J. and Jones, P.W. 2000. Response of *Globodera rostochiensis* to exogenously applied hatching factors in soil. *Annals of Applied Biology*. **137**(1), pp.21–29.

Dingley, S., Polyak, E., Lightfoot, R., Ostrovsky, J., Rao, M., Greco, T., Ischiropoulos, H. and Falk, M.J. 2010. Mitochondrial respiratory chain dysfunction variably increases oxidant stress in *Caenorhabditis elegans*. *Mitochondrion*. **10**(2), pp.125–136.

Duceppe, M.O., Lafond-Lapalme, J., Palomares-Rius, J.E., Sabeh, M., Blok, V., Moffett, P. and Mimee, B. 2017. Analysis of survival and hatching transcriptomes from potato cyst nematodes, *Globodera rostochiensis* and *G. pallida*. *Scientific Reports*. **7**(1), pp.1–13.

Dungan, R.S., Gan, J. and Yates, S.R. 2001. Effect of temperature, organic amendment rate and moisture content on the degradation of 1,3-dichloropropene in soil. *Pest Management Science*. **57**(12), pp.1107–1113.

Eaton, S. 2002. Control of mitochondrial β-oxidation flux. *Progress in Lipid Research*. **41**(3), pp.197–239.

Ebrahimi, N. 2015. Optimizing Trehalose-Based Quantification of Live Eggs in Potato Cyst Nematodes (*Globodera rostochiensis* and *G. pallida*). *Plant Disease*. **99**(7), pp.947–953.

Edinger, A.L. and Thompson, C.B. 2004. Death by design: Apoptosis, necrosis and autophagy. *Current Opinion in Cell Biology*. **16**, pp.663–669.

Eisenback, J. and Triantaphyllou, H. 1991. Root-Knot Nematodes: *Meloidogyne* species and races *In*: W. Nickle, ed. *Manual of agricultural nematology*., p.191.

Elle, I.C., Rodkaer, S.V., Fredens, J. and Faergeman, N.J. 2012. A method for measuring fatty acid oxidation in *C. elegans*. *Landes Bioscience*. **Worm 1**(1), pp.26–30.

Ellenby, C. and Perry, R.N. 1976. The Influence of the Hatching Factor on the Water Uptake of the Second Stage Larva of the Potato Cyst Nematode *Heterodera Rostochiensis*. *Journal of Experimental Biology*. **64**(1), pp.141–147.

Erkut, C., Gade, V.R., Laxman, S. and Kurzchalia, T. V. 2016. The glyoxylate shunt is essential for desiccation tolerance in *C. elegans* and budding yeast. *eLife*. **5**, p.e13614.

Erkut, C. and Kurzchalia, T. V. 2015. The *C. elegans* dauer larva as a paradigm to study metabolic suppression and desiccation tolerance. *Planta*. **242**, pp.389–396.

Erkut, C., Penkov, S., Khesbak, H., Vorkel, D., Verbavatz, J.M., Fahmy, K. and Kurzchalia, T. V. 2011. Trehalose renders the dauer larva of *Caenorhabditis elegans* resistant to extreme desiccation. *Current Biology*. **21**, pp.1331–1336.

Escorcia, W., Ruter, D.L., Nhan, J. and Curran, S.P. 2018. Quantification of lipid abundance and evaluation of lipid distribution in *Caenorhabditis elegans* by nile red and oil red o staining. *Journal of Visualized Experiments*. **2018**(133), pp.1–6.

Evans, C.L. and Xie, X.S. 2008. Coherent anti-Stokes Raman scattering microscopy: Chemical imaging for biology and medicine. *Annual Review of Analytical Chemistry*. **1**(1), pp.883–909.

Fahy, E., Cotter, D., Sud, M. and Subramaniam, S. 2011. Lipid classification, structures and tools. *Biochim Biophys Acta.* **1811**(11), pp.637–647.

Fahy, E., Subramaniam, S., Murphy, R.C., Nishijima, M., Raetz, C.R.H., Shimizu, T., Spener, F., Van Meer, G., Wakelam, M.J.O. and Dennis, E.A. 2009. Update of the LIPID MAPS comprehensive classification system for lipids. *Journal of Lipid Research*. **50**(SUPPL.), pp.9–14.

Faske, T.R. and Hurd, K. 2015. Sensitivity of *Meloidogyne incognita* and *Rotylenchulus reniformis* to Fluopyram. *Journal of Nematology*. **47**(2), pp.216–321.

Faske, T.R. and Starr, J.L. 2007. Cotton Root Protection from Plant-Parasitic Nematodes by Abamectin-Treated Seed. *Journal of Nematology*. **39**(1), pp.27–30.

Faske, T.R. and Starr, J.L. 2006. Sensitivity of *Meloidogyne incognita* and *Rotylenchulus reniformis* to Abamectin. *Journal of Nematology*. **38**(2), pp.240–244.

Feist, E., Kearn, J., Gaihre, Y., O'Connor, V. and Holden-Dye, L. 2020. The distinct profiles of the inhibitory effects of fluensulfone, abamectin, aldicarb and fluopyram on *Globodera pallida* hatching. *Pesticide Biochemistry and Physiology*. **165** (2020) 104541.

Ferriss, R. 1984. Effects of microwave oven treatment on microorganisms in soil. *Phytopathology*. **74**, pp.121–126.

Fielenbach, N. and Antebi, A. 2008. *C. elegans* dauer formation and the molecular basis of plasticity. *Genes and Development*. **22**(16), pp.2149–2165.

Fisher, M.H. and Mrozik, H. 1992. The Chemistry and Pharmacology of Avermectins. *Annual Review of Pharmacology and Toxicology*. **32**(1), pp.537–553.

Fuchs, G. and Berg, I.A. 2014. Unfamiliar metabolic links in the central carbon metabolism. *Journal of Biotechnology*. **192**(PB), pp.314–322.

Gaihre, Y.K., Feist, E., Blok, V.C., O'Connor, V. and Holden-dye, L. 2019. Optimization of an egg hatching assay in *G . rostochiensis*. *Aspects of Applied Biology*. **142**, pp.59–70.

Gao, A.W., Chatzispyrou, I.A., Kamble, R., Liu, Y.J., Herzog, K., Smith, R.L., Van Lenthe, H., Vervaart, M.A.T., Van Cruchten, A., Luyf, A.C., Van Kampen, A., Pras-Raves, M.L., Vaz, F.M. and Houtkooper, R.H. 2017. A sensitive mass spectrometry platform identifies metabolic changes of life history traits in *C. elegans*. *Scientific Reports*. **7**(1), pp.1–14.

Garcia-Segura, L., Abreu-Goodger, C., Hernandez-Mendoza, A., Dinkova, T.D.D., Padilla-Noriega, L., Perez-Andrade, M.E. and Miranda-Rios, J. 2015. High-Throughput profiling of *Caenorhabditis elegan*s starvation-responsive microRNAs. *PLoS ONE*. **10**(11), pp.1–22.

Gems, D., Sutton, A.J., Sundermeyer, M.L., Albert, P.S., King, K. V., Edgley, M.L., Larsen, P.L. and Riddle, D.L. 1998. Two pleiotropic classes of daf-2 mutation affect larval arrest, adult behavior, reproduction and longevity in *Caenorhabditis elegans*. *Genetics*. **150**(1), pp.129–155.

Giannakou, I.O., Karpouzas, D.G., Anastasiades, I., Tsiropoulos, N.G. and Georgiadou, A. 2005. Factors affecting the efficacy of non-fumigant nematicides for controlling root-knot nematodes. *Pest Management Science*. **61**(10), pp.961–972.

Giannakou, I.O. and Panopoulou, S. 2019. The use of fluensulfone for the control of root-knot nematodes in greenhouse cultivated crops: Efficacy and phytotoxicity effects. *Cogent Food & Agriculture*. **5**(1643819).

Gibson, D.M., Moreau, R.A., Mcneil, G.P. and Brodie, B.B. 1995. Lipid Composition of Cyst Stages of *Globodera rostochiensis*. *Journal of Nematology*. **27**(3), pp.304–311.

Golden, J. and Riddle, D. 1984. The *Caenorhabditis elegans* dauer larva: Developmental effects of pheromone, food, and temperature. *Developmental Biology*. **102**(2), pp.368–378.

Gortari, M.C. and Hours, R.A. 2008. Fungal chitinases and their biological role in the antagonism onto nematode eggs. A review. *Mycological Progress*. **7**, pp.221–238.

Grabau, Z.J., Noling, J.W. and Navia Gine, P.A. 2019. Fluensulfone and 1,3-dichloroprene for plant-parasitic nematode management in potato production. *Journal of Nematology*. **51**(1), pp.1–12.

Greco, N. and Elia, F. 2000. Effects of the nematicides aldicarb and fenamiphos on the egg hatch, movement, and root penetration of the carrot cyst nematode, *Hereradera carotae In*: *Proceedings of the international symposium on chemical and non-chemical soil and substrate disinfestation*., pp.189–194.

Greenspan, Phillip, Mayer, E.P. and Fowler, S.D. 1985. Nile red: A selective fluorescent stain for intracellular lipid droplets. *Journal of Cell Biology*. **100**(3), pp.965–973.

Grewal, P.S., Bornstein-Forst, S., Burnell, A.M., Glazer, I. and Jagdale, G.B. 2006. Physiological, genetic, and molecular mechanisms of chemoreception, thermobiosis, and anhydrobiosis in entomopathogenic nematodes. *Biological Control*. **38**, pp.54–65.

Guo, Y., Walther, T.C., Rao, M., Stuurman, N., Goshima, G., Terayama, K., Wong, J.S., Vale, R.D., Walter, P. and Farese, R. V. 2008. Functional genomic screen reveals genes involved in lipid-droplet formation and utilization. *Nature*. **453**(7195), pp.657–661.

Gutbrod, P., Gutbrod, K., Nauen, R., Elashry, A., Siddique, S., Benting, J., Dörmann, P. and Grundler, F. 2020. Inhibition of acetyl-CoA carboxylase by spirotetramat causes growth arrest and lipid depletion in nematodes. *Scientific Reports*. **10**, p.12710.

Hameed, S., Ikegami, K., Sugiyama, E., Matsushita, S., Kimura, Y., Hayasaka, T., Sugiura, Y., Masaki, N., Waki, M., Ohta, I., Hossen, M.A. and Setou, M. 2015. Direct profiling of the phospholipid composition of adult *Caenorhabditis elegans* using whole-body imaging mass spectrometry. *Analytical and Bioanalytical Chemistry*., pp.7589–7602.

Hänel, V., Pendleton, C. and Witting, M. 2019. The sphingolipidome of the model organism *Caenorhabditis elegans*. *Chemistry and Physics of Lipids*. **222**(April), pp.15–22.

Hastings, J., Mains, A., Virk, B., Rodriguez, N., Murdoch, S., Pearce, J., Bergmann, S., Le Novère, N. and Casanueva, O. 2019. Multi-omics and genome-scale modeling reveal a metabolic shift during *C. elegans* aging. *Frontiers in Molecular Biosciences*. **6**(FEB), pp.1–18.

Haydock, P.P.J., Woods, S., Grove, I.G. and Hare, M.C. 2013. Chemical Control of Nematodes *In*: R. N. Perry and M. Moens, eds. *Plant Nematology*. CABI, pp.459–479.

Hellerer, T., Axäng, C., Brackmann, C., Hillertz, P., Pilon, M. and Enejder, A. 2007. Monitoring of lipid storage in *Caenorhabditis elegans* using coherent anti-Stokes Raman scattering (CARS) microscopy. *Proceedings of the National Academy of Sciences of the United States of America*. **104**(37), pp.14658–14663.

Hokkanen, H. 1991. Trap Cropping in Pest Management. *Annual review of entomology*. **36**, pp.119–138.

Holt, S.J. and Riddle, D.L. 2003. SAGE surveys *C. elegans* carbohydrate metabolism: Evidence for an anaerobic shift in the long-lived dauer larva. *Mechanisms of Ageing and Development*. **124**(7), pp.779–800.

Holz, R.A., Wright, D.J. and Perry, R.N. 1998a. Changes in the lipid content and fatty acid composition of 2nd-stage juveniles of *Globodera rostochiensis* after rehydration, exposure to the hatching stimulus and hatch. *Parasitology*. **116**, pp.183–190.

Holz, R.A., Wright, D.J. and Perry, R.N. 1998b. The effect of long term storage on the lipid reserves and fatty acid composition of cysts and hatched juveniles of *Globodera rostochtensis* and *G. pallida*. *Journal of Helminthology*. **72**(2), pp.133–141.

Holz, R.A., Wright, D.J. and Perry, R.N. 1997. The lipid content and fatty acid composition of hatched second stage juveniles of *Globodera rostochiensis* and *G. pallida*. *Fundamental and Applied Nematology*. **20**(3), pp.291–298.

Horsefield, R., Yankovskaya, V., Sexton, G., Whittingham, W., Shiomi, K., Omura, S., Byrne, B., Cecchini, G. and Iwata, S. 2006. Structural and computational analysis of the quinone-binding site of complex II (succinate-ubiquinone oxidoreductase): A mechanism of electron transfer and proton conduction during ubiquinone reduction. *Journal of Biological Chemistry*. **281**(11), pp.7309–7316.

Hough, A. and Thomason, I.J. 1975. Effects of aldicarb on the behavior of *Heterodera schachtii* and *Meloidogyne javanica*. *Journal of nematology*. **7**(3), pp.221–229.

Hough, A., Thomason, I.J. and Farmer, W.J. 1975. Behaviour of Aldicarb in Soil Relative to Control of *Heterodera schachtii*. *Journal of Nematology*. **7**(3), pp.214–221.

Huang, S.P., Resende, I.C., de Souza, D.E. and Campos, V.P. 1983. Effect of Aldicarb, Ethoprop, and Carbofuran on Control of Coffee Root-knot Nematode, *Meloidogyne exigua*. *Journal of nematology*. **15**(4), pp.510–4.

Huyer, G., Liu, S., Kelly, J., Moffat, J., Payette, P., Kennedy, B., Tsaprailis, G., Gresser, M.J. and Ramachandran, C. 1997. Mechanism of inhibition of protein-tyrosine phosphatases by vanadate and pervanadate. *Journal of Biological Chemistry*. **272**(2), pp.843–851.

Indarti, S., Widianto, D., Kim, Y.H., Mulyadi and Suryanti 2010. Survey of egg- and cyst-parasitic fungi of potato cyst nematode in Indonesia. *Plant Pathology Journal*. **26**(1), pp.32–36.

Ioannou, M.S., Jackson, J., Sheu, S.H., Chang, C.L., Weigel, A. V., Liu, H., Pasolli, H.A., Xu, C.S., Pang, S., Matthies, D., Hess, H.F., Lippincott-Schwartz, J. and Liu, Z. 2019. Neuron-Astrocyte Metabolic Coupling Protects against Activity-Induced Fatty Acid Toxicity. *Cell*. **177**(6), pp.1522-1535.e14.

Ishihara, A., Hashimoto, Y., Tanaka, C., Dubouzet, J.G., Nakao, T., Matsuda, F., Nishioka, T., Miyagawa, H. and Wakasa, K. 2008. The tryptophan pathway is involved in the defense responses of rice against pathogenic infection via serotonin production. *Plant Journal*. **54**(3), pp.481–495.

Issa, N., Lachance, G., Bellmann, K., Laplante, M., Stadler, K. and Marette, A. 2018. Cytokines promote lipolysis in 3T3-L1 adipocytes through induction of NADPH oxidase 3 expression and superoxide production. *Journal of Lipid Research*. **59**(12), pp.2321–2328.

James, C.E. and Davey, M.W. 2007. A rapid colorimetric assay for the quantitation of the viability of free-living larvae of nematodes in vitro. *Parasitology Research*. **101**(4), pp.975–980.

Jatala, P. 1986. Biological control of plant-parasitic nematodes. *Annual Review of Phytopathology*. **24**, pp.453–489.

Jenzer, C., Simionato, E., Largeau, C., Scarcelli, V., Lefebvre, C. and Legouis, R. 2019. Autophagy mediates phosphatidylserine exposure and phagosome degradation during apoptosis through specific functions of GABARAP/LGG-1 and LC3/LGG-2. *Autophagy*. **15**(2), pp.228–241.

Jones, F. 1970. The control of the potato cyst- nematode. *Journal of the Royal Society of Arts*. **118**(5164), pp.179–199.

Jones, J.G., Kleczewski, N.M., Desaeger, J., Meyer, S.L.F. and Johnson, G.C. 2017. Evaluation of nematicides for southern root-knot nematode management in lima bean. *Crop Protection*. **96**, pp.151–157.

Jones, J.T., Kumar, A., Pylypenko, L.A., Thirugnanasambandam, A., Castelli, L., Chapman, S., Cock, P.J.A., Grenier, E., Lilley, C.J., Phillips, M.S. and Blok, V.C. 2009. Identification and functional characterization of effectors in expressed sequence tags from various life cycle stages of the potato cyst nematode *Globodera pallida*. *Molecular Plant Pathology*. **10**(6), pp.815–828.

Jones, L.M., Koehler, A., Trnka, M., Balek, J., Challinor, A.J., Atkinson, H.J. and Urwin, P.E. 2017. Climate change is predicted to alter the current pest status of *Globodera pallida* and G . rostochiensis in the United Kingdom. *Global Change Biology*. **23**, pp.4497–4507.

Jones, R.L. and Norris, F.A. 1998. Factors Affecting Degradation of Aldicarb and Ethoprop. *Journal of Nematology*. **30**(1), pp.45–55.

K, A., FY, C., JL, W., AG, F., RS, K., J, A. and G, R. 2003. Genome-wide RNAi analysis of *Caenorhabditis elegans* fat regulatory genes. *Nature*. **421**(January), pp.268–272.

Kawanobe, M., Toyota, K., Fujita, T. and Hatta, D. 2019. Evaluation of nematicidal activity of fluensulfone against non-target free-living nematodes under field conditions. *Agronomy*. **9**(12), pp.1–16.

Kearn, J. 2015. *Mode of action studies on the nematicide fluensulfone*. University of Southampton, Centre for Biological Sciences, PhD Thesis.

Kearn, J., Lilley, C., Urwin, P., Connor, V.O. and Holden-dye, L. 2017. Progressive metabolic impairment underlies the novel nematicidal action of fluensulfone on the potato cyst nematode *Globodera pallida*. *Pesticide Biochemistry and Physiology*. **142**, pp.83–90.

Kearn, J., Ludlow, E., Dillon, J., O'Connor, V. and Holden-Dye, L. 2014. Fluensulfone is a nematicide with a mode of action distinct from anticholinesterases and macrocyclic lactones. *Pesticide Biochemistry and Physiology*. **109**, pp.44–57.

Kennedy, J.A., Unger, S.A. and Horowitz, J.D. 1996. Inhibition of Camitine Palmitoyltransferase-1 in Rat Heart and Liver by Perhexiline and Amiodarone. . **52**(October 1995), pp.273–280.

Kerry, B. 1988. Fungal parasites of cyst nematodes. *Agriculture, Ecosystems and Environment*. **24**(1–3), pp.293–305.

Kerry, B.R. 2000. Rhizosphere interactions and the exploitation of microbial agents for the biological control of plant -parasitic nematodes. *Annual Review of Phytopathology.* **38**, pp.423–441.

Khan, F.R. and McFadden, B.A. 1982. *Caenorhabditis elegans*: Decay of isocitrate lyase during larval development. *Experimental Parasitology*. **54**(1), pp.47–54.

Kikuchi, T., Cotton, J.A., Dalzell, J.J., Hasegawa, K., Kanzaki, N., McVeigh, P., Takanashi, T., Tsai, I.J., Assefa, S.A., Cock, P.J.A., Da Otto, T., Hunt, M., Reid, A.J., Sanchez-Flores, A., Tsuchihara, K., Yokoi, T., Larsson, M.C., Miwa, J., Maule, A.G., Sahashi, N., Jones, J.T. and Berriman, M. 2011. Genomic insights into the origin of parasitism in the emerging plant pathogen bursaphelenchus xylophilus. *PLoS Pathogens*. **7**(9).

Kim, H.E., Grant, A.R., Simic, M.S., Kohnz, R.A., Nomura, D.K., Durieux, J., Riera, C.E., Sanchez, M., Kapernick, E., Wolff, S. and Dillin, A. 2016. Lipid Biosynthesis Coordinates a Mitochondrial-to-Cytosolic Stress Response. *Cell*. **166**(6), pp.1539-1552.e16.

Kim, J., Mwamula, A.O., Kabir, F., Shin, J.H., Choi, Y.H., Lee, J.-K. and Lee, D. 2016. Efficacy of Different Nematicidal Compounds on Hatching and Mortality of Heterodera schachtii Infective Juveniles. *The Korean Journal of Pesticide Science*. **20**(4), pp.293–299.

Köfeler, H.C., Fauland, A., Rechberger, G.N. and Trötzmüller, M. 2012. Mass Spectrometry Based Lipidomics: An Overview of Technological Platforms. *Metabolites*. **2**(4), pp.19–38.

Kondrashov, F.A., Koonin, E. V, Morgunov, I.G., Finogenova, T. V and Kondrashova, M.N. 2006. Evolution of glyoxylate cycle enzymes in Metazoa: evidence of multiple horizontal transfer events and pseudogene formation. *Biology direct*. **1**(31).

Kroese, D., Zasada, I.A. and Ingham, R.E. 2011. Comparison of Meldola's Blue Staining and Hatching Assay with Potato Root Diffusate for Assessment of *Globodera* sp. Egg Viability. *Journal of Nematology*. **43**(3–4), pp.182–186.

Krusberg, L.R., Hussey, R.S. and Fletcher, C.L. 1973. Lipid and fatty acid composition of females and eggs of *Meloidogyne incognita* and *M. arenaria*. *Comparative Biochemistry and Physiology*. **45**(2), pp.335–341.

Kurzchalia, T. V. and Ward, S. 2003. Why do worms need cholesterol? *Nature Cell Biology*. **5**(8), pp.684–688.

Kwong, S.C., Jamil, A.H.A., Rhodes, A., Taib, N.A. and Chung, I. 2019. Metabolic role of fatty acid binding protein 7 in mediating triple-negative breast cancer cell death via PPAR-α signaling. *Journal of Lipid Research*. **60**(11), pp.1807–1817.

Lahm, G.P., Desaeger, J., Smith, B.K., Pahutski, T.F., Rivera, M.A., Meloro, T., Kucharczyk, R., Lett, R.M., Daly, A., Smith, B.T., Cordova, D., Thoden, T. and Wiles, J.A. 2017. The discovery of fluazaindolizine: A new product for the control of plant parasitic nematodes. *Bioorganic and Medicinal Chemistry Letters*. **27**(7), pp.1572–1575.

Lam, S.M., Wang, Z., Li, J., Huang, X. and Shui, G. 2017. Sequestration of polyunsaturated fatty acids in membrane phospholipids of *Caenorhabditis elegans* dauer larva attenuates eicosanoid biosynthesis for prolonged survival. *Redox Biology*. **12**(April), pp.967–977.

Lampropoulou, V., Sergushichev, A., Bambouskova, M., Nair, S., Vincent, E.E., Loginicheva, E., Cervantes-barragan, L., Ma, X., Huang, S.C., Griss, T., Weinheimer, C.J., Khader, S., Randolph, G.J., Pearce, E.J., Jones, R.G. and Diwan, A. 2017. Itaconate links inhibition of succinate dehydrogenase with macrophage metabolic remodeling and regulation of inflammation. *Cell Metabolism*. **24**(1), pp.158–166.

Lauble, H., Kennedy, M.C., Emptage, M.H., Beinert, H. and Stout, C.D. 1996. The reaction of fluorocitrate with aconitase and the crystal structure of the enzyme-inhibitor complex. *Proceedings of the National Academy of Sciences of the United States of America*. **93**(24), pp.13699–13703.

Le, T.T., Duren, H.M., Slipchenko, M.N., Hu, C.D. and Cheng, J.X. 2010. Label-free quantitative analysis of lipid metabolism in living *Caenorhabditis elegans*. *Journal of Lipid Research*. **51**(3), pp.672–677.

Lee, D. 2002. Life Cycles *In*: D. Lee, ed. *The Biology of Nematodes*. Taylor and Francis, pp.61–72.

Lee, J.M., Lee, Y.K., Mamrosh, J.L., Busby, S.A., Griffin, P.R., Pathak, M.C., Ortlund, E.A. and Moore, D.D. 2011. A nuclear-receptor-dependent phosphatidylcholine pathway with antidiabetic effects. *Nature*. **474**(7352), pp.506–511.

Li, J., Zou, C., Xu, J., Ji, X., Niu, X., Yang, J., Huang, X. and Zhang, K.-Q. 2015. Molecular Mechanisms of Nematode-Nematophagous Microbe Interactions: Basis for Biological Control of Plant-Parasitic Nematodes. *Annual Review of Phytopathology*. **53**(1), pp.67–95.

Li, S., Xu, S., Ma, Y., Wu, S., Feng, Y., Cui, Q., Chen, L., Zhou, S., Kong, Y., Zhang, X., Yu, J., Wu, M. and Zhang, S.O. 2016. A genetic screen for mutants with supersized lipid droplets in *Caenorhabditis elegans*. *G3: Genes, Genomes, Genetics*. **6**(8), pp.2407–2419.

Lingwood, D. and Simons, K. 2010. Lipid rafts as a membrane-organizing principle. *Science*. **327**(5961), pp.46–50.

Liu, F., Thatcher, J.D., Barral, J.M. and Epstein, H.F. 1995. Bifunctional glyoxylate cycle protein of *Caenorhabditis elgans*: A developmentally regulated protein of intestine and muscle. *Developmental Biology*. **169**, pp.399–414.

Liu, F., Thatcher, J.D. and Epstein, H.F. 1997. Induction of glyoxylate cycle expression in *Caenorhabditis elegans*: A fasting response throughout larval development. *Biochemistry*. **36**(1), pp.255–260.

Liu, Y., Fang, S., Sun, Q. and Liu, B. 2016. Anthelmintic drug ivermectin inhibits angiogenesis, growth and survival of glioblastoma through inducing mitochondrial dysfunction and oxidative stress. *Biochemical and Biophysical Research Communications*. **480**(3), pp.415–421.

Lourenço-Tessutti, I.T., Souza Junior, J.D.A., Martins-de-Sa, D., Viana, A.A.B., Carneiro, R.M.D.G., Togawa, R.C., de Almeida-Engler, J., Batista, J.A.N., Silva, M.C.M., Fragoso, R.R. and Grossi-de-Sa, M.F. 2015. Knock-down of heat-shock protein 90 and isocitrate lyase gene expression reduced root-knot nematode reproduction. *Phytopathology*. **105**(5), pp.628–37.

Luciani, G.M., Magomedova, L., Rachel, P., Urbanus, M.L., Wallace, I.M., Giaever, G., Nislow, C., Cummins, C.L. and Roy, P.J. 2011. Dafadine inhibits DAF-9 to promote dauer formation and longevity of *Caenorhabditis elegans*. *Nature Chemical Biology*. **7**, pp.891–893.

Lundquist, M.R., Goncalves, M.D., Loughran, R.M., Possik, E., Vijayaraghavan, T., Yang, A., Pauli, C., Ravi, A., Verma, A., Yang, Z., Johnson, J.L., Wong, J.C.Y., Ma, Y., Hwang, K.S.K., Weinkove, D., Divecha, N., Asara, J.M., Elemento, O., Rubin, M.A., Kimmelman, A.C., Pause, A., Cantley, L.C. and Emerling, B.M. 2018. Phosphatidylinositol-5-Phosphate 4-Kinases Regulate Cellular Lipid Metabolism By Facilitating Autophagy. *Molecular Cell*. **70**(3), pp.531-544.e9.

Ma, G., Wang, T., Korhonen, P.K., Young, N.D., Nie, S., Ang, C.S., Williamson, N.A., Reid, G.E. and Gasser, R.B. 2019. Dafachronic acid promotes larval development in *Haemonchus contortus* by modulating dauer signalling and lipid metabolism. *PLoS Pathogens*. **15**(7), pp.1–20.

Madin, K.A.C. and Crowe, J.H. 1975. Anhydrobiosis in nematodes: Carbohydrate and lipid metabolism during dehydration. *Journal of Experimental Zoology*. **193**(3), pp.335–342.

Maioli, M.A., de Medeiros, H.C.D., Guelfi, M., Trinca, V., Pereira, F.T.V. and Mingatto, F.E. 2013. The role of mitochondria and biotransformation in abamectin-induced cytotoxicity in isolated rat hepatocytes. *Toxicology in Vitro*. **27**(2), pp.570–579.

Mak, H.Y., Nelson, L.S., Basson, M., Johnson, C.D. and Ruvkun, G. 2006. Polygenic control of *Caenorhabditis elegans* fat storage. *Nature Genetics*. **38**(3), pp.363–368.

Mateos, M. V., Uranga, R.M., Salvador, G.A. and Giusto, N.M. 2008. Activation of phosphatidylcholine signalling during oxidative stress in synaptic endings. *Neurochemistry International*. **53**(6–8), pp.199–206.

McCarter, J.P., Mitreva, M.D., Martin, J., Dante, M., Wylie, T., Rao, U., Pape, D., Bowers, Y., Theising, B., Murphy, C. V, Kloek, A.P., Chiapelli, B.J., Clifton, S.W., Bird, D.M. and Waterston, R.H. 2003. Analysis and functional classification of transcripts from the nematode *Meloidogyne incognita*. *Genome Biology*. **4**(R26).

McElwee, J.J., Schuster, E., Blanc, E., Thornton, J. and Gems, D. 2006. Diapause-associated metabolic traits reiterated in long-lived daf-2 mutants in the nematode *Caenorhabditis elegans*. *Mechanisms of Ageing and Development*. **127**(12), pp.922–936.

Middendorf, P.J. and Dusenbery, D.B. 1993. Fluoroacetic Acid Is a Potent and Specific Inhibitor of Reproduction in the Nematode *Caenorhabditis elegans*. *Journal of nematology*. **25**(4), pp.573–7.

Minnis, S.T., Haydock, P.P.J. and Evans, K. 2004. Control of potato cyst nematodes and economic benefits of application of 1,3-dichloropropene and granular nematicides. *Annals of Applied Biology*. **145**, pp.145–156.

Momma, N., Kobara, Y., Uematsu, S., Kita, N. and Shinmura, A. 2013. Development of biological soil disinfestations in Japan. *Applied Microbiology and Biotechnology*. **97**(9), pp.3801–3809.

Momma, N., Yamamoto, K., Simandi, P. and Shishido, M. 2006. Role of organic acids in the mechanisms of biological soil disinfestation (BSD). *Journal of General Plant Pathology*. **72**(4), pp.247–252.

Morgunov, I.G., Kondrashova, M.N., Kamzolova, S. V, Sokolov, A.P., Fedotcheva, N.I. and Finogenova, T. V 2005. Evidence of the glyoxylate cycle in the liver of newborn rats. *Medical science monitor : international medical journal of experimental and clinical research*. **11**(2), pp.BR57-R60.

Morris, K.A., Langston, D.B., Davis, R.F., Noe, J.P., Dickson, D.W. and Timper, P. 2016. Efficacy of Various Application Methods of Fluensulfone for Managing Root-knot Nematodes in Vegetables. *Journal of Nematology*. **48**(482), pp.65–71.

Morris, K.A., Langston, D.B., Dickson, D.W., Davis, R.F., Timper, P. and Noe, J.P. 2015. Efficacy of fluensulfone in a tomato-cucumber double cropping system. *Journal of Nematology*. **47**(4), pp.310–315.

Mosmann, T. 1983. Rapid colorimetric assay for cellular growth and survival: Application to proliferation and cytotoxicity assays. *Journal of immunological methods*. **65**(1–2), pp.55–63.

Motola, D.L., Cummins, C.L., Rottiers, V., Sharma, K.K., Li, T., Li, Y., Suino-Powell, K., Xu, H.E., Auchus, R.J., Antebi, A. and Mangelsdorf, D.J. 2006. Identification of Ligands for DAF-12 that Govern Dauer Formation and Reproduction in *C. elegans*. *Cell*. **124**(6), pp.1209–1223.

Mulcahy, B., Holden-Dye, L. and O'Connor, V. 2012. Pharmacological assays reveal age-related changes in synaptic transmission at the *Caenorhabditis elegans* neuromuscular junction that are modified by reduced insulin signalling. *Journal of Experimental Biology*. **4**, pp.492–501.

Nauen, R., Reckmann, U., Thomzik, J. and Thielert, W. 2008. Biological profile of spirotetramat (Movento®) – a new two-way systemic (ambimobile) insecticide against sucking pest species. *Bayer CropScience Journal*. **61**(2).

Needham, T. 1742. A Letter from Mr. Turbevil Needham, to the President; Concerning Certain Chalky Tubulous Concretions, Called Malm: With Some Microscopical Observations on the Farina of the Red Lily, and of Worms Discovered in Smutty Corn. *Philosophical Transactions of the Royal Society of London*. **42**, pp.462–471.

Newhall, A.G. 1955. Disinfestation of soil by heat, flooding and fumigation. *The Botanical Review*. **21**(4), pp.189–249.

Nguyen, D., Alavi, M. V., Kim, K.Y., Kang, T., Scott, R.T., Noh, Y.H., Lindsey, J.D., Wissinger, B., Ellisman, M.H., Weinreb, R.N., Perkins, G.A. and Ju, W.K. 2011. A new vicious cycle involving glutamate excitotoxicity, oxidative stress and mitochondrial dynamics. *Cell Death and Disease*. **2**(12), pp.1–10.

Nordbring-Hertz, B., Jansson, H.-B. and Tunlid, A. 2006. Nematophagous Fungi. *eLS*., pp.1–13.

Norshie, P.M., Grove, I.G. and Back, M.A. 2016. Field evaluation of the nematicide fluensulfone for control of the potato cyst nematode *Globodera pallida*. *Pest Management Science*. **72**, pp.2001–2007.

Norshie, Patrick M., Grove, I.G. and Back, M.A. 2017. Persistence of the nematicide fluensulfone in potato (*Solanum tuberosum ssp. tuberosum*) beds under field conditions. *Nematology*. **19**(6), pp.739–747.

Ogawa, A., Streit, A., Antebi, A. and Sommer, R.J. 2009. A conserved endocrine mechanism controls the formation of dauer and infective larvae in nematodes. *Current Biology*. **19**(1), pp.67–71.

Oka, Y., Shuker, S. and Tkachi, N. 2009. Nematicidal efficacy of MCW-2, a new nematicide of the fluoroalkenyl group, against the root-knot nematode *Meloidogyne javanica*. *Pest Management Science*. **65**, pp.1082–1089.

Oka, Y., Shuker, S. and Tkachi, N. 2012. Systemic nematicidal activity of fluensulfone against the root-knot nematode *Meloidogyne incognita* on pepper. *Pest Management Science*. **68**, pp.268–275.

Oka, Y. 2014. Nematicidal activity of fluensulfone against some migratory nematodes under laboratory conditions. *Pest Management Science*. **70**, pp.1850–1858.

Oka, Y. and Saroya, Y. 2019. Effect of fluensulfone and fluopyram on the mobility and infection of second-stage juveniles of *Meloidogyne incognita* and *M. javanica. Pest Management Science*. **75**(8), pp.2095–2106.

Oka, Y. 2020a. From Old-Generation to Next-Generation Nematicides. *Agronomy.* **2020**, 10, 1387.

Oka, Y. 2020b. Sensitivity to fluensulfone of inactivated *Meloidogyne spp*. second-stage juveniles. *Pest Management Science*. **76**(7), pp.2379–2387.

Olzmann, J.A. and Carvalho, P. 2019. Dynamics and functions of lipid droplets. *Nature Reviews Molecular Cell Biology*. **20**(3), pp.137–155.

Opperman, C.H., Bird, D.M., Williamson, V.M., Rokhsar, D.S., Burke, M., Cohn, J., Cromer, J., Diener, S., Gajan, J., Graham, S., Houfek, T.D., Liu, Q., Mitros, T., Schaff, J., Schaffer, R., Scholl, E., Sosinski, B.R., Thomas, V.P. and Windham, E. 2008. Sequence and genetic map of *Meloidogyne hapla*: A compact nematode genome for plant parasitism. *Proceedings of the National Academy of Sciences*. **105**(39), pp.14802–14807.

Opperman, C.H. and Chang, S. 1991. Effects of Aldicarb and Fenamiphos on Acetylcholinesterase and Motility of *Caenorhabditis elegans*. *Test*. **23**(1), pp.20–27.

Osborne, P. 1973. The effect of aldiarb on the hatching of *Heterodera rostochiensis* larvae. *Nematologica*. **19**, pp.7–14.

Ou, L.-T. 1998. Enhanced Degradation of the Volatile Fumigant-Nematicides 1,3-D and Methyl Bromide in Soil. *Journal of Nematology*. **30**(1), pp.56–64.

Palomares-Rius, J.E., Hedley, P., Cock, P.J.A., Morris, J.A., Jones, J.T. and Blok, V.C. 2016. Gene expression changes in diapause or quiescent potato cyst nematode, *Globodera pallid*a, eggs after hydration or exposure to tomato root diffusate. *PeerJ*. **4**(e1654).

Palomares-Rius, J.E., Jones, J.T., Cock, P.J., Castillo, P. and Blok, V.C. 2013. Activation of hatching in diapaused and quiescent *Globodera pallida*. *Parasitology*. **140**, pp.445–454.

Palumbo, M.C., Colosimo, A., Giuliani, A. and Farina, L. 2007. Essentiality is an emergent property of metabolic network wiring. *FEBS Letters*. **581**(13), pp.2485–2489.

Pang, S., Lynn, D.A., Lo, J.Y., Paek, J. and Curran, S.P. 2014. SKN-1 and Nrf2 couples proline catabolism with lipid metabolism during nutrient deprivation. *Nature Communications*. **5**(5048).

Patel, T.R. and McFadden, B.A. 1978. *Caenorhabditis elegans* and *Ascaris suum*: Inhibition of isocitrate lyase by itaconate. *Experimental Parasitology*. **44**(2), pp.262–268.

Pelagio-Flores, R., Ortíz-Castro, R., Méndez-Bravo, A., Macías-Rodríguez, L. and López-Bucio, J. 2011. Serotonin, a tryptophan-derived signal conserved in plants and animals, regulates root system architecture probably acting as a natural auxin inhibitor in *Arabidopsis thaliana*. *Plant and Cell Physiology*. **52**(3), pp.490–508.

Penkov, S., Kaptan, D., Erkut, C., Sarov, M., Mende, F. and Kurzchalia, T. V. 2015. Integration of carbohydrate metabolism and redox state controls dauer larva formation in *Caenorhabditis elegans*. *Nature Communications*. **6**(8060).

Penkov, S., Mende, F., Zagoriy, V., Erkut, C., Martin, R., Pässler, U., Schuhmann, K., Schwudke, D., Gruner, M., Reichert-Müller, T., Shevchenko, A., Knölker, H.J. and Kurzchalia, T. V. 2010. Maradolipids: Diacyltrehalose glycolipids specific to dauer larva in *Caenorhabditis elegans*. *Angewandte Chemie - International Edition*. **49**(49), pp.9430–9435.

Penkov, S., Ogawa, A., Schmidt, U., Tate, D., Zagoriy, V., Boland, S., Gruner, M., Vorkel, D., Verbavatz, J.M., Sommer, R.J., Knölker, H.J. and Kurzchalia, T. V. 2014. A wax ester promotes collective host finding in the nematode *Pristionchus pacificus*. *Nature Chemical Biology*. **10**(4), pp.281–285.

Penkov, S., Raghuraman, B.K., Erkut, C., Oertel, J., Galli, R., Ackerman, E.J.M., Vorkel, D., Verbavatz, J.-M., Koch, E., Fahmy, K., Shevchenko, A. and Kurzchalia, T. V 2020. A metabolic switch regulates the transition between growth and diapause in *C. elegans*. *BMC Biology*. **18**(31).

Perez, C.L. and Van Gilst, M.R. 2008. A 13C Isotope Labeling Strategy Reveals the Influence of Insulin Signaling on Lipogenesis in *C. elegans*. *Cell Metabolism*. **8**(3), pp.266–274.

Perry, R.N. 1996. Chemoreception in Plant Parasitic Nematodes. *Annual Review of Phytopathology*. **34**(1), pp.181–199.

Perry, R.N. and Clarke, A.J. 1981. Trends and Perspectives Hatching mechanisms of nematodes. *Parasitology*. **83**, pp.435–449.

Perry, R.N. and Moens, M. 2011. Survival of Parasitic Nematodes outside the Host *In*: *Molecular and physiological basis of nematode survival*.

Perry, R.N. and Trett, M.W. 1986. Ultrastructure of the eggshell of *Heterodera schachtii* and *H. glycines* (Nematoda : Tylenchida). *Revue de Nématologie*. **9**(4), pp.399–403.

Perry, R.N., Wright, D. and Chitwood, D.J. 2013. Reproduction, Physiology and Biochemistry *In*: R. N. Perry and M. Moens, eds. *Plant Nematology*. CABI, pp.220–235.

Petrat, F., Pindiur, S., Kirsch, M. and De Groot, H. 2003. NAD(P)H, a primary target of 1O2 in mitochondria of intact cells. *Journal of Biological Chemistry*. **278**(5), pp.3298–3307.

Phillips, M.J. and Voeltz, G.K. 2016. Structure and function of ER membrane contact sites with other organelles. *Nature Reviews Molecular Cell Biology*. **17**(2), pp.69–82.

Proudfoot, A.T., Bradberry, S.M. and Vale, J.A. 2006. Sodium Fluoroacetate Poisoning. *Toxicological reviews*. **25**(4), pp.2113–219.

Qiao, K., Liu, X., Wang, H., Xia, X., Ji, X. and Wang, K. 2012. Effect of abamectin on root-knot nematodes and tomato yield. *Pest Management Science*.**68**, pp.853–857.

857Rajasekharan, S.K. and Lee, J. 2020. Hydropic anthelmintics against parasitic nematodes. *PLoS Pathogens*. **16**(1), pp.1–7.

Rajasekharan, S.K., Lee, J.H., Ravichandran, V., Kim, J.C., Park, J.G. and Lee, J. 2019. Nematicidal and insecticidal activities of halogenated indoles. *Scientific Reports*. **9**(1), pp.1–14.

Rambold, A.S., Cohen, S. and Lippincott-Schwartz, J. 2015. Fatty Acid Trafficking in Starved Cells: Regulation by Lipid Droplet Lipolysis, Autophagy, and Mitochondrial Fusion Dynamics. *Developmental Cell*. **33**(4), pp.489–490.

Rauthan, M. and Pilon, M. 2011. The mevalonate pathway in *C. elegans*. *Lipids in Health and Disease*. **10**, pp.2431476–511.

Reuner, A., Hengherr, S., Brümmer, F. and Schill, R.O. 2010. Comparative studies on storage cells in tardigrades during starvation and anhydrobiosis. *Current Zoology*. **56**(2), pp.259–263.

Ristaino, J.B. and Thomas, W. 1996. Agriculture, Methyl Bromide and the Ozone Hole: Can We Fill the Gaps? *Plant Disease*. **81**(9), pp.964–977.

Rockenfeller, P., Ring, J., Muschett, V., Beranek, A., Buettner, S., Carmona-Gutierrez, D., Eisenberg, T., Khoury, C., Rechberger, G., Kohlwein, S.D., Kroemer, G. and Madeo, F. 2010. Fatty acids trigger mitochondrion-dependent necrosis. *Cell Cycle*. **9**(14), pp.2908–2914.

Rolfe, R.N. and Perry, R.N. 2001. Electropharyngeograms and stylet activity of second stage juveniles of *Globodera rostochiensis. Nematology*. **3**(1), pp.31–34.

Roshchina, V. 2001. *Neurotransmitters in plant life*. CRC Press.

Salgueiro, W.G., Goldani, B.S., Peres, T. V., Miranda-Vizuete, A., Aschner, M., da Rocha, J.B.T., Alves, D. and Ávila, D.S. 2017. Insights into the differential toxicological and antioxidant effects of 4-phenylchalcogenil-7-chloroquinolines in *Caenorhabditis elegans*. *Free Radical Biology and Medicine*. **110**(December 2016), pp.133–141.

Sasanelli, N., Toderas, I., Veronico, P., Iurcu-Straistaru, E., Rusu, S., Melillo, M.T. and Caboni, P. 2020. Abamectin efficacy on the potato Cyst nematode *Globodera pallid*a. *Plants*. **9**(1), pp.1–13.

Scholte, K. 2000. Effect of potato used as a trap crop on potato cyst nematodes and other soil pathogens and on the growth of a subsequent main potato crop. *Annals of Applied Biology*. **136**(3), pp.229–238.

Schumacher, L.A., Grabau, Z.J., Wright, D.L., Small, I.M. and Liao, H.L. 2020. Nematicide influence on cotton yield and plant-parasitic nematodes in conventional and sod-based crop rotation. *Journal of Nematology*. **52**, pp.1–14.

Settembre, C., Fraldi, A., Medina, D.L., Ballabio, A. and Children, T. 2013. Signals from the lysosome. *Nat Rev Mol Cell Biol.* **14**(5), pp.283–296.

Shai, N., Schuldiner, M. and Zalckvar, E. 2016. No peroxisome is an island - Peroxisome contact sites. *Biochimica et Biophysica Acta - Molecular Cell Research*. **1863**(5), pp.1061–1069.

Shi, X., Li, J., Zou, X., Greggain, J., Rødkær, S. V., Færgeman, N.J., Liang, B. and Watts, J.L. 2013. Regulation of lipid droplet size and phospholipid composition by stearoyl-CoA desaturase. *Journal of Lipid Research*. **54**(9), pp.2504–2514.

Siddiqui, A.A., Stanley, C.S. and Berk, S.L. 2000. Cloning and expression of isocitrate lyase from human round worm *Strongyloides stercoralis*. *Parasite*. **7**, pp.233–236.

Siddiqui, Z.A. and Mahmood, I. 1999. Role of bacteria in the management of plant parasitic nematodes: A review. *Bioresource Technology*. **69**(2), pp.167–179.

Sierotzki, H. and Scalliet, G. 2013. A Review of Current Knowledge of Resistance Aspects for the Next-Generation Succinate Dehydrogenase Inhibitor Fungicides. *Phytopathology*. **103**(9), pp.880–887.

Smiley, R.W., Marshall, J.M. and Yan, G.P. 2011. Effect of Foliarly Applied Spirotetramat on Reproduction of *Heterodera avenae* on Wheat Roots. *Plant Disease*. **95**(8), pp.983–989.

Smus, J.P., Ludlow, E., Dallière, N., Luedtke, S., Monfort, T., Lilley, C., Urwin, P., Walker, R.J., O'Connor, V., Holden-Dye, L. and Mahajan, S. 2017. Coherent anti-Stokes Raman scattering (CARS) spectroscopy in *Caenorhabditis elegans* and *Globodera pallida*: evidence for an ivermectin-activated decrease in lipid stores. *Pest Management Science*. **73**(12), pp.2550–2558.

Sostare, J., Di Guida, R., Kirwan, J., Chalal, K., Palmer, E., Dunn, W.B. and Viant, M.R. 2018. Comparison of modified Matyash method to conventional solvent systems for polar metabolite and lipid extractions. *Analytica Chimica Acta*. **1037**, pp.301–315.

Stapleton, J.J. 2000. Soil solarization in various agricultural production systems. *Crop Protection*. **19**(8–10), pp.837–841.

Steele, A.E. 1977. Effects of selected carbamate and organophosphate nematicides on hatching and emergence of *Heterodera schachtii*. *Journal of nematology*. **9**(2), pp.149–14954.

Steele, A.E. and Hodges, L.R. 1975. In-Vitro and In-Vivo Effects of Aldicarb on Survival and Development of *Heterodera schachtii*. *Journal of Nematology.* **7**(3), pp.305–312.

Stirling, G. 2011. An Ecological Perspective, a Review of Progress and Opportunities for Further Research *In*: K. Davies and Y. Spiegel, eds. *Biological control of plant-parasitic nematodes*. Springer Netherlands, pp.1–38.

Stockert, J.C., Blázquez-Castro, A., Cañete, M., Horobin, R.W. and Villanueva, Á. 2012. MTT assay for cell viability: Intracellular localization of the formazan product is in lipid droplets. *Acta Histochemica*. **114**(8), pp.785–796.

Stoltzfus, J.D., Bart, S.M. and Lok, J.B. 2014. cGMP and NHR Signaling Co-regulate Expression of Insulin-Like Peptides and Developmental Activation of Infective Larvae in *Strongyloides stercoralis*. *PLoS Pathogens*. **10**(7).

Storelli, A., Keiser, A., Eder, R., Jenni, S. and Kiewnick, S. 2020. Evaluation of fluopyram for the control of *Ditylenchus dipsaci* in sugar beet. *Journal of Nematology*. **52**(January), pp.1–10.

Storey, R.M.J. 1984. The relationship between neutral lipid reserves and infectivity for hatched and dormant juveniles of *Globodera spp*. *Annals of Applied Biology*. **104**(3), pp.511–520.

Tatsuta, T., Scharwey, M. and Langer, T. 2014. Mitochondrial lipid trafficking. *Trends in Cell Biology*. **24**(1), pp.44–52.

Taylor, C.M., Wang, Q., Rosa, B.A., Huang, S.C.C., Powell, K., Schedl, T., Pearce, E.J., Abubucker, S. and Mitreva, M. 2013. Discovery of Anthelmintic Drug Targets and Drugs Using Chokepoints in Nematode Metabolic Pathways. *PLoS Pathogens*. **9**(8), e1003505.

Tefft, P.M. and Bone, L.W. 1985. Plant-Induced Hatching of Eggs of the Soybean Cyst Nematode *Heterodera glycines*. *Journal of nematology*. **17**(3), pp.275–279.

Teuscher, A. and Ewald, C. 2018. Overcoming Autofluorescence to Assess GFP Expression During Normal Physiology and Aging in *Caenorhabditis elegans*. *Bio-Protocol*. **8**(14).

Thoden, T., Pardavella, I. V. and Tzortzakakis, E.A. 2019. In vitro sensitivity of different populations of *Meloidogyne javanica* and *M. incognita* to the nematicides Salibro™ and Vydate®. *Nematology*. **21**(8), pp.889–893.

Thoden, T.C. and Wiles, J.A. 2019. Biological attributes of Salibro™, a novel sulfonamide nematicide. Part 1: Impact on the fitness of *Meloidogyne incognita*, *M. hapla* and *Acrobeloides buetschlii*. *Nematology*. **21**(6), pp.625–639.

Thorn, M.B. 1953. Inhibition by malonate of succinic dehydrogenase in heart-muscle preparations. *The Biochemical journal*. **54**(4), pp.540–547.

Tian, B., Yang, J. and Zhang, K.Q. 2007. Bacteria used in the biological control of plant-parasitic nematodes: Populations, mechanisms of action, and future prospects. *FEMS Microbiology Ecology*. **61**(2), pp.197–213.

Timper, P. 2011. Utilization of Biological Control for Managing Plant-Parasitic Nematodes *In*: K. Davies and Y. Spiegel, eds. *Biological control of plant-parasitic nematodes*. Springer Netherlands, pp.259–289.

Tobin, J.D., Haydock, P.P.J., Hare, M.C., Woods, S.R. and Crump, D.H. 2008. Effect of the fungus *Pochonia chlamydosporia* and fosthiazate on the multiplication rate of potato cyst nematodes (*Globodera pallida* and *G . rostochiensis*) in potato crops grown under UK field conditions. *Biological control*. **46**, pp.194–201.

Trivedi, P.C. and Barker, K.R. 1986. Management of Nematodes by Cultural Practices. *Nematropica*. **16**(2), pp.213–236.

Tyagi, R., Rosa, B.A., Lewis, W.G. and Mitreva, M. 2015. Pan-phylum Comparison of Nematode Metabolic Potential. *PLoS Neglected Tropical Diseases*. **9**(5), pp.1–32.

Urwin, P.E., Lilley, C.J. and Atkinson, H.J. 2002. Ingestion of double-stranded RNA by preparasitic juvenile cyst nematodes leads to RNA interference. *Molecular Plant-Microbe Interactions*. **15**(8), pp.747–752.

Valm, A.M., Cohen, S., Legant, W.R., Melunis, J., Hershberg, U., Wait, E., Cohen, A.R., Davidson, M.W., Betzig, E. and Lippincott-Schwartz, J. 2017. Applying systems-level spectral imaging and analysis to reveal the organelle interactome. *Nature*. **546**(7656), pp.162–167.

Vang, Leah E, Opperman, C.H., Schwarz, M.R. and Davis, E.L. 2016. Spirotetramat causes an arrest of nematode juvenile development. *Nematology*. **18**, pp.121–131.

Vergano, S.S., Rao, M., McCormack, S., Ostrovsky, J., Clarke, C., Preston, J., Bennett, M.J., Yudkoff, M., Xiao, R. and Falk, M.J. 2014. In vivo metabolic flux profiling with stable isotopes discriminates sites and quantifies effects of mitochondrial dysfunction in *C. elegans*. *Mol Genet Metab*. **111**(3), pp.331–341.

Viane, N., Coyne, D. and Davies, K. 2013. Biological and Cultural Management *In*: R. N. Perry and M. Moens, eds. *Plant Nematology*. CABI, pp.383–410.

Villafranca, J.J. 1974. The Mechanism of Aconitase Action. *The Journal of Biological Chemistry*. **249**(19), pp.6149–6155.

Waldo, B.D., Grabau, Z.J., Mengistu, T.M. and Crow, W.T. 2019. Nematicide effects on non-target nematodes in bermudagrass. *Journal of Nematology*. **51**(1).

Walker, A.K., Jacobs, R.L., Watts, J.L., Rottiers, V., Jiang, K., Finnegan, D.M., Shioda, T., Hansen, M., Yang, F., Niebergall, L.J., Vance, D.E., Tzoneva, M., Hart, A.C. and Näär, A.M. 2011. A conserved SREBP-1/phosphatidylcholine feedback circuit regulates lipogenesis in metazoans. *Cell*. **147**(4), pp.840–852.

Wandsworth, W. and Riddle, D. 1989. Developmental regulation of energy metabolism in *Caenorhabditis elegans*. *Developmental Biology*. **132**(1), pp.167–173.

Wang, Z., Zhou, X.E., Motola, D.L., Gao, X., Suino-Powell, K., Conneely, A., Ogata, C., Sharma, K.K., Auchus, R.J., Lok, J.B., Hawdon, J.M., Kliewer, S.A., Xu, H.E. and Mangelsdorf, D.J. 2009. Identification of the nuclear receptor DAF-12 as a therapeutic target in parasitic nematodes. *Proceedings of the National Academy of Sciences of the United States of America*. **106**(23), pp.9138–9143.

Watanabe, M. 2006. Anhydrobiosis in invertebrates. *Appl. Entomol. Zool.* **41**(1), pp.15–31.

Watts, J.L. 2009. Fat synthesis and adiposity regulation in *Caenorhabditis elegans*. *Trends Endocrinol Metab.* **20**(2), pp.58–65.

Watts, J.L. and Browse, J. 2002. Genetic dissection of polyunsaturated fatty acid synthesis in *Caenorhabditis elegans*. *Proceedings of the National Academy of Sciences of the United States of America*. **99**(9), pp.5854–5859.

Watts, J.L. and Ristow, M. 2017. Lipid and Carbohydrate Metabolism in *Caenorhabditis elegans*. *Genetics*. **207**(October), pp.413–446.

Williamson, V.M. and Gleason, C.A. 2003. Plant-nematode interactions. *Current Opinion in Plant Biology*. **6**, pp. 1–7.

Witting, M. and Schmitt-Kopplin, P. 2016. The *Caenorhabditis elegans* lipidome: A primer for lipid analysis in *Caenorhabditis elegans*. *Archives of Biochemistry and Biophysics*. **589**, pp.27–37.

Wram, C.L. and Zasada, I.A. 2019. Short-term effects of sublethal doses of nematicides on *Meloidogyne incognita. Phytopathology*. **109**(9), pp.1605–1613.

Wright, D. 1981. Nematicides:Mode of action and new approaches to chemical control *In*: B. Zuckerman, ed. *Plant Parasitic nematodes*., p.421.

Wright, D.J., Roberts, I.T.J. and Evans, S.G. 1989. Effect Of The Nematicide Oxamyl On Lipid Utilization And Infectivity In *Globodera Rostochiensis*. *Parasitology*. **98**(1), pp.151–154.

Yen, K., Le, T.T., Bansal, A., Narasimhan, S.D., Cheng, J.X. and Tissenbaum, H.A. 2010. A comparative study of fat storage quantitation in nematode *Caenorhabditis elegans* using label and label-free methods. *PLoS ONE*. **5**(9), pp.1–10.

Zasada, I.A., Halbrendt, J.M., Kokalis-Burelle, N., LaMondia, J., McKenry, M. V. and Noling, J.W. 2010. Managing Nematodes Without Methyl Bromide. *Annual Review of Phytopathology*. **48**(1), pp.311–328.

Zhang, S.O., Box, A.C., Xu, N., Men, J. Le, Yu, J., Guo, F., Trimble, R. and Mak, H.Y. 2010. Genetic and dietary regulation of lipid droplet expansion in *Caenorhabditis elegans*. *Proceedings of the National Academy of Sciences of the United States of America*. **107**(10), pp.4640–4645.

Zhang, Y., Xu, J., Dong, F., Liu, X., Wu, X. and Zheng, Y. 2014. Response of microbial community to a new fungicide fluopyram in the silty-loam agricultural soil. *Ecotoxicology and Environmental Safety*. **108**, pp.273–280.

Zhang, Y., Zhao, Z., Ke, B., Wan, L., Wang, H. and Ye, J. 2016. Induction of posttranslational modifications of mitochondrial proteins by ATP contributes to negative regulation of mitochondrial function. *PLoS ONE*. **11**(3), pp.1–13.

Zhang, Y., Zou, X., Ding, Y., Wang, H., Wu, X. and Liang, B. 2013. Comparative genomics and functional study of lipid metabolic genes in *Caenorhabditis elegans*. *BMC Genomics*. **14**(1).

Zhu, H., Shen, H., Sewell, A.K., Kniazeva, M. and Han, M. 2013. A novel sphingolipid-TORC1 pathway critically promotes postembryonic development in *Caenorhabditis elegans. eLife*. **2013**(2), pp.1–19.